Institute of Veterinary Medicine

Nicolaus Copernicus University

Department of Basic and Clinical Sciences

Doctoral Thesis

Transcriptome analysis of early stages of bovine embryos obtained *in vivo* from Polish Holstein-Friesian cows

Klaudia Miętkiewska

Ph.D. thesis under the supervision of:

Prof. dr hab. n. wet. Chandra S. Pareek

Department of Infectious, Invasive Diseases and Veterinary Administration

Institute of Veterinary Medicine

Faculty of Biological and Veterinary Sciences

Nicolaus Copernicus University

Toruń, 2026

Acknowledgments

The author expresses her gratitude to the supervisor, Prof. dr hab. n. wet. Chandra Shekhar Pareek for supervising the doctoral research and helping to prepare the doctoral thesis.

Spis treści

Abstract

Background: The objective of the research was to investigate how maternal age and season affect the transcriptome of bovine embryos derived in vivo from Holstein-Friesian cows. The study aimed to analyze changes in gene expression and metabolic pathways related to embryo quality and developmental potential. Previous studies have documented the impact of maternal age on reproductive outcomes; however, the mechanisms underlying transcriptomic changes in early bovine embryos remain unclear. Therefore, by comparing embryos collected during warm and cold seasons and of younger and older cows, the dissertation study sought to identify molecular markers of embryo competence and environmental adaptation.

Methods: The RNA-Seq-based transcriptome profiling was conducted on 34 in vivo-derived embryos collected from seven Polish Holstein-Friesian dairy cows differing in age (2–7 years) and season (spring and summer). Embryos were obtained after superovulation, artificial insemination, and uterine flushing according to IETS guidelines, morphologically evaluated, and stored at -80 °C. RNA extraction, cDNA synthesis, amplification, and library preparation were performed according to the Takara Smart-seq2 protocol. Sequencing was carried out on the Illumina NovaSeq6000 platform (2×150 bp, 30 million reads per embryo). The raw reads were filtered for quality and mapped to the Bos taurus UMD3.0 reference genome (assembly accession GCA_002263795.3). Differential gene expression analysis was performed in DESeq2, comparing embryos by maternal age and seasons. The functional annotation of differentially expressed genes was conducted using PANTHER and STRING databases. The enrichment analysis of Gene Ontology Biological Processes and KEGG pathways was performed in Cytoscape (v3.9.1) with ClueGO (v2.5.9), applying Bonferroni step-down correction (adjusted $p<0.05$). Networks of enriched functional terms were generated separately for up- and downregulated gene sets to visualize molecular processes potentially affected by age and seasonal conditions. Additionally, deconvolution analysis employing the MuSiC and DeTREM algorithm was applied to estimate the contribution of specific embryonic developmental stages to the bulk transcriptomes, using reference single-cell RNA-seq datasets.

Results: Transcriptome analysis revealed that both advanced maternal age and seasonal conditions significantly influenced gene expression profiles in bovine embryos, affecting pathways essential for embryonic development, metabolism, implantation, immune regulation, and stress adaptation. In cotext to maternal age, the study identified the top 30 age-dependent

upregulated differentially expressed gene (DEG) transcripts, including: *Inducible T cell costimulator (ICOS), Signal Transducer and Activator of Transcription 4 (STAT4), Matrix Gla Protein (MGP), Cancer/Testis Antigen Family 47 Member B1 (CT47B1), Family With Sequence Similarity 13 Member C (FAM13C), Cytochrome P450 Family 11 Subfamily A Member 1 (CYP11A1), Cytochrome P450 Family 4 Subfamily V Member 2 (CYP4V2), Hypoxanthine Phosphoribosyltransferase 1 (HPRT1), C-C Motif Chemokine Ligand 24 (CCL24), Phospholipase A2 Group VII (PLA2G7), SYT 4 (Synaptotagmin 4), Phosphodiesterase 10A (PDE10A), MAGE Family Member B2 (MAGE B2), INSC Spindle Orientation Adaptor Protein (INSC), Leucine rich repeats and calponin homology domain containing 2 (LRCH2), Zinc Finger Protein 514 (ZNF514), Molybdenum Cofactor Sulfurase (MOCOS), Homer Scaffold Protein 1 (HOMER1), RNA binding motif protein 46 (RBM46), Pyruvate Dehydrogenase Kinase 4 (PDK 4), Carbonic Anhydrase 2 (CA2), Transketolase Like 2 (TKTL2), Early growth response 2 (Egr 2), Zinc finger B-box domain (ZBBX), Chromosome 5 Open Reading Frame 75 (C5H12orf75)* and 5 novel unannotated genes. The study identified the top 30 age-dependent downregulated differentially expressed gene (DEG) transcripts, including: *Neuropeptide S Receptor 1 (NPSR1), Synaptotagmin (SYT9), ADP Ribosylation Factor Like GTPase 13A (Arl13a), Prominin 1 (PROM1), RNA binding motif single-stranded interacting protein 3 (RBMS3), Fibronectin type III and SPRY domain containing 1 like (FSD1L), ATPase copper transporting alpha (ATP7A), Inosine monophosphate dehydrogenase 1 (IMPDH1), Serpin family B member 4 (SERPINB4), Calcyphosine-like (CAPSL), Fanconi anaemia, complementation group A (FANCA), CAMP Responsive Element Binding Protein 5 (CREB5), LY6/PLAUR Domain Containing 6B (LYPD6B), SANT and BTB domain regulator of CSR (SANBR), Lysozyme (LYZ), Ubiquinol-cytochrome c reductase core protein 2 (UQCRC2), FEM-1-Like Death Receptor Binding Protein (FEM1B), Junction-Mediating And -Regulatory Protein (JMY), V-Akt Murine Thymoma Viral Oncogene Homolog 2 (AKT2)* along with eleven unannotated genes. In context to season, the study identified the top 30 season-dependent upregulated differentially expressed gene (DEG) transcripts, including: *HSPA6 (Heat shock protein family A (Hsp70) member 6), NR1I3 (Nuclear Receptor Subfamily 1 Group I Member 3), Cytochrome P450 Family 4 Subfamily V Member 2 (CYP4V2), C-X-C Motif Chemokine Receptor 4 (CXCR4), Immunoglobulin Heavy Constant Mu (IGHM), Hypoxanthine Phosphoribosyltransferase 1 (HPRT1), Follicle Stimulating Hormone Receptor (FSHR), MAGE Family Member B2 (MAGEB2), FosB Proto-Oncogene, AP-1 Transcription Factor Subunit (FOSB), Cytochrome P450 Family 11 Subfamily A Member 1 (CYP11A1), Zinc Finger B-Box Domain Containing (ZBBX), Forkhead Box A1 (FOXA1), Lysosomal Protein*

Transmembrane 5 (LAPTM5), MAGE Family Member D2 (MAGED2), Eva-1 Homolog C (EVA1C), SH3 Domain Binding Glutamate Rich Protein (SH3BGR), Carbonic Anhydrase 2 (CA2), Branched Chain Amino Acid Transaminase 2 (BCAT2), SH3 Domain Containing GRB2 Like 2, Endophilin A1 (SH3GL2), BMP Binding Endothelial Regulator (BMPER), Fibrinogen Beta Chain (FGB), Family With Sequence Similarity 13 Member C (FAM13C), Kallikrein Related Peptidase 8 (KLK8), Myosin Light Chain 7 (MYL7), CD8 Subunit Beta (CD8B) and 4 novel unannotaed genes. However, the study identified the top 30 season-dependent downregulated differentially expressed gene (DEG) transcripts, including: *RNA binding motif single stranded interacting protein 3 (RBMS3), Ubiquinol-cytochrome c reductase core protein 2 (UQCRC2), Proteasome 26S subunit, ATPase 6 (PSMC6), Dynein axonemal heavy chain 12 (DNAH12), ETS variant transcription factor 5 (ETV5), Synaptotagmin 9 (SYT9), Fibronectin type III and SPRY domain containing 1 like (FSD1L), F-box protein 48 (FBXO48), Dedicator of cytokinesis 8 (DOCK8), Adrenoceptor beta 2 (ADRB2), Zinc finger protein 845 (ZNF845), Fem-1 homolog B (FEM1B), Hepcidin antimicrobial peptide (HAMP), BEN domain containing 4 (BEND4), Aquaporin 7 (AQP7), Corneodesmosin (CDSN), and ATP binding cassette subfamily C member 3 (ABCC3),* and 13 novel unannotated genes. In the context of deconvolution-based gene expression analysis, the study identified several overlapping marker genes across four successive stages of embryo development: the early-stage group comprising 2-cell and 4-cell embryos, the 8-cell stage, the morula stage, and the late blastocyst stage. Most of these marker genes exhibit stage specificity, with the majority being unique to the 8-cell stage (2832; 45.6%) and the early-stage group (1444; 23.3%), followed by morula (895; 14.4%) and late blastocyst (640; 10.3%). Only limited overlap was detected between clusters, indicating that each developmental stage is characterized by a distinct gene expression profile.

Conclusions: The findings demonstrate that maternal age and season jointly shape the bovine embryonic transcriptome, affecting key developmental, metabolic, and stress-adaptive processes. This knowledge may help improve embryo selection criteria, refine assisted reproduction protocols in cattle, and offer insights relevant to reproductive management in other mammalian species. In the context of maternal age, the study concludes that relative to embryos derived from younger cows, embryos obtained from older cows exhibited up-regulation of genes involved in the metabolic pathways of steroidogenesis, metabolic regulation, and immune signaling, including *CYP11A1, PDK4, HPRT1, STAT4, and EGR2,* suggesting compensatory activation of endocrine and metabolic pathways. In contrast, embryos from older cows showed down-regulation of key developmental and mitochondrial genes, such

as *AKT2, UQCRC2, FANCA, JMY,* and *PROM1,* indicating impaired energy metabolism, cytoskeletal organization, genomic stability, and implantation-related processes. In context to season, the study concludes that when embryos collected during the warm season were compared with those obtained during the cold season, warm-season embryos displayed increased expression of stress-response, endocrine, and implantation-associated genes, including *HSPA6, FSHR, CXCR4, CYP11A1, BMPER, and FGB*, consistent with enhanced cellular stress adaptation and altered hormonal signaling. Conversely, reduced expression of genes involved in mitochondrial function, cytoskeletal dynamics, vesicle trafficking, and epigenetic regulation, such as *UQCRC2, DNAH12, SYT9, ETV5, and RBMS3*, was observed in warm-season embryos, suggesting a slower developmental tempo and altered metabolic homeostasis under elevated environmental temperatures. A deconvolution-inspired analytical framework was applied to bulk RNA-seq data from individual in vivo–derived bovine embryos to assess transcriptional similarity across stages of preimplantation development. This approach enabled the identification of shared gene expression signatures and stage-specific transcriptional programs. Clustering and dimensionality reduction analyses revealed a clear separation of developmental stages, with pronounced transcriptomic transitions between early cleavage stages and later stages. Comparative analyses using MuSiC and DeTREM indicated a predominance of late blastocyst–associated transcriptional signatures in whole-embryo transcriptomes, highlighting the dominance of later-stage gene expression programs in bulk RNA-seq data.

Keywords: Holstein-Friesian cattle, Bovine embryos, Maternal age, Transcriptome analysis, RNA-seq

1. Introduction

In recent years, the field of dairy cattle reproduction has seen dynamic progress in the development of assisted reproductive technologies, which play a pivotal role in accelerating breeding advancement and optimizing herd productivity. In the face of ever-increasing demands to maximize reproductive potential and the numerous challenges encountered by both breeders and veterinarians responsible for herd health management, gaining an in-depth understanding of the factors that determine embryo quality has become particularly important [1]. This dissertation is dedicated to analyzing the impact of cow age and the influence of varying temperatures on the quality of preimplantation bovine embryos. The assessment of embryo quality was conducted at the transcriptomic level by identifying changes in the expression of genes involved in key developmental processes. The study was conducted using advanced Next-Generation Sequencing (NGS) technologies, which enabled a detailed and precise characterization of the molecular determinants that may significantly impact further embryo development and the overall success of biotechnological procedures applied in bovine reproduction.

1.1. The influence of cow age on the transcriptome of bovine embryos obtained in vivo.

The age at which cattle reach puberty and sexual maturity is crucial for the reproductive and economic efficiency of beef and dairy production [2]. The onset of puberty in cattle is influenced by a complex set of factors, and interpreting these factors requires caution due to the many parameters that shape the phenotype of both heifers and bulls. [3]. The process of sexual maturation is regulated by complex biochemical mechanisms involving the metabolic, neuroendocrine, and reproductive systems [2]. In heifers, puberty is marked by ovulation, visible signs of oestrus, the formation of a corpus luteum (CL), and a regular oestrous cycle [4]. Typically, the onset of puberty is identified by measuring systemic progesterone concentrations, with two consecutive readings above 1 ng/mL considered evidence of the first ovulation. Studies show that improved metabolic status in early life accelerates the maturation of the hypothalamic–pituitary–gonadal axis, promoting earlier sexual development without compromising fertility [2]. Factors such as age and season are often related to animal fertility quality [5]. The age of cows significantly influences their reproductive efficiency, particularly the quality of bovine embryos, as it affects oocyte maturation and subsequent embryonic

development [6]. Older cows often experience diminished embryo viability due to age-associated declines in oocyte quality and changes in uterine receptivity [7]. Additionally, genetic and epigenetic modifications in embryos are increasingly recognized as contributing factors to developmental outcomes and potential intergenerational effects [8]. Age-related alterations in gene expression profiles within bovine embryos can influence their ability to implant and develop properly [9]. These findings underscore the importance of understanding the interplay between maternal age, genetic modifications, and embryo quality to improve reproductive technologies and management strategies in cattle breeding programs [10]. Furthermore, researching the influence of cow age on the quality of bovine embryos may contribute to expanding knowledge about assisted reproductive techniques in humans of advanced age [5].

Assisted reproductive technologies (ART) are gaining increasing popularity, and the application of OMICs methods, such as transcriptomics, proteomics, and metabolomics offers the opportunity to identify effective biomarkers and analyze gene expression in pre-implantation cattle embryos, thereby providing a deeper understanding of molecular changes occurring at the transcriptome level [11, 12]. In this context, transcriptomic profiling has become a key tool for elucidating the physiological, biochemical, and metabolic mechanisms underlying early embryonic development, as well as for assessing embryonic competence in dairy cows [13]. Importantly, the transcriptome of a single bovine embryo can vary significantly depending on the maternal age, reflecting a cascade of specific regulatory pathways [14]. Since the female reproductive system is highly susceptible to aging [15], maternal age also impacts several molecular processes within the oocyte, including a decline in the maturation-promoting factor (MPF) and mitogen-activated protein kinase (MAPK) activity [16]. Therefore, a solid understanding of molecular biology is essential for interpreting how maternal aging affects early embryonic development in cattle [17]. In this dissertation, we investigated *in vivo*-derived bovine embryos using bulk RNA-seq analysis of individual embryos to identify differentially expressed genes (DEGs) and associated metabolic pathways (upregulated and downregulated) in Polish Holstein-Friesian cows of different ages. Advanced bioinformatics approaches were applied to elucidate molecular factors determining gene expression profiles in the context of fertility and reproduction in the studied population.

1.2. Changes in bovine embryos collected in vivo caused by seasonal changes in temperature.

Global warming has recently had a significant impact across the globe. The rise in ambient temperatures, particularly during summer, poses a serious challenge to the agricultural sector. Exposure of livestock to high ambient temperatures leads to substantial economic losses worldwide, with estimates in the United States alone reaching approximately 1.2 billion dollars annually, underscoring the economic consequences of elevated temperatures on animal productivity and health [18]. Exposure of dairy cattle to high ambient temperatures during the summer months negatively impacts livestock productivity, leading to reductions in milk yield, feed intake, daily weight gain, and reproductive performance [19]. One of the most critical outcomes of elevated environmental temperatures affecting cattle is the decline in fertility. Since the 1990s, the success rate of artificial insemination (AI) in dairy cattle has significantly dropped during the summer, primarily due to increased maternal body temperature, which disrupts ovarian and uterine function [20]. Moreover, the impact of high ambient temperatures on dairy cattle is widely recognized as a contributing factor to increased embryonic mortality. Elevated maternal body temperature affects various aspects of pregnancy, including reproductive hormone secretion, oocyte quality, fertilization success, and embryo development. [21]. Exposure of cows to elevated environmental temperatures is proposed to reduce oocyte quality and impair subsequent embryo development [20]. Studies report that when GV-stage cumulus–oocyte complexes (COCs) are exposed to elevated temperatures (40.0°C to 41.0°C) in vitro, they exhibit impaired nuclear and cytoplasmic maturation, as well as a higher incidence of abnormal spindle formation [22, 20]. Consequently, heat-stressed oocytes frequently fail to progress beyond the metaphase I stage [22]. Some studies also indicate that oocytes are especially vulnerable during the initial 12 hours of maturation, as the impact of high temperatures may accelerate both cytoplasmic and nuclear maturation processes [23]. At the GV stage, maternal exposure to high environmental temperatures compromises oocyte function, induces apoptosis, disrupts cytoskeletal components, alters maternal gene expression, and impairs mitochondrial function and ATP levels. Additionally, it affects surrounding cumulus cells, disrupting matrix metallopeptidase 9 (MMP9) activity and progesterone secretion. These alterations interfere with protein synthesis, thereby compromising oocyte maturation and further development [19, 24]. Exposure of dairy cows to high environmental temperatures also induces oxidative stress, increasing the production of

reactive oxygen species (ROS) within oocytes. ROS can damage DNA, trigger apoptosis, and impair organelle function, particularly within mitochondria [25].

Considering the negative impact of high temperatures on oocyte development and quality, it is intriguing to explore how exposure to heat affects bovine embryo development. Studies report that an increase in maternal internal temperature above 39°C during the first six days of embryo development impairs cytoskeletal integrity, promotes oxidative stress, and reduces transcriptional competence prior to embryonic genome activation. More advanced embryos, such as blastocysts, gradually acquire thermotolerance through the expression of heat shock proteins and accumulation of antioxidants [26]. Research has demonstrated that exposure of dairy cattle to high environmental temperatures during the preimplantation period significantly decreases the proportion of embryos that develop to the blastocyst stage [27]. Preimplantation embryos are especially sensitive to thermal stress, and early embryonic loss frequently occurs during this period [28]. The vulnerability of embryos to elevated environmental temperatures is stage-dependent, with early-stage embryos (1- to 8-cell) being more susceptible than later stages such as morulae or blastocysts [29]. Exposure to temperatures between 40.0°C and 42.0°C significantly impairs the developmental potential of 1- to 8-cell embryos, whereas morulae and blastocysts are less affected [30]. Even when early-stage embryos survive initial exposure to high environmental temperatures, they frequently show a reduction in total cell number, especially in the trophectoderm of the blastocyst. [31]. Early-stage embryos subjected to elevated environmental temperatures also exhibit disrupted microfilaments and microtubules, mitochondrial swelling, and increased apoptosis at the 2-cell stage [30]. Collectively, these findings confirm that exposure of dairy cattle to elevated environmental temperatures directly damages early-stage embryos and reduces their developmental competence [32]. Interestingly, two-cell and four-cell embryos are capable of initiating a heat shock-induced transcriptional response even before major embryonic genome activation [30]. However, the overall ability of early embryos to survive heat shock remains debated. Some studies suggest that exposure of dairy cattle to moderately elevated environmental temperatures induces the synthesis of heat shock proteins (HSPs) in two-cell embryos, promoting cellular resilience, while others report that these embryos fail to survive induced thermotolerance [33]. Thermotolerance is believed to be associated with the transcriptional activation of HSP genes [34].

In early bovine embryogenesis, exposure to elevated environmental temperatures not only upregulates genes related to heat shock proteins but also induces epigenetic modifications that alter the transcriptome. Key HSPs such as HSP70 and HSPA14 are significantly upregulated at the 2-cell, 4-cell, and morula stages, contributing to protein stabilization and apoptosis inhibition [29, 35]. As embryos develop, they gradually gain thermotolerance. For instance, exposure to 41°C on days 0 and 2 of development significantly reduces embryo viability, whereas exposure on days 4 and 6 does not show a notable effect [18]. Bovine morulae exposed to 40°C for 8 hours show increased expression of heat shock proteins (HSPs), such as HSPB11 and HSPA1A, which play a protective role by stabilizing ribosomal RNA [29]. Elevated expression of HSP90AA1 has also been reported. At the same time, exposure to elevated temperatures can downregulate crucial developmental genes, including AQP3 and ATP1A1, which are involved in blastocyst cavitation and ion transport, thus compromising embryo viability [36]. Epigenetic disturbances include increased acetylation of the HSP70 promoter and abnormal nuclear accumulation of H3K9me3 and HP1, which disrupt chromatin structure and impair transcription of essential developmental genes [36]. The expression of DNMT1, a gene essential for DNA methylation during epigenetic reprogramming, is also altered under thermal stress, indicating instability in the epigenetic landscape [37]. Antioxidant treatments such as coagulansin-A have been shown to mitigate the molecular effects of exposure to elevated environmental temperatures by modulating genes associated with oxidative stress and apoptosis-upregulating BCL-2 and PI3K, and downregulating CASP3, BAX, and NF-κB [38]. Therefore, this study aimed to investigate how environmental conditions experienced by donor cows, specifically during hot and thermoneutral seasons, affect the transcriptomic profile of bovine embryos. By analyzing gene expression patterns, we sought to identify temperature-related molecular changes that may influence early embryonic development and viability in dairy cattle.

1.3 RNA sequencing (RNAseq) technology

Various molecular biology techniques have been employed to study gene expression in bovine embryos. Reverse transcription combined with PCR (RT-PCR) remains a commonly used method for detecting rare transcripts, and is particularly useful in distinguishing qualitative differences between morulae and blastocysts derived in vivo and in vitro [39, 40]. Furthermore, RT-qPCR, which enables real-time monitoring of cDNA amplification, is frequently applied to quantify gene expression [40]. Over time, additional techniques such as hybridization have

been developed to facilitate transcriptome-wide analysis [11, 12]. Among the most advanced tools is high-throughput next-generation sequencing (HT-NGS), particularly RNA-seq, which allows for comprehensive transcriptome analysis through direct sequencing of cDNA [41]. RNA-seq is known for its sensitivity, scalability, and ability to detect novel transcripts. It was first applied to single bovine embryos in 2013 [42], and since then, it has become a powerful approach in studying early embryo development. In this study, we utilized single-embryo RNA-seq to characterize transcriptomic profiles at early developmental stages. This method was selected because early-stage embryos are small in size and cellular complexity, which makes it feasible to bulk mRNA from the whole embryo and obtain an averaged gene expression profile. The transcriptome profile is now recognized as essential to understanding the physiological, biochemical, and metabolic processes underlying preimplantation development and embryo competence in dairy cows. Notably, in vivo-derived embryos can exhibit distinct transcriptome patterns depending on the maternal age, which is known to affect various molecular pathways, including reductions in maturation-promoting factor (MPF) and mitogen-activated protein kinase (MAPK) levels [43]. The female reproductive system is particularly sensitive to aging, and understanding these molecular changes is crucial to improving reproductive efficiency.

Previous studies have shown that gene expression profiles-especially differentially expressed genes (DEGs)-vary depending on experimental design and the specific aim of the research. In vivo-derived embryos exhibit higher expression of nuclear-encoded genes related to mitochondrial function [44]. Candidate genes implicated in embryo development include sperm-associated antigen 1 (SPAG1), microtubule-associated protein 1A (MAP1A), and gasdermin B (GSDMB) [45]. EIF2B2 was reported to be overexpressed 33-fold in blastocysts, alongside other genes such as TNK1, UBE3A, and PSMA1 [46]. In addition, sex-specific differences in transcriptomic profiles have been identified. For instance, one study reported 7,369 DEGs between male and female preimplantation embryos, with 5,197 upregulated and 2,172 downregulated genes. Among them, 34 genes were simultaneously upregulated in both sexes, highlighting substantial sex-related differences in early embryo development [47]. Such findings underline the importance of analyzing the transcriptomes of in vivo-derived embryos to better understand the molecular impact of various biological and environmental factors. Moreover, determining whether in vivo or in vitro-derived embryos offer better developmental potential remains an open question. Evidence suggests that in vitro fertilization and culture conditions may significantly alter the embryonic transcriptome compared to in vivo

counterparts, particularly in genes related to glucose metabolism [46, 47]. For instance, genes such as GLU and CS exhibit higher expression in embryos produced in vivo. Overall, comprehensive transcriptomic analysis using advanced molecular techniques is essential for unraveling the complex regulatory networks governing early bovine embryo development. In this study, we performed bulk RNA-seq analysis of individual in vivo-derived embryos from Polish Holstein-Friesian cows of different ages and seasons to identify differentially expressed genes (DEGs) and associated metabolic pathways. The dissertation aim was to elucidate temperature- and age-dependent gene expression changes relevant to fertility and reproductive efficiency in cattle.

1.4 Deconvolution

Deconvolution is a computational technique used in the analysis of bulk RNA-seq data that allows the estimation of the composition and abundance of different cell types in a heterogeneous population based on gene expression profiles. Deconvolution algorithms compare gene expression profiles from single cells to reference profiles of known cell types. Based on these comparisons, the algorithm can estimate the relative proportions of different cell types in the sample. In our study, deconvolution was applied to bulk RNA-seq data obtained from individual in vivo-derived bovine embryos to estimate the contribution of different cell types within the whole-embryo transcriptome. This is particularly useful where gene expression profiles of individual cells are examined. Deconvolution is critical because bulk sRNA-seq analyses measure average gene expression across the entire sample, which can hide differences between individual cell types. Undoubtedly, the advantage of deconvolution is the identification of specific changes, which allows us to distinguish which changes in gene expression are related to changes in the proportions of these cells and which result from changes in gene expression within these cells. There are various deconvolution methods, one of them is MuSiC (and its extension MuSiC 2), which was developed to improve deconvolution, i.e., separation of cell types, which enables precise analysis of the obtained results. MuSiC is a method that utilizes cell-type-specific gene expression from single-cell RNA sequencing data to characterize cell type compositions from bulk RNA-seq data in complex tissues [48]. By appropriate weighting of genes showing cross-subject and cross-cell consistency, MuSiC enables the transfer of cell-type-specific gene expression information from one dataset to another. In general, the MuSiC uses two types of input data: i) Bulk expression obtained from RNA sequencing, which is a mixture of the expression of various cell types.

These are the data we want to deconvolve: ii) Multi-subject single-cell expression obtained from single-cell RNA sequencing (scRNA-seq). The cell types of scRNA-seq are pre-determined. These serve as a reference for estimating cell type proportions of bulk data.

In the present study, the concept of deconvolution was adapted and applied to bulk RNA-seq data from individual in vivo-derived bovine embryos. Rather than directly comparing single-cell and bulk datasets, we used the deconvolution framework as an analytical inspiration to explore similarities and differences in gene expression among embryos at various developmental stages. This approach allowed us to observe which genes were commonly expressed across stages, such as morula and blastocyst, and to identify those whose expression changed as development progressed.

2. Dissertation's research hypothesis

The experimental research was designed to generate the transcriptome profiles of early developmental stages of bovine embryos obtained in vivo.

Hypothesis 1: Maternal age influences early bovine embryo development through physiological and metabolic mechanisms, resulting in measurable transcriptomic differences between embryos collected *in vivo* from young cows (2 years) and older cows (>5 years).
Hypothesis 2: Elevated ambient temperature impairs cow early embryonic development *in vivo* and is associated with transcriptomic changes in genes involved in key developmental and metabolic pathways.
Hypothesis 3: Embryo transcriptomes vary by developmental stage, and deconvolution-oriented analyses applied to single-embryo bulk RNA-seq can help resolve stage-specific gene-expression signatures in *in vivo*–derived embryos.

Dissertation's research objective and goals.

The advanced innovative transcriptome analysis studies involving comprehensive transcriptome investigations on bovine blastocyst stages and preimplantation of embryos obtained in vivo will provide new insights and novel research findings on animal reproduction, such as identification of the potential candidate genes (CGs) for animal reproduction and fertility traits, and the metabolic pathways based on the gene network interactions. By generating the differentially expressed RNA gene profiles in bovine blastocysts and advanced

bioinformatics analysis of bulk RNA-seq analysis of single embryos data will help to elucidate factors determining the potential putative RNA genes in the context of fertility and animal reproduction in Polish HF breeds used in the experiment. The present dissertation aimed to investigate the transcriptome analysis (bulk RNA-seq analysis of single embryos) of early stages of blastocysts and preimplantation of embryos in vivo in Polish HF cows and to identify the physiological and molecular processes associated with differentially expressed (DE) genes (upregulated and downregulated) at the preimplantation of embryos transcriptomic level in Polish HF cows. The genome-wide RNA expression in the bovine blastocysts was assessed using the bulk RNA-seq analysis of single embryos. The bovine blastocyst transcriptomes changed at the early developmental stages of embryos, and preimplantation of embryos was compared to identify the novel genes. In this dissertation, the DEGs analysis of early stages of bovine blastocysts and preimplantation of embryos of bulk RNA-seq analysis of single embryos data was carried out to achieve the following research objectives and aims:

1. To generate the FASTq data set of bovine blastocysts from bulk RNA-seq analysis of single embryos of the Polish HF (submission to NCBI resource database, after the PhD dissertation: 34 embryos).
2. Alignment and mapping of the 34 embryos at different early developmental stages in Polish HF cows to the Bos Taurus UMD 3,0 reference genome.
3. To identify the differentially expressed gene transcripts (DEG-transcripts) in preimplantation embryos by comparing cows' age (younger cows - 2 years vs older cows - over 5 years).
4. To identify the differentially expressed gene (DEGs) transcripts of preimplantation embryos by comparing embryos stages developed during the spring (May) and summer (August) period.
5. Based on bulk RNA-seq analysis of single embryos deconvolution, it was determined how changes in gene expression affect the developmental stages of bovine embryos.

3. Materials and Methods

3.1. Animal selection and seasonal framework of the study

Animals, housing, and ethics

In vivo embryo collections were performed on a commercial dairy farm in Łódź, Poland, using seven multiparous, lactating, clinically healthy Polish Holstein–Friesian (HF) donor

cows. Cows were maintained in a free-stall system with ad libitum access to drinking water and were fed a balanced total mixed ration (TMR). Donor ages were 2 years (n = 2), 5 years (n = 1), 6 years (n = 2), and 7 years (n = 2).

Eligibility for embryo collection was restricted to animals confirmed as clinically healthy at enrolment, based on herd health records and a brief veterinary examination. Cows with evidence of infectious disease or other clinical conditions that could confound reproductive performance were excluded. Management variables, including parity and days-in-milk, were recorded prospectively for sensitivity analyses. All procedures complied with national regulations and EU Directive 2010/63/EU and were approved by the Local Ethical Committee in Bydgoszcz (32/2023; 17 October 2023).

Seasonal framework and on-farm temperature monitoring

To evaluate whether embryos collected under different ambient temperature conditions differed in developmental stage and quality parameters, collections were performed at two time points: late summer (August 25, 2022) and spring (May 4, 2023). Seasonal classification was defined operationally based on on-site ambient temperature measurements recorded at the farm where donor cows were housed. The two collection periods are therefore referred to as warmer and cooler conditions, based solely on recorded environmental temperature.

Ambient temperature was monitored for one month preceding each embryo collection. Measurements were performed three times daily-morning (07:00), midday (13:00), and evening (19:00)-to capture diurnal variation. Temperature was also recorded on the day of embryo collection at approximately the time of the procedure; at 11:00, the temperature was approximately 21 °C on August 25, 2022 and approximately 16 °C on May 4, 2023.

For the late-summer period (July 25 to August 25, 2022), the average daily maximum temperature was 23.2 °C and the average daily temperature was 19.25 °C, indicating warmer ambient conditions. For the spring period (April 4 to May 4, 2023), the average daily temperature was 9.9 °C and the average maximum temperature was 13.6 °C, indicating cooler ambient conditions. These two monitoring windows (warmer vs cooler) were used as the exposure framework for downstream comparisons.

Because multiple embryos could be obtained from the same donor cow, donor identity was retained to enable explicit consideration of within-cow clustering in the statistical modeling described in subsequent Methods sections.

3.2. Embryo collection procedures

Oestrous synchronization, superovulation, and insemination

In vivo-derived (IVD) embryos were obtained following oestrous synchronization, superovulation, and artificial insemination of donor cows, according to Bó et al. [49]. Briefly, the ovarian cycle was synchronized using a progestin vaginal insert (PRID delta, 1.55 g vaginal therapeutic system for cattle; Ceva Santé Animale, 133500 Libourne, France) and intramuscular hormone administrations as follows: day 1, 3 ml GnRH (Ovarelin, 50 μg/ml; Ceva Santé Animale, 133500 Libourne, France); day 7, 2 ml PGF2α (Cyclix, 250 μg/ml; VIRBAC, France) with PRID removal; day 8, 2 ml PGF2α (Cyclix); day 9, 3 ml GnRH (Ovarelin). All injections were administered intramuscularly into the gluteal muscles.

Superovulation was induced using a four-day decreasing-dose regimen of FSH + LH (Follicle-stimulating hormone 500 IU + Luteinizing hormone 500 IU), Pluset (LABORATORIOS CALIER, S.A., Spain), administered twice daily at 12 h intervals: day 1, 3 ml per injection; day 2, 2.5 ml per injection; day 3, 1.5 ml per injection; day 4, 1 ml per injection.

Bull semen was deposited intrauterine by a qualified inseminator. Insemination was performed three times at 12 h intervals to increase the probability of fertilization of ovulated oocytes.

Embryo recovery and sample structure

Embryos were recovered by non-surgical uterine flushing. A Foley catheter was placed into each uterine horn, and flushing was performed using a commercial flushing medium containing buffering agents, bovine serum albumin (BSA), and antibiotics (BoviFlush, Minitube). Recovered embryos were collected and enumerated for each donor cow. Individual embryo recovery outcomes per donor are summarized in Table 1. For downstream analyses, embryos were additionally grouped using two operational schemes: an age-based grouping (younger vs older donors) and a collection-time grouping reflecting cooler vs warmer on-farm conditions (spring vs late-summer collection), as summarized in Table 2.

Table 1. Individual embryo recovery outcomes by donor cow and age.

Donor ID	Age (years)	Number of embryos
Cow 1	2	13
Cow 2	6	3
Cow 3	2	4
Cow 4	6	2
Cow 5	7	3
Cow 6	7	3
Cow 7	5	6

Table 2. Embryo yield under two operational grouping schemes: age-based and collection-time-based.

Comparison framework ‡	Group	Donor cows	n*	Total embryos †
Age-based	Younger (2 years)	Cow 1, Cow 3	2	17
Age-based	Older (5–7 years)	Cow 2, Cow 4, Cow 5, Cow 6, Cow 7	5	17
Collection-time-based	Spring (cooler conditions)	Cow 5, Cow 6, Cow 7	3	12
Collection-time-based	Summer (warmer conditions)	Cow 1, Cow 2, Cow 3, Cow 4	4	22

n = number of donor cows per group.
† Multiple embryos were obtained from some donor cows; donor identity was retained for downstream analyses to allow consideration of within-donor clustering where applicable.
‡ The age-based and collection-time-based groupings represent overlapping classification schemes applied to the same set of donors and embryos and were used to address distinct analytical objectives in subsequent sections.

3.3. Embryo evaluation

Embryo recovery, evaluation, and staging

All recovered in vivo-derived (IVD) embryos were evaluated and classified according to the International Embryo Transfer Society (IETS) standards [50,51]. Embryos were examined under a stereomicroscope and classified using two descriptors: developmental stage (IETS stage code) and morphological quality (IETS quality code).

After non-surgical uterine flushing of both uterine horns using a Foley catheter and a sterile commercial flushing medium containing physiological buffers, bovine serum albumin, and antibiotics (BoviFlush, Minitube), recovered material was screened systematically under a stereomicroscope to identify embryos. Recovered embryos were transferred into 0.1% PBS/PVA and washed three times in fresh aliquots. Embryos were then assessed under transmitted light at 40–60× working magnification. Staging and grading were performed according to predefined IETS morphological criteria by trained personnel to ensure consistent application of the classification system.

The classification followed IETS criteria (Figure 1; Table 3). Developmental stage was recorded using IETS stage codes (1-9). In the present dataset, embryos were assigned to compact morula (stage code 4), early blastocyst (stage code 5), or blastocyst (stage code 6). Morphological quality was recorded using the IETS quality code (1-4), reflecting overall morphological integrity and the proportion of viable embryonic mass.

Immediately after classification, single embryos were placed into labelled 0.2 mL PCR tubes containing 5 µL of 0.1% PBS/PVA buffer, snap-frozen on dry ice, and stored at -80°C until downstream processing.

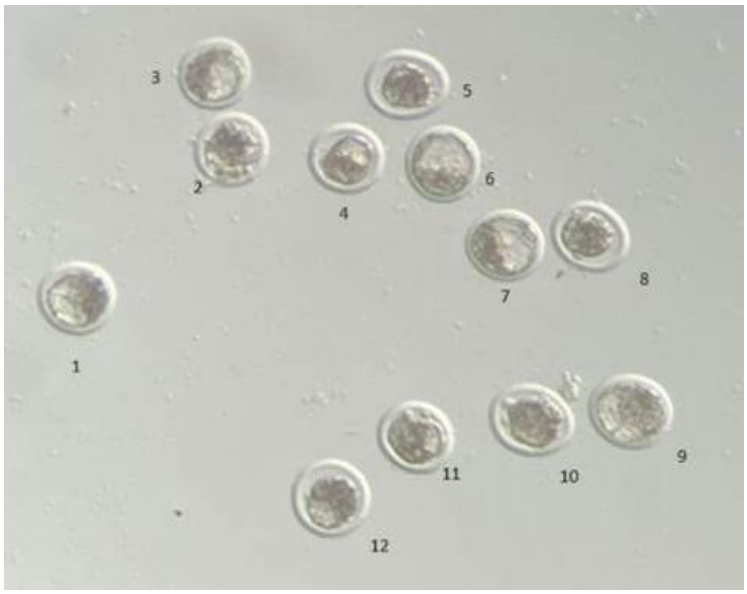

Figure 1. Representative images of bovine embryos derived in vivo from seven Holstein–Friesian cows, examined under a stereomicroscope (transmitted light; working magnification 40–60×) and classified according to IETS developmental stage and morphological quality criteria [50,51].

Table 3. Morphological classification and quality assessment of in vivo-derived bovine embryos according to IETS criteria.

Embryo No.	Stage code	Developmental stage	Quality code	Morphological description
1	5	Early blastocyst	1	Blastocoel visible with ring-like appearance; embryo occupies ~70–80% of the perivitelline space; early differentiation of inner cell mass and trophectoderm; zona pellucida intact; uniform morphology with ≥85% viable embryonic mass.
2	6	Blastocyst	2	Large blastocoel occupying most of the perivitelline space; inner cell mass and trophectoderm distinguishable with mild irregularities; zona pellucida intact; moderate irregularities in morphology with ≥50% viable embryonic mass.
3	5	Early blastocyst	2	Blastocoel present (~70–80% of the perivitelline space); inner cell mass and trophectoderm forming but not sharply distinct; zona pellucida intact; moderate irregularities with ≥50% viable embryonic mass.

4	4	Compact morula	1	Compact mass of blastomeres without visible blastocoel; indistinct cell borders due to compaction; zona pellucida intact; uniform morphology without fragmentation with ≥85% viable embryonic mass.
5	5	Early blastocyst	1	Clear blastocoel cavity; inner cell mass and trophectoderm visible; zona pellucida intact; uniform morphology with ≥85% viable embryonic mass.
6	5	Early blastocyst	2	Blastocoel present; early differentiation of inner cell mass and trophectoderm; zona pellucida intact; moderate irregularities in shape or cell density with ≥50% viable embryonic mass.
7	5	Early blastocyst	2	Blastocoel present; initiation of inner cell mass and trophectoderm differentiation; zona pellucida intact; moderate irregularities in cell arrangement/density with ~50–75% viable embryonic mass.
8	5	Early blastocyst	1	Clear blastocoel cavity; inner cell mass and trophectoderm visible and evenly distributed; zona pellucida intact; uniform morphology without fragmentation with ≥85% viable embryonic mass.
9	6	Blastocyst	1	Large blastocoel occupying nearly all perivitelline space; clear inner cell mass and trophectoderm differentiation; zona pellucida intact and slightly thinned; uniform morphology with ≥85% viable embryonic mass.
10	5	Early blastocyst	1	Blastocoel occupying ~70–80% of the perivitelline space; organized inner cell mass and trophectoderm; zona pellucida intact; uniform morphology with ≥85% viable embryonic mass.
11	4	Compact morula	1	Compact morula; no visible blastocoel; zona pellucida intact; no visible fragmentation with ≥85% viable embryonic mass.
12	5	Early blastocyst	1	Well-formed blastocoel cavity; organized inner cell mass and trophectoderm; zona pellucida intact; uniform morphology with ≥85% viable embryonic mass.

Explanatory notes (IETS classification) [50,51].
Stage code (1–9): 1, unfertilized oocyte or 1-cell; 2, 2–4 cells; 3, morula; 4, compact morula; 5, early blastocyst; 6, blastocyst; 7, expanded blastocyst; 8, hatching blastocyst; 9, hatched blastocyst.
Quality code (1–4): 1, excellent/good (≥85% intact viable embryonic mass; symmetrical and uniform morphology); 2, fair (moderate irregularities; ≥50% viable embryonic mass); 3, poor (major irregularities; ≥25% viable embryonic mass); 4, dead/degenerating (non-viable).

3.4. RNA-seq experiment

A next-generation sequencing (NGS)-based RNA sequencing (RNA-seq) experiment was conducted to generate embryo-level transcriptomic profiles from in vivo-derived bovine preimplantation embryos. The dataset comprised 34 embryos collected in vivo from seven Polish Holstein-Friesian (HF) donor cows (Sections 3.1-3.2; Tables 3-4) and processed as separate low-input RNA-seq libraries. Sequencing was performed on an Illumina NovaSeq platform using paired-end 150 bp reads.

3.4.1. Experimental design

Each embryo constituted one RNA-seq library and one embryo-level transcriptome profile. A unique sample identifier was assigned to each embryo, and embryo-level and donor-level metadata were recorded at recovery and retained throughout molecular processing and sequencing, including donor cow identity, age-based grouping (younger vs older donors), and collection-time grouping reflecting cooler vs warmer on-farm conditions (as defined in Sections 3.1–3.2). Because multiple embryos were recovered from some donors, the sample structure is nested (embryos within donor cows); donor identity was therefore retained to enable explicit consideration of within-donor clustering in the statistical modeling framework described in subsequent Methods sections. Embryos were processed individually using sterile consumables to minimize cross-sample contamination. A schematic overview of the experimental design and the laboratory and analytical workflow is provided in Figure 2.

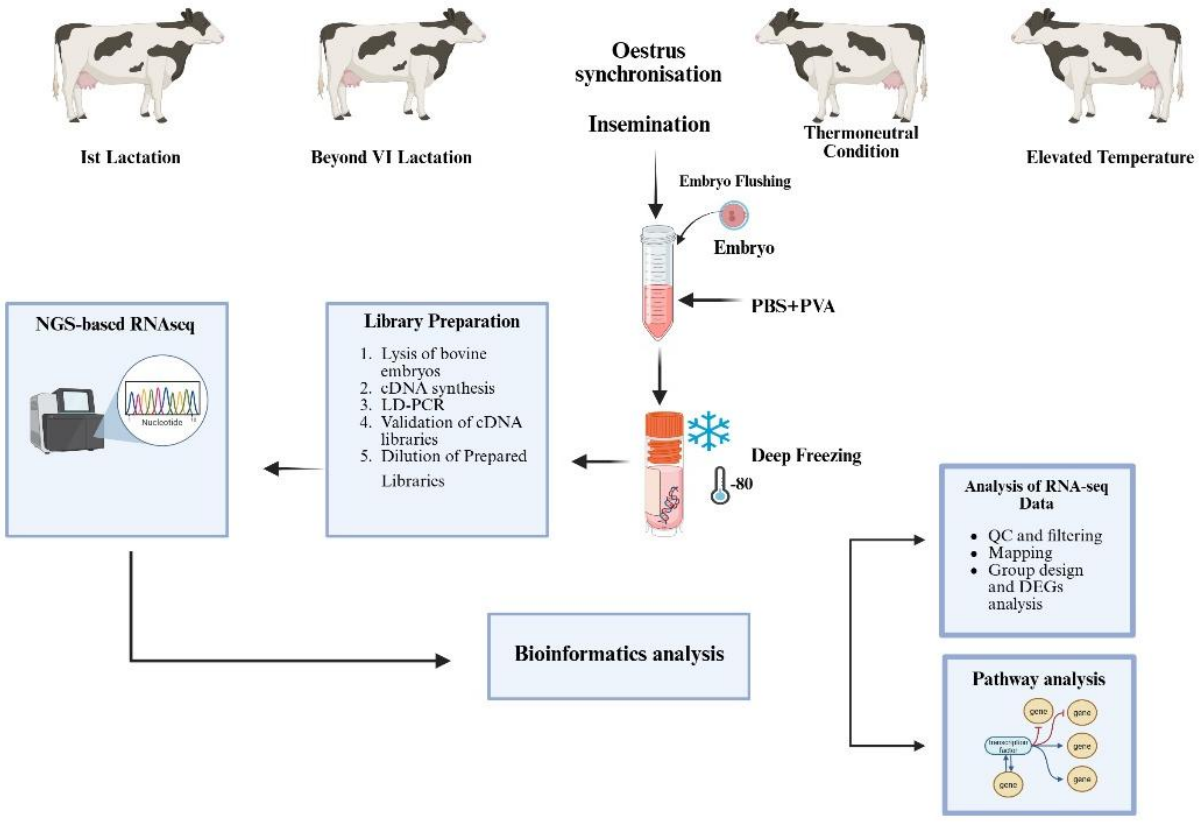

Figure 2. Experimental design and RNA-seq workflow for in vivo-derived bovine embryos. Schematic overview of the experimental design and analytical workflow. In vivo-derived bovine embryos were recovered by uterine flushing, transferred to PBS supplemented with PVA, and stored at -80°C. RNA-seq libraries were generated from individual embryos using a low-input workflow including embryo lysis, first-strand cDNA synthesis, long-distance PCR (LD-PCR) amplification, purification, and library quality control. Sequencing data were subjected to primary read-level quality assessment and downstream bioinformatic processing (quality filtering, mapping/quantification, and differential expression analysis), followed by functional interpretation.

3.4.2. Low-input RNA-seq library preparation from individual in vivo-derived embryos (n = 34)

Low-input library preparation was performed directly in 0.2 mL PCR tubes containing individual embryos in 5 µL of RNase-free 0.1% PBS/PVA buffer using a Takara kit, following the manufacturer's protocol (Takara SmartSeq v4 Ultra Low Input RNA Kit). The workflow consisted of embryo lysis, first-strand cDNA synthesis, amplification of full-length cDNA by long-distance PCR (LD-PCR), purification, and pre-sequencing quality control.

Embryo lysis was initiated by adding 1 µL of 10× lysis buffer supplemented with RNase inhibitor. First-strand cDNA synthesis was performed by adding an RT master mix prepared according to the kit protocol, including 5× ultra-low first-strand buffer, SMART-seq v4 oligonucleotide, RNase inhibitor, and SMARTScribe II reverse transcriptase. Reverse transcription was carried out in a BIO-RAD thermocycler with incubation at 42°C for 3 h followed by enzyme inactivation at 70°C for 10 min.

Amplification of double-stranded cDNA was performed using SeqAmp PCR buffer, PCR Primer IIA, and SeqAmp DNA polymerase, applying the LD-PCR cycling program specified by the manufacturer. Purification of amplified cDNA was performed using AMPure XP beads (30 µL per library) with magnetic separation, followed by two washes with 150 µL freshly prepared 70% ethanol and air-drying on the magnetic stand (10 min) prior to elution.

Library quantity and fragment-size distribution were assessed prior to sequencing using predefined QC criteria to ensure that libraries met sequencing input and performance requirements. Quantitative assessment was performed using the Qubit 3.0 Fluorometer (Thermo Fisher Scientific, USA) with the Qubit dsDNA HS Assay Kit. Qualitative assessment of fragment-size distribution and electropherogram profile was performed using the Agilent 2100 Bioanalyzer (Agilent Technologies, USA) with a high-sensitivity DNA assay. Libraries were considered suitable for sequencing based on an expected insert-size distribution and a stable electropherogram peak shape without prominent impurity peaks, and with no detectable adapter or primer-dimer peaks. Library molarity was additionally evaluated by qPCR; libraries with qPCR concentration >1.5 nM met sequencing input requirements. Based on these criteria, 34 libraries passed quality control and were advanced to sequencing (Table 4; Figure 2). All laboratory steps were performed according to the manufacturer's protocol, and any deviations were documented.

3.4.3. NGS sequencing and primary quality control of sequencing read data

Prior to sequencing, libraries were normalized to 2 nM using 10 mM Tris-HCl (pH 8.5). Denaturation was performed by combining 5 µL of the 2 nM library with 5 µL of 0.2 N NaOH, followed by vortexing, brief centrifugation (280×g for 1 min), and incubation at room temperature for 5 min. Denatured libraries were prepared for loading according to Illumina NovaSeq requirements and combined with a PhiX control as a run performance control. Sequencing was performed on the Illumina NovaSeq instrument to generate paired-end reads (2 × 150 bp), targeting approximately 30 million paired-end reads per library. For each embryo, approximately 9 GB of raw sequencing data were generated.

Primary read-data quality control was performed at both run level and library level prior to downstream analyses to verify sequencing performance and sample-level read quality and to identify potential technical artifacts. Primary QC included evaluation of sequencing yield, per-base quality distributions, GC-content profiles, and signals consistent with technical artifacts (including adapter-related features) prior to subsequent bioinformatic processing and statistical analyses described in later Methods sections.

3.5. Bioinformatic analysis

3.5.1. Primary processing of embryo RNA-seq reads and NCBI submission

Raw sequencing reads (FASTQ) generated from low-input RNA-seq libraries prepared from individual embryos were subjected to primary quality assessment using FastQC [52,53,54,55]. Quality assessment was performed on a per-embryo basis to verify sequencing yield and base-call quality and to identify technical artifacts that can influence downstream inference (e.g., adapter contamination, low-complexity sequence, atypical base-composition profiles, and abnormal quality-score distributions). Key read-level QC metrics are summarized in Table 4, while complete sample-level QC outputs were retained in Supplementary Table 4 to ensure end-to-end traceability between raw sequencing output and downstream analyses.

Adapter sequences and low-complexity artifacts, including poly-A sequences, were removed using fastp [57]. Unless otherwise specified, recommended/default parameters were applied. Quality assessment was repeated after read processing to confirm effective removal of technical sequence content and to ensure that read-quality profiles remained suitable for alignment and quantification. Libraries showing atypical sequencing yield or read-quality profiles relative to the cohort were flagged during QC review and documented explicitly. All QC outputs, sample-retention decisions, and any deviations from the standard processing

workflow were recorded per embryo (Supplementary Table S2) to provide a transparent audit trail from raw data to analysis-ready inputs [58].

Raw sequencing data were deposited in NCBI under BioProject accession PRJNA1026627.

Table 4. Read-level quality control summary for embryo RNA-seq libraries generated from in vivo-derived Polish Holstein–Friesian embryos.

SN	Sample	Library_Flowcell_Lane	Raw reads	Raw data	Effective (%)	Error (%)	Q20 (%)	Q30 (%)	GC (%)
1	Embryo_2022_24	EKDL230007736-1A_HF557DSX7_L3	61680062	9.3	100.00	0.10	77.25	68.66	43.35
2	U033	EKDL230007737-1A_HF557DSX7_L2	70238996	10.5	100.00	0.05	88.95	82.64	49.77
3	Embryo_2022_1	EKDL230007713-1A_HF7WWDSX7_L4	83968024	12.6	100.00	0.04	89.88	83.59	45.04
4	Embryo_2022_2	EKDL230007714-1A_HF7WWDSX7_L4	68055062	10.2	100.00	0.05	87.93	81.33	41.17
5	Embryo_2022_3	EKDL230007715-1A_HF7WWDSX7_L4	68703484	10.3	100.00	0.07	81.53	73.69	43.50
6	Embryo_2022_4	EKDL230007716-1A_HF7WWDSX7_L4	70190760	10.5	100.00	0.05	87.84	81.50	40.96
7	Embryo_2022_5	EKDL230007717-1A_HF7WWDSX7_L4	65548074	9.8	100.00	0.04	90.87	84.96	43.56
8	Embryo_2022_6	EKDL230007718-1A_HF7WWDSX7_L4	61860038	9.3	100.00	0.04	90.80	84.74	44.20
9	Embryo_2022_7	EKDL230007719-1A_HF7WWDSX7_L4	65574172	9.8	100.00	0.03	93.38	87.85	44.34
10	Embryo_2022_8	EKDL230007720-1A_HF7WWDSX7_L4	59335714	8.9	100.00	0.06	83.40	76.64	39.71
11	Embryo_2022_9	EKDL230007721-1A_HF7WWDSX7_L4	52650254	7.9	100.00	0.05	88.12	81.62	47.03
12	Embryo_2022_10	EKDL230007722-1A_HF7WWDSX7_L4	60178382	9.0	100.00	0.05	88.19	82.00	44.72
13	Embryo_2022_11	EKDL230007723-1A_HF3NCDSX7_L4	5620112	6.8	100.00	0.05	86.38	79.90	45.42
14	Embryo_2022_12	EKDL230007724-1A_HF7WWDSX7_L4	53887842	8.1	100.00	0.05	86.62	79.88	43.41
15	Embryo_2022_13	EKDL230007725-1A_HF3NCDSX7_L4	7881242	10.2	100.00	0.06	84.59	77.82	42.77
16	Embryo_2022_14	EKDL230007726-1A_HF7WWDSX7_L4	55063072	8.3	100.00	0.06	85.79	79.02	41.51
17	Embryo_2022_15	EKDL230007727-1A_HF7WWDSX7_L4	73360376	11.0	100.00	0.08	81.05	73.36	35.47

SN	Sample	Library_Flowcell_Lane	Raw reads	Raw data	Effective (%)	Error (%)	Q20 (%)	Q30 (%)	GC (%)
18	Embryo_2022_16	EKDL230007728-1A_HF7WWDSX7_L4	47840402	7.2	100.00	0.06	84.24	77.26	42.77
19	Embryo_2022_17	EKDL230007729-1A_HF7WWDSX7_L4	62732614	9.4	100.00	0.04	89.73	83.62	42.52
20	Embryo_2022_18	EKDL230007730-1A_HF557DSX7_L2	51542312	7.7	100.00	0.04	90.85	85.54	43.34
21	Embryo_2022_19	EKDL230007731-1A_HF557DSX7_L2	63310004	9.5	100.00	0.04	91.05	85.41	43.78
22	Embryo_2022_20	EKDL230007732-1A_HF557DSX7_L3	60987078	9.1	100.00	0.04	91.27	85.58	46.91
23	Embryo_2022_23	EKDL230007735-1A_HF557DSX7_L2	54787812	8.2	100.00	0.05	86.80	80.26	45.51
24	U035	EKDL230007738-1A_HF557DSX7_L3	76346396	11.5	100.00	0.03	93.40	88.28	47.98
25	U034	EKDL230007739-1A_HF557DSX7_L3	51462060	7.7	100.00	0.03	93.64	88.42	49.58
26	Embryo_2023_4	EKDL230007740-1A_HF557DSX7_L2	59139282	8.9	100.00	0.05	88.43	82.20	47.25
27	U037	EKDL230007741-1A_HF557DSX7_L3	50541816	7.6	100.00	0.04	93.08	87.51	47.53
28	U032	EKDL230007742-1A_HF557DSX7_L2	60853740	9.1	100.00	0.04	89.46	83.39	46.99
29	Embryo_2023_7	EKDL230007743-1A_HF557DSX7_L3	67014506	10.1	100.00	0.10	76.97	68.36	45.92
30	U040	EKDL230007744-1A_HF557DSX7_L3	49849202	7.5	100.00	0.03	95.59	91.10	49.56
31	Embryo_2023_12	EKDL230007748-1A_HF557DSX7_L2	45180134	6.8	100.00	0.03	96.49	92.28	46.92
32	Embryo_2023_15	EKDL230007751-1A_HF557DSX7_L3	55579414	8.3	100.00	0.04	92.70	87.01	47.85
33	U038	EKDL230007752-1A_HF557DSX7_L2	54299398	8.1	100.00	0.03	94.82	90.05	46.98
34	Embryo_2023_17	EKDL230007753-1A_HF557DSX7_L3	67497038	10.1	100.00	0.07	82.55	74.78	44.52

Abbreviations and definitions.
Sample: sample identifier.
Library_Flowcell_Lane: library and sequencing run identifier used for raw-file naming (Library ID_Flowcell ID_Lane ID).
Raw reads: total number of reads in raw data; for paired-end sequencing, corresponds to read1 + read2.
Raw data: sequencing yield derived from read count and read length (reported in G).
Effective (%): (clean reads/raw reads) × 100%.
Error (%): base error rate.
Q20, Q30 (%): fraction of bases with Phred quality score > 20 or > 30.
GC (%): fraction of G and C bases among all bases.

3.5.2. Alignment, quantification, and gene-level summarization

Processed reads were aligned to the Bos taurus reference genome (Bos taurus UMD3.0; assembly accession GCA_002263795.3) using STAR [60]. Transcript and gene-level abundance estimates were generated using RSEM [59] with the corresponding Ensembl transcriptome/GTF annotation. Alignment and mapping-quality summaries were generated using SAMStat [61] and RNA-SeQC [62]. MultiQC [63] was used to aggregate QC and alignment summaries across all embryos and to generate consolidated reporting of read processing, alignment performance, and sample-level statistics for the complete dataset.

Gene-level expression matrices were constructed from RSEM outputs for downstream analyses. Reference build, annotation, and feature definitions were held constant across samples to ensure consistent gene-level summarization and comparability across embryos. To strengthen reproducibility and prevent reference drift, quantification outputs and reference metadata were imported into R using tximeta, which records reference provenance and metadata.

3.5.3. Normalization, exploratory assessment, and diagnostic evaluation

For differential expression inference, gene-level count data were retained as the primary input to preserve the mean–variance relationship required for count-based modeling. In parallel, normalized expression values were generated to support exploratory analyses and visualization. Between-sample compositional differences were addressed using trimmed mean of M values (TMM) normalization, and voom with quality weights was applied where appropriate for exploratory analyses and diagnostic plots assessing sample-level structure.

Exploratory assessment included evaluation of global sample relationships (e.g., PCA-based inspection), detection of potential outliers, and examination of latent structure consistent with technical variation prior to formal group comparisons. Where embryos exhibited atypical QC patterns, these were reviewed and documented, and their influence on downstream results was assessed during model checking and interpretation.

3.5.4. Differential expression analysis and definition of contrasts

Differentially expressed genes (DEGs) were identified to evaluate transcriptomic differences between embryo groups defined by donor age (2-year donors vs 5-7-year donors; Table 2) and by collection-time grouping reflecting cooler vs warmer on-farm conditions (Table 2). Differential expression testing was performed using DESeq2 [64]. Hypothesis testing was conducted using the Wald test, and p-values were adjusted to control the false discovery rate

(FDR) due to multiple testing. Genes were considered differentially expressed at an adjusted p-value (FDR) threshold of ≤ 0.05. For effect-size filtering, genes with an absolute log fold change of ≥ 1.0 were retained for downstream functional interpretation.

For reporting and prioritization, DEGs were ranked based on statistical significance (adjusted p-value/FDR) and effect size (absolute log fold change). External resources and pathway databases were used exclusively for functional interpretation after DEG identification rather than for defining the DEG set.

3.5.5. Control of batch effects, unwanted variation, and sample-structure considerations

To mitigate the influence of unwanted technical variation on group comparisons, batch effects were addressed using surrogate variable analysis (SVA) [65]. Surrogate variables estimated by SVA were incorporated into downstream modeling to account for latent technical factors and improve robustness of DEG inference.

Because multiple embryos were obtained from some donor cows, donor identity was retained in the metadata to support sensitivity assessment of conclusions with respect to within-donor clustering during downstream analysis and interpretation.

3.5.6. Gene annotation, functional enrichment, and pathway analysis

Following DEG identification, functional interpretation was performed to characterize biological processes and pathways associated with transcriptional differences between embryo groups. Functional annotation and enrichment analyses were performed using Panther (classification system v.14) and STRING v.11 (default settings). Network-based functional interpretation was conducted using Cytoscape (version 3.9.1) with the ClueGO plugin (version 2.5.9) [66], using Gene Ontology Biological Processes and KEGG pathway terms. Multiple testing correction was applied using Bonferroni step-down correction, and only terms with adjusted p-values < 0.05 were considered significant. Enrichment networks were generated separately for upregulated and downregulated gene sets to support interpretation of directional biological changes associated with donor age and collection-time grouping.

Principal component analysis (PCA), volcano plots, Gene Ontology enrichment summaries, and heatmaps were generated using SRplot [67].

3.5.7. Deconvolution

As introduced in Section 1.4, deconvolution was incorporated to estimate the relative contribution of transcriptomic programs associated with distinct preimplantation developmental stages from embryo-level low-input ("bulk") RNA-seq profiles. The objective of this analysis was to quantify, for each embryo, the degree of transcriptomic concordance with stage-resolved reference signatures, rather than to assert definitive biological staging or to infer cell-type composition.

Deconvolution was performed using MuSiC (Multi-subject Single Cell deconvolution), a regression-based framework that leverages a single-cell reference to estimate mixture proportions in bulk RNA-seq samples. MuSiC incorporates gene-weighting strategies that prioritize genes showing stable expression across reference subjects and across stage groups, thereby reducing sensitivity to highly variable genes and improving robustness of stage-associated proportion estimates [48].

Reference dataset and cross-dataset harmonization

Stage-resolved reference expression profiles were derived from the publicly available single-cell RNA-seq dataset generated by Yan et al. [68] and deposited in the NCBI Gene Expression Omnibus (GEO) under accession GSE36552 [69]. This dataset comprises single-cell transcriptomes spanning key preimplantation stages, including zygote, 2-cell, 4-cell, 8-cell, morula, and blastocyst.

To ensure identifier compatibility between bovine bulk embryo RNA-seq data and the reference dataset, bovine gene identifiers were harmonized to human gene symbols using Ensembl homology relationships (Ensembl version 111) [70]. Specifically, bovine embryos were quantified at the gene level using a fixed bovine reference build and annotation (Bos taurus UMD3.0; assembly accession GCA_002263795.3), and gene identifiers were translated to corresponding human ortholog symbols to match the identifier namespace of the reference matrix. Because orthology relationships are not one-to-one for all genes, only genes with an unambiguous orthology relationship suitable for identifier translation were retained. This step yielded a shared gene set used consistently across all embryos for deconvolution.

To strengthen reproducibility and minimize analytical drift, the reference dataset accession (GSE36552), the Ensembl release used for orthology mapping (version 111), and the bovine reference assembly accession (GCA_002263795.3) were fixed for the entire deconvolution workflow, and the same harmonization rules were applied uniformly across all samples.

Definition of developmental stage categories

Because embryonic transcriptomes exhibit rapid transitions and high inter-stage variability, reference stages were aggregated into broader developmental categories prior to deconvolution to stabilize estimation and improve interpretability. Four categories were defined: (i) oocyte/zygote/2-cell/4-cell, (ii) 8-cell, (iii) morula, and (iv) late blastocyst. Aggregation reduces sensitivity to fine-grained stage boundaries and supports more robust comparative assessment across embryos.

Deconvolution workflow, quality constraints, and outputs

Deconvolution was conducted using the following standardized steps:

1. Construction of a gene-level bulk embryo expression matrix following alignment/quantification and orthology-based identifier harmonization.
2. Generation of reference expression profiles representing the defined developmental categories from the single-cell reference dataset.
3. Estimation of relative stage-associated contributions for each embryo using MuSiC, producing a per-embryo vector of proportional weights across the four developmental categories.

To increase technical robustness while remaining conservative, the analysis incorporated the following neutral-ground constraints: (i) only genes shared between bulk and reference matrices after harmonization were retained; (ii) the same processing rules and reference resources were applied to all embryos; and (iii) inferred proportions were interpreted as continuous similarity-based estimates of stage-associated transcriptional programs, rather than as discrete stage calls. Stage-associated proportions were subsequently used as quantitative descriptors of developmental heterogeneity across embryos for downstream comparative analyses.

Sensitivity analysis using an alternative deconvolution implementation

As an additional robustness check, the DeTREM algorithm, an adaptation of MuSiC optimized for single-nuclei reference data [71], was applied as a sensitivity analysis. Concordance between MuSiC- and DeTREM-derived proportion estimates was used to evaluate the stability of inferred stage-associated contributions to alternative implementation choices.

Deconvolution outputs were used to support interpretation of between-embryo developmental variability and to evaluate associations with donor age grouping and collection-time grouping. Interpretation was framed cautiously given the cross-species orthology mapping and the fact that deconvolution estimates reflect transcriptomic similarity to reference developmental signatures rather than direct experimental staging.

4. Results

4.1. NGS-based bulk scRNASeq experiment on bovine embryos

4.1.1. Transcriptomic profiling of bovine embryos and quality control metrics

We sequenced 34 in vivo–derived Holstein–Friesian (Bos taurus) embryos spanning the donor-age classes. After pre-specified QC, 34 libraries met the inclusion thresholds and yielded 34 unique single-embryo transcriptomes for downstream analyses. The sequencing run produced 309.4 Gbp of raw data. Reads were aligned to the Bos taurus UMD3.0 reference genome (assembly accession GCA_002263795.3) using STAR, and transcript abundances were estimated with RSEM; gene-level summaries (Ensembl stable IDs) were derived via tximport (type = "rsem").

4.1.2. Quantification, normalization, and gene-level summarization

For gene-level analyses, we summarized transcripts with tximport using countsFromAbundance="lengthScaledTPM" (transcripts per million), yielding bias-adjusted counts suitable for count-based differential testing. Ensembl stable IDs were retained as primary gene identifiers (**Supplementary Table S2**). The Fragments Per Kilobase of transcript per Million (FPKM) /TPM values were not used as inputs for differential expression. Across the cohort, 27,607 gene transcripts (**Supplementary Table S2**) had nonzero estimates; expression filtering with filterByExpr defined 11,571 reliably expressed gene transcripts (**Supplementary Table S2**), which constituted the tested universe for all subsequent analyses.

4.2 Transcriptome analysis of bovine embryos based on the bulk scRNA-seq experiment (age comparison between young vs older cows)

A summary of differential expression results for the age contrast (younger vs older cows) is presented below. After expression filtering, 11,571 gene transcripts were retained and constituted the tested gene set (Supplementary Table S3). Based on nominal p-value distributions, 159 genes showed $P < 0.001$, 236 $P < 0.002$, 488 $P < 0.005$, and 647 $P < 0.01$.
At the pre-specified statistical threshold ($P \leq 0.05$), genes were classified as upregulated or downregulated in embryos derived from older versus younger donor cows. Among the tested genes, 6,023 exhibited positive log2 fold change values and 5,548 negative log2 fold change values in the age contrast. Full differential expression results are provided in Supplementary Table S4.

4.2.1. Identification of top 30 upregulated (Log2FoldChange ≥2 and P-value <0.05) putative DEGs transcripts in embryos of Polish HF cows at different ages.

By comparing embryos derived from 2-year-old cows with those obtained from cows aged 5–7 years, we identified the top 30 significantly upregulated differentially expressed genes (DEGs) using a threshold of log2 fold change ≥ 2 and P-value < 0.05 (Table 5). Functional annotations were retrieved from the GeneCards database: *Inducible T cell costimulator (ICOS), Signal transducer and activator of transcription 4 (STAT4), Matrix Gla Protein (MGP), Cancer/Testis Antigen Family 47 Member B1 (CT47B1), Family With Sequence Similarity 13 Member C (FAM13C), Cytochrome P450 Family 11 Subfamily A Member 1 (CYP11A1), Cytochrome P450 Family 4 Subfamily V Member 2 (CYP4V2), Hypoxanthine Phosphoribosyltransferase 1 (HPRT1), C-C Motif Chemokine Ligand 24 (CCL24), Phospholipase A2 Group VII (PLA2G7), SYT 4 (Synaptotagmin 4), Phosphodiesterase 10A (PDE10A), MAGE Family Member B2 (MAGE B2), INSC Spindle Orientation Adaptor Protein (INSC), Leucine rich repeats and calponin homology domain containing 2 (LRCH2), Zinc finger protein 514 (ZNF514), Molybdenum Cofactor Sulfurase (MOCOS), Homer Scaffold Protein 1 (HOMER1), RNA binding motif protein 46 (RBM46), Pyruvate Dehydrogenase Kinase 4 (PDK 4), Carbonic Anhydrase 2 (CA2), Transketolase Like 2 (TKTL2), Early growth response 2 (Egr 2), Zinc finger B-box domain (ZBBX), Chromosome 5 Open Reading Frame 75 (C5H12orf75)* and 5 novel genes.

Table 5. TOP 30 Age-dependent up-regulated genes from in vivo-derived embryo of Polish HF cattle

SN	gene_id	chr	start	end	*gene_name*	Transcript count	Gene biotype	log2 FoldChange	lfcSE	stat	pvalue	padj
1	ENSBTAG00000021596	2	92144625	92169974	*ICOS*	43	protein_coding	22,32418	2.9756376157693	7.50231923587495	6,27E-14	2.15891647184355e-11
2	ENSBTAG00000067628	1	88717610	88724186	*unannotated*	6	lncRNA	15,48947	2.00605001312123	7.72137536755967	1,15E-14	4.45795392308243e-12
3	ENSBTAG00000012370	5	95025092	95028634	*MGP*	14	protein_coding	15,27421	2.74328555418515	5.56785259024145	2,58E-08	2.82911661009928e-06
4	ENSBTAG00000046699	2	79568840	79673336	*STAT4*	207	protein_coding	14,66967	2.29488513994451	6.39233083856894	1,63E-10	3.26646451444399e-08
5	ENSBTAG00000049471	X	5568550	5572125	*CT47B1*	22	protein_coding	14,15418	2.97417349753441	4.75902945290029	1,95E-06	0.000110054142567161
6	ENSBTAG00000017540	28	14882652	15023646	*FAM13C*	243	protein_coding	13,89982	1.49393359933493	9.30417468506588	1,35E-20	1.59305707206147e-17
7	ENSBTAG00000006934	21	34328574	34342887	*CYP11A1*	24	protein_coding	13,34327	1.53030836207851	8.71933475289151	2,80E-18	2.31260664685246e-15
8	ENSBTAG00000063990	18	58779423	58816639	*unannotated*	28	protein_coding	12,65134	1.53152275314548	8.26062809990038	1,45E-16	7.18511404193299e-14
9	ENSBTAG00000021263	27	16250292	16266690	*CYP4V2*	28	protein_coding	12,46279	2.01823945227624	6.17508001385981	6,61E-10	1.15457341313381e-07
10	ENSBTAG00000013919	23	25723424	25735337	*unannotated*	18	protein_coding	12,45776	1.45026657645747	8.58997837152228	8,70E-18	6.73921696832331e-15
11	ENSBTAG00000046220	3	102735258	102744921	*HPRT1*	42	protein_coding	12,42859	2.28766976387434	5.43286053215259	5,55E-08	5.72878583866608e-06
12	ENSBTAG00000026275	25	34065905	34069221	*CCL24*	12	protein_coding	12,20665	1.57465116597133	7.75197356239992	9,05E-15	3.61784179019474e-12
13	ENSBTAG00000019315	23	19925027	19963093	*PLA2G7*	77	protein_coding	11,80839	1.03804687055116	11.3755877382602	5,53E-30	1.71464173051051e-26
14	ENSBTAG00000001801	24	12650269	12660064	*SYT4*	25	protein_coding	11,77102	1.07632615772192	10.936298895899	7,73E-28	1.91620146698812e-24
15	ENSBTAG00000007758	9	100468650	101036385	*PDE10A*	300	protein_coding	11,66367	1.83724051381174	6.3484738913745	2,17E-10	4.08431921912242e-08
16	ENSBTAG00000034437	11	27016	32430	*MAGEB2*	10	protein_coding	11,65986	1.36262870150463	8.55688914148287	1,16E-17	8.11782767076541e-15
17	ENSBTAG00000050382	X	63643323	63745866	*LRCH2*	191	protein_coding	11,52566	1.90720669443806	6.04321652091517	1,51E-09	2.43205811506969e-07
18	ENSBTAG00000032782	15	37342362	37482577	*INSC*	91	protein_coding	11,42762	1.79249975656507	6.37524406124847	1,83E-10	3.53812465745124e-08
19	ENSBTAG00000001947	11	1961360	1975352	*ZNF514*	90	protein_coding	11,40660	1.78254606751906	6.39904662473958	1,56E-10	3.17723905609519e-08
20	ENSBTAG00000001696	17	2540688	2599539	*RBM46*	45	protein_coding	11,37839	1.50779170513343	7.54639235038696	4,47E-14	1.63146171386385e-11
21	ENSBTAG00000012252	24	20886994	20946894	*MOCOS*	180	protein_coding	11,35065	1.08083588441088	10.5017331312408	8,48E-26	1.75214412952358e-22
22	ENSBTAG00000025853	10	10413731	10546778	*HOMER1*	117	protein_coding	11,32502	2.05843036634337	5.50177626516433	3,76E-08	3.98350110734908e-06
23	ENSBTAG00000014069	4	12881889	12895362	*PDK4*	28	protein_coding	11,23360	1.50422473504241	7.46803037727581	8,14E-14	2.65548594398558e-11
24	ENSBTAG00000017733	14	76994568	77012262	*CA2*	54	protein_coding	11,09927	1.7707841081593	6.26799878359601	3,66E-10	6.57019690559947e-08
25	ENSBTAG00000061340	29	32327586	32329448	*unannotated*	3	lncRNA	10,97394	1.30382032178232	8.41675693963897	3,87E-17	2.18084832234046e-14
26	ENSBTAG00000008947	6	2142353	2171074	*TKTL2*	12	protein_coding	10,90345	1.05126956735703	10.3716977886544	3,34E-25	5.90661008414409e-22
27	ENSBTAG00000046409	28	18935996	18942471	*EGR2*	23	protein_coding	10,80607	2.20070827184023	4.9102672800616	9,10E-07	5.93392200754714e-05

28	ENSBTAG00000061471	1	63748226	63749234	*unannotated*	3	lncRNA	10,79430	1.31230160795381	8.22547321804577	1,94E-16	9.26942887326641e-14
29	ENSBTAG00000035710	1	100083002	100206264	*ZBBX*	109	protein_coding	10,76947	1.90336734624258	5.65811170913525	1,53E-08	1.82420860817747e-06
30	ENSBTAG00000058538	5	68823269	68887033	*C5H12orf75*	100	protein_coding	10,73683	1.89427281130398	5.6680499157931	1,44E-08	1.75527230562011e-06

4.2.2 Identification of downregulated (Log2FoldChange ≤ -2 and p-value <0.05) putative DEGs transcripts in embryos of Polish HF cows at different ages.

The top 30 downregulated genes (Log2FoldChange ≤ -2, $p < 0.05$) were identified based on differential expression analysis and subsequently annotated using the GeneCards database: *Neuropeptide S Receptor 1 (NPSR1), Synaptotagmin (SYT9), ADP Ribosylation Factor Like GTPase 13A (Arl13a), Prominin 1 (PROM1), RNA binding motif single-stranded interacting protein 3 (RBMS3), Fibronectin type III and SPRY domain containing 1 like (FSD1L), ATPase copper transporting alpha (ATP7A), Inosine monophosphate dehydrogenase 1 (IMPDH1), Serpin family B member 4 (SERPINB4), Calcyphosine-like (CAPSL), Fanconi anaemia, complementation group A (FANCA), CAMP Responsive Element Binding Protein 5 (CREB5), LY6/PLAUR Domain Containing 6B (LYPD6B), SANT and BTB domain regulator of CSR (SANBR), Lysozyme (LYZ), Ubiquinol-cytochrome c reductase core protein 2 (UQCRC2), FEM-1-Like Death Receptor Binding Protein (FEM1B), Junction-Mediating And -Regulatory Protein (JMY), V-Akt Murine Thymoma Viral Oncogene Homolog 2 (AKT2).*

Table 6. TOP 30 Age-dependent down-regulated genes from in vivo-derived embryo of Polish HF cattle

SN	gene_id	chr	start	end	gene_name	Transcript count	gene_biotype	log2 FoldChange	lfcSE	stat	pvalue	padj
1	ENSBTAG00000013768	4	62120709	62274639	*NPSR1*	75	protein_coding	-11,30654	2.11370263731923	-5.34916365974351	8,84E-08	8.17410837289958e-06
2	ENSBTAG00000032079	15	45274682	45653531	*SYT9*	199	protein_coding	-10,21480	1.19401611973663	-8.55499146026698	1,18E-17	8.11782767076541e-15
3	ENSBTAG00000020390	X	51168144	51188536	*ARL13A*	26	protein_coding	-10,04031	2.48828810266337	-4.03502750999843	5,46E-05	0.00160496965590101
4	ENSBTAG00000013736	6	111165303	111279631	*PROM1*	56	protein_coding	-9,84888	1.31673590228959	-7.47976859345171	7,45E-14	2.49439665160128e-11
5	ENSBTAG00000044062	22	2984947	4652965	*RBMS3*	172	protein_coding	-8,14288	1.08043079329819	-7.53669455206556	4,82E-14	1.70722531347654e-11
6	ENSBTAG00000013420	8	95277011	95346595	*FSD1L*	151	protein_coding	-7,87927	1.47970171684616	-5.32490685126113	1,01E-07	9.07286467532218e-06
7	ENSBTAG00000010018	X	74364046	74490947	*ATP7A*	311	protein_coding	-7,05522	1.49139704149725	-4.73060821457992	2,24E-06	0.000123325414423904
8	ENSBTAG00000066381	3	43242908	43243997	*unannotated*	3	lncRNA	-6,95694	1.19281505539366	-5.83237295248364	5,46E-09	7.83291008601929e-07
9	ENSBTAG00000069414	13	11068109	11092862	*unannotated*	42	protein_coding	-6,81254	1.90914426581128	-3.56837121732121	0,000359207	0.00627830861930322
10	ENSBTAG00000000296	4	92569436	92586784	*IMPDH1*	69	protein_coding	-6,50868	2.34677187532689	-2.77346011445442	0,005546364	0.0430405734182132
11	ENSBTAG00000065630	24	61843746	61850653	*SERPINB4*	20	protein_coding	-6,45172	1.72096429156099	-3.74890026835894	0,000177612	0.00380912550908743
12	ENSBTAG00000012688	20	38234955	38266312	*CAPSL*	28	protein_coding	-5,84724	1.65966085617926	-3.52315626445098	0,00042644	0.00713380352531963
13	ENSBTAG00000060764	6	85497254	85506606	*unannotated*	13	protein_coding	-5,78744	1.81587330763286	-3.18713852824852	0,001436879	0.00000000000000000
14	ENSBTAG00000062664	18	59722555	59723532	*unannotated*	4	protein_coding	-5,65289	1.95846067262504	-2.88639413624749	0,003896838	0.0338508802905567
15	ENSBTAG00000055617	29	43671267	43673690	*unannotated*	3	lncRNA	-5,55031	0.836904696479577	-6.63194692093646	3,31E-11	7.60489370502629e-09
16	ENSBTAG00000046383	18	62448171	62454926	*unannotated*	24	protein_coding	-5,42052	0.956654326597844	-5.66611932134642	1,46E-08	1.75791919661232e-06
17	ENSBTAG00000001906	18	14606881	14645127	*FANCA*	183	protein_coding	-5,38009	1.33447638673087	-4.0316133877797	5,54E-05	0.00161952744360751
18	ENSBTAG00000059862	18	62472348	62481588	*unannotated*	18	protein_coding	-5,37303	1.06721777187224	-5.03461313723163	4,79E-07	3.47555320666025e-05
19	ENSBTAG00000018909	4	67314290	67749124	*CREB5*	73	protein_coding	-5,17486	1.47517169683645	-3.50797461093611	0,000451532	0.00741349987909386
20	ENSBTAG00000055919	6	65401598	65469087	*unannotated*	25	protein_coding	-5,07557	1.40876438951579	-3.602850215304	0,000314747	0.00568054395106648
21	ENSBTAG00000019683	2	46965865	47080837	*LYPD6B*	17	protein_coding	-4,86329	1.55902061204533	-3.11945462273411	0,001811862	0.0197016115528811
22	ENSBTAG00000054531	11	43812633	43874209	*SANBR*	195	protein_coding	-4,84097	1.50453182151239	-3.21759312027021	0,001292711	0.0153785414206031
23	ENSBTAG00000057161	29	47387547	47400668	*unannotated*	25	lncRNA	-4,72687	1.62049501054183	-2.91693024433292	0,003534948	0.00000000000000000
24	ENSBTAG00000020564	5	44246008	44303575	*LYZ*	29	protein_coding	-4,70441	0.820213259965352	-5.73558838091281	9,72E-09	1.28146158638729e-06
25	ENSBTAG00000034662	9	18251167	18252696	*UQCRC2*	8	protein_coding	-4,62877	0.485007905847031	-9.54370541429289	1,38E-21	1.89821437499436e-18
26	ENSBTAG00000055520	3	13811803	13843135	*unannotated*	10	protein_coding	-4,58711	0.954463790168987	-4.80595513305412	1,54E-06	9.13475109686139e-05
27	ENSBTAG00000008378	10	15106163	15118280	*FEM1B*	10	protein_coding	-4,58365	1.23737350497795	-3.70433903103615	0,000211943	0.00428721895985614

28	ENSBTAG00000025856	10	10306075	10375814	*JMY*	28	protein_coding	-4,57091	1.22385669839099	-3.73484410186941	0,000187832	0.00394873593515385
29	ENSBTAG00000045854	18	62459660	62476390	*unannotated*	103	protein_coding	-4,46757	0.96340756813299	-4.63726347282253	3,53E-06	0.000175760473638966
30	ENSBTAG00000001400	18	49628437	49674930	*AKT2*	154	protein_coding	-4,45704	1.20986550085492	-3.68390997891648	0,000229683	0.00454824722555834

4.2.3. Visualization of gene expression of identified upregulated and downregulated putatively significant DE gene transcripts according to age

The expression distributions were consistent across the embryos: the kernel density curves of log-scaled normalized expression (Figure 3) overlapped closely, indicating effective normalization and the absence of multimodal artifacts. Principal component analysis (PCA) of variance-stabilized counts (Figure 4) resolved two partially overlapping clusters; separation along PC1 was consistent with the recorded age classes once the developmental stage was accounted for and was not explained by run-level metrics. The bar plot (Figure 5) revealed that PC1, PC2, and PC3 explained 29.7%, 13.7%, and 8.9% of the variance, respectively, which was consistent with a structured biological signal rather than technical noise.

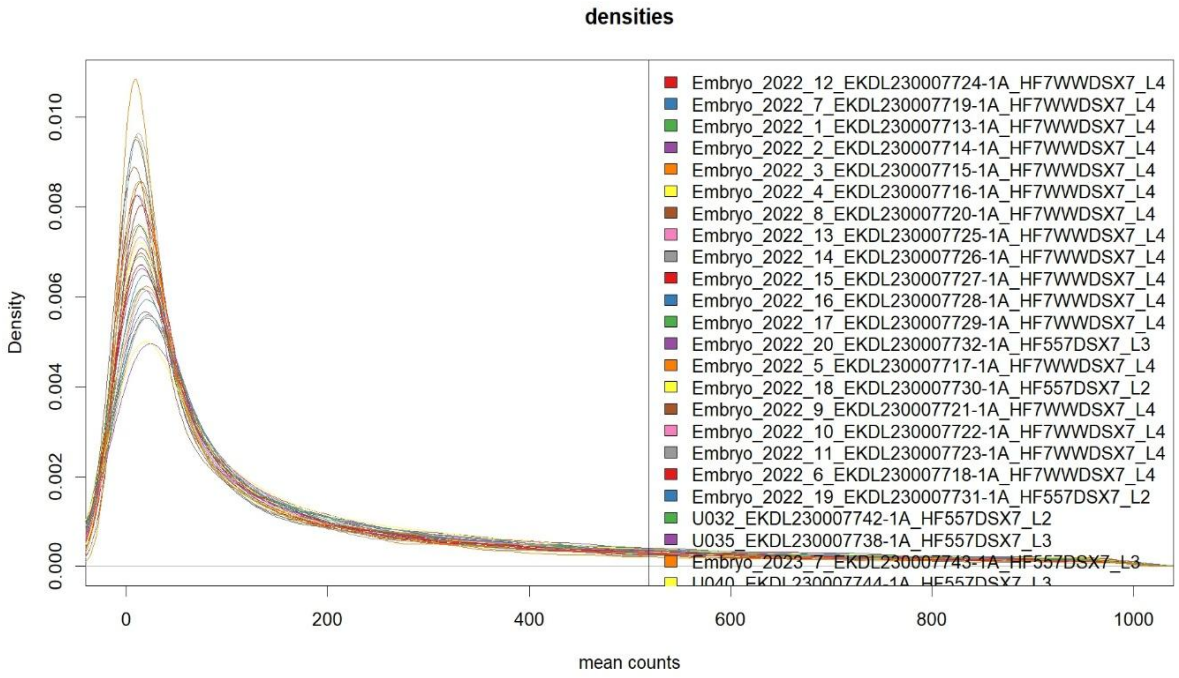

Figure 3. Density plot displaying the distribution of raw gene expression counts across individual bovine embryo RNA-seq samples. The X-axis indicates mean gene expression counts, while the Y-axis represents density. Each coloured curve corresponds to a unique embryo sample (legend). The high degree of overlap among curves reflects consistent expression distributions across samples, supporting uniform sequencing depth and sample quality prior to normalization.

Figure 4. Principal component analysis (PCA) plot showing sample classification of embryo samples based on their gene expression profiles. Each point represents an individual sample plotted according to its scores on principal components PC1 (x-axis) and PC2 (y-axis), reflecting the highest variability within the dataset. Samples are classified by developmental stage (blastocyst, cleavage, or embryo) indicated by different shapes (circle, triangle, and square, respectively) and grouped into two distinct clusters (Group 1 in red and Group 2 in blue). Clear separation between these two groups on PC1 suggests pronounced differences in gene expression profiles related to distinct biological conditions or developmental characteristics.

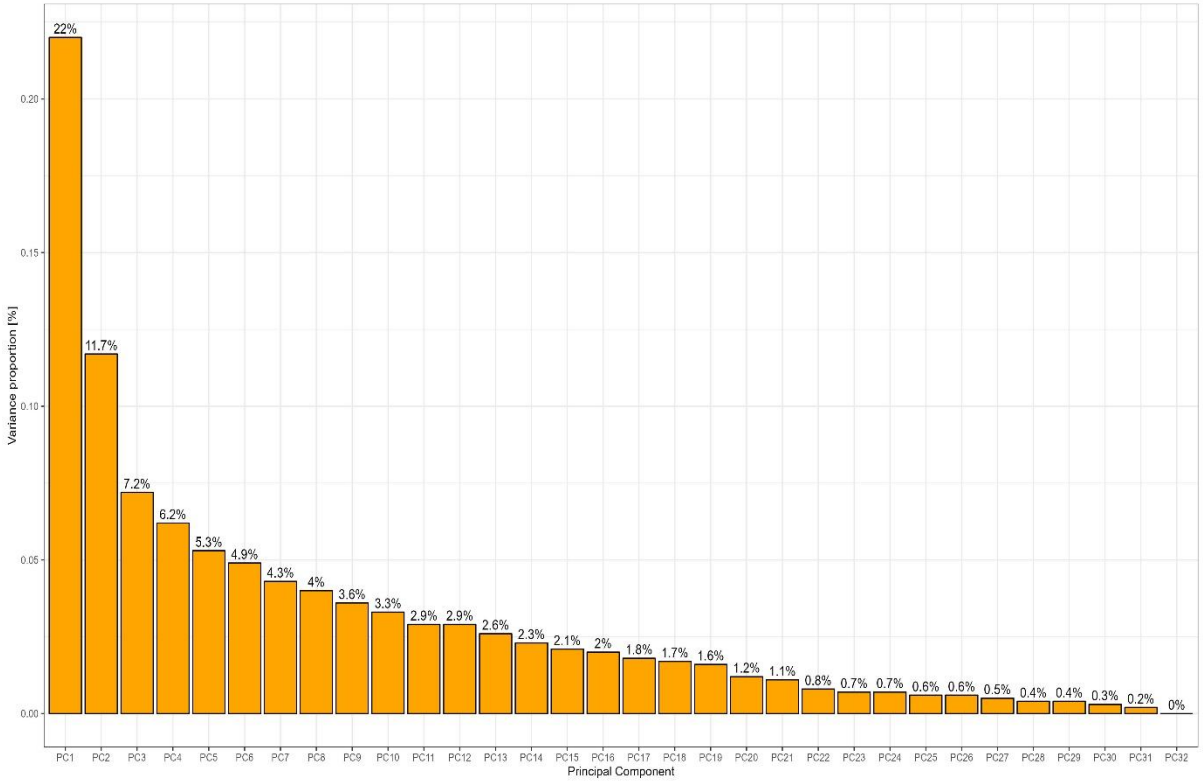

Figure 5. Bar plot showing the proportion of variance explained by each principal component (PC) in the PCA analysis. PC1 explains the largest proportion (29.7%) of total variance, followed by PC2 (13.7%) and PC3 (8.9%), indicating that these first few components capture most of the variability present in the gene expression data. This plot emphasizes the significance of the first principal components in differentiating embryo samples based on their gene expression profiles.

Differential expression was evaluated on the filtered gene set via the covariate structure specified in the Methods section. The p-value histogram (Figure 6) shows the expected near-uniform bulk with enrichment near zero under the true signal after adjustment. The Q-Q plot (Figure 7) displayed tail departures compatible with genuine alternatives rather than systematic curvature. The per-gene effect sizes and significance are summarized in the volcano plot (Figure 8), which delineates the dominant up- and downregulated components of the age contrast.

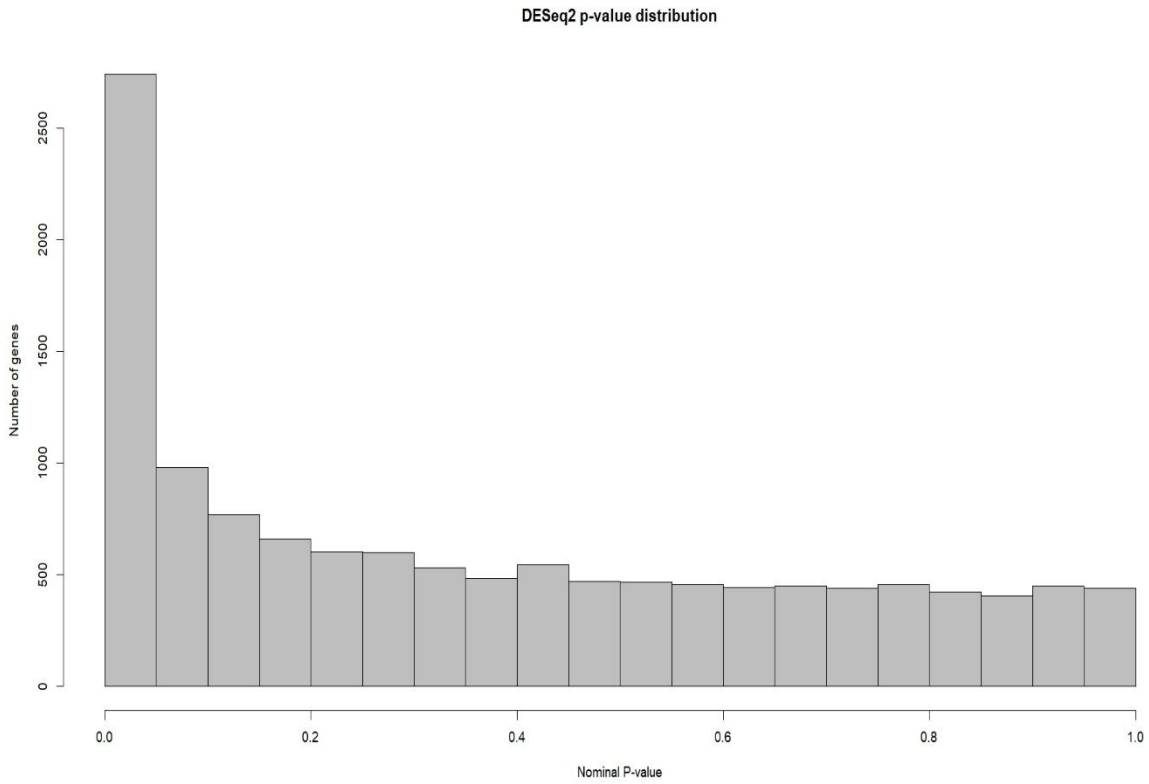

Figure 6. Histogram showing the distribution of nominal p-values obtained from differential gene expression analysis using DESeq2. The X-axis represents nominal p-value ranges, and the Y-axis indicates the number of genes falling within each range. The noticeable peak near zero indicates a substantial proportion of genes with statistically significant differential expression between the analysed conditions. This p-value distribution highlights the robustness and sensitivity of the differential expression analysis performed in this study.

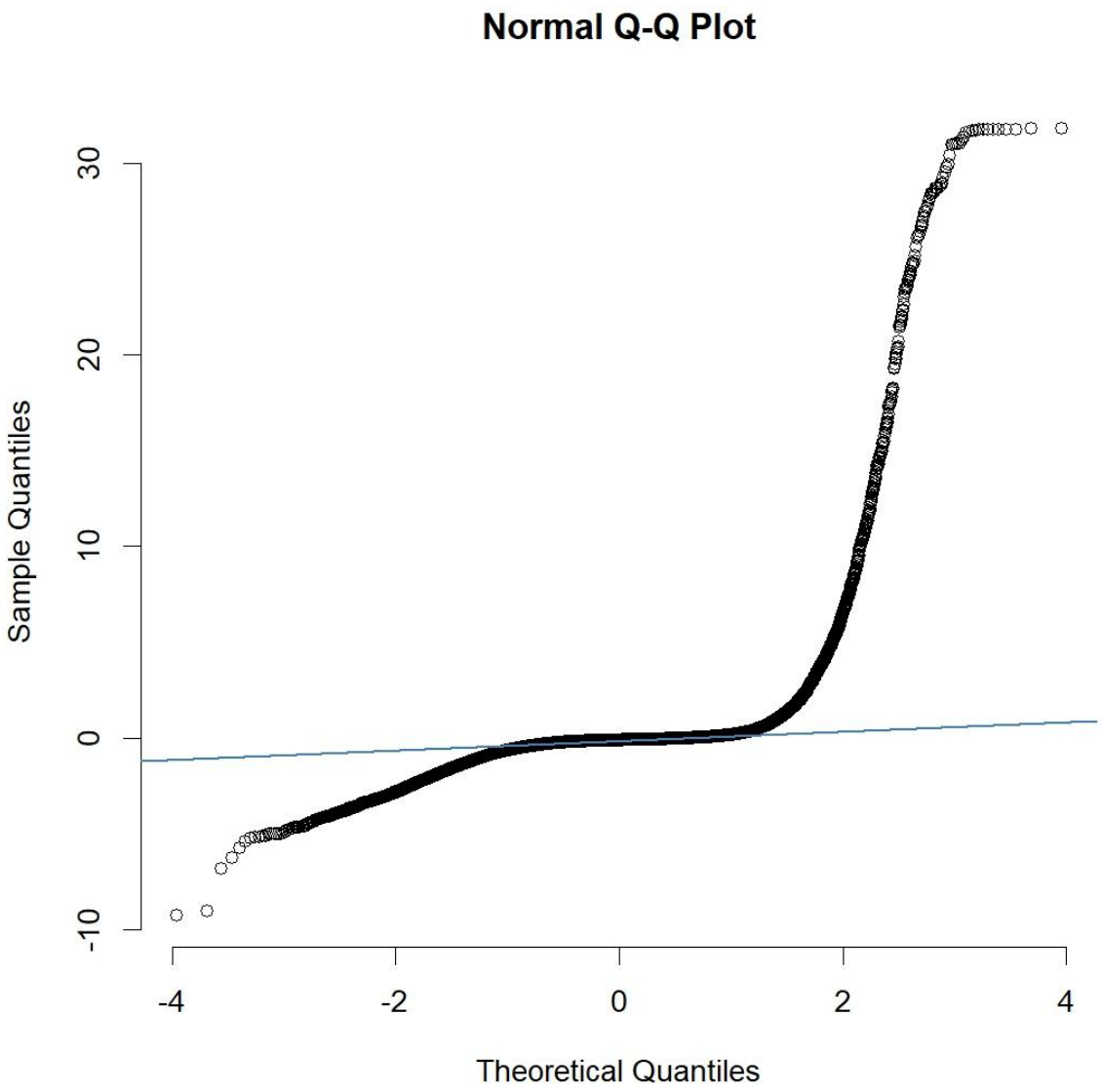

Figure 7. Normal Q-Q plot representing the distribution of the gene expression data residuals against a theoretical normal distribution. The X-axis shows theoretical quantiles, while the Y-axis shows observed sample quantiles. Points deviating significantly from the diagonal line indicate departures from normality, suggesting the potential presence of outliers or non-normal distribution in the data. Notable deviations observed at both tails of the plot indicate that some genes significantly differ from a normal distribution, a common scenario in high-throughput gene expression datasets.

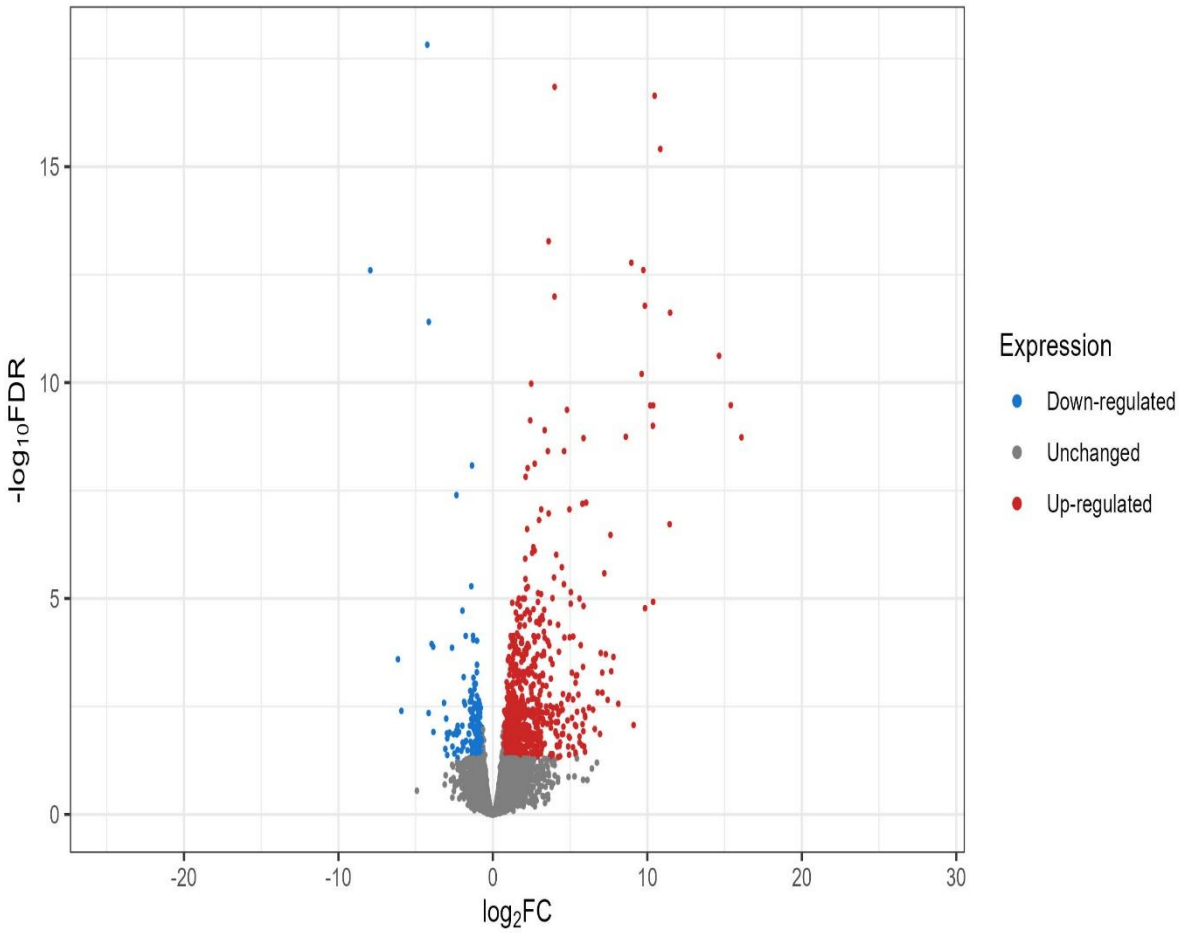

Figure 8. Volcano plots illustrating the differential gene expression between the compared embryo conditions. The x-axis represents the magnitude of change in gene expression (log2 Fold Change), while the y-axis shows the statistical significance (-log10 False Discovery Rate, FDR). Each dot represents a gene: Red dots indicate significantly upregulated genes, blue dots indicate significantly downregulated genes, and grey dots indicate genes without significant expression changes. Genes located in the upper corners of each plot represent those with the highest fold change and greatest statistical significance, highlighting key differentially expressed genes that may have biological importance.

Among the 11571 gene transcripts tested (Supplementary Table S4), 6023 were upregulated (Supplementary Table S5), and 5548 (Supplementary Table S6) were downregulated in embryos from older donors at pre-specified thresholds. The genome-wide relationship between effect size and abundance is shown in the MA plot (Figure 9), which displays a log2-fold change against the mean expression for the fully tested set.

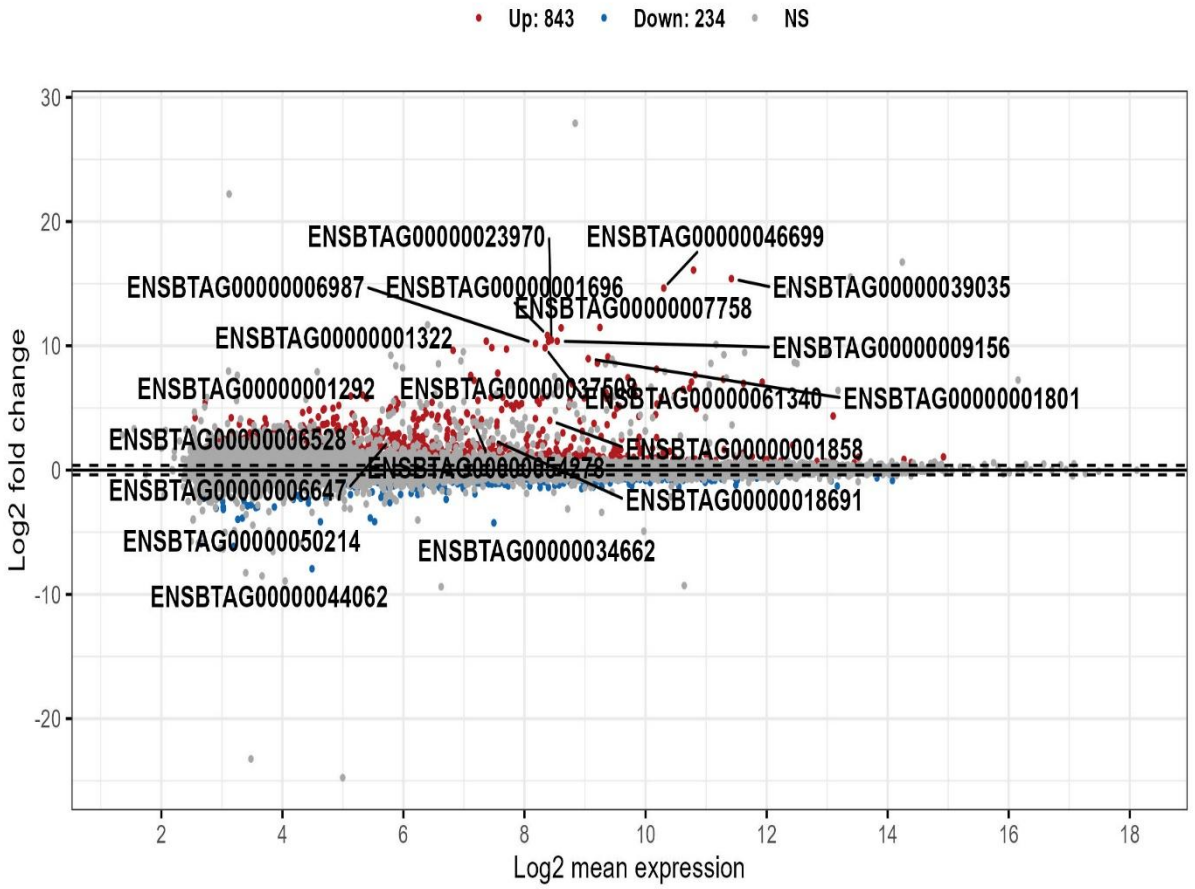

Figure 9. MA plot showing differential gene expression between embryos derived from younger (≤3 years) and older (6–7 years) Holstein–Friesian cows. Each dot represents a gene, plotted by its $\log_2$ mean expression (x-axis) and $\log_2$ fold change (y-axis). Red and blue dots indicate significantly up- and downregulated transcripts, respectively (FDR-adjusted $p < 0.05$), while grey dots represent non-significant genes. The top 20 differentially expressed genes are annotated by Ensembl IDs based on effect size. Dashed lines denote the fold change thresholds used to determine biological significance.

4.2.4. Transcriptomic signatures of upregulated genes in embryos

Upregulated transcripts in embryos derived from older donors could be grouped into functional categories related to immune/cytokine signalling, metabolism, and early cell division processes rather than representing isolated single-gene changes. Immune-associated genes included ICOS and STAT4, and increased expression of the chemokine CCL24 was also observed. Metabolic regulators included CYP11A1 and CYP4V2 (steroidogenesis and lipid metabolism), alongside PDK4, PLA2G7, CA2, and TKTL2, consistent with altered metabolic pathway activity. Genes linked to cell polarity and division, such as MGP, INSC, and RBM46, were also upregulated, whereas HOMER1 and PDE10A are involved in calcium and cyclic-nucleotide signalling pathways. Additional upregulated transcripts included ZNF514, LRCH2, EGR2, HPRT1, MOCOS, and MAGEB2. The top 25 upregulated genes ranked by log2 fold change are shown in Figures 8–9; full per-gene results (effect size, standard error, adjusted P

value) are presented in Supplementary Table S4. For context, Table 7 summarizes representative upregulated genes with reported roles in embryogenesis and reproduction, and Table 8 lists statistically significant candidates whose functions in bovine preimplantation embryos remain unconfirmed (e.g., CT47B1, PDE10A, ICOS). Several consistently increased but uncharacterized loci (e.g., C5H12orf75, ZBBX) are noted as potential regulatory candidates for future investigation.

Table 7. Age-dependent up-regulated genes in bovine embryos with established roles in embryogenesis and reproductive pathways.

Gene	Functional Annotation
STAT4	Regulates immune responses and cellular differentiation during early embryogenesis.
MGP	Modulates calcium and phosphorus homeostasis and supports epithelial-mesenchymal transition during embryonic development.
CYP11A1	Catalyses the conversion of cholesterol to pregnenolone, initiating steroidogenesis critical for pregnancy maintenance.
CYP4V2	Involved in lipid metabolism and antioxidant defense, potentially protecting embryos from oxidative stress.
HPRT1	Facilitates purine recycling to support rapid cell proliferation during early embryonic stages.
CCL24	Mediates cell migration within the inner cell mass, contributing to embryo patterning and implantation.
PDE10A	Regulates intracellular cAMP levels, influencing cell proliferation and early embryonic developmental potential.
RBM46	Controls post-transcriptional regulation of genes essential for germ cell development and meiosis.
PDK4	Modulates glucose and fatty acid metabolism to maintain embryonic energy homeostasis.
EGR2	Regulates implantation, folliculogenesis, and early neural development.
ZBBX	Putatively involved in embryo–endometrium interactions and early reproductive development.
LRCH2	Supports immune system development and motor neuron formation during embryogenesis.

This table lists genes that were significantly up regulated in embryos obtained from cows of different ages and whose documented functions are directly linked to embryogenesis or reproductive processes. The annotations highlight key pathways-including steroidogenesis (e.g., CYP11A1), immune and cellular differentiation signalling (STAT4, LRCH2), metabolic support for rapid cell proliferation (HPRT1, PDK4), and cell migration crucial for implantation (CCL24). Collectively, the elevated expression of these transcripts may underpin age-related variations in embryo competence, developmental trajectory, and implantation potential observed in the study.

Table 8. Age-dependent up-regulated genes in bovine embryos with no currently validated roles in embryogenesis or reproduction

Gene	***Functional Annotation***
ICOS	Activates T-cell signalling pathways; embryonic function remains unconfirmed.
CT47B1	Cancer/testis antigen with expression restricted to testes; no evidence for embryonic roles.
FAM13C	Implicated in oncogenesis; embryonic relevance unestablished.
PLA2G7	Participates in lipid metabolism and cardiovascular pathophysiology; embryonic functions unknown.
SYT4	Modulates synaptic vesicle exocytosis; potential but unconfirmed role in early neuronal development.
MAGEB2	Regulates rRNA transcription in cancer; lacks documented embryonic expression.

INSC	Governs mitotic spindle orientation; potentially influences early cell division processes.
ZNF514	Transcription factor involved in cellular differentiation; may contribute to embryonic transcriptional regulation.
MOCOS	Activates molybdenum-dependent enzymes; supports purine metabolism and oxidative stress defense.
HOMER1	Links calcium signalling to synaptic plasticity; influenced by hormonal and stress responses during development.
CA2	Maintains acid–base equilibrium and cellular pH homeostasis under dynamic metabolic conditions.
TKTL2	Functions in the pentose phosphate pathway, facilitating nucleotide biosynthesis and antioxidative responses.
C5H12orf75	No functional characterization available; embryonic role undetermined.

This table compiles genes that were significantly up regulated in embryos derived from cows of different ages but for which the literature does not yet provide clear evidence of direct involvement in embryogenesis or reproductive processes. Although many encode proteins with well-characterised functions-such as immune-cell activation (ICOS), lipid and pH homeostasis (PLA2G7, CA2), neuronal signalling (SYT4, HOMER1) and nucleotide metabolism (MOCOS, TKTL2)-their contribution to early bovine development remains speculative. Several genes (e.g., CT47B1, MAGEB2) are chiefly known as cancer/testis antigens, while others (C5H12orf75) are largely uncharacterized. Their differential expression may reflect age-related systemic influences on the embryo rather than direct developmental roles, underscoring the need for functional validation to determine whether any of these transcripts modulate embryo quality, stress resilience, or later physiological traits.

4.2.5. Transcriptomic signatures of downregulated genes in embryos

The downregulated set of 5548 tested gene transcripts (FDR-adjusted) comprised loci annotated to ciliogenesis/polarity, genome surveillance, nucleotide metabolism, vesicle trafficking, metal–ion homeostasis, mitochondrial respiration, and signal transduction. Examples include *NPSR1 and SYT9* (neuronal excitability/synaptic vesicle exocytosis), *PROM1 and ARL13A* (epithelial polarity/primary cilium), FANCA and RBMS3 (DNA damage handling/posttranscriptional control), *FSD1L and ATP7A* (matrix organization/copper transport), IMPDH1 (guanine nucleotide biosynthesis), and UQCRC2 (respiratory complex III). Additional reductions were observed for signalling and stress-response transcripts (AKT2, *FEM1B, SERPINB4, CAPSL, CREB5*). The top 25 downregulated genes ranked by log2 fold change are shown in Figure 8-9; full per-gene results (effect size, standard error, adjusted *P*) are presented in Supplementary Table S5. The principal downregulated genes with established developmental or reproductive relevance are summarized in Table 9; statistically significant transcripts without validated preimplantation roles in cattle are listed in Table 10.

Table 9. Age-dependent down-regulated genes in bovine embryos with established roles in embryogenesis and reproduction

Gene	Functional Annotation
NPSR1	Regulates foetal blood circulation and placental inflammatory responses; associated with foetal demise.

SYT9	Mediates exocytosis; mutation results in embryonic lethality in murine models.
ARL13A	Critical for primary cilia formation and signal transduction during embryogenesis.
PROM1	Stem cell surface marker involved in cell proliferation and uterine epithelial integrity during implantation.
FSD1L	Regulates proteolytic enzymes; impacts angiogenesis and invasive cell behaviour in early development.
ATP7A	Copper transporter; deficiency leads to severe developmental defects and embryonic lethality.
AKT2	Controls cell survival, proliferation, and metabolism; essential for blastomere division and embryo maturation.
JMY	Organizes the actin cytoskeleton; required for oocyte maturation and asymmetric cleavage during early development.
FEM1B	Influences cell differentiation and growth; it contributes to oogenesis and early embryonic development.
UQCRC2	Component of mitochondrial respiratory complex III; critical for ATP generation in embryonic cells.
IMPDH1	Catalyses purine nucleotide biosynthesis; supports energy metabolism during foetal development.
FANCA	Facilitates DNA repair and hematopoietic progenitor cell development; preserves genomic stability in embryos.
CREB5	Regulates FGF18 expression; crucial for pharyngeal muscle formation and embryonic tissue morphogenesis.
SANBR	Modulates transcription and chromatin remodelling during early embryonic tissue differentiation.

This table lists genes whose transcript levels decreased significantly in embryos collected from cows of different ages and whose documented functions are tightly linked to core developmental or reproductive pathways. The downregulation affects diverse processes, including cilia-mediated signalling (ARL13A), copper and purine metabolism essential for energy production (ATP7A, IMPDH1, UQCRC2), cytoskeletal dynamics during oocyte maturation and cleavage (JMY, AKT2), and placental or uterine interactions critical for implantation (PROM1, NPSR1). Reduced expression of key genome-maintenance and DNA-repair factors (FANCA) further suggests compromised genomic stability. Collectively, these changes may help explain age-related declines in embryo viability, altered metabolic competence, and reduced implantation success observed in the study.

Table 10. Age-dependent down-regulated genes in bovine embryos lacking documented roles in embryogenesis or reproduction

Gene	**Functional Annotation**
SERPINB4	Involved in protease inhibition and inflammatory responses; no established role in embryogenesis.
CAPSL	Associated with adipogenesis and retinal angiogenesis; embryonic function remains uncertain.
LYPD6B	Modulates acetylcholine receptor activity; primarily studied in neurobiology and oncology.
LYZ	Encodes lysozyme, an immune defense enzyme; no direct evidence for involvement in embryonic development.

This table summarises transcripts whose abundance fell significantly in embryos derived from cows of different ages, yet whose known functions do not presently include embryogenesis or reproductive regulation. The genes encode proteins mainly associated with innate immunity (SERPINB4, LYZ), neuromodulation (LYPD6B), and metabolic or angiogenic processes (CAPSL). Although their direct contribution to early bovine development is unverified, age-related repression of these genes might still influence the embryonic micro-environment—for example, by altering inflammatory tone or nutrient signalling-thereby indirectly affecting embryo quality. Functional studies will be needed to determine whether their down-regulation is merely correlative or plays a contributory role in age-linked developmental differences.

4.2.6. Biological gene networks and pathways analysis of RNA-seq upregulated and downregulated genes related to different cows' ages using Cytoscape ClueGo

4.2.6.1. Identification of RNA-seq upregulated target genes associated with GO Biological Processes and KEGG pathways related to cow's age (Gene ontology and pathway enrichment analysis)

ClueGO GO/KEGG enrichment for the older-donor contrast (Bonferroni step-down, adjusted $p < 0.05$; kappa ≥ 0.3) was performed using the 11571 tested gene transcripts as the background universe and term redundancy controlled by kappa grouping. ClueGO analysis identified 124 GO/pathway-specific terms associated with upregulated genes related to cow's age (Figure 10). Most enriched terms include 17: *rhombomere morphogenesis, rhombomere formation, rhombomere 3 morphogenesis, rhombomere 5 morphogenesis, rhombomere 3 formation, rhombomere 5 formation, regulation of retrograde trans-synaptic signaling by neuropeptide, negative regulation of retrograde trans-synaptic signaling by neuropeptide, retrograde trans-synaptic signaling by neuropeptide, negative regulation of short-term neuronal synaptic plasticity, positive regulation of oligopeptide transport, positive regulation of dipeptide transport, dipeptide transport, regulation of dipeptide transport, regulation of dipeptide transmembrane transport, positive regulation of dipeptide transmembrane transport, dipeptide transmembrane transport.* The identified 124 significant upregulated terms were concentrated in peptide/lipid transport, oxidative metabolism, morphogenesis, and neurodevelopment; the highest-frequency categories were "dipeptide transmembrane transport" (18.18%), "negative regulation of short-term neuronal synaptic plasticity" (18.18%), "fatty-acid ω-oxidation" (16.67%) and "hombomere morphogenesis" (14.39%) (Figure 10).

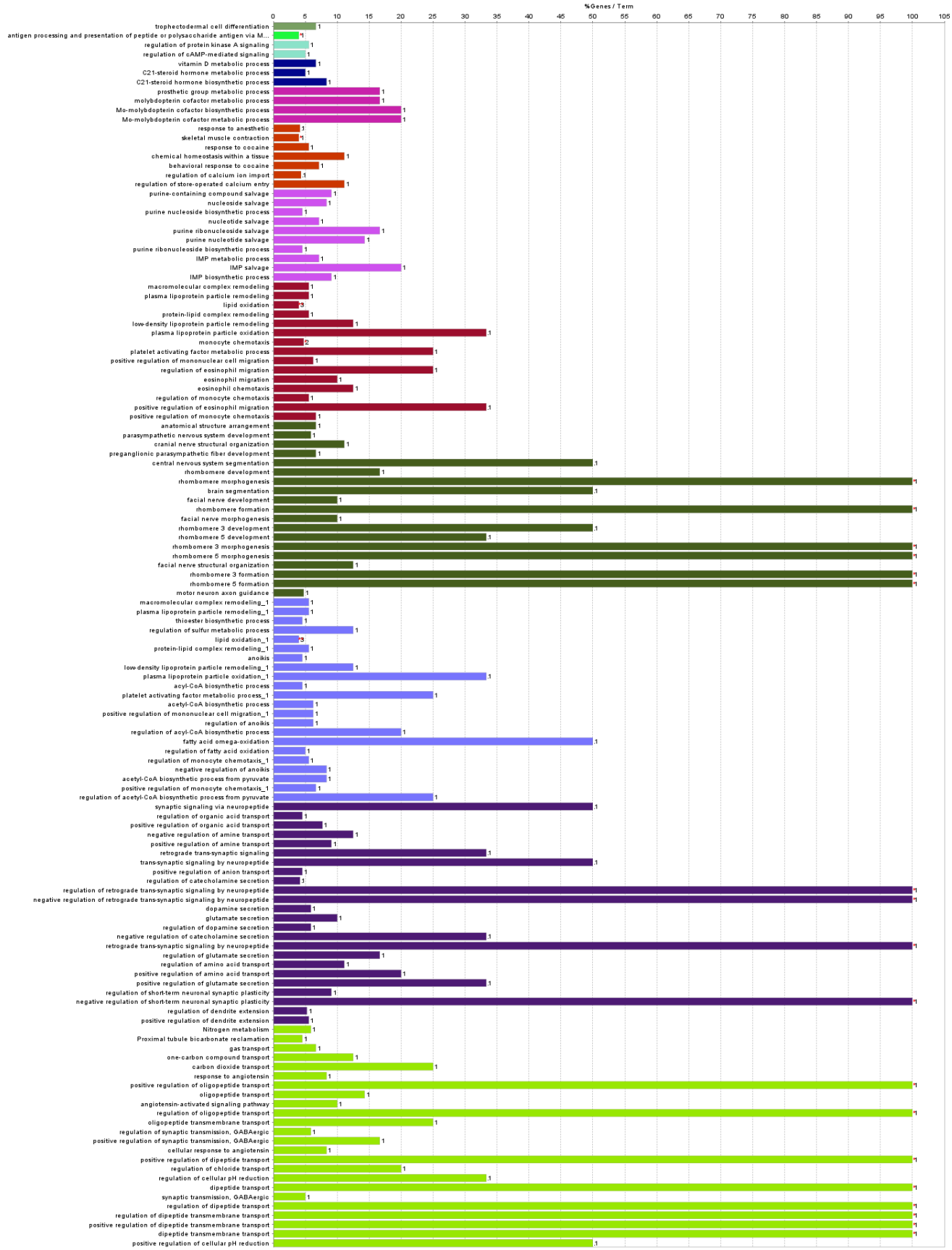
%Genes / Term
0 5 10 15 20 25 30 35 40 45 50 55 60 65 70 75 80 85 90 95 100 105
trophectodermal cell differentiation
antigen processing and presentation of peptide or polysaccharide antigen via M...
regulation of protein kinase A signaling
regulation of cAMP-mediated signaling
vitamin D metabolic process
C21-steroid hormone metabolic process
C21-steroid hormone biosynthetic process
prosthetic group metabolic process
molybdopterin cofactor metabolic process
Mo-molybdopterin cofactor biosynthetic process
Mo-molybdopterin cofactor metabolic process
response to anesthetic
skeletal muscle contraction
response to cocaine
chemical homeostasis within a tissue
behavioral response to cocaine
regulation of calcium ion import
regulation of store-operated calcium entry
purine-containing compound salvage
nucleoside salvage
purine nucleoside biosynthetic process
nucleotide salvage
purine ribonucleoside salvage
purine nucleotide salvage
purine ribonucleoside biosynthetic process
IMP metabolic process
IMP salvage
IMP biosynthetic process
macromolecular complex remodeling
plasma lipoprotein particle remodeling
lipid oxidation
protein-lipid complex remodeling
low-density lipoprotein particle remodeling
plasma lipoprotein particle oxidation
monocyte chemotaxis
platelet activating factor metabolic process
positive regulation of mononuclear cell migration
regulation of eosinophil migration
eosinophil migration
eosinophil chemotaxis
regulation of monocyte chemotaxis
positive regulation of eosinophil migration
positive regulation of monocyte chemotaxis
anatomical structure arrangement
parasympathetic nervous system development
cranial nerve structural organization
preganglionic parasympathetic fiber development
central nervous system segmentation
rhombomere development
rhombomere morphogenesis
brain segmentation
facial nerve development
rhombomere formation
facial nerve morphogenesis
rhombomere 3 development
rhombomere 5 development
rhombomere 3 morphogenesis
rhombomere 5 morphogenesis
facial nerve structural organization
rhombomere 3 formation
rhombomere 5 formation
motor neuron axon guidance
macromolecular complex remodeling_1
plasma lipoprotein particle remodeling_1
thioester biosynthetic process
regulation of sulfur metabolic process
lipid oxidation_1
protein-lipid complex remodeling_1
anoikis
low-density lipoprotein particle remodeling_1
plasma lipoprotein particle oxidation_1
acyl-CoA biosynthetic process
platelet activating factor metabolic process_1
acetyl-CoA biosynthetic process
positive regulation of mononuclear cell migration_1
regulation of anoikis
regulation of acyl-CoA biosynthetic process
fatty acid omega-oxidation
regulation of fatty acid oxidation
regulation of monocyte chemotaxis_1
negative regulation of anoikis
acetyl-CoA biosynthetic process from pyruvate
positive regulation of monocyte chemotaxis_1
regulation of acetyl-CoA biosynthetic process from pyruvate
synaptic signaling via neuropeptide
regulation of organic acid transport
positive regulation of organic acid transport
negative regulation of amine transport
positive regulation of amine transport
retrograde trans-synaptic signaling
trans-synaptic signaling by neuropeptide
positive regulation of anion transport
regulation of catecholamine secretion
regulation of retrograde trans-synaptic signaling by neuropeptide
negative regulation of retrograde trans-synaptic signaling by neuropeptide
dopamine secretion
glutamate secretion
regulation of dopamine secretion
negative regulation of catecholamine secretion
retrograde trans-synaptic signaling by neuropeptide
regulation of glutamate secretion
regulation of amino acid transport
positive regulation of amino acid transport
positive regulation of glutamate secretion
regulation of short-term neuronal synaptic plasticity
negative regulation of short-term neuronal synaptic plasticity
regulation of dendrite extension
positive regulation of dendrite extension
Nitrogen metabolism
Proximal tubule bicarbonate reclamation
gas transport
one-carbon compound transport
carbon dioxide transport
response to angiotensin
positive regulation of oligopeptide transport
oligopeptide transport
angiotensin-activated signaling pathway
regulation of oligopeptide transport
oligopeptide transmembrane transport
regulation of synaptic transmission, GABAergic
positive regulation of synaptic transmission, GABAergic
cellular response to angiotensin
positive regulation of dipeptide transport
regulation of chloride transport
regulation of cellular pH reduction
dipeptide transport
synaptic transmission, GABAergic
regulation of dipeptide transport
regulation of dipeptide transmembrane transport
positive regulation of dipeptide transmembrane transport
dipeptide transmembrane transport
positive regulation of cellular pH reduction

Figure 10. ClueGO Gene Ontology (GO) and KEGG pathway enrichment analysis of RNA-seq upregulated target genes associated with cow's age. Bar chart displaying significantly enriched GO biological process terms and KEGG pathways among RNA-seq target genes upregulated in association with age in cattle. The y-axis lists enriched terms, while the x-axis represents the percentage of genes annotated to each term within the input set. Numbers at the end of each bar indicate the number of associated genes. Functional terms are color-coded based on biological groupings. The analysis reveals age-associated upregulation of key processes, including development (e.g., lung and forebrain development, urogenital system development), immune signaling, lipid metabolism, synaptic transmission, and peptide transport, highlighting molecular pathways potentially linked to physiological aging in cattle.

4.2.6.2. Identification of functional groups affected by upregulated target genes related to the cow's age.

ClueGO analysis identified 12 functional groups (Figure 11) and 11 metabolic pathways (**Supplementary** Figure 3) for the upregulated RNA-seq target genes affected by cow's age: namely: trophectoderm cell differentiation (0,76%); antigen processing and presentation of peptide or polysaccharide antigen via MHC class II (0,76%); regulation of cAMP-mediated signaling (1,52%); C21-steroid hormone metabolic process (2,27%); Mo-molybdopterin cofactor biosynthetic process (3,03%); skeletal muscle contraction (5,3%); purine nucleoside biosynthetic process (7,58%); lipid oxidation (11,36%); rhombomere morphogenesis (14,39%); fatty acid omega-oxidation (16,67%); negative regulation of short-term neuronal synaptic plasticity (18,18%); dipeptide transmembrane transport (18,18%). The identified twelve functional clusters formed a single connected network centered on metabolite transport and oxidation, with edges to developmental and signalling nodes (Figure 11).

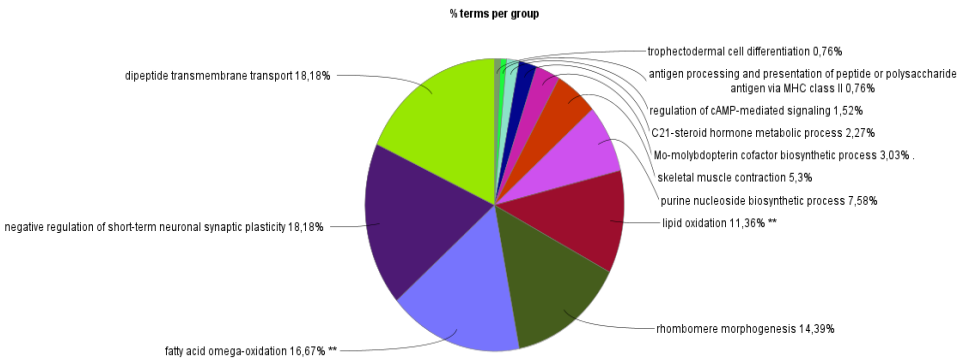

Figure 11. ClueGO pie chart showing GO biological process and KEGG pathway enrichment of RNA-seq upregulated target genes associated with cow's age.
Pie chart illustrating the distribution of significantly enriched GO biological processes and KEGG pathways identified by ClueGO among RNA-seq target genes upregulated with advancing age in cattle. Each slice represents a functional term or pathway group, with its proportion expressed as a percentage of the total enriched terms. Major enriched categories include *dipeptide transmembrane transport* (18.18%), *negative regulation of short-term neuronal synaptic plasticity* (18.18%), *fatty acid omega-oxidation* (16.67%), *rhombomere morphogenesis* (14.39%), and *lipid oxidation* (11.36%).

Additional pathways include *purine nucleoside biosynthetic process* (7.58%), *skeletal muscle contraction* (5.3%), and others. Asterisks (**) indicate statistically significant enrichment after multiple testing corrections. Functional groups are color-coded to reflect biological similarity. This analysis highlights age-associated changes in metabolism, neuroregulation, morphogenesis, and transport processes in cattle.

4.2.6.3. Identification of RNA-seq downregulated target genes associated with GO Biological Processes and KEGG pathways related to cow's age (Gene ontology and pathway enrichment analysis)

ClueGO GO/KEGG enrichment for the older-donor contrast (Bonferroni step-down, adjusted $p < 0.05$; kappa ≥ 0.3) was performed using the 11571 tested gene transcripts as the background universe and term redundancy controlled by kappa grouping. ClueGO analysis identified 80 GO/pathway-specific terms associated with downregulated genes related to the cow's age. The most enriched terms include de novo actin filament nucleation; positive regulation processes such as positive regulation of vesicle fusion, positive regulation of synaptic vesicle transport, positive regulation of anion transport, positive regulation of organic acid transport, positive regulation of lipid catabolic process, positive regulation of fatty acid biosynthetic process, and positive regulation of glucose transmembrane transport; as well as retinal and light-related terms including retinal cell apoptotic process, retinal rod cell apoptotic process, and cellular response to light intensity. The identified 80 significant downregulated terms were met significance criteria and were resolved into comparatively sparse, weakly connected clusters; the dominant category was "cellular response to light intensity" (55.7%), with additional terms related to cytoskeletal assembly, vesicle-mediated trafficking, CD40 signalling, and copper-ion homeostasis (Figure 12).

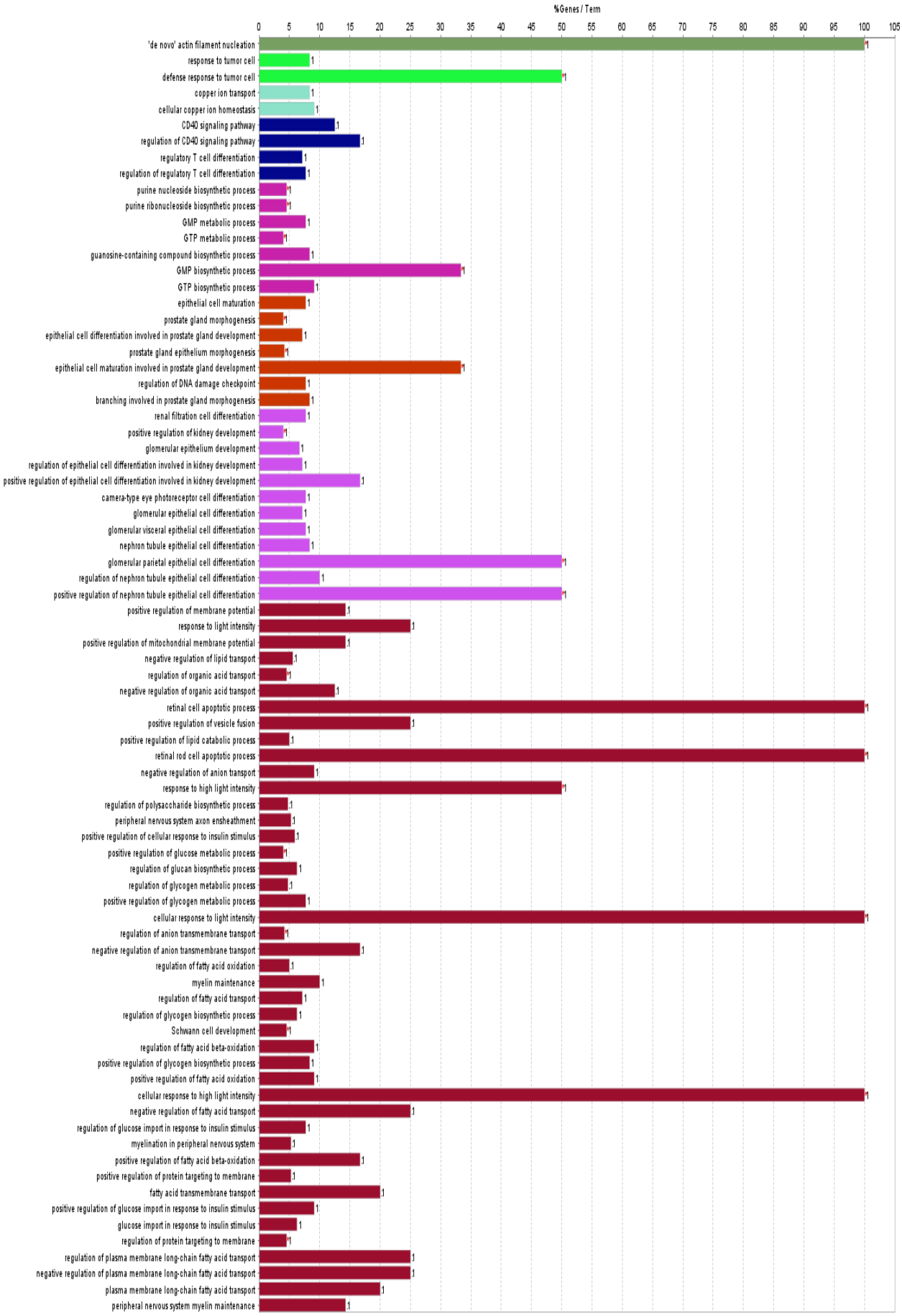
%Genes / Term
0 5 10 15 20 25 30 35 40 45 50 55 60 65 70 75 80 85 90 95 100 105
'de novo' actin filament nucleation
response to tumor cell
defense response to tumor cell
copper ion transport
cellular copper ion homeostasis
CD40 signaling pathway
regulation of CD40 signaling pathway
regulatory T cell differentiation
regulation of regulatory T cell differentiation
purine nucleoside biosynthetic process
purine ribonucleoside biosynthetic process
GMP metabolic process
GTP metabolic process
guanosine-containing compound biosynthetic process
GMP biosynthetic process
GTP biosynthetic process
epithelial cell maturation
prostate gland morphogenesis
epithelial cell differentiation involved in prostate gland development
prostate gland epithelium morphogenesis
epithelial cell maturation involved in prostate gland development
regulation of DNA damage checkpoint
branching involved in prostate gland morphogenesis
renal filtration cell differentiation
positive regulation of kidney development
glomerular epithelium development
regulation of epithelial cell differentiation involved in kidney development
positive regulation of epithelial cell differentiation involved in kidney development
camera-type eye photoreceptor cell differentiation
glomerular epithelial cell differentiation
glomerular visceral epithelial cell differentiation
nephron tubule epithelial cell differentiation
glomerular parietal epithelial cell differentiation
regulation of nephron tubule epithelial cell differentiation
positive regulation of nephron tubule epithelial cell differentiation
positive regulation of membrane potential
response to light intensity
positive regulation of mitochondrial membrane potential
negative regulation of lipid transport
regulation of organic acid transport
negative regulation of organic acid transport
retinal cell apoptotic process
positive regulation of vesicle fusion
positive regulation of lipid catabolic process
retinal rod cell apoptotic process
negative regulation of anion transport
response to high light intensity
regulation of polysaccharide biosynthetic process
peripheral nervous system axon ensheathment
positive regulation of cellular response to insulin stimulus
positive regulation of glucose metabolic process
regulation of glucan biosynthetic process
regulation of glycogen metabolic process
positive regulation of glycogen metabolic process
cellular response to light intensity
regulation of anion transmembrane transport
negative regulation of anion transmembrane transport
regulation of fatty acid oxidation
myelin maintenance
regulation of fatty acid transport
regulation of glycogen biosynthetic process
Schwann cell development
regulation of fatty acid beta-oxidation
positive regulation of glycogen biosynthetic process
positive regulation of fatty acid oxidation
cellular response to high light intensity
negative regulation of fatty acid transport
regulation of glucose import in response to insulin stimulus
myelination in peripheral nervous system
positive regulation of fatty acid beta-oxidation
positive regulation of protein targeting to membrane
fatty acid transmembrane transport
positive regulation of glucose import in response to insulin stimulus
glucose import in response to insulin stimulus
regulation of protein targeting to membrane
regulation of plasma membrane long-chain fatty acid transport
negative regulation of plasma membrane long-chain fatty acid transport
plasma membrane long-chain fatty acid transport
peripheral nervous system myelin maintenance

Figure 12. ClueGO Gene Ontology (GO) and KEGG pathway enrichment analysis of RNA-seq downregulated target genes associated with cow's age.
Bar chart displaying significantly enriched GO biological process terms and KEGG pathways among RNA-seq target genes downregulated with increasing age in cattle, as identified using ClueGO. The y-axis lists the enriched GO terms, while the x-axis represents the percentage of genes in the input set annotated to each term. Numbers at the end of each bar indicate the gene count per term. Terms are color-coded based on functional groupings. Notable enriched terms include 'de novo' actin filament nucleation, defense response to tumor cell, epithelial cell differentiation, prostate gland morphogenesis, positive regulation of kidney development, glucose and glycogen metabolic processes, regulation of fatty acid beta-oxidation, fatty acid transport, anion transmembrane transport, regulation of membrane potential, and cellular response to light intensity. These results reflect age-associated downregulation of genes involved in cellular signaling, transport, metabolism, and developmental processes in cattle.

4.2.6.4. Identification of functional groups affected by downregulated target genes related to the cow's age.

ClueGO analysis identified eight functional groups (Figure 13) and eight metabolic pathways (Supplementary Figure 4) for the downregulated RNA-seq target genes affected by cow's age: namely: 'de novo' actin filament nucleation (1,27%), defense response to tumor cell (2,53%), cellular copper ion homeostasis (2,53%), regulation of CD40 signaling pathway (5,06%), GTP metabolic process (8,86%), prostate gland morphogenesis (8,86%), positive regulation of kidney development (15,19%), cellular response to light intensity (55,7%). (Figure 13). The identified eight functional clusters in Figure 13 revealed the modular organization of these terms, with node size proportional to enrichment significance and colour denoting functional groups.

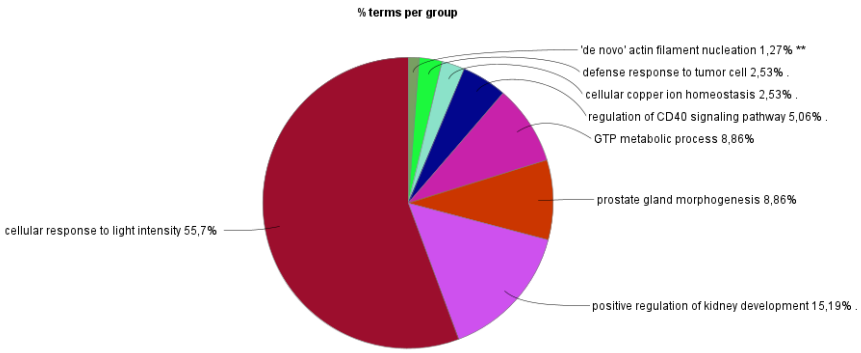

Figure 13. ClueGO pie chart showing GO biological process and KEGG pathway enrichment of RNA-seq downregulated target genes associated with cow's age.

Pie chart illustrating the proportional distribution of significantly enriched GO biological process terms and KEGG pathways among RNA-seq target genes downregulated with advancing age in cattle, identified using ClueGO. Each slice represents a functional group, with its proportion expressed as a

percentage of the total number of enriched terms. Dominant categories include *cellular response to light intensity* (55.7%), *positive regulation of kidney development* (15.19%), and *prostate gland morphogenesis* (8.86%), with additional terms such as *GTP metabolic process* (8.86%), *regulation of CD40 signaling pathway* (5.06%), *cellular copper ion homeostasis* (2.53%), *defense response to tumor cell* (2.53%), and *'de novo' actin filament nucleation* (1.27%). Terms marked with asterisks (**) are statistically significant after multiple testing corrections. Color coding represents functionally grouped biological processes. This analysis highlights age-related downregulation of pathways linked to cellular signaling, immune function, development, and environmental response in cattle.

4.3 Transcriptome analysis of bovine embryos according to season based on the bulk scRNA-seq experiment

Transcriptomic profiling of bovine embryos and quality control metrics: Similar to the age experiment, we sequenced 34 in vivo-derived Holstein-Friesian (*Bos taurus*) embryos of Polish HF cows obtained during summer and spring seasons. After pre-specified QC, 34 libraries met the inclusion thresholds and yielded 34 unique single-embryo transcriptomes for downstream analyses. The run produced 309.4 Gbp of raw data. Reads were aligned to the Bos Taurus UMD 3,0 reference genome with STAR, and transcript abundances were estimated with RSEM; gene-level summaries (Ensembl stable IDs) were derived via tximport (*type* = "rsem").

Summary of identified DE gene transcripts with significant p values, upregulated and downregulated gene transcripts expressed in Polish HF cows: according to season, based on the bulk scRNA-seq experiment: Across the cohort, 27,607 gene transcripts had nonzero estimates (without filtering); expression filtering with filterByExpr defined (filtered with P<1,0) 12,752 reliably expressed gene transcripts (Supplementary Table S6), which constituted the tested universe for all subsequent analyses. Overall, 7167 upregulated (Supplementary Table S7 season) and 5585 downregulated (Supplementary Table S8 season) putative DEGs transcripts in embryos of Polish HF cows at different seasons (summer and spring) were identified.

4.3.1. Identification of top 30 upregulated (Log2FoldChange ≥2 and p-value <0.05) putative DEGs transcripts in embryos of Polish HF cows at different seasons.

By comparing the seasonal groups (in vivo embryos collected from cows in summer and spring), results revealed the identification of 30 top significant upregulated DEGs transcripts with Log2FoldChange ≥2 in bovine embryos at different ages (Table 11).

The top 30 upregulated genes were identified using the Gene cards website: *HSPA6 (Heat shock protein family A (Hsp70) member 6), NR1I3 (Nuclear Receptor Subfamily 1 Group I Member 3), Cytochrome P450 Family 4 Subfamily V Member 2 (CYP4V2), C-X-C Motif Chemokine Receptor 4 (CXCR4), Immunoglobulin Heavy Constant Mu (IGHM), Hypoxanthine Phosphoribosyltransferase 1 (HPRT1), Follicle Stimulating Hormone Receptor (FSHR), MAGE Family Member B2 (MAGEB2), FosB Proto-Oncogene, AP-1 Transcription Factor Subunit (FOSB), Cytochrome P450 Family 11 Subfamily A Member 1 (CYP11A1), Zinc Finger B-Box Domain Containing (ZBBX), Forkhead Box A1 (FOXA1), Lysosomal Protein Transmembrane 5 (LAPTM5), MAGE Family Member D2 (MAGED2), Eva-1 Homolog C (EVA1C), SH3 Domain Binding Glutamate Rich Protein (SH3BGR), Carbonic Anhydrase 2 (CA2), Branched Chain Amino Acid Transaminase 2 (BCAT2), SH3 Domain Containing GRB2 Like 2, Endophilin A1 (SH3GL2), BMP Binding Endothelial Regulator (BMPER), Fibrinogen Beta Chain (FGB), Family With Sequence Similarity 13 Member C (FAM13C), Kallikrein Related Peptidase 8 (KLK8), Myosin Light Chain 7 (MYL7), CD8 Subunit Beta (CD8B)* and 4 novel genes.

Table 11. TOP 30 season-dependent up-regulated genes from in vivo-derived embryo of Polish HF cattle

SN	gene_id	chr	start	end	Gene name	Transcript count	gene_biotype	log2 FoldChange	lfcSE	stat	pvalue	padj
1	ENSBTAG00000067628	1	88717610	88724186	*unannotated*	6	lncRNA	16,64890992	2.05996716002186	8.08212394927719	6,3648E-16	1.62328785868061e-12
2	ENSBTAG00000039035	3	8031683	8034120	*HSPA6*	9	protein_coding	15,47987749	1.92658457997871	8.03488082075548	9,3670E-16	1.99079775090934e-12
3	ENSBTAG00000009215	3	8271461	8276698	*NR1I3*	112	protein_coding	9,66880668	2.40425411579201	4.02154107450685	5,7819E-05	0.00281413390220918
4	ENSBTAG00000021263	27	16250292	16266690	*CYP4V2*	28	protein_coding	9,076330842	1.88412619064344	4.81726271158922	1,4554E-06	0.000231992371627141
5	ENSBTAG00000001060	2	61250084	61254502	*CXCR4*	28	protein_coding	8,494988163	2.94956645440013	2.88008027416896	3,9757E-03	0.047205425937131
6	ENSBTAG00000001219	21	18874	193160	*IGHM*	78	protein_coding	7,551485091	2.09365651104768	3.60684049727456	3,0995E-04	0.00914920734251924
7	ENSBTAG00000046220	3	102735258	102744921	*HPRT1*	42	protein_coding	7,517573966	2.07398014585301	3.62470874248755	2,8929E-04	0.00863932427249042
8	ENSBTAG00000032424	11	31255653	31450417	*FSHR*	138	protein_coding	7,204598745	1.68823070914236	4.26754394741044	1,9764E-05	0.0013405665134
9	ENSBTAG00000034437	11	27016	32430	*MAGEB2*	10	protein_coding	7,154539981	1.84072003691602	3.88681594006146	1,0157E-04	0.00397297976900326
10	ENSBTAG00000008182	18	53074714	53081288	*FOSB*	49	protein_coding	7,111583408	1.58270529692317	4.49330865439673	7,0125E-06	0.000693204959252207
11	ENSBTAG00000006934	21	34328574	34342887	*CYP11A1*	24	protein_coding	7,045289641	1.64021904636077	4.29533461203335	1,7443E-05	0.00124962462986124
12	ENSBTAG00000035710	1	100083002	100206264	*ZBBX*	109	protein_coding	6,773500721	2.07725006167023	3.26080179060647	1,1110E-03	0.0210659825410954
13	ENSBTAG00000013888	21	47772978	47787583	*FOXA1*	41	protein_coding	6,763136652	2.04647136195464	3.30477952353395	9,5051E-04	0.0191181726018533
14	ENSBTAG00000048049	21	200614	207113	*IGHM*	16	protein_coding	6,697910204	2.50784439997103	2.67078380323375	7,5674E-03	0.0698768692011072
15	ENSBTAG00000005477	2	122806844	122833480	*LAPTM5*	24	protein_coding	6,674225632	2.72495039376643	2.44930169993062	1,4313E-02	0.104898758402205
16	ENSBTAG00000039888	X	92287353	92293899	*MAGED2*	28	protein_coding	6,581016952	1.59721490774096	4.12030774352327	3,7837E-05	0.0020887151079003
17	ENSBTAG00000017310	1	2953876	3081872	*EVA1C*	207	protein_coding	6,532429435	1.61009352610268	4.05717390260844	4,9670E-05	0.00257476866326762
18	ENSBTAG00000007068	1	139458039	139600025	*SH3BGR*	43	protein_coding	6,50307304	1.64274478518296	3.95866302474881	7,5370E-05	0.00332437516444505
19	ENSBTAG00000017733	14	76994568	77012262	*CA2*	54	protein_coding	6,469205989	1.85211413187054	3.49287653389505	4,7785E-04	0.0120898041611892
20	ENSBTAG00000009172	18	55411008	55425212	*BCAT2*	77	protein_coding	6,363380521	1.94027401988124	3.27962981308844	1,0394E-03	0.0201524998054651
21	ENSBTAG00000066217	X	37944064	37945684	*unannotated*	12	protein_coding	6,333795179	0.724136775699689	8.74668348839312	2,1971E-18	7.0045099889993e-15
22	ENSBTAG00000014103	8	26598507	26825777	*SH3GL2*	64	protein_coding	6,323939646	1.77511113663966	3.5625598394143	3,6726E-04	0.0102447938615545
23	ENSBTAG00000010866	4	62664288	62917005	*BMPER*	258	protein_coding	6,169643009	1.63819084893805	3.76613201903759	1,6580E-04	0.00580833095686082
24	ENSBTAG00000066428	4	70173365	70190061	*unannotated*	8	lncRNA	6,159994632	1.52891639687686	4.02899376604959	5,6016E-05	0.00276867190946697
25	ENSBTAG00000022120	17	2893368	2919644	*FGB*	141	protein_coding	5,921980871	1.7859294410832	3.3159097638061	9,1345E-04	0.0186756049240074
26	ENSBTAG00000017540	28	14882652	15023646	*FAM13C*	243	protein_coding	5,800169718	1.55826168715387	3.72220517618324	1,9749E-04	0.00666242882425808
27	ENSBTAG00000068554	10	42629551	42629850	*Metazoa_SRP*	3	misc_RNA	5,78176603	1.45169416825311	3.98277141042713	6,81E-05	0.00318175318200442

28	ENSBTAG00000015128	18	56971922	56978107	*KLK8*	28	protein_coding	5,668223776	1.14924838768131	4.93211375048142	8,13E-07	0.000157167473188826
29	ENSBTAG00000002066	4	77178486	77181131	*MYL7*	49	protein_coding	5,647634125	1.21575850195672	4.64535852769595	3,39E-06	0.000412298092972455
30	ENSBTAG00000008956	11	48044725	48064460	*CD8B*	31	protein_coding	5,642547046	1.19870274920253	4.70721123305819	2,51E-06	0.000348086145807118

4.3.2 Identification of downregulated (Log2FoldChange ≤ -2 and p-value <0.05) putative DEGs transcripts in embryos of Polish HF cows at different seasons.

The top 30 downregulated genes were identified using the Gene cards website: *RNA binding motif single stranded interacting protein 3 (RBMS3), Ubiquinol-cytochrome c reductase core protein 2 (UQCRC2), Proteasome 26S subunit, ATPase 6 (PSMC6), Dynein axonemal heavy chain 12 (DNAH12), ETS variant transcription factor 5 (ETV5), Synaptotagmin 9 (SYT9), Fibronectin type III and SPRY domain containing 1 like (FSD1L), F-box protein 48 (FBXO48), Dedicator of cytokinesis 8 (DOCK8), Adrenoceptor beta 2 (ADRB2), Zinc finger protein 845 (ZNF845), Fem-1 homolog B (FEM1B), Hepcidin antimicrobial peptide (HAMP), BEN domain containing 4 (BEND4), Aquaporin 7 (AQP7), Corneodesmosin (CDSN), and ATP binding cassette subfamily C member 3 (ABCC3),* ENSBTAG00000069414, ENSBTAG00000060764, ENSBTAG00000046383, ENSBTAG00000059862, ENSBTAG00000045854, ENSBTAG00000057054, ENSBTAG00000062664, ENSBTAG00000062826, ENSBTAG00000064207, ENSBTAG00000055919, ENSBTAG00000055520, ENSBTAG00000064201, and ENSBTAG00000062365.

Table 12. TOP 30 season-dependent down-regulated genes from in vivo-derived embryo of Polish HF cattle

SN	gene_id	chr	start	end	gene_name	Transcript count	gene_biotype	log2 FoldChange	lfcSE	stat	pvalue	padj
1	ENSBTAG00000044062	22	2984947	4652965	*RBMS3*	172	protein_coding	-7,687081124	1.31447776812314	-5.84801151481161	4,97E-09	3.02091311569591e-06
2	ENSBTAG00000069414	13	11068109	11092862	*unannotated*	42	protein_coding	-6,287933541	1.43028635838851	-4.39627596559608	1,10E-05	0.000888797530837977
3	ENSBTAG00000060764	6	85497254	85506606	*unannotated*	13	protein_coding	-5,671042841	1.66809153736781	-3.39971920841879	0,000674551	0.0152786367795371
4	ENSBTAG00000046383	18	62448171	62454926	*unannotated*	24	protein_coding	-5,591721557	0.982244908143969	-5.69279770349963	1,25E-08	6.63849290405761e-06
5	ENSBTAG00000059862	18	62472348	62481588	*unannotated*	18	protein_coding	-4,711400967	0.919562875101361	-5.12352237615673	3,00E-07	7.35398127694792e-05
6	ENSBTAG00000045854	18	62459660	62476390	*unannotated*	103	protein_coding	-4,242818796	0.887410689959565	-4.78112202640465	1,74E-06	0.00026463360957514
7	ENSBTAG00000057054	1	117666912	117670643	*unannotated*	3	lncRNA	-4,212603282	1.21890479803498	-3.45605603391183	0,000548141	0.0132635647499093
8	ENSBTAG00000034662	9	18251167	18252696	*UQCRC2*	8	protein_coding	-4,119209401	0.551522579327714	-7.46879557675817	8,09E-14	1.4743525814686e-10
9	ENSBTAG00000062664	18	59722555	59723532	*unannotated*	4	protein_coding	-3,949899646	1.3532229988862	-2.91888302941072	0,00351288	0.0437890979528667
10	ENSBTAG00000050214	16	30386725	30387045	*PSMC6*	6	protein_coding	-3,910920716	0.61641017563775	-6.34467254200395	2,23E-10	1.89493908421499e-07
11	ENSBTAG00000062826	19	8736608	8742038	*unannotated*	10	protein_coding	-3,68830903	1.25483286940363	-2.93928308728946	0,003289725	0.0419506311670285
12	ENSBTAG00000064207	29	43112165	43116421	*unannotated*	4	lncRNA	-3,608629455	0.839825056845389	-4.29688233889451	1,73E-05	0.00124826749068727
13	ENSBTAG00000020802	22	43652878	43832046	*DNAH12*	348	protein_coding	-3,598282696	0.814282653123341	-4.41896027354712	9,92E-06	0.000843135664194907
14	ENSBTAG00000014915	1	81135305	81194599	*ETV5*	86	protein_coding	-3,556337734	0.813139361034939	-4.3735894533984	1,22E-05	0.000980220815148898
15	ENSBTAG00000055919	6	65401598	65469087	*unannotated*	25	protein_coding	-3,523611929	1.05938746509829	-3.32608421812867	0,000880753	0.0182031829338577
16	ENSBTAG00000032079	15	45274682	45653531	*SYT9*	199	protein_coding	-3,484132453	0.900031535858386	-3.8711226377537	0,000108335	0.00408725247956243
17	ENSBTAG00000013420	8	95277011	95346595	*FSD1L*	151	protein_coding	-3,380468508	1.2456867578048	-2.71373881695443	0,00665286	0.0646359881183376
18	ENSBTAG00000047772	11	66861021	66864669	*FBXO48*	14	protein_coding	-3,09432485	1.04794424077717	-2.95275715070387	0,003149496	0.0410972423674156
19	ENSBTAG00000002190	8	44032278	44271335	*DOCK8*	620	protein_coding	-3,044436331	0.866349995448319	-3.51409516565679	0,000441255	0.0115304916326572
20	ENSBTAG00000002144	7	60232646	60271233	*ADRB2*	103	protein_coding	-3,005360627	0.46047631689695	-6.52663452379038	6,73E-11	7.14791103253372e-08
21	ENSBTAG00000055520	3	13811803	13843135	*unannotated*	10	protein_coding	-2,976515172	0.861828903480711	-3.45371936327267	0,000552912	0.0133032815319312
22	ENSBTAG00000064201	10	15934431	15948936	*unannotated*	21	lncRNA	-2,937921604	0.912628892254634	-3.21918539841161	0,001285553	0.023319170366434
23	ENSBTAG00000059258	18	59417368	59434063	*ZNF845*	36	protein_coding	-2,872191247	0.788953421345514	-3.64050800630539	0,000272101	0.00830102257642266
24	ENSBTAG00000062365	11	43665665	43668643	*unannotated*	4	lncRNA	-2,860646735	0.863309179305995	-3.31358313310005	0,000921087	0.0187331803457917
25	ENSBTAG00000008378	10	15106163	15118280	*FEM1B*	10	protein_coding	-2,842498889	0.848534878797565	-3.34989045246455	0,000808435	0.0173527422190623
26	ENSBTAG00000017042	18	45994911	45996355	*HAMP*	12	protein_coding	-2,831821303	0.585820418996405	-4.83394093366118	1,34E-06	0.000218837918407614
27	ENSBTAG00000005567	6	60981592	61011643	*BEND4*	16	protein_coding	-2,804303795	1.04972024474035	-2.67147729070526	0,007551818	0.0697831782184124

28	ENSBTAG00000020105	8	75137786	75154391	*AQP7*	88	protein_coding	-2,780731441	0.85477924783511	-3.25315740670384	0,001141303	0.0214976222760419
29	ENSBTAG00000021721	23	28019813	28026890	*CDSN*	71	protein_coding	-2,758876089	0.934075046560243	-2.95359146873073	0,003140995	0.0410587693609312
30	ENSBTAG00000020070	19	36047549	36095574	*ABCC3*	70	protein_coding	-2,747404761	0.822314780642751	-3.34106211539989	0,000834585	0.0176787943240414

4.3.3. Visualization of gene expression of identified upregulated and downregulated putatively significant DE gene transcripts according to seasonal variations

The expression distributions were consistent across the embryos: the kernel density curves of log-scaled normalized expression (Figure 14) overlapped closely, indicating effective normalization and the absence of multimodal artifacts. Principal component analysis (PCA) of variance-stabilized counts (Figure 15) resolved two partially overlapping clusters; separation along PC1 was consistent with the recorded seas classes once the developmental stage was accounted for and was not explained by run-level metrics. The bar plot (Figure 16) revealed that PC1, PC2, and PC3 explained 29.7%, 13.7% and 8.9% 22.9%, 11.7% and 7.2% of the variance, respectively, which was consistent with a structured biological signal rather than technical noise.

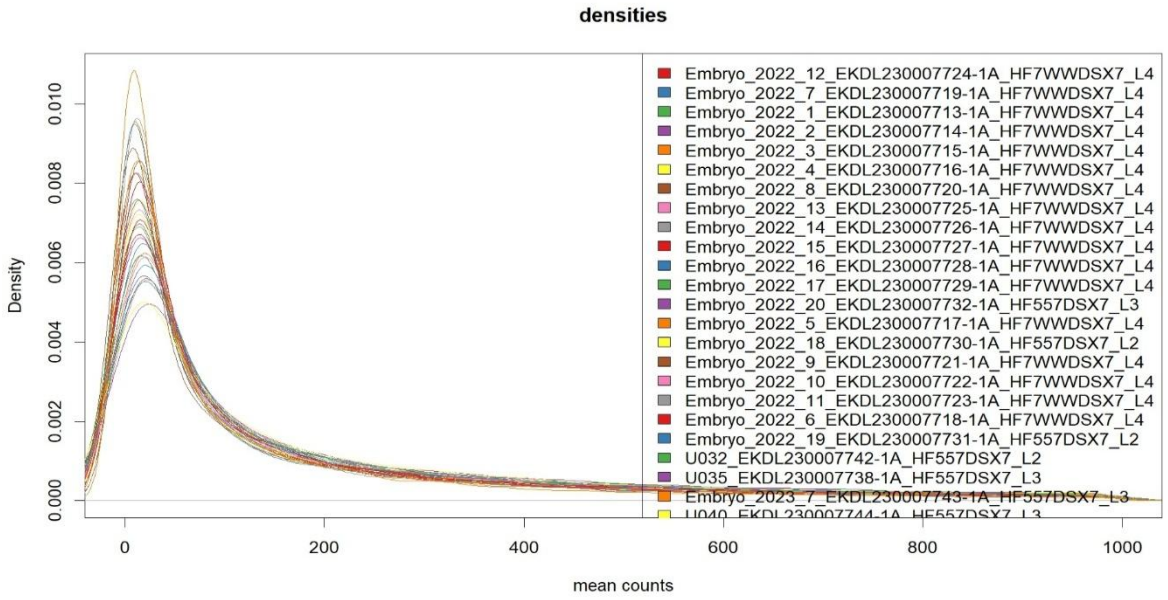

Figure 14. Density plot displaying the distribution of raw gene expression counts across individual bovine embryo RNA-seq samples. The X-axis indicates mean gene expression counts, while the Y-axis represents density. Each coloured curve corresponds to a unique embryo sample (legend). The high degree of overlap among curves reflects consistent expression distributions across samples, supporting uniform sequencing depth and sample quality prior to normalization.

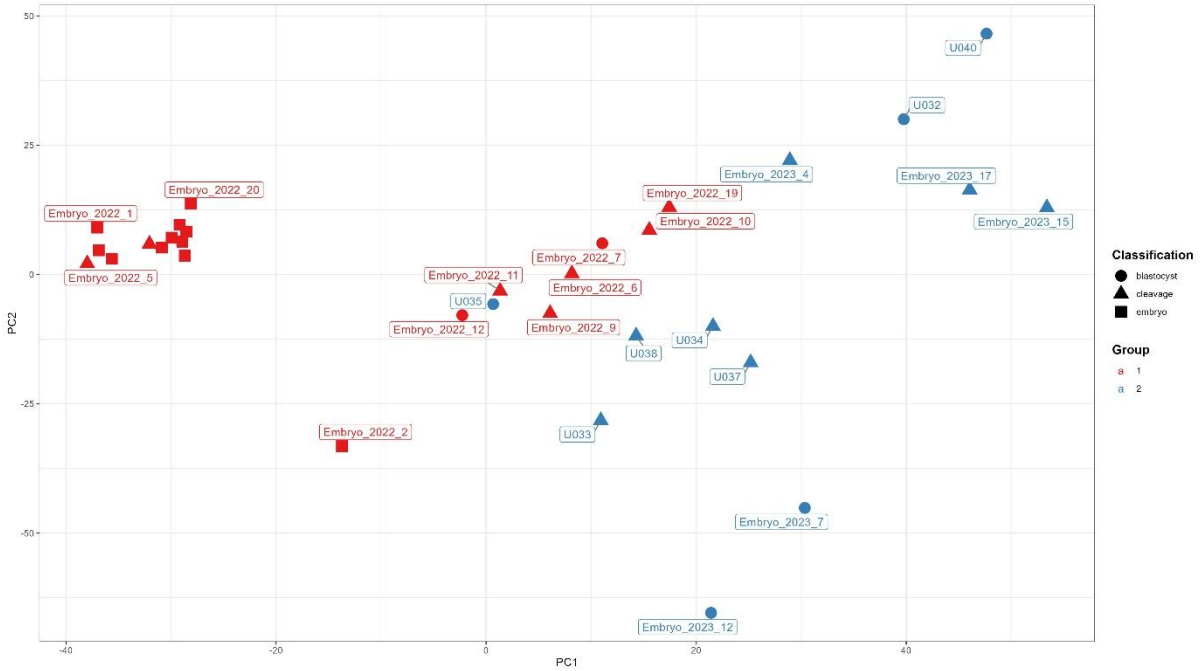

Figure 15. Principal component analysis (PCA) plot showing sample classification of embryo samples based on their gene expression profiles. Each point represents an individual sample plotted according to their scores on principal components PC1 (x-axis) and PC2 (y-axis), reflecting the highest variability within the dataset. Samples are classified by developmental stage (blastocyst, cleavage, or embryo) indicated by different shapes (circle, triangle, and square, respectively), and grouped into two distinct clusters (Group 1 in red and Group 2 in blue). Clear separation between these two groups on PC1 suggests pronounced differences in gene expression profiles related to distinct biological conditions or developmental characteristics.

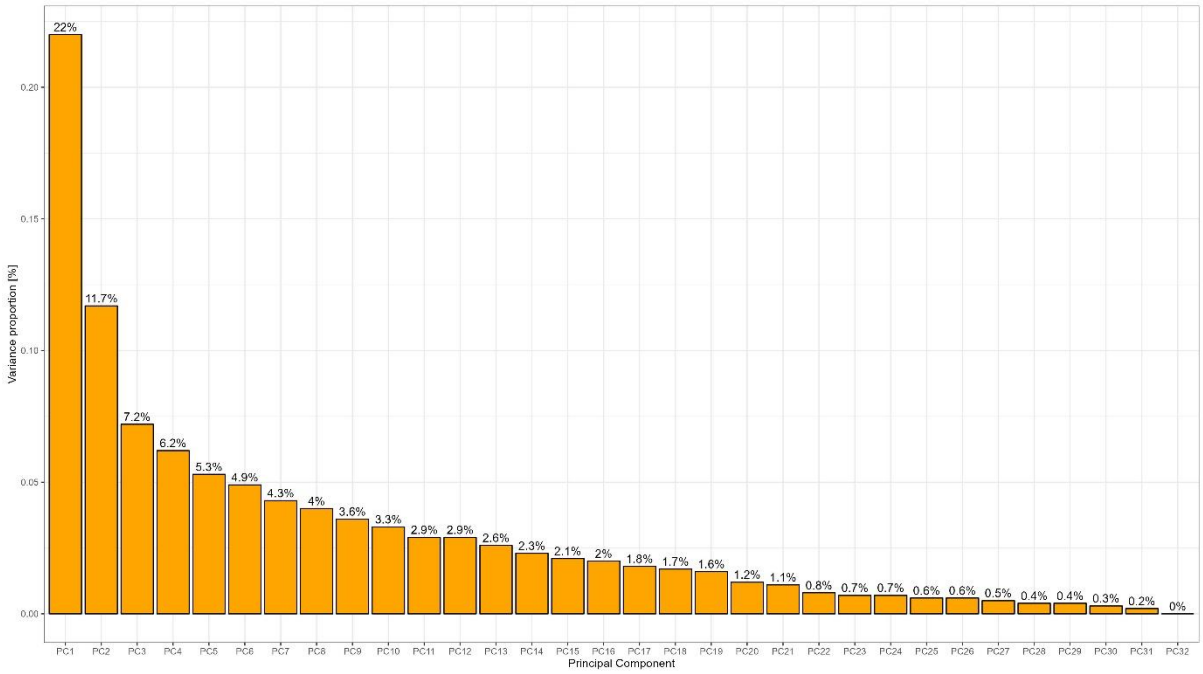

Figure 16**.** Bar plot showing the proportion of variance explained by each principal component (PC) in the PCA analysis. PC1 explains the largest proportion (29.7%) of total variance, followed by PC2 (13.7%) and PC3 (8.9%), indicating that these first few components capture most of the variability

present in the gene expression data. This plot emphasizes the significance of the first principal components in differentiating embryo samples based on their gene expression profiles.

Differential expression was evaluated on the filtered gene set via the covariate structure specified in the Methods section. The p-value histogram (Figure 17) shows the expected near-uniform bulk with enrichment near zero under the true signal after adjustment. The Q–Q plot (Figure 18) displayed tail departures compatible with genuine alternatives rather than systematic curvature. The per-gene effect sizes and significance are summarized in the volcano plot (Figure 19), which delineates the dominant up- and downregulated components of the season contrast (summer vs spring).

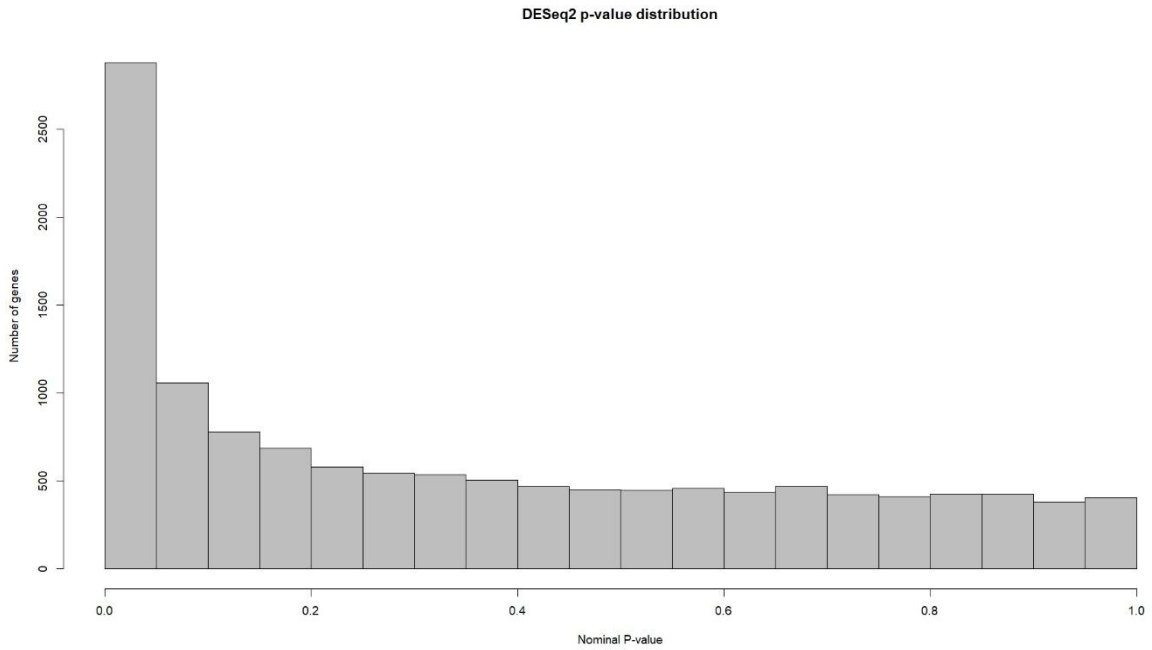

Figure 17. Histogram showing the distribution of nominal p-values obtained from differential gene expression analysis using DESeq2. The X-axis represents nominal p-value ranges, and the Y-axis indicates the number of genes falling within each range. The noticeable peak near zero indicates a substantial proportion of genes with statistically significant differential expression between the analysed conditions. This p-value distribution highlights the robustness and sensitivity of the differential expression analysis performed in this study.

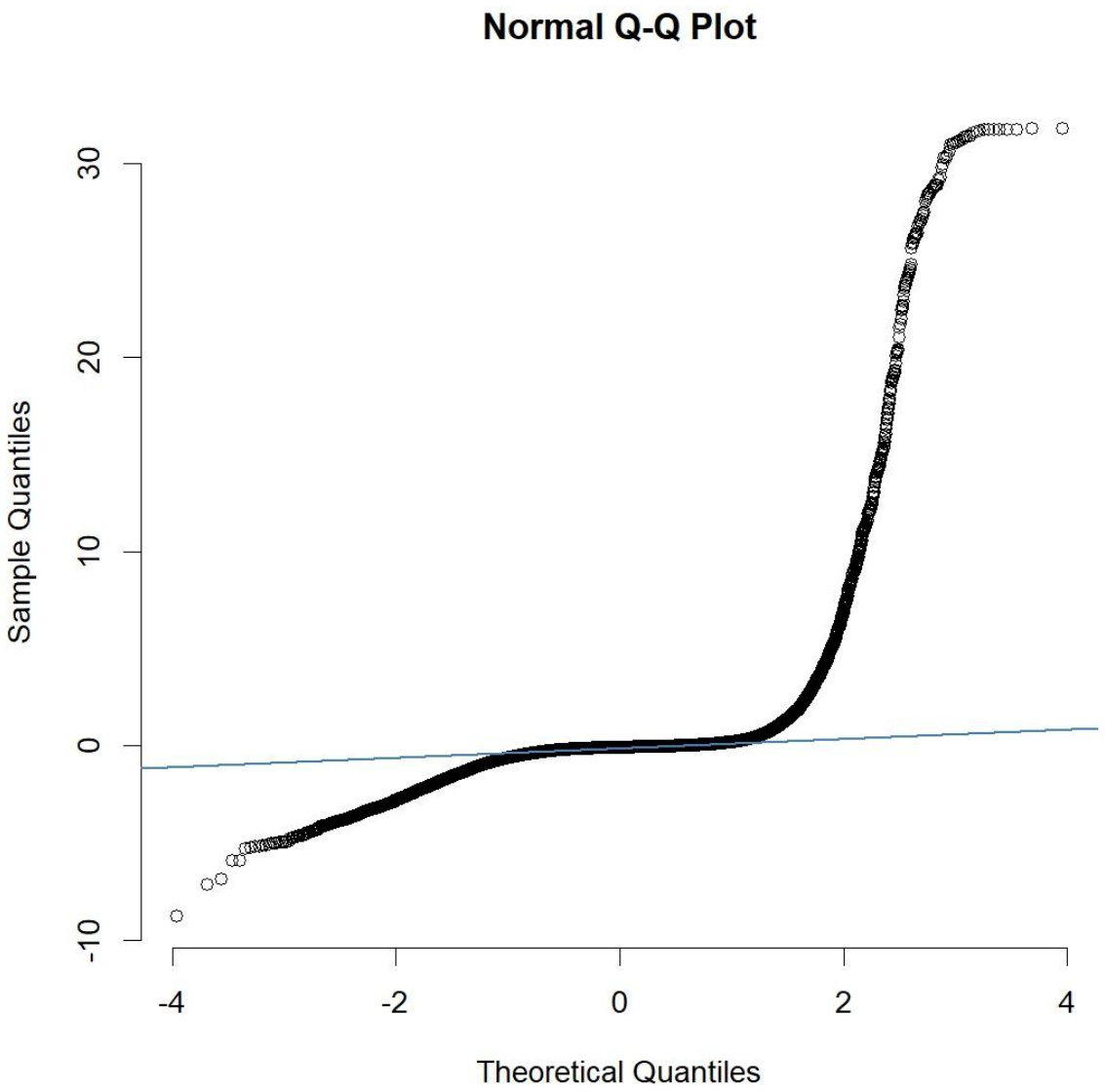

Figure 18**.** Normal Q-Q plot representing the distribution of the gene expression data residuals against a theoretical normal distribution. The X-axis shows theoretical quantiles, while the Y-axis shows observed sample quantiles. Points deviating significantly from the diagonal line indicate departures from normality, suggesting potential presence of outliers or non-normal distribution in the data. Notable deviations observed at both tails of the plot indicate that some genes significantly differ from a normal distribution, a common scenario in high-throughput gene expression datasets.

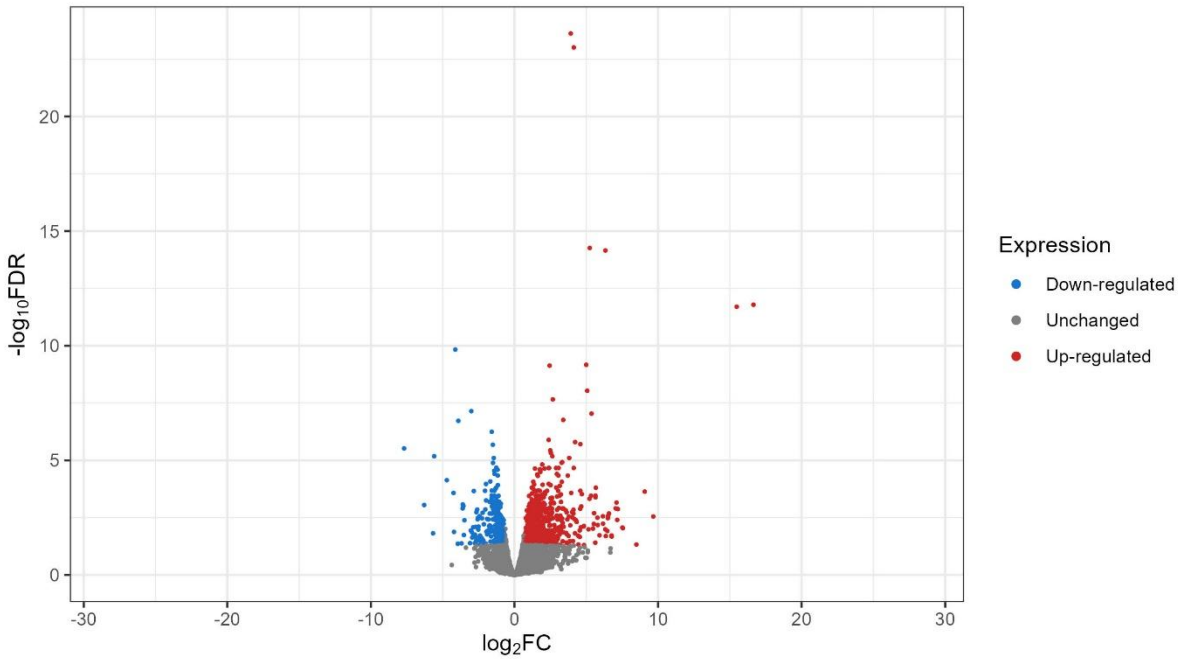

Figure 19. Volcano plots illustrating the differential gene expression between the compared embryo conditions. The x-axis represents the magnitude of change in gene expression (log2 Fold Change), while the y-axis shows the statistical significance (-log10 False Discovery Rate, FDR). Each dot represents a gene: Red dots indicate significantly upregulated genes, blue dots indicate significantly downregulated genes, and grey dots indicate genes without significant expression changes. Genes located in the upper corners of each plot represent those with the highest fold change and greatest statistical significance, highlighting key differentially expressed genes that may have biological importance.

Among the 12752 gene transcripts tested after filtering (P<1,0) (Supplementary Table S6), 7167 were upregulated (Supplementary Table S7) and 5585 (Supplementary Table S8) were downregulated in embryos from Polish HF cows at pre-specified thresholds. The genome-wide relationship between effect size and abundance is shown in the MA plot (Figure 20), which displays a log2-fold change against the mean expression for the fully tested set.

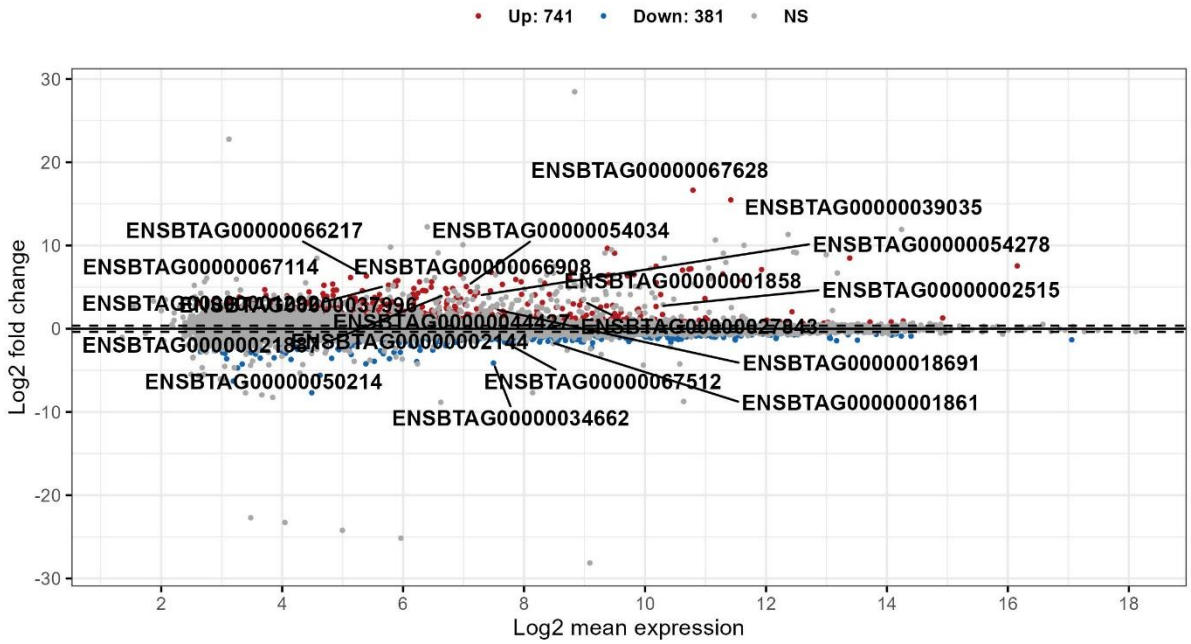

Figure 20**.** MA plot showing differential gene expression between embryos derived from sumer and spring seasons of Polish Holstein–Friesian cows. Each dot represents a gene, plotted by its $\log_2$ mean expression (x-axis) and $\log_2$ fold change (y-axis). Red and blue dots indicate significantly up- and downregulated transcripts, respectively (FDR-adjusted $p < 0.05$), while grey dots represent non-significant genes. The top 20 differentially expressed genes are annotated by Ensembl IDs based on effect size. Dashed lines denote the fold change thresholds used to determine biological significance.

4.3.4. Transcriptomic signatures of upregulated genes in embryos

Upregulated transcripts in embryos derived from dams exposed to elevated ambient temperatures clustered into functional modules related to stress response, immune signalling, steroidogenesis, and metabolic adaptation. Increased expression of the heat-shock protein HSPA6 and the transcription factor FOSB suggests engagement of cellular stress-response pathways. Immune-associated transcripts, including IGHM, CXCR4, and CD8B, indicate modulation of immune and inflammatory signalling. Genes involved in steroidogenesis and lipid metabolism (CYP11A1, CYP4V2) were also elevated, alongside metabolic regulators such as CA2 and BCAT2, consistent with adaptive adjustments in energy balance and acid–base homeostasis. Transcripts linked to reproductive and endocrine regulation (FSHR, NR1I3, FOXA1) may reflect altered endocrine signalling under elevated temperature conditions. The top 25 upregulated genes ranked by log2 fold change are shown in Figure 6-7; full per-gene results are presented in Supplementary Table S7.

Table 13. Season-dependent up-regulated genes in bovine embryos with established roles in embryogenesis and reproductive pathways

Gene	*Functional Annotation*
HSPA6	Member of the HSP70 family; mediates stress protection, protein folding, and recovery during embryogenesis.
CXCR4	Chemokine receptor critical for cell migration, stem cell maintenance, primordial germ cell survival, and organogenesis.
FSHR	Follicle-stimulating hormone receptor; essential for folliculogenesis, oocyte maturation, and early embryonic quality.
CYP11A1	Catalyzes cholesterol conversion to pregnenolone, initiating steroidogenesis necessary for embryonic hormonal support.
BCAT2	Enzyme involved in branched-chain amino acid metabolism; supports fetal growth and energy homeostasis during development.
BMPER	Regulates BMP signaling pathways; essential for endothelial migration, angiogenesis, and early vascular formation.
FGB	Encodes fibrinogen beta chain; facilitates endometrial receptivity, maternal–fetal interactions, and embryo implantation.
KLK8	Member of the kallikrein family; involved in extracellular matrix remodeling and protein activation during implantation.
MYL7	Myosin light chain isoform; critical for myocardial structure and cardiac development during embryogenesis.
CD8B	Encodes T-cell surface glycoprotein beta chain; supports immune system maturation and T-cell activation during pregnancy.

The genes listed here showed significantly higher transcript abundance in embryos collected during the warm-season versus the cold-season (or vice-versa, depending on directionality in the dataset) and have well-documented functions directly supporting embryogenesis or reproductive success. Several transcripts enhance cellular stress tolerance and proper protein folding under thermal challenge (HSPA6) or guide chemotactic cell movements critical for organ patterning and germ-cell survival (CXCR4). Up-regulation of endocrine regulators-including FSHR and the steroidogenic enzyme CYP11A1-suggests seasonal modulation of folliculogenesis, oocyte competence, and early hormonal signalling. Metabolic support genes (BCAT2) and vascular/implantation mediators (BMPER, FGB, KLK) may bolster nutrient delivery and embryo–maternal interactions when environmental conditions fluctuate. Cardiac (MYL7) and immune-maturation factors (CD8B) further indicate that seasonally altered expression profiles could influence organogenesis and immunological priming. Together, these expression changes provide molecular evidence that ambient temperature or photoperiod affects key developmental pathways, potentially contributing to seasonal variation in embryo quality and implantation success observed in vivo.

The genes listed here were detected as differentially expressed transcripts in embryos collected across seasons but currently lack well-established, direct roles in mammalian preimplantation embryogenesis. Several transcripts are primarily involved in systemic metabolic or stress-response pathways rather than embryo-specific developmental programs. For example, NR1I3 and CYP4V2 participate in xenobiotic and lipid metabolism, while MAGED2 and EVA1C are associated with stress adaptation and hypoxia-responsive mechanisms. IGHM and LAPTM5 are predominantly linked to immune system development, and HPRT1 functions in nucleotide salvage and genomic maintenance.

Other transcripts, including FOSB, FOXA1, and ZBBX, encode transcriptional regulators with broad roles in chromatin accessibility or cellular differentiation but without clearly defined functions in early bovine embryos. SH3GL2 and CA2 are involved in vesicular trafficking and acid–base regulation, respectively, reflecting metabolic adjustments rather than direct morphogenetic control. Similarly, FAM13C and Metazoa_SRP remain poorly characterized in the context of embryogenesis.

Overall, although these genes may contribute to systemic metabolic, endocrine, or stress-adaptive responses associated with seasonal environmental variation, their precise functional relevance to early bovine embryonic development remains to be experimentally validated.

Table 14. Season-dependent up-regulated genes in bovine embryos with no currently validated roles in embryogenesis or reproduction

Gene	*Functional Annotation*
NR1I3	Nuclear receptor involved in xenobiotic and endogenous metabolism; affects systemic metabolic homeostasis.
CYP4V2	Cytochrome P450 enzyme; implicated in lipid metabolism with limited evidence for embryonic functions.
IGHM	Encodes the immunoglobulin heavy chain mu; early marker of immune competence during development.
HPRT1	Key enzyme in the purine salvage pathway; essential for nucleotide synthesis and genomic stability.
MAGEB2	Melanoma antigen family member; involved in apoptosis regulation, cell cycle control, and differentiation.
FOSB	Transcription factor regulating cellular stress responses and differentiation; associated with embryonic pathways.

ZBBX	Zinc finger transcription factor; putatively involved in cilia function and transcriptional regulation during early development.
FOXA1	Pioneer transcription factor; modulates chromatin accessibility and activates liver and urogenital developmental programs.
LAPTM5	Lysosomal-associated protein; plays a role in hematopoietic cell maturation, with possible developmental relevance.
MAGED2	Stress-responsive gene; regulates autophagy under hypoxic conditions and is expressed in mesodermal tissues.
EVA1C	Mediates axon guidance and neural circuitry formation; important for nervous system development under hypoxia.
SH3BGR	Regulates endothelial migration and sarcomere assembly; critical for muscle and cardiac development.
CA2	Carbonic anhydrase enzyme; maintains acid–base balance and adapts to metabolic stress during early embryogenesis.
SH3GL2	Involved in vesicular trafficking and lipid metabolism; associated with reproductive traits and nutrient transport.
FAM13C	Poorly characterized; linked to conditions favorable for embryo development.
Metazoa_SRP	Encodes signal recognition particle RNA; limited evidence supporting a direct role in embryogenesis.

The transcripts listed here increased significantly in abundance when comparing embryos obtained in the warm versus cold season (direction as indicated by the dataset), yet current literature does not assign them a primary, validated role in early embryogenesis or reproductive biology. Many encode factors that respond to systemic or environmental stressors-including xenobiotic-metabolism regulators (NR1I3), hypoxia-responsive proteins (MAGED2, EVA1C), and acid–base homeostasis enzymes (CA2)-suggesting that seasonal shifts in maternal physiology may be relayed to the embryo through metabolic and stress-adaptation pathways rather than through direct developmental cues. Others participate broadly in immunity (IGHM, LAPTM5), nucleotide salvage (HPRT1), lipid handling (CYP4V2, SH3GL2), or chromatin regulation (FOSB, FOXA1, ZBBX), but their contribution to embryo fitness remains speculative. The collective up-regulation of this diverse gene set may therefore reflect indirect adjustments to ambient temperature, photoperiod, or associated changes in maternal endocrine and metabolic status. Functional studies will be required to determine whether these expression changes modulate embryo resilience to seasonal stressors or simply mirror maternal systemic adaptations.

4.3.5. Transcriptomic signatures of downregulated genes in embryos

The downregulated transcript set identified in embryos derived from cows exposed to seasonal environmental variation comprised genes involved in mitochondrial respiration, proteostasis, cytoskeletal organization, transcriptional regulation, vesicle trafficking, and metabolic homeostasis. Reduced expression of UQCRC2 and AQP7 suggests potential alterations in mitochondrial ATP production and cellular energy balance. Downregulation of PSMC6 points to modified proteasomal activity and protein turnover, whereas decreased DNAH12 and SYT9 expression may reflect changes in cytoskeletal dynamics and vesicle-mediated communication. Transcriptional and regulatory factors, including ETV5 and BEND4, were also reduced, indicating possible modulation of differentiation-related pathways. Additional transcripts involved in metabolic and stress-response regulation (HAMP, FEM1B, ADRB2) showed decreased abundance, suggesting that seasonal environmental conditions may influence iron metabolism, cell survival signalling, and endocrine responsiveness. The top 25 downregulated genes ranked by log2 fold change are shown in Figure 19-20; full per-gene results (effect size, standard error, p values, and adjusted P) are presented in Supplementary Table S8. The principal genes with established developmental or reproductive relevance are summarized in Table 15, whereas transcripts without validated preimplantation roles in cattle are listed in Table 16.

Table 15. Season-dependent down-regulated genes in bovine embryos with established roles in embryogenesis and reproduction

Gene	***Functional Annotation***
RBMS3	Stabilizes TGF-β pathway mRNAs; regulates cranial neural crest development, pancreatic organogenesis, and microRNA-mediated developmental networks.
UQCRC2	Component of mitochondrial respiratory complex III; essential for ATP production and embryonic cell viability.
PSMC6	Involved in proteasomal degradation; regulates cell cycle, immune responses, and implantation during early development.
DNAH12	Axonemal dynein heavy chain; contributes to cytoskeletal architecture and embryonic morphogenesis.

ETV5	Transcription factor governing epiblast specification, lipid metabolism, and embryo implantation processes.
SYT9	Calcium sensor required for vesicle exocytosis; critical for cellular communication and embryonic viability.
FSD1L	Potential regulator of epigenetic reprogramming and metabolic adaptation during early embryogenesis; associated with reproductive maturation.
BEND4	Modulates chromatin architecture and germ cell differentiation during early embryonic stages.
AQP7	Aquaglyceroporin facilitating water and glycerol transport; supports preimplantation embryo metabolism and homeostasis.
FEM1B	Regulates cell growth and differentiation; contributes to oocyte development and embryogenesis.
HAMP	Hormonal regulator of iron metabolism; ensures iron availability for hematopoiesis and oxidative stress defense in embryos.

Table 15. The genes listed here were identified as differentially expressed transcripts in bovine embryos and are implicated in essential developmental pathways. Several encode key regulators of metabolism and energy balance (UQCRC2, AQP7, HAMP), ensuring adequate ATP production, nutrient transport, and iron homeostasis critical for rapid cellular proliferation. Transcripts involved in cytoskeletal organization and morphogenesis (DNAH12) or vesicle-mediated communication (SYT9) highlight the orchestration of intracellular trafficking and structural integrity during cleavage and implantation. Factors such as RBMS3 and FSD1L participate in stabilizing mRNA networks and epigenetic programming, underscoring their importance for lineage specification and adaptive responses to environmental cues. Transcriptional modulators (ETV5, BEND4) further govern early differentiation events and germ cell maturation. Additionally, components of proteasomal degradation and cell cycle regulation (PSMC6, FEM1B) reflect dynamic turnover and precise control of embryonic protein homeostasis. Together, these expression profiles provide insight into the molecular mechanisms driving preimplantation development and reveal potential pathways sensitive to maternal or environmental influences on embryonic competence.

Table 16. Season-dependent down-regulated genes in bovine embryos lacking documented roles in embryogenesis or reproduction

Gene	*Functional Annotation*
ADRB2	β2-adrenergic receptor; mediates stress hormone signaling affecting reproductive tissues; potential role in stress-related embryonic responses.
DOCK8	Involved in cytoskeletal rearrangement and immune signaling; indirect role in embryogenesis via immunomodulation.
FBXO48	Ubiquitin ligase subunit controlling AMPKα turnover; no direct embryonic role established, but linked to metabolic regulation.
CDSN	Cornified envelope component; supports epithelial proliferation and adhesion, mainly relevant to placental and tissue remodeling.
ABCC3	ATP-binding cassette transporter; facilitates detoxification and placental xenobiotic transfer; embryonic functions unconfirmed.
ZNF845	Zinc finger transcription factor implicated in cell differentiation in cnidarians; no characterized function in mammalian embryogenesis.

Table 16 The genes listed here were detected as differentially expressed transcripts in the analyzed embryos but lack well-established functions directly supporting mammalian embryogenesis. Some, such as ADRB2 and DOCK8, may indirectly influence early development through modulation of stress signaling or immune pathways potentially affecting reproductive tissues and maternal–embryo interactions. Other transcripts (FBXO48, ABCC3) are primarily involved in cellular metabolism or detoxification processes, suggesting ancillary roles in maintaining tissue homeostasis during gestation. CDSN, while critical for epithelial proliferation and placental remodeling, does not have a clearly defined role in preimplantation embryos. Finally, ZNF845 has been characterized in invertebrate developmental systems without known functions in bovine or mammalian embryogenesis. Overall, while these genes may contribute to broader physiological processes surrounding reproduction, their specific relevance to early bovine embryonic development requires further investigation.

4.3.6. Biological gene networks and pathways analysis of RNA-seq upregulated and downregulated genes related to different seasons using Cytoscape ClueGo

4.3.6.1.Identification of RNA-seq upregulated target genes associated with GO Biological Processes and KEGG pathways related to seasonal variations in Polish HF cow (Gene ontology and pathway enrichment analysis):

ClueGO GO/KEGG enrichment for the summer–spring contrast (Bonferroni step-down, adjusted $p < 0.05$; kappa ≥ 0.3) was performed using the 12,752 tested gene transcripts as the background universe and term redundancy controlled by kappa grouping. ClueGO analysis identified 124 GO/pathway-specific terms associated with upregulated genes related to seasonal variation. Most enriched terms include: *dipeptide transmembrane transport*, *positive regulation of dipeptide transmembrane transport*, *regulation of dipeptide transmembrane transport*, *positive regulation of oligopeptide transport*, *branched-chain amino acid metabolic process*, *isoleucine metabolic process*, *leucine metabolic process*, *valine metabolic process*, *fatty acid omega-oxidation*, *retrograde trans-synaptic signaling by neuropeptide*, *axon regeneration*, *rhombomere morphogenesis*, *intracellular estrogen receptor signaling pathway*, and *positive regulation of intracellular estrogen receptor signaling pathway*.

The identified significant upregulated terms were primarily concentrated in peptide and amino acid transport, branched-chain amino acid metabolism, oxidative metabolism, neurodevelopmental signaling, morphogenesis, and steroid hormone receptor–mediated pathways, indicating that seasonal variation is associated with coordinated alterations in metabolic regulation, neuronal processes, and hormone-dependent signaling in bovine embryos.

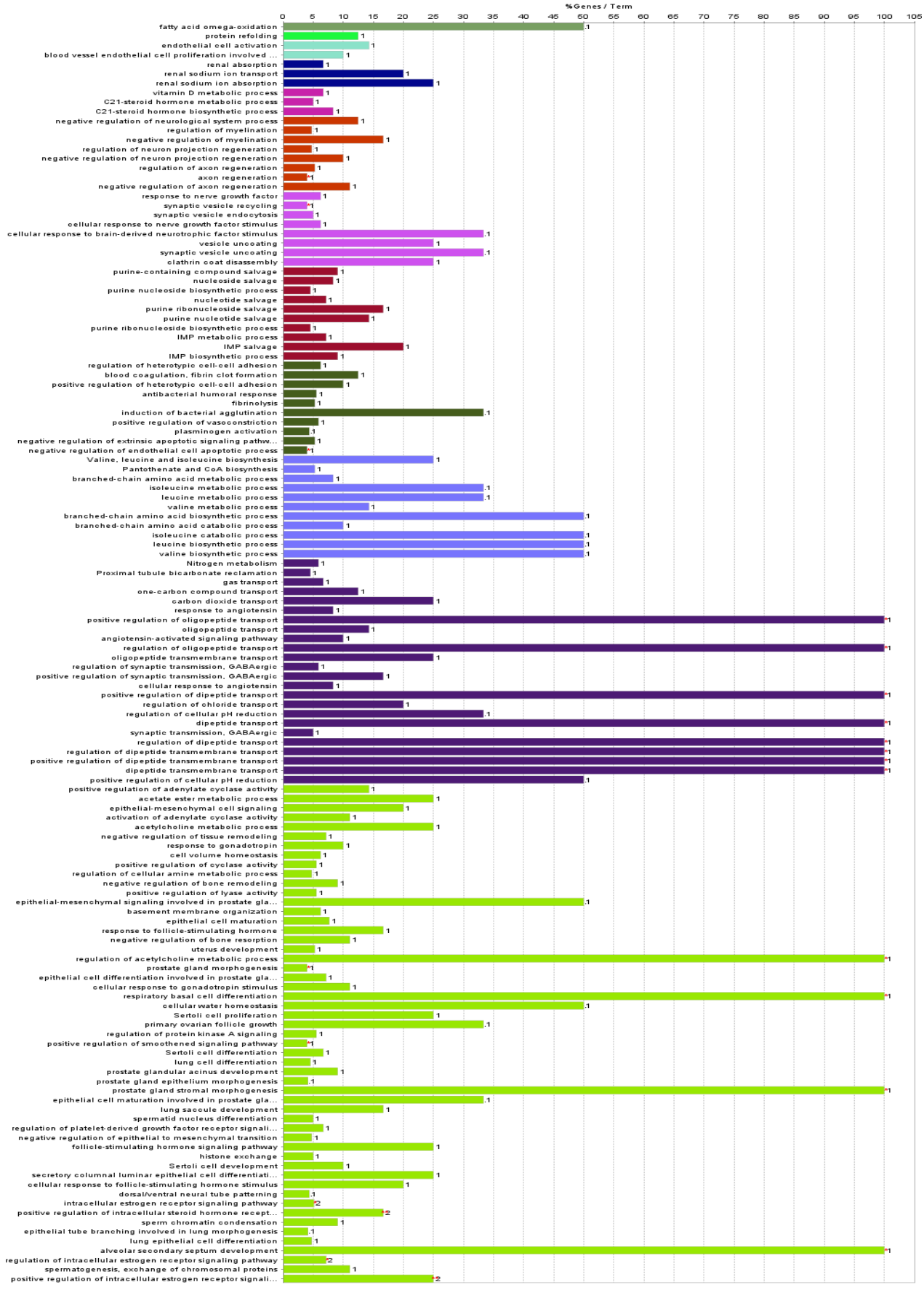
%Genes / Term
0 5 10 15 20 25 30 35 40 45 50 55 60 65 70 75 80 85 90 95 100 105
fatty acid omega-oxidation
protein refolding
endothelial cell activation
blood vessel endothelial cell proliferation involved ...
renal absorption
renal sodium ion transport
renal sodium ion absorption
vitamin D metabolic process
C21-steroid hormone metabolic process
C21-steroid hormone biosynthetic process
negative regulation of neurological system process
regulation of myelination
negative regulation of myelination
regulation of neuron projection regeneration
negative regulation of neuron projection regeneration
regulation of axon regeneration
axon regeneration
negative regulation of axon regeneration
response to nerve growth factor
synaptic vesicle recycling
synaptic vesicle endocytosis
cellular response to nerve growth factor stimulus
cellular response to brain-derived neurotrophic factor stimulus
vesicle uncoating
synaptic vesicle uncoating
clathrin coat disassembly
purine-containing compound salvage
nucleoside salvage
purine nucleoside biosynthetic process
nucleotide salvage
purine ribonucleoside salvage
purine nucleotide salvage
purine ribonucleoside biosynthetic process
IMP metabolic process
IMP salvage
IMP biosynthetic process
regulation of heterotypic cell-cell adhesion
blood coagulation, fibrin clot formation
positive regulation of heterotypic cell-cell adhesion
antibacterial humoral response
fibrinolysis
induction of bacterial agglutination
positive regulation of vasoconstriction
plasminogen activation
negative regulation of extrinsic apoptotic signaling pathw...
negative regulation of endothelial cell apoptotic process
Valine, leucine and isoleucine biosynthesis
Pantothenate and CoA biosynthesis
branched-chain amino acid metabolic process
isoleucine metabolic process
leucine metabolic process
valine metabolic process
branched-chain amino acid biosynthetic process
branched-chain amino acid catabolic process
isoleucine catabolic process
leucine biosynthetic process
valine biosynthetic process
Nitrogen metabolism
Proximal tubule bicarbonate reclamation
gas transport
one-carbon compound transport
carbon dioxide transport
response to angiotensin
positive regulation of oligopeptide transport
oligopeptide transport
angiotensin-activated signaling pathway
regulation of oligopeptide transport
oligopeptide transmembrane transport
regulation of synaptic transmission, GABAergic
positive regulation of synaptic transmission, GABAergic
cellular response to angiotensin
positive regulation of dipeptide transport
regulation of chloride transport
regulation of cellular pH reduction
dipeptide transport
synaptic transmission, GABAergic
regulation of dipeptide transport
regulation of dipeptide transmembrane transport
positive regulation of dipeptide transmembrane transport
dipeptide transmembrane transport
positive regulation of cellular pH reduction
positive regulation of adenylate cyclase activity
acetate ester metabolic process
epithelial-mesenchymal cell signaling
activation of adenylate cyclase activity
acetylcholine metabolic process
negative regulation of tissue remodeling
response to gonadotropin
cell volume homeostasis
positive regulation of cyclase activity
regulation of cellular amine metabolic process
negative regulation of bone remodeling
positive regulation of lyase activity
epithelial-mesenchymal signaling involved in prostate gla...
basement membrane organization
epithelial cell maturation
response to follicle-stimulating hormone
negative regulation of bone resorption
uterus development
regulation of acetylcholine metabolic process
prostate gland morphogenesis
epithelial cell differentiation involved in prostate gla...
cellular response to gonadotropin stimulus
respiratory basal cell differentiation
cellular water homeostasis
Sertoli cell proliferation
primary ovarian follicle growth
regulation of protein kinase A signaling
positive regulation of smoothened signaling pathway
Sertoli cell differentiation
lung cell differentiation
prostate glandular acinus development
prostate gland epithelium morphogenesis
prostate gland stromal morphogenesis
epithelial cell maturation involved in prostate gla...
lung saccule development
spermatid nucleus differentiation
regulation of platelet-derived growth factor receptor signali...
negative regulation of epithelial to mesenchymal transition
follicle-stimulating hormone signaling pathway
histone exchange
Sertoli cell development
secretory columnal luminar epithelial cell differentiati...
cellular response to follicle-stimulating hormone stimulus
dorsal/ventral neural tube patterning
intracellular estrogen receptor signaling pathway
positive regulation of intracellular steroid hormone recept...
sperm chromatin condensation
epithelial tube branching involved in lung morphogenesis
lung epithelial cell differentiation
alveolar secondary septum development
regulation of intracellular estrogen receptor signaling pathway
spermatogenesis, exchange of chromosomal proteins
positive regulation of intracellular estrogen receptor signali...

Figure 21. Gene Ontology (GO) Biological Process and KEGG pathway enrichment analysis of genes significantly upregulated in bovine embryos derived from cows of different seasons, performed using ClueGO. The bar plot illustrates enriched GO terms and KEGG pathways, with bar length proportional to the number of genes associated with each term. The x-axis represents the percentage of genes annotated to a given term within the input gene set, while numbers at the end of each bar indicate the absolute number of associated genes. Functionally related terms are grouped and color-coded according to shared biological categories. The analysis reveals season-associated upregulation of key biological processes, including developmental pathways (e.g., lung and forebrain development, urogenital system development), immune signaling, lipid metabolism, synaptic transmission, and peptide transport, highlighting molecular pathways potentially linked to physiological aging in cattle.

4.3.6.2. Identification of functional groups affected by upregulated target genes related to the seasonal variations in Polish HF cow.

ClueGO analysis identified 12 functional groups enriched among the upregulated RNA-seq target genes affected by seasonal variation (Figure 22). The most represented biological process was positive regulation of the *intracellular estrogen receptor signaling pathway (39.55%)*, indicating a strong involvement of hormone-dependent regulatory mechanisms. Other highly represented clusters included *dipeptide transmembrane transport (17.91%), isoleucine catabolic process (8.21%), and purine nucleoside biosynthetic process (7.46%)*, suggesting enhanced metabolic activity and substrate transport. Processes related to neuronal and cellular regulation were also identified, including *synaptic vesicle recycling (5.97%)*, *axon regeneration (5.97%)*, and *negative regulation of endothelial cell apoptotic process (7.46%).* Smaller clusters were associated with *C21-steroid hormone metabolic process (2.24%), renal sodium ion absorption (2.24%), endothelial cell activation (1.49%), protein refolding (0.75%), and fatty acid omega-oxidation (0.75%)*. Altogether, the identified functional groups indicate that seasonal upregulation of genes in bovine embryos is primarily associated with intracellular hormone signaling, metabolite transport, amino acid catabolism, and cellular regulatory processes.

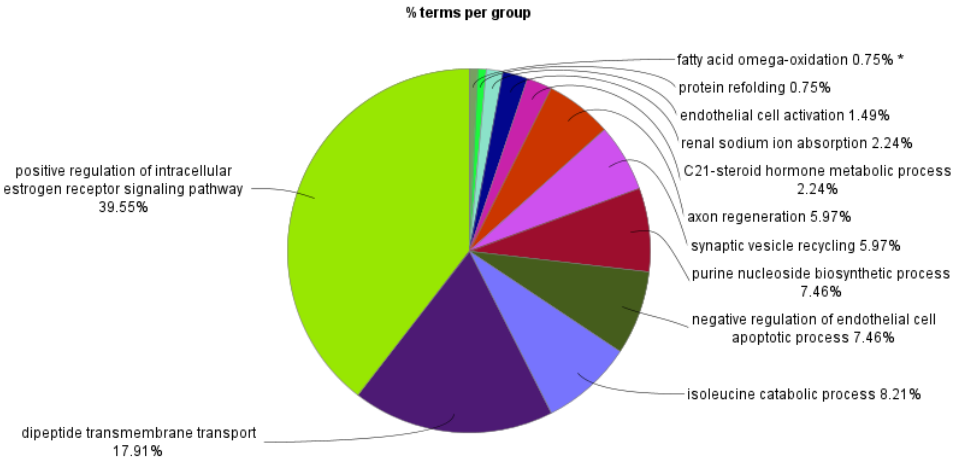

Figure 22. ClueGO pie chart of GO Biological Process and KEGG pathway enrichment for season-associated upregulated genes in bovine embryos.
Pie chart illustrating the distribution of significantly enriched Gene Ontology (GO) Biological Process terms and KEGG pathways identified by ClueGO among RNA-seq target genes upregulated in response to seasonal variation. Each slice represents an enriched functional term, expressed as a percentage of the total identified terms. The most prominent category was positive regulation of intracellular estrogen receptor signaling pathway (39.55%), followed by dipeptide transmembrane transport (17.91%), isoleucine catabolic process (8.21%), and purine nucleoside biosynthetic process (7.46%). Additional enriched processes included negative regulation of endothelial cell apoptotic process (7.46%), synaptic vesicle recycling (5.97%), axon regeneration (5.97%), C21-steroid hormone metabolic process (2.24%), renal sodium ion absorption (2.24%), endothelial cell activation (1.49%), protein refolding (0.75%), and fatty acid omega-oxidation (0.75%). Asterisks (*) indicate statistically significant enrichment after multiple testing correction. Functional groups are color-coded according to biological similarity. Overall, the enrichment analysis indicates that seasonal upregulation of genes in bovine embryos is primarily associated with intracellular hormone signaling, metabolite transport, amino acid catabolism, and cellular regulatory mechanisms.

The pie chart illustrates the percentage distribution of significantly enriched Gene Ontology (GO) biological process terms identified using ClueGO among RNA-seq target genes upregulated in response to seasonal variation. Each slice represents a functional group of GO terms, with the proportion calculated based on the total number of enriched terms. The enriched categories include: fatty acid omega-oxidation (0.75%*), protein refolding (0.75%), endothelial cell activation (1.49%), renal sodium ion absorption (2.24%), C21-steroid hormone metabolic process (2.24%), axon regeneration (5.97%), synaptic vesicle recycling (5.97%), purine nucleoside biosynthetic process (7.46%), negative regulation of endothelial cell apoptotic process (7.46%), isoleucine catabolic process (8.21%), dipeptide transmembrane transport (17.91%), and positive regulation of intracellular estrogen receptor signaling pathway (39.55%). Functional groups are color-coded, and categories marked with an asterisk (*) indicate statistically significant enrichment after correction for multiple testing. This analysis highlights key biological processes involved in hormonal signaling, transport, metabolism, neuroregeneration, and vascular regulation.

4.3.6.3. Identification of RNA-seq downregulated target genes associated with GO Biological Processes and KEGG pathways related to seasonal variations in Polish HF cow (Gene ontology and pathway enrichment analysis)

ClueGO GO/KEGG enrichment for the summer vs spring contrast (Bonferroni step-down, adjusted $p < 0.05$; kappa ≥ 0.3) was performed using the 12,752 tested gene transcripts as the background universe and term redundancy controlled by kappa grouping. ClueGO analysis identified 80 GO/pathway-specific terms associated with downregulated genes related to seasonal variation.

The most represented terms based on the highest percentage of genes per term included *negative regulation of ion transmembrane transport*, *negative regulation of iron ion transport*, *mini excitatory postsynaptic potential*, *positive regulation of mini excitatory postsynaptic potential*, *positive regulation of establishment of T cell polarity*, and *regulation of oligopeptide transport*. Additional highly represented terms included *positive regulation of dipeptide transport*, *dipeptide transport*, *regulation of dipeptide transmembrane transport*, and *desensitization of G-protein coupled receptor protein signaling pathway*.

Overall, the enrichment profile of the longest bars indicates that seasonal downregulation predominantly affected ion transport regulation, excitatory postsynaptic signaling, peptide transport mechanisms, and immune-related polarity and signaling processes in bovine embryos.

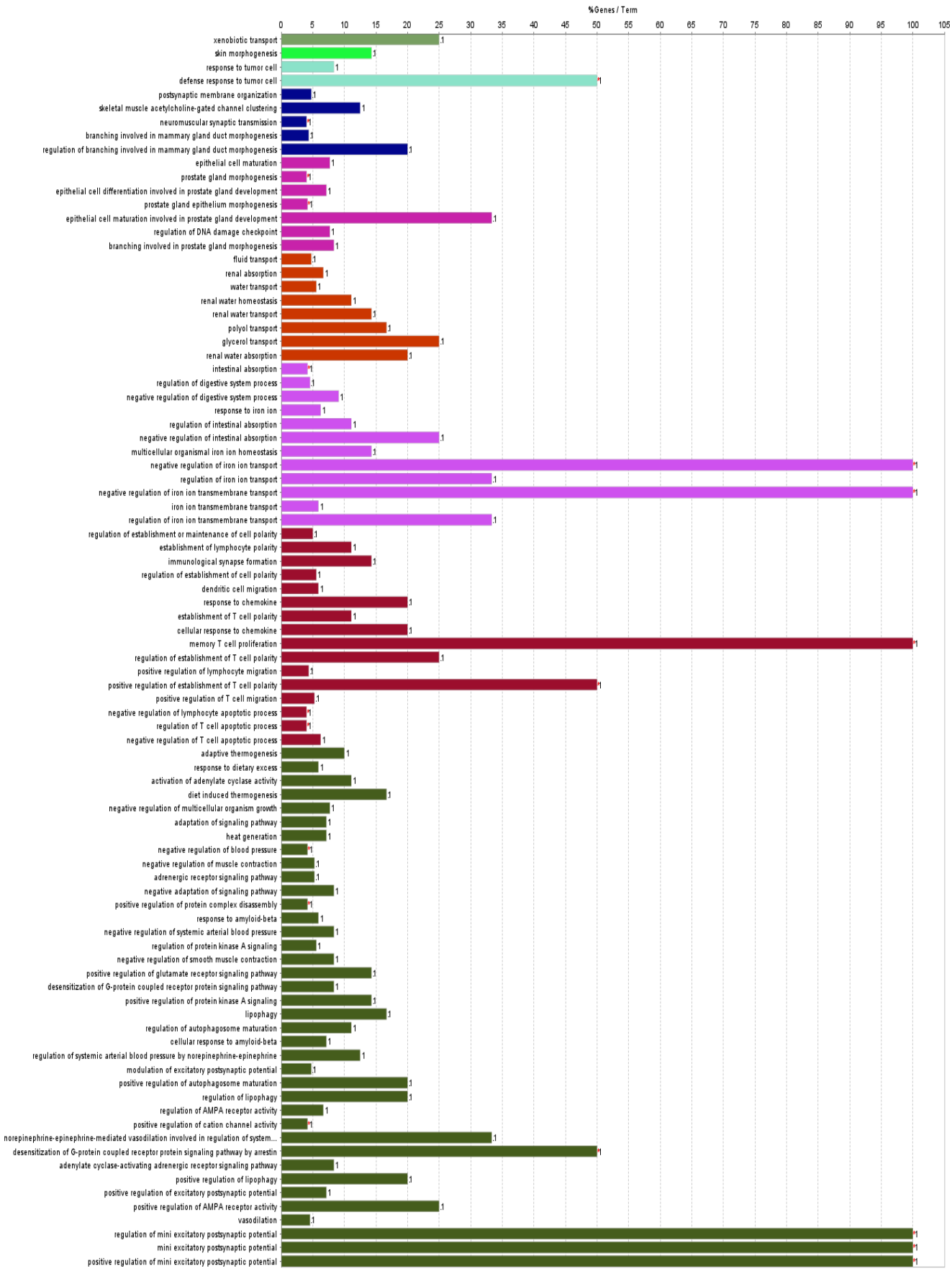
%Genes / Term
0 5 10 15 20 25 30 35 40 45 50 55 60 65 70 75 80 85 90 95 100 105
xenobiotic transport
skin morphogenesis
response to tumor cell
defense response to tumor cell
postsynaptic membrane organization
skeletal muscle acetylcholine-gated channel clustering
neuromuscular synaptic transmission
branching involved in mammary gland duct morphogenesis
regulation of branching involved in mammary gland duct morphogenesis
epithelial cell maturation
prostate gland morphogenesis
epithelial cell differentiation involved in prostate gland development
prostate gland epithelium morphogenesis
epithelial cell maturation involved in prostate gland development
regulation of DNA damage checkpoint
branching involved in prostate gland morphogenesis
fluid transport
renal absorption
water transport
renal water homeostasis
renal water transport
polyol transport
glycerol transport
renal water absorption
intestinal absorption
regulation of digestive system process
negative regulation of digestive system process
response to iron ion
regulation of intestinal absorption
negative regulation of intestinal absorption
multicellular organismal iron ion homeostasis
negative regulation of iron ion transport
regulation of iron ion transport
negative regulation of iron ion transmembrane transport
iron ion transmembrane transport
regulation of iron ion transmembrane transport
regulation of establishment or maintenance of cell polarity
establishment of lymphocyte polarity
immunological synapse formation
regulation of establishment of cell polarity
dendritic cell migration
response to chemokine
establishment of T cell polarity
cellular response to chemokine
memory T cell proliferation
regulation of establishment of T cell polarity
positive regulation of lymphocyte migration
positive regulation of establishment of T cell polarity
positive regulation of T cell migration
negative regulation of lymphocyte apoptotic process
regulation of T cell apoptotic process
negative regulation of T cell apoptotic process
adaptive thermogenesis
response to dietary excess
activation of adenylate cyclase activity
diet induced thermogenesis
negative regulation of multicellular organism growth
adaptation of signaling pathway
heat generation
negative regulation of blood pressure
negative regulation of muscle contraction
adrenergic receptor signaling pathway
negative adaptation of signaling pathway
positive regulation of protein complex disassembly
response to amyloid-beta
negative regulation of systemic arterial blood pressure
regulation of protein kinase A signaling
negative regulation of smooth muscle contraction
positive regulation of glutamate receptor signaling pathway
desensitization of G-protein coupled receptor protein signaling pathway
positive regulation of protein kinase A signaling
lipophagy
regulation of autophagosome maturation
cellular response to amyloid-beta
regulation of systemic arterial blood pressure by norepinephrine-epinephrine
modulation of excitatory postsynaptic potential
positive regulation of autophagosome maturation
regulation of lipophagy
regulation of AMPA receptor activity
positive regulation of cation channel activity
norepinephrine-epinephrine-mediated vasodilation involved in regulation of system...
desensitization of G-protein coupled receptor protein signaling pathway by arrestin
adenylate cyclase-activating adrenergic receptor signaling pathway
positive regulation of lipophagy
positive regulation of excitatory postsynaptic potential
positive regulation of AMPA receptor activity
vasodilation
regulation of mini excitatory postsynaptic potential
mini excitatory postsynaptic potential
positive regulation of mini excitatory postsynaptic potential

Figure 23. ClueGO Gene Ontology (GO) enrichment analysis of season-associated downregulated genes in bovine embryos. ClueGO-based GO Biological Process enrichment analysis of RNA-seq target genes significantly downregulated in bovine embryos in association with seasonal variation. The bar chart displays enriched GO terms, with bar length representing the percentage of genes assigned to each term (% Genes / Term). The most represented categories are related to regulation of ion transmembrane transport, excitatory postsynaptic potential, peptide transport, immune cell polarity, and G-protein coupled receptor signaling processes.

Bar chart displaying significantly enriched GO biological process terms among RNA-seq target genes downregulated with seasonal variation in cattle, as identified using ClueGO. The y-axis lists the enriched GO terms, while the x-axis represents the percentage of genes in the input set annotated to each term (% Genes / Term). Numbers at the end of each bar indicate the gene count per term, and terms are color-coded according to functional grouping. Notable enriched terms include *negative regulation of ion transmembrane transport*, *negative regulation of iron ion transport*, *memory T cell proliferation*, *mini excitatory postsynaptic potential*, *positive regulation of mini excitatory postsynaptic potential*, and *positive regulation of establishment of T cell polarity*. These results indicate that seasonal downregulation predominantly affects ion transport regulation, excitatory postsynaptic signaling, and immune-related polarity processes in bovine embryos.

4.3.6.4. Identification of functional groups affected by downregulated target genes related to the seasonal variations in Polish HF cow

ClueGO analysis identified 9 functional groups (Figure 24) and 9 metabolic pathways (Supplementary Figure 6) for the down regulated RNA-seq target genes affected by season (Figure 24): namely: xenobiotic transport (1.11%), skin morphogenesis (1.11%), defense response to tumor cell (2.22%), neuromuscular synaptic transmission (5.56%), prostate gland morphogenesis (7.78%), glycerol transport (8.89%), negative regulation of iron ion transport (13.33%), negative regulation of lymphocyte apoptotic process (17.78%), and regulation of mini excitatory postsynaptic potential (42.22%).

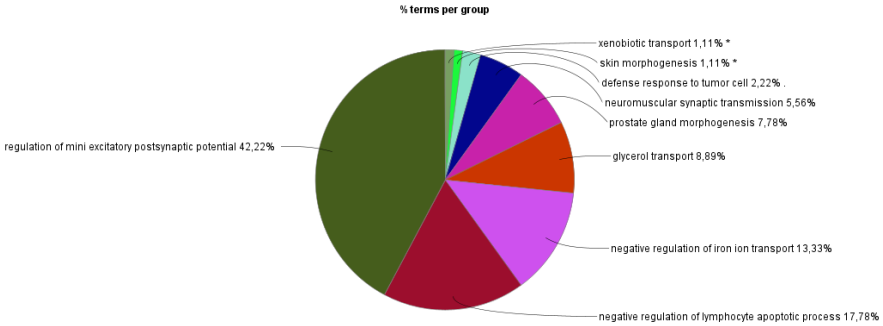

Figure 24. ClueGO pie chart showing GO biological process and KEGG pathway enrichment of RNA-seq downregulated target genes associated with seasonal variation.

Pie chart illustrating the proportional distribution of significantly enriched Gene Ontology (GO) biological process terms and KEGG pathways among RNA-seq target genes downregulated with seasonal variation in cattle, identified using ClueGO. Each slice represents a functional group, with its proportion expressed as a percentage of the total number of enriched terms. Dominant categories include: xenobiotic transport (1.11%*), skin morphogenesis (1.11%*), defense response to tumor cell (2.22%), neuromuscular synaptic transmission (5.56%), prostate gland morphogenesis (7.78%), glycerol transport (8.89%), negative regulation of iron ion transport (13.33%), negative regulation of lymphocyte apoptotic process (17.78%), and regulation of mini excitatory postsynaptic potential (42.22%). Terms marked with an asterisk (*) are statistically significant after multiple testing corrections. Color coding represents functionally grouped biological processes and pathways. This analysis highlights season-associated downregulation of pathways linked to cellular signaling, immune function, development, and environmental response in cattle.

4.4. Deconvolution

Deconvolution-based analyses revealed clear, stage-dependent transcriptional patterns across bovine preimplantation development and provided insight into the relative contribution of developmental-stage–specific transcriptional signatures within whole-embryo RNA-seq profiles.

Expression profiling of selected developmentally relevant marker genes (Figure 25) demonstrated pronounced differences across preimplantation stages, confirming strong stage specificity of key regulatory pathways. Genes associated with steroidogenesis and metabolic regulation (*CYP11A1*) showed minimal expression during early cleavage stages and markedly increased expression at the morula and late blastocyst stages. In contrast, AKT2 displayed a gradual increase in expression beginning at the 2-cell stage and continuing toward the late blastocyst, consistent with its role in cell survival, proliferation, and metabolic regulation during rapid embryonic divisions. *UQCRC2* exhibited high expression at the morula and late blastocyst stages, reflecting increased mitochondrial activity and energy demand associated with compaction and differentiation. *CXCR4* expression emerged predominantly at later stages, indicating involvement in cell signaling and lineage allocation, whereas BMPER showed generally low expression during early cleavage with increased prominence at the zygote and late blastocyst stages, suggesting a regulatory role in BMP signaling during embryonic patterning.

Hierarchical clustering based on both the design matrix and MuSiC-derived mean relative abundance values (Figure 26) consistently separated early developmental stages (oocyte, zygote, 2-cell, and 4-cell) from later stages (8-cell, morula, and late blastocyst). This separation reflects high transcriptional similarity within early-stage embryos and progressive divergence of gene expression profiles as development advances. These results provided a rationale for grouping developmental stages into broader categories for subsequent deconvolution analyses. UMAP visualization further supported this stage-based structure (Figure 27), revealing well-defined clusters corresponding to late blastocyst, morula, 8-cell stage, and a combined early-stage group. The clear spatial separation of clusters indicates robust stage-specific transcriptional programs and validates the categorization strategy used for downstream deconvolution-based comparisons.

Analysis of marker gene overlap using a Venn diagram (Figure 28) demonstrated that the majority of marker genes were unique to individual developmental stages. The highest number of stage-specific markers was observed for the 8-cell stage and for the combined early-stage

group, followed by morula and late blastocyst. Only minimal overlap was detected between clusters, underscoring the dynamic and tightly regulated nature of transcriptomic transitions during preimplantation development.

Application of the MuSiC algorithm enabled estimation of developmental-stage–specific transcriptional contributions within bulk RNA-seq profiles of individual embryos (Figure 29). Heatmap visualization indicated that transcriptional signatures characteristic of the late blastocyst stage predominated across all analyzed samples. Contributions from early developmental stages were detectable at low levels in several embryos, whereas 8-cell and morula signatures were largely absent. This pattern suggests that whole-embryo transcriptomes are strongly influenced by later-stage gene expression programs, potentially reflecting increased transcriptional activity and biological dominance of late-stage regulatory processes in bulk RNA-seq data.

Results obtained using the DeTREM algorithm showed overall concordance with MuSiC-based estimates (Figure 30), particularly with respect to the predominance of late blastocyst–associated transcriptional signatures. However, DeTREM detected slightly stronger low-level contributions from early developmental stages and the 8-cell stage in a subset of samples. These differences likely reflect methodological distinctions between algorithms and differences in sensitivity to subtle transcriptional variation.

Collectively, deconvolution-inspired analyses demonstrated that bovine preimplantation development is characterized by distinct, stage-specific gene expression programs, with whole-embryo transcriptomes largely dominated by signatures of later developmental stages. These findings provide a coherent framework for interpreting transcriptomic variability across embryos and establish a robust basis for subsequent analyses examining the effects of maternal age and seasonal conditions on embryonic gene expression.

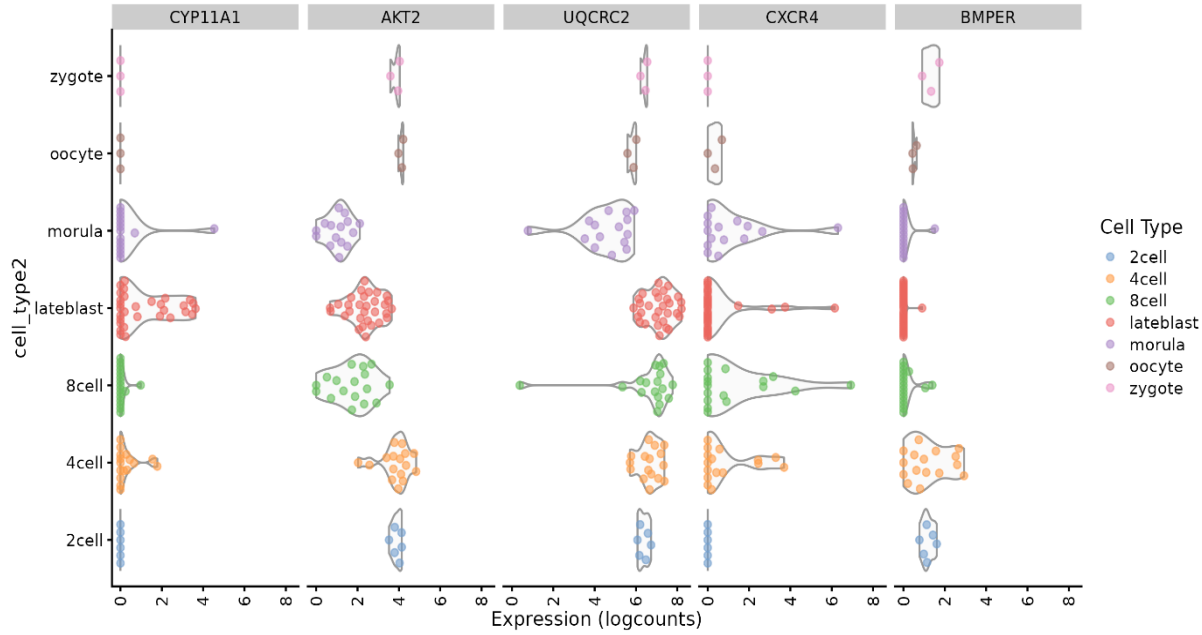

Figure 25. Expression profiles of five developmentally relevant genes during bovine preimplantation stages. The violin plot illustrates the expression profiles of CYP11A1, AKT2, UQCRC2, CXCR4, and BMPER during bovine preimplantation development, from oocyte to late blastocyst.

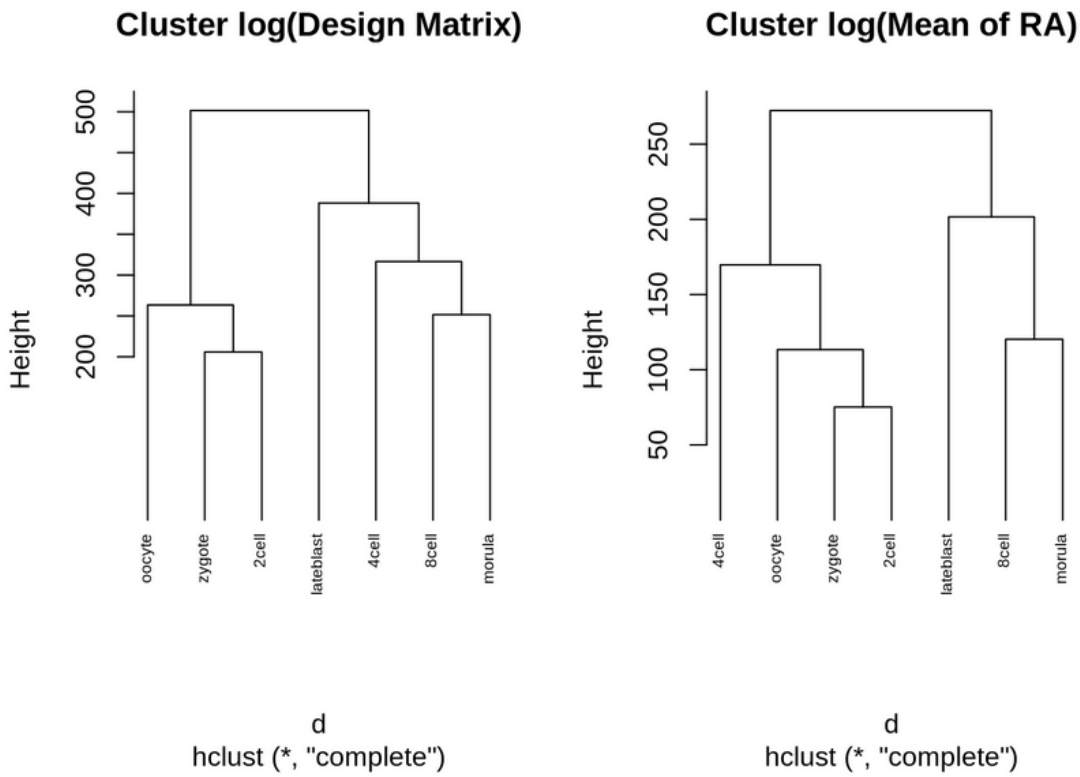

Figure 26. MuSiC dendrograms visualizing hierarchical clustering of bovine preimplantation embryos based on the design matrix (left) and the mean relative abundance (right) following group revision. The dendrograms showing hierarchical clustering of developmental stage structure (left) and MuSiC-derived mean relative abundance across bovine preimplantation embryos (right). The left panel presents clustering based on the design matrix of gene expression, while the right panel depicts the clustering based on the mean relative abundance (RA). Both approaches consistently demonstrate the separation of early developmental stages (oocyte, zygote, 2-cell, 4-cell), from later stages (8-cell, morula, late blastocyst), reflecting transcriptional similarities within these groups. The clustering results served as the basis for grouping developmental stages into broader categories for deconvolution analysis.

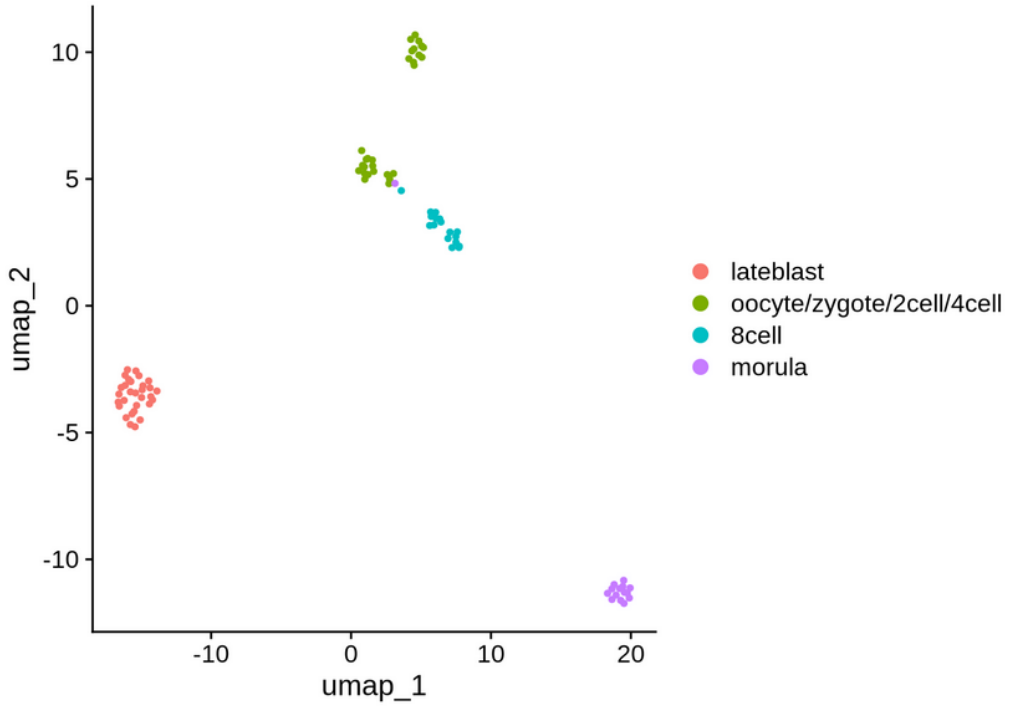

Figure 27. UMAP visualization of RNA-seq samples across developmental stages

The Uniform Manifold Approximation and Projection (UMAP) plot displaying the transcriptional similarity between RNA-seq samples corresponding to distinct developmental stages: late blastocyst (red), morula (purple), 8-cell (blue), and the combined early-stage group comprising oocyte, zygote, 2-cell, and 4-cell (green). The clear separation between clusters indicates consistent stage-specific expression profiles across the samples, validating the categorization strategy applied for further analyses.

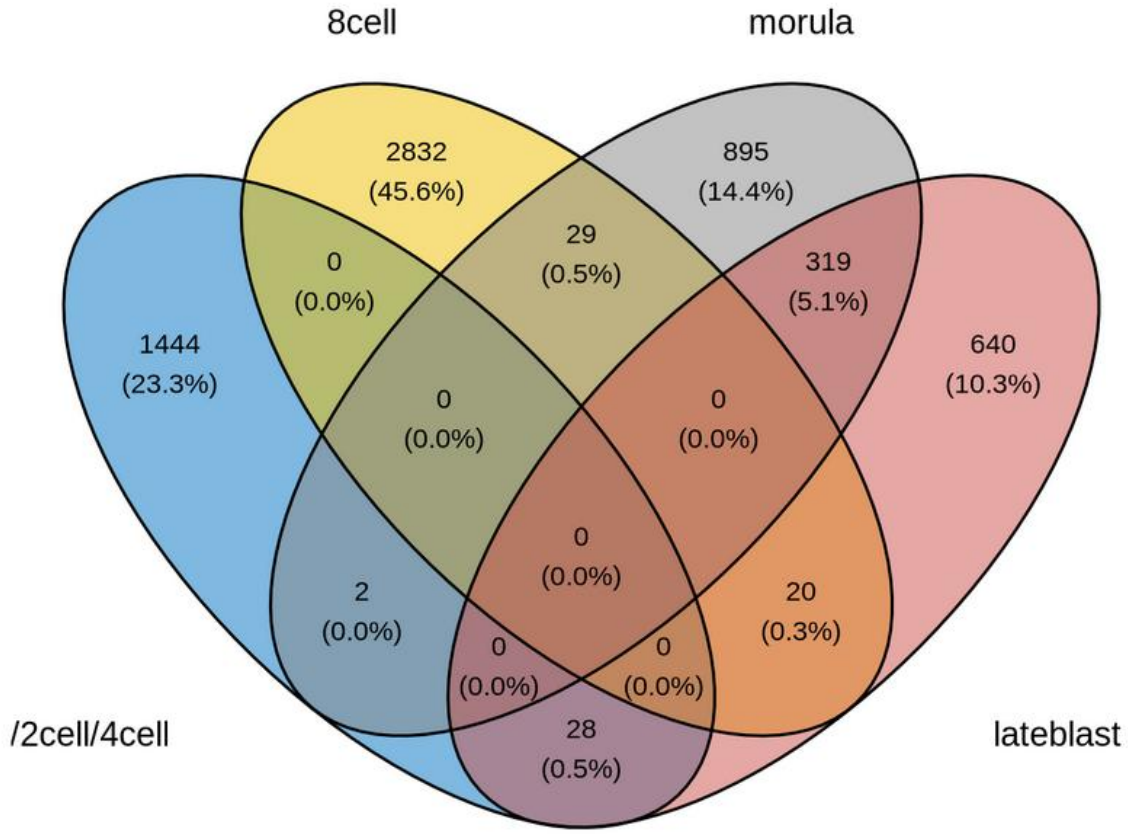

Figure 28. Venn diagram of marker genes assigned to developmental stage clusters

The Venn diagram shows the overlap of marker genes identified for four embryo developmental stages: 8-cell (yellow), morula (grey), late blastocyst (red), and the early-stage group comprising 2-cell/4-cell embryos (blue). Most marker genes exhibit stage specificity, with the majority being unique to the 8-cell stage (2832; 45.6%) and the early-stage group (1444; 23.3%), followed by morula (895; 14.4%) and late blastocyst (640; 10.3%). Only limited overlap was detected between clusters, indicating that each developmental stage is characterized by a distinct gene expression profile.

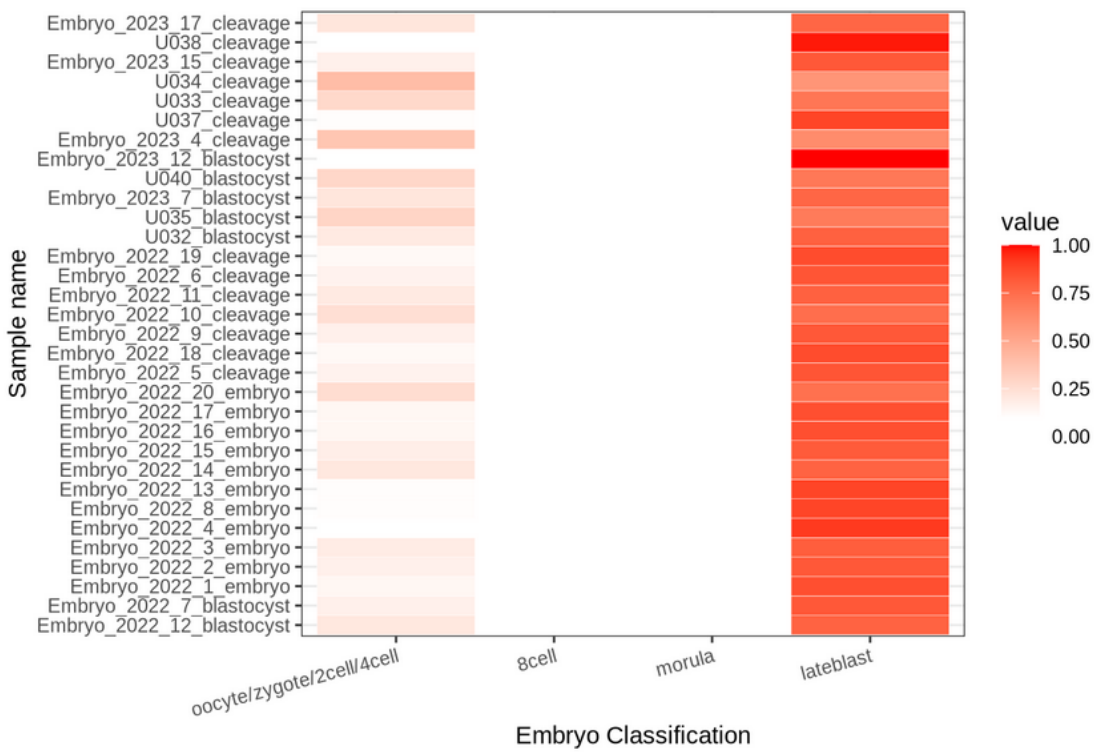

Figure 29. Heatmap of MuSiC-estimated developmental stage contributions across embryo RNA-seq samples.

The heatmap displays the estimated proportions of transcriptional signatures characteristic of four developmental stages - oocyte/zygote/2-cell/4-cell, 8-cell, morula, and late blastocyst - across individual embryo RNA-seq samples. Each row represents one sample, and the color gradient (0–1) reflects the relative abundance of each signature. Late-blastocyst transcriptional profiles dominate all samples, while 8-cell and morula signatures are absent. A faint signal corresponding to the oocyte/zygote/2-cell/4-cell group is detectable in several samples.

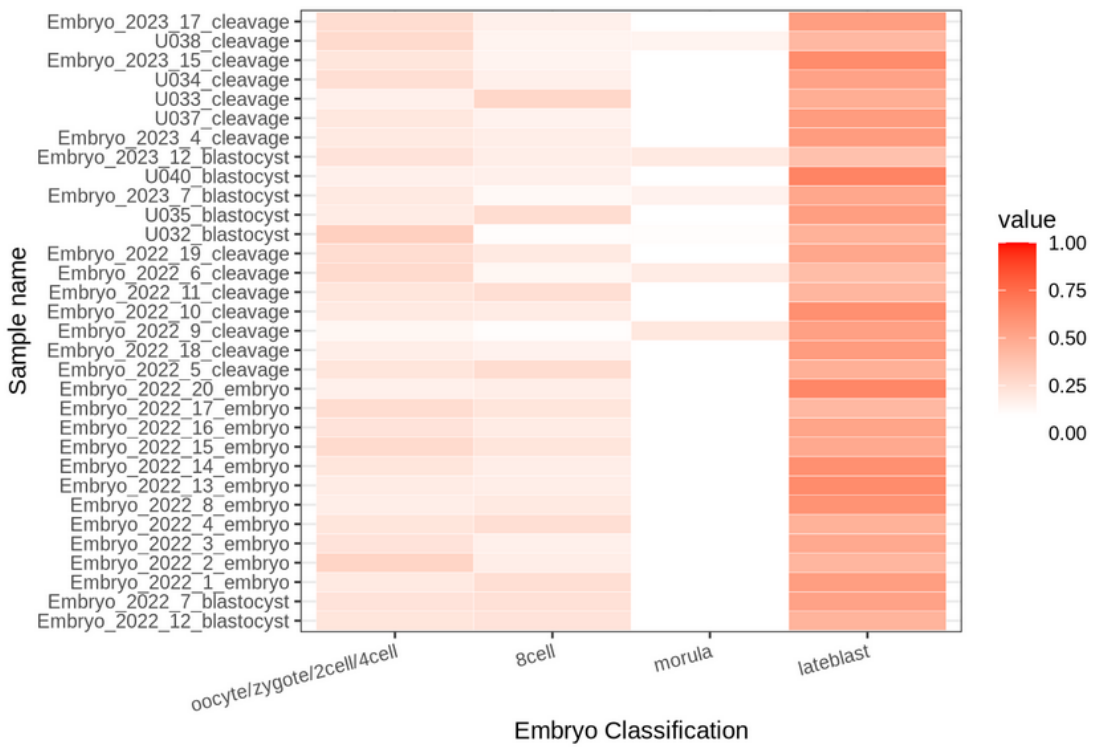

Figure 30. Heatmap of estimated developmental stage proportions in embryo RNA-seq samples using DeTREM

The heatmap displays the estimated proportions of transcriptional signatures characteristic of four developmental stages - oocyte/zygote/2-cell/4-cell, 8-cell, morula, and late blastocyst - across individual embryo RNA-seq samples. Each row represents one sample, and the color gradient (0–1) reflects the relative abundance of each signature. Late-blastocyst transcriptional profiles dominate most samples. Low-level contributions from the oocyte/zygote/2-cell/4-cell group and the 8-cell stage are detectable in several samples, whereas morula signatures are nearly absent.

5. Discussion

5.1. Transcriptome analysis of bovine embryos based on the bulk scRNA-seq experiment (age comparison between young vs older cows)

5.1.1. Age-dependent upregulated genes

In the analysis of upregulated genes, genes were divided according to their function and their previously determined association with embryos or pregnancy quality. First, upregulated genes whose role is associated with embryos from cows of different ages were described. Among the genes important in embryo development, up-expressed in our experiment, is the STAT 4 gene. The STAT protein group consists of 7 proteins that are functionally and structurally related [72]. This group includes: *STAT 1, STAT 2, STAT 3, STAT 4, STAT 5A, STAT 5B, STAT 6* [73]. Studies have shown that STAT 1 and STAT 3 are expressed in oocytes and preimplantation embryos in mice, which suggests that these genes may influence embryo development due to the association of these genes with apoptosis and the cell cycle [74]. Moreover, it has been shown that STAT 3 is necessary for the early survival of embryos, but it is assumed that other proteins from the STAT group may compensate its deficiency [72], especially since studies have shown that STAT proteins they take part in the process of fertilization and initial embryonic development [75]. STAT 4 is an essential component of the IL-12 signaling pathway, which stimulates the production of IFN-γ and supports the development of cellular immunity [76]. Direct studies on the expression of STAT-4 in bovine embryos are limited, therefore the increase in the expression of STAT 4 in bovine cells is puzzling. However, the increase in STAT 4 gene expression in cow embryos may be related to its role in regulating cell differentiation processes and the immune response [77].

The functions of MGP (*Matrix Gla Protein*) include, among others, the regulation of phosphorus and calcium transport [78]. This gene is expressed in embryonic tissues, and it has been suggested that this expression may be associated with cell differentiation and proliferation [79]. It has been shown that the increase in MGP expression at the early stage of bird embryo development may be related to its participation in epithelial-mesenchymal changes [80]. Perhaps the increase in the expression of this gene in the group of younger cows indicates the advancement of these processes and their better expression in this group.

CYP11A1 (*Cytochrome P450 Family 11 Subfamily A Member 1*) gene is crucial in embryonic development due to its role in steroidogenesis, which produces essential steroid hormones from cholesterol [81]. Upregulation of CYP11A1 in trophoblast cells leads to increased production of pregnenolone and progesterone, vital for maintaining pregnancy and supporting fetal development. However, excessive CYP11A1 activity can cause oxidative stress and mitochondrial damage in trophoblasts, potentially impacting fetal development adversely. [82]. The observed increase in CYP11A1 gene expression in embryos from older cows may indicate increased activity of the steroidogenic pathway at the early stage of embryonic development in this group of cows. This may promote the intensification of the production of pregnenolone and progesterone, which is beneficial for maintaining pregnancy and supporting the development of the embryo. However, excessive CYP11A1 activity may be associated with the risk of oxidative stress and mitochondrial damage, which could potentially negatively impact the quality and developmental capacity of embryos. Further research is needed to assess whether the increase in expression of this gene in younger cows has a beneficial or adverse effect on long-term embryo development.

The functions of the CYP4V2 (*Cytochrome P450 Family 4 Subfamily V Member 2*) gene are related to the coding of an enzyme belonging to the cytochrome P450 family, which plays a key role in the biotransformation of endogenous compounds and xenobiotics [83].

During chicken embryo development, the CYP4V2 gene was identified as one of the key proteins with altered abundance at different stages of incubation. Changes in the expression level of this gene indicate its potential involvement in the regulation of metabolic processes, including arachidonic acid metabolism and steroid biosynthesis. Functional analyzes showed that CYP4V2 is associated with important cellular processes such as oxidation-reduction reactions, lipid transport, and binding of iron, heme, and lipid ions. Although this gene has not been directly implicated as a master regulator, its presence among proteins with significant changes in abundance suggests its possible role in the regulation of lipid metabolism and antioxidant response during embryonic development. The obtained results contribute to a better understanding of the mechanisms related to lipid metabolism and the activity of antioxidant enzymes in chicken embryos, and CYP4V2 itself may be a potential marker for assessing the lipid composition and the level of activity of enzymes responsible for protection against oxidative stress [84]. To date, no increase in CYP4V2 gene expression has been demonstrated in bovine embryos, and available data mainly concern other species such as birds. However,

considering its functions in other organisms, it can be assumed that increased expression of CYP4V2 in bovine embryos could influence metabolic processes, especially in the context of regulating lipid metabolism and the response to oxidative stress.

The HPRT1 (*Hypoxanthine Phosphoribosyltransferase 1*) gene plays an important role in purine metabolism, participating in the purine recovery pathway. In the context of embryos, its expression in caprine embryos has been shown to be increased in parthenogenetic embryos, especially at the 2–4 cell stage and at the morula stage in diploid parthenots [85]. The observed increase in HPRT1 gene expression in embryos from older cows may indicate an increased demand for nucleotides associated with more intensive cell division and higher metabolic activity in the initial stages of development. Increased HPRT1 expression may be beneficial to the developmental potential of embryos by supporting efficient nucleic acid synthesis. However, its excessive activity may also indicate a reaction to metabolic stress or compensation for disorders in the nucleotide biosynthetic pathways.

The CCL24 (*C-C motif chemokine ligand 24*) gene encodes a chemokine known as eotaxin-2, which is involved in the recruitment of eosinophils, basophils, and Th2 lymphocytes during inflammatory responses [86]. CCL24 stimulates the proliferation and apoptosis of DSCs (decidual stromal cells); however, it overall increases their number, indicating that the CCL24/CCR3 axis is a beneficial factor supporting the process of decidualization (the physiological process in which cells in the lining of the uterus (endometrium) develop into specialized decidua tissue that supports embryo development and pregnancy) in early pregnancy [87, 88].

The conducted research showed that the CCL24 gene plays an important role in the spatial organization of the inner cell mass (ICM) of bovine embryos. Its expression was clearly higher in the ICM than in the trophectoderm, suggesting its involvement in the regulation of cell migration and distribution in the developing embryo. CCL24 levels increased with blastocyst formation, reaching the highest values on day 7 of development, and then decreased until day 9. Moreover, blocking the action of CCL24 (both via CCR3 receptor antagonists and CCL24-specific morpholino) resulted in a reduction in the number of GATA6+ cells (hypoblast precursors) in the outer parts of the ICM, indicating that this chemokine may influence the proper distribution of cells in the blastocyst [89]. Our studies showed an increase in CCL24 expression in embryos from older cows, suggesting that the age of the oocyte donor may influence the level of this chemokine. This may mean that CCL24 plays a role in molecular

mechanisms related to embryo quality and implantation potential, and its level may be modulated by environmental and physiological factors dependent on maternal age.

The PDE gene superfamily is divided into 11 families that influence cAMP and cGMP. PDE10 affects cAMP more and is mainly associated with neurological disorders, which is why this gene is mainly studied in the brain [90]. Scientists have demonstrated an increase in phosphodiesterase 10A (PDE10A) gene expression in bovine testes, primary spermatocytes and spermatids [90]. Additionally, PDE10A transcripts were localized in the thyroid and other tissues [91]. The studies also showed an increase in the expression of genes from the PDE superfamily (PDE 8 and PDE 8A) in granulosa cells of follicles larger than 10 mm. Greater PDE10A expression was also observed in cummulus cells [92]. Moreover, the presence of PDE10A transcripts in human oocytes has also been demonstrated [Hetman et al., 2000]. Inhibition of PDE10A (together with PDE8) by dipyridamole increases cAMP levels in COCs and delays oocyte maturation [92].

The increase in PDE10A expression in embryos from younger cows may be important both for the regulation of cAMP levels and for the potential developmental capacity of the embryos. PDE10A is a phosphodiesterase that breaks down cAMP and cGMP, key signaling molecules for the regulation of maturation and early development of embryos. The increase in PDE10A expression in embryos from younger cows may indicate a more intense regulation of cAMP levels in these embryos, which may affect the rate of cell division, synchronization of cellular metabolism or potential implantation ability. In younger cows, oocytes and embryos may have a different metabolic profile than in older animals. Higher PDE10A activity may indicate more intensive regulation of metabolic processes in the embryos of young cows, which may be related to their greater ability to compensate for possible disturbances in cAMP levels. Moreover, higher PDE10A activity may result in a more effective reduction of cAMP levels, which may accelerate cell division.

RBM46 (*RNA binding motif protein 46*) is a germ cell-specific RNA-binding protein crucial for gametogenesis, as it binds distinct motifs in the 3'UTRs of mRNAs for meiotic cohesin components, and its loss impairs translation, ultimately disrupting synaptonemal complex formation and causing meiotic arrest [93]. Moreover, RBM46 is essential for gametogenesis because its loss leads to masculinization, impaired spermatogenesis, and meiotic arrest by disrupting the posttranscriptional regulation of key genes like DALZ, NANOS3, and SYCP3 independently of p53-mediated apoptosis [94]. Based on the above information, it can be

concluded that the increase in the expression of the RBM46 gene in embryos from younger cows results from a stronger maternal transmission of this protein, which is crucial for the regulation of the development of reproductive cells and the proper course of prophase I of meiosis.

PDK4 (*Pyruvate dehydrogenase kinase 4*) plays a role in regulating glucose and lipid metabolism [95]. PDK4 expression is significantly lower in the endometrium of women with hyperandrogenism [96]. PDK4 levels increase during the preparation of the endometrium for embryo implantation [96]. PDK4 is mentioned as one of the main genes associated with the development of insulin resistance (along with the AHSG gene). In the perinatal period, increased expression of PDK4 in hepatocytes is observed in dairy cows [97]. PDK4 participates in the early proliferation and differentiation of muscle cells, which translates into muscle development and growth. In chicken embryos, PDK4 is expressed in the pectoral muscle from days 7 to 17 of incubation [98].

Although no increase in PDK4 has been shown in bovine embryos to date, considering previous reports on this topic, its increase in bovine embryos from younger cows is intriguing. PDK4 is a key regulator of glucose and lipid metabolism. In younger cows, which are usually characterized by a more active metabolism and a higher ability to effectively manage nutrients, there may be increased expression of PDK4 in embryonic tissues. This supports the adaptation of the embryo to variable energy sources (glucose and fatty acids). From studies on the endometrium, it is known that PDK4 increases during preparation for implantation, which may also translate into the development of the early embryo. More efficient hormonal and metabolic regulation in younger cows promotes appropriate "programming" of the embryo, expressed, among others, by increased levels of PDK4. PDK4 is one of the genes associated with the development of insulin resistance, but under conditions of physiological homeostasis (more common in younger cows), its role may consist in maintaining the balance between the use of glucose and fatty acids. As a result, this promotes proper embryo development and adaptation to the conditions of the uterine environment. Studies in the poultry model indicate that PDK4 plays a role in early proliferation and differentiation of skeletal muscles. Although in the case of bovine embryos the context may be broader, similar mechanisms of tissue development (including muscle) may also contribute to higher levels of PDK4 in more "dynamically" developing embryos from younger cows.

The *Early growth response 2 (*Egr 2) gene is involved in the regulation of both folliculogenesis and ovulation. This gene was shown to be accumulated around the blastocyst on day 5 of pregnancy. Moreover, studies report that estrogens induce the expression of this gene in the uterine epithelium. Egr2 is also said to influence the embryo implantation process [99]. This gene plays an important role in the development of the hindbrain, the mineralization of bones and peripheral nerves, and the differentiation of immune cells [100].

According to GeneCards, the *zinc finger B-box domain* (ZBBX) is overexpressed, among others, in the ovary, testes and fallopian tube. The function of this gene in the female reproductive system is not well understood [101]. It is hypothesized that the ZBBX gene is upregulated in the intercaruncular areas of the endometrium (ICAR) due to dysregulated interaction between the endometrium and the embryo produced in vitro in cattle [102]. Higher expression of the cilia-related ZBBX gene was demonstrated in women with ectopic pregnancy (ECT), compared to expression in women with abnormal intrauterine pregnancy (AIUP) [101].

The LRCH gene family is involved in the development of immunity and cell migration [103]. LRCH2 (*Leucine Rich Repeats And Calponin Homology Domain Containing 2*) is expressed in the developing brain, particularly in areas responsible for motor function in humans. It was confirmed that the period of the highest expression of the LRCH2 gene in the embryonic development of the cerebellum coincides with the development of the pathology of early ataxia with cerebellar hypoplasia in humans [104]. Studies also report that amplification of the LRCH2 and LRCH3 genes is associated with the development of cancers such as low-grade gliomas [103].

A total of 12 genes were descripted (including STAT4, MGP, CYP11A1, CYP4V2, HPRT1, CCL24, PDE10A, RBM46, PDK4, Egr2, ZBBX and LRCH2), which in our studies showed higher expression in embryos from younger cows and their role has already been determined in publications and their functions are important for embryos and pregnancy development. Particular attention should be paid to: CYP11A1 (effect on steroidogenesis), PDE10A (cAMP regulation, important for early embryo development), PDK4 (key regulator of glucose and fatty acid metabolism), CCL24 (important for proper organization of ICM and potential implantation) and HPRT1 (high demand for nucleotides and active cell division). Their increased expression may reflect more dynamic metabolic and developmental processes in the embryos of younger cows, which may translate into better quality and higher implantation potential of these embryos. We also described the remaining upregulated genes, most of whose

functions described so far do not indicate a connection with embryos, but in the case of some of them their role may be important for embryo development and pregnancy.

The transcriptome analysis of bovine embryos based on the RNA-seq experiment identified 13 age-dependent up-regulated genes (*ICOS, CT47B1, FAM13C, PLA2G7, SYT4, MAGE B2, INSC, ZNF514, MOCOS, HOMER1, CA2, TKTL2, and C5H12orf75*) in bovine embryos with unclear or insufficiently described roles in the development of bovine embryos (Table 8). Among them, the following genes can be considered as particularly interesting for embryogenesis: INSC (control of the mitotic spindle), CA2 (maintenance of acid-base balance and cellular homeostasis), TKTL2 (metabolism in the pentose phosphate pathway, NADPH production), ICOS (functions related to the activation of T lymphocytes and dendritic cells), MOCOS (activation of molybdenum-dependent enzymes important for purine metabolism). Their increased expression in embryos from younger cows may suggest a more favorable metabolic-hormonal profile and more intensive proliferative processes, but further studies are needed to confirm the possible influence of these genes on embryo quality and development.

The gene ICOS (*Inducible T cell costimulatory*) is part of the CD28/CTLA4 protein family and is located on the surface of activated CD4+ T-lymphocytes. Moreover, it is highly expressed on dendritic cells and B lymphocytes. It is suggested that ICOS is important in the immune response [105]. A study demonstrated that ICOS expression is significantly upregulated in several tumor types, including gliomas, breast cancer, and lung cancer. This upregulation is associated with enhanced immune checkpoint activity and can serve as a biomarker for T-cell-mediated responses to immunotherapy [106]. There is no information yet about the expression of this gene in embryos.

The CT47B1 gene, known as *Cancer/Testis Antigen Family 47 Member B1*, is part of the CT47 gene family. It is predominantly expressed in the cytoplasm of cells within the seminiferous ducts of the human testis (https://www.proteinatlas.org/ENSG00000236446-CT47B1?utm_source=chatgpt.com). Regarding bovine embryos, current research does not indicate the presence or expression of the CT47B1 gene. However, it is predominantly expressed in the cytoplasm of cells within the seminiferous ducts of the human testis [107]. So far, the expression of this gene has not been reported in bovine embryos, so the increase in the expression of this gene in embryos from younger cows is puzzling.

The FAM13C *(Family with sequence similarity 13, Member C*) gene is one of 857 genes belonging to the FAM family, but its exact functions and location are not fully known [108]. Scientists recognize the role of the FAM13C gene and other genes from this group in the pathogenesis of various types of cancer and consider changes in the expression of these genes to be prognostic in the diagnosis of cancer [109]. So far, there is no data on the role this gene plays in the processes of embryogenesis.

PLA2G7 (*Phospholipase A2 group VII*) encodes the enzyme lipoprotein phospholipase A2 (Lp-PLA2), which is involved in lipid metabolism and in metabolic states [106]. PLA2G7 is considered a biomarker of cardiovascular diseases, and the influence of this gene on the development of immunity in humans and mice has been demonstrated [110]. The increase in its expression in embryos is a phenomenon unknown so far.

The SYT4 (*Synaptotagmin 4*) gene encodes a member of the synaptotagmin family of proteins, which are involved in the regulation of neurotransmitter release and other aspects of synaptic function. Synaptotagmins are integral to the exocytosis of synaptic vesicles and play a role in the nervous system's response to calcium signals [111]. Increased neuronal activity can lead to the upregulation of SYT4. Synaptic activity and calcium influx through voltage-gated calcium channels can enhance the transcription of the SYT4 gene [112]. Upregulation of the SYT4 gene in embryos from younger cows may result from increased neuronal activity and increased calcium influx through voltage-dependent channels, leading to increased transcription of this gene. This may suggest more dynamic signaling processes in developing embryos from younger cows, potentially affecting their ability to differentiate and continue to develop.

MAGE B2 (*Melanoma Antigen Family B Member 2)* plays a key role in regulating rRNA transcription and ribosome biogenesis in cancer cells [113]. So far, the expression of this gene has only been observed in healthy tissues [114]. So far, there is no information regarding the expression of this gene in embryos, either human or animal.

INSC (*INSC Spindle Orientation Adaptor Protein*) is a gene encoding an adapter protein responsible for the orientation of the spindle during cell division [115].

The increase in INCS gene expression in embryos from younger cows may be the result of the fact that younger cows may show higher proliferative activity, which may lead to increased expression of genes involved in cell division, such as INCS. Perhaps differences in metabolic

and hormonal status between younger and older cows may also affect the expression of genes related to embryo development.

Zinc finger proteins, including ZNF514 (*Zinc Finger Protein 514*), are key transcription factors that regulate processes such as differentiation, proliferation, metabolism, and apoptosis, and changes in their expression are linked to the development and progression of colorectal cancer, indicating their potential as prognostic biomarkers and therapeutic targets [43, 116]. The result of increased expression of the ZNF514 gene in embryos from younger cows may result from a more favorable hormonal and epigenetic profile that favors more intense transcriptional activity. Additionally, younger cows are characterized by a better metabolic and reproductive condition, which may also result in a higher level of expression of this gene.

The MOCOS (*Molybdenum Cofactor Sulfurase*) gene encodes an enzyme that is essential for the activation of molybdenum-dependent enzymes, such as xanthine dehydrogenase and aldehyde oxidase. These enzymes play crucial roles in purine degradation and the metabolism of various endogenous and exogenous compounds. Upregulation of the MOCOS gene can impact cellular metabolism and is relevant in the context of certain diseases and physiological conditions [117]. In conditions of oxidative stress or cellular damage, the upregulation of MOCOS can occur as part of a broader response to maintain cellular homeostasis and facilitate the repair of damaged molecules. Increased metabolic activity, particularly in tissues with high turnover rates, can lead to the upregulation of MOCOS to ensure adequate levels of active molybdenum-dependent enzymes [118]. The HOMER1 gene encodes a protein that is part of the Homer family of proteins, which are involved in the regulation of synaptic signaling and plasticity. Homer proteins play a crucial role in linking cell surface receptors to intracellular calcium release and signal transduction pathways, which are essential for synaptic function and neural communication [119].

Increased neuronal activity can lead to the upregulation of HOMER1. Activity-dependent transcription factors such as CREB (*cAMP response element-binding protein*) can enhance HOMER1 expression in response to synaptic activity and calcium influx. Upregulation of HOMER1 can occur during these processes to modulate synaptic strength and connectivity. Stress and hormonal changes can influence the expression of HOMER1. For example, stress-induced activation of the hypothalamic-pituitary-adrenal (HPA) axis can lead to changes in HOMER1 expression in specific brain regions [120, 121].

The carbonic anhydrase 2 (CA2) gene encodes carbonic anhydrase II, an enzyme that catalyzes the reversible hydration of carbon dioxide [122]. This enzyme plays a crucial role in various physiological processes, including acid-base balance, respiration, and the formation of bodily fluids such as cerebrospinal fluid, saliva, and gastric acid [123]. Upregulation of the CA2 gene can occur in response to various physiological and pathological conditions. Hypoxic conditions can lead to the upregulation of CA2. Hypoxia-inducible factors (HIFs) activate the transcription of genes involved in pH regulation, including CA2, to adapt to low oxygen levels. Hormones such as glucocorticoids and thyroid hormones can influence the expression of CA2. These hormones can upregulate CA2 as part of their role in maintaining metabolic and physiological homeostasis [124]. In our study, the increase in CA2 expression in embryos from younger cows is likely due to a more dynamic hormonal and metabolic environment (including responses to factors such as hypoxia) that favors increased activation of genes responsible for maintaining acid-base balance and overall cellular homeostasis.

The TKTL2 gene encodes the transketolase-like 2 enzyme, which is involved in the non-oxidative part of the pentose phosphate pathway. This pathway is crucial for cellular metabolism, providing ribose-5-phosphate for nucleotide synthesis and NADPH for reductive biosynthesis and antioxidant defense [125]. Upregulation of the TKTL2 gene can impact cellular metabolism, particularly in the context of cancer and other proliferative diseases. Hypoxic conditions within tumors can lead to the upregulation of genes involved in glycolysis and the pentose phosphate pathway, including TKTL2. Hypoxia-inducible factors (HIFs) play a key role in this regulatory process. Cells experiencing oxidative stress may upregulate TKTL2 to increase the production of NADPH, which is crucial for counteracting oxidative damage and maintaining cellular redox homeostasis [126, 127]. In our study, the increased expression of the TKTL2 gene in embryos from younger cows is likely due to more intensive proliferation and metabolism processes (including the response to hypoxia), which increase the demand for NADPH and antioxidant support. No reports have been found so far about the C5H12orf75 gene, chromosome 5 C12orf75 homolog.

5.1.2. Age-dependent downregulated genes

In this dissertation, the age-dependent down-regulated genes in bovine embryos with established roles in embryogenesis and reproduction are summarized in Table 9. *Study identified the folowing significantly dowregulated genes transcripts in embryos collected from cows of different ages and whose documented functions are tightly linked to core*

developmental or reproductive pathways. The down-regulation affects diverse processes, including cilia-mediated signalling (ARL13A), copper and purine metabolism essential for energy production (ATP7A, IMPDH1, UQCRC2), cytoskeletal dynamics during oocyte maturation and cleavage (JMY, AKT2), and placental or uterine interactions critical for implantation (PROM1, NPSR1). Reduced expression of key genome-maintenance and DNA-repair factors (FANCA) further suggests compromised genomic stability. Collectively, these changes may help explain age-related declines in embryo viability, altered metabolic competence, and reduced implantation success observed in the study.

The downregulated genes obtained from cows of different ages are discussed below. First, genes with clearly defined and previously established roles in embryogenesis are described. This is followed by the characterization of genes whose role in embryogenesis has not yet been determined but which may have significant importance in shaping embryo quality.

NPSR1 (*Neuropeptide S Receptor 1*) belongs to GPCR (*G protein-coupled receptor superfamily*). It is activated by neuropeptide S (NPS). The NPSR-NPS system is important in many physiological processes in vertebrates and has signaling functions in the central nervous system [128]. NPSR1 and neuropeptide S (NPS) are associated with stress regulation and stress-related disorders. Taking into account the results from animal models related to genetic studies, it appears that the study of the NPS/NPSR1 system is a promising topic in neurobiological research regarding the regulation of chronic stress [129]. Studies report that the expression of NPSR1 increases during inflammatory processes, which proves that this gene plays a major role in inflammatory reactions [130]. The NPSR1 gene is expressed in two mRNA isoforms (A and B) [131]. Strong NPSR1A mRNA expression was detected in bovine fetal cotyledons, but no NPSR1A mRNA expression was detected in other fetal tissues or in maternal muscles. It has been shown that this gene is associated with blood circulation in the fetus, but also in the placenta, and is involved in the pro-inflammatory immune response in the fetus. It has been shown that changes in placental gene expression influence the subsequent functioning of the fetus and changes in its development. It has been shown that abnormal expression of NPSR1A in the placenta may be associated with fetal death [132]. NPSR1 downregulation may be influenced by differences in rs740347 [130].

SYT 9 (*Synaptotagmin 9*) is part of the synaptotagmin family, which as a whole group have tandem C2A and C2B domains that are contained in the cytoplasm and are linkers between calcium ions and phospholipids. SYT isoforms regulate the process of exocytosis, mainly in

neurotransmission, and have different subcellular locations [133]. The best-studied isoform is SYT1, whose close homolog is SYT9 [134]. However, SYT9 has a different biological role than SYT1 because it has special binding properties that bind Ca and phospholipids [135]. Research on mouse models has shown that mutations in SYT9 can lead to significant developmental issues, including embryonic lethality. Mice homozygous for a null allele of SYT9 exhibit 50% embryonic lethality, highlighting its critical role in development. These findings underscore the gene's importance in cellular signaling pathways essential for normal embryogenesis.

Arl13a (*ADP Ribosylation Factor Like GTPase 13A*) belongs to the ADP-ribosylation-factor-like (Arl) family of GTPases [136]. The ARL13A gene (*ADP-ribosylation factor-like GTPase 13A*) plays a significant role in embryonic development, particularly in the formation and function of primary cilia, which are crucial for various signaling pathways during development [136]. Primary cilia are specialized, single, short, non-motile projections located on almost all human cells. These structures are present in the cell during the G0/G1 phase, but are resorbed before entering mitosis. Primary cilia are microtubule-based structures that protrude from the surface of many cell types and are involved in signal transduction. These structures play a critical role in sensing extracellular signals and transducing them into cellular responses, which are vital during embryonic development for processes such as cell differentiation and organogenesis. Primary cilia play an important role in transmitting chemical and physical stimuli from the outside to the inside of the cell; for this reason, it is believed that primary cilia play an important role in the proper functioning of tissues and organs and contribute to maintaining homeostasis [137]. Studies show that mutations in Arl13b cause several defects in animal organisms, but there are no such reports in the case of Arl13a [138].

PROM1 (*Prominin1*) - is a pentaspan membrane protein also known as CD133 and is considered a stem cell marker [139]. It is a gene for cholesterol-binding membrane glycoproteins and is found throughout the animal kingdom [140]. CD133 mRNA was shown to be expressed in bovine ovaries at all luteal stages and at each ovary location [139]. It was found that CD133 could modulate late cell proliferation as well as glucose uptake [141]. Studies show that downregulation of CD133 leads to downregulation of the nuclear factor-κB (NF-κB) pathway [142], which plays an important role in tumor necrosis factor (TNF) and Interleukin 1 (IL-1) transcriptional activation [143]. Studies also report that CD133 is a significant stem cell factor that enhances glioma progression [144]. As is known, in early

pregnancy the embryo attaches to the uterine wall, so it is essential to know the influence of uterine luminal epithelial cells on the embryo. It is believed that the expression of Prom 1 in uterine epithelial cells should be higher in the first days of pregnancy and then decrease [145].

RBMS3 (*RNA binding motif single-stranded interacting protein 3*) is a member of the MSSP group, which are involved in transcription, DNA replication, apoptosis and cell cycle progression [146]. This is a gene that encodes a protein involved in RNA processing and has been implicated in various cellular processes and plays an important role in embryonic development [147]. Studies suggest that RBMS3 expression may influence the regulatory mechanisms of embryonic pancreas development in mice [147]. This gene is also a prognostic marker for various types of cancer [148]. RBMS3 is associated with pancreatic development. The increase in Rbsm3 expression corresponds to the increase in Ptf1 expression, which also plays an important role in the initial development of cells that ultimately form the pancreas [149]. Rbm3 has been shown to be limited in expression in the embryonic pancreas, dorsal root ganglion, and neural tube [149].

The FSD1L (*Fibronectin type III and SPRY domain containing 1 like*) gene encodes a protein from the cystatin group, which may, among others, regulate the activity of proteolytic enzymes involved in processes related to angiogenesis or cell invasiveness [150]. The FSD1L gene was detected in cattle on chromosome 8. In humans, the region of the genome containing, among others, the homolog of this gene is associated with the age of puberty in females [151]. Furthermore, in humans, the FSD1L gene has been shown to influence the onset of menarche [152]. Studies have shown an increase in the expression of this gene in the posterior lobe of the pituitary gland in humans [153]. Studies have shown that higher maternal blood glucose levels during pregnancy are significantly associated with lower levels of DNA methylation (DNAm) in the FSD1L gene region in children, both immediately after birth (in cord blood) and at the age of 5 years [154]. Based on the above information, it can be concluded that the reduction in FSD1L gene expression in embryos from cows at a younger age may result from epigenetic mechanisms related to exposure to hyperglycemia (high glucose level) in the perinatal environment.

ATP7A (*ATPase copper transporting alpha*) is associated with determining sensitivity to copper deficiency, which indicates that copper metabolism is influenced by genetic factors. Research says copper metabolism may contribute to birth defects [155]. The ATP7A gene plays a crucial role in embryonic development due to its function in copper transport. This gene

encodes a protein that is essential for regulating copper levels within cells, which is vital for numerous biological processes, including the development of the nervous system and connective tissue [156]. Analyses using a mouse model have shown that ATP7A plays a key role in normal embryonic development and in ensuring fetal survival. In mice with a complete deletion of the Atp7a gene (global silencing), embryonic death occurs around day 10–10.5 of pregnancy, resulting in severe morphological anomalies and vascular disorders. Moreover, in some genetic backgrounds, even partial (heterozygous) deletion of the gene results in high postnatal mortality, while in others (e.g., in the Mottled strain), heterozygous females retain the ability to reproduce and transmit lethal mutations to their offspring. These results clearly demonstrate the importance of ATP7A in supplying copper ions to enzymes necessary for embryo development, and also indicate that a diverse genetic background may affect the intensity of negative consequences in the area of fertility and development [157].

IMPDH1 (*Inosine monophosphate dehydrogenase 1*) serves as a critical regulatory enzyme in the biosynthetic pathway of purine nucleotides, which are essential for the synthesis of ATP and GTP [158]. This gene is responsible for the assembly [158] of filaments in the event of changes in metabolic requirements [159]. Research conducted by Giroto et al. (2019) examined the effect of exogenous pregnancy-associated plasma protein-A (PAPP-A), which increases IGF-1 bioavailability in reproductive tissues, on the quality of oocytes and embryos. It was observed that the IMPDH1 gene was downregulated in PAPP-A-treated oocytes, suggesting potential metabolic adjustments [160]. The *IMPDH Cytoophidium Couples Metabolism and Fetal Development in Mice* explores how cytoophidia-subcellular structures formed by IMPDH-play a role in regulating metabolism and supporting fetal development. The research highlights the significance of IMPDH cytoophidium in maintaining cellular metabolism during embryogenesis, shedding light on its crucial function in early development [130].

The FANCA (Fanconi anaemia, complementation group A) gene is integral to the process of embryonic development, with particular emphasis on hematopoiesis, which refers to the generation of cellular components of the blood. Empirical research has demonstrated that FANCA is transcribed at multiple phases of embryogenesis, notably within hematopoietic locales that are pivotal for the production of hematopoietic stem cells and progenitor cells [161]. Research involving human embryonic stem cells (hESCs) has demonstrated that knockdown of FANCA leads to a reduction in hematopoietic progenitor cells. This effect can be rescued by complementing the FA gene, highlighting FANCA's essential role in early

hematopoietic development [162]. The FANCA gene, a key component of the Fanconi anemia (FA) pathway, is involved in DNA repair and maintaining genomic stability. Downregulation of the FANCA gene has significant implications, especially in relation to certain diseases [163]. FANCA mutations or reduced expression are often associated with Fanconi anemia, a genetic disorder characterized by bone marrow failure, congenital abnormalities, and an increased risk of cancer. Patients with FA typically exhibit hypersensitivity to DNA cross-linking agents, leading to increased chromosomal breakage and instability. In some cases, downregulation of FANCA can lead to hematologic issues like myelodysplastic syndromes (MDS) and acute myeloid leukemia (AML). Abnormal FANCA function is linked to the clonal progression of AML, where gene deletions and reduced expression promote genetic instability and tumor development [164]. Research shows that the expression level of FANCA can influence patient outcomes. For instance, MDS/AML patients with high FANCA expression tend to have a better prognosis compared to those with lower expression. However, mutations in FANCA, despite leading to reduced gene function, sometimes confer better overall survival in these patients due to increased sensitivity to chemotherapy. FANCA operates within a complex network of proteins involved in DNA repair. The FA pathway includes the upstream core complex and downstream elements that coordinate various DNA repair mechanisms. Downregulation or dysfunction of FANCA disrupts this network, compromising the cell's ability to repair DNA damage effectively, which is particularly detrimental under stress conditions that induce DNA lesions [165]. These insights underscore the critical role of FANCA in genomic stability and its broader implications for understanding and treating related disorders.

CREB5 (CAMP Responsive Element Binding Protein 5) is a transcription factor that plays a role in gene regulation and is involved in several cellular functions, including proliferation, differentiation, and stress response. The downregulation of the CREB5 gene has been linked to various biological and disease processes.In the context of cancer, CREB5 has been observed to promote tumor growth and metastasis. For example, in colorectal cancer, CREB5 promotes invasiveness and metastasis by activating the MET gene, which is involved in cell growth and differentiation. Downregulation of CREB5 in this scenario can inhibit these processes, potentially reducing the aggressiveness of the tumor [166]. In Alzheimer’s disease, CREB5 expression is significantly reduced in the brain. This downregulation is associated with increased levels of amyloid-beta (Aβ) peptides, which are characteristic of Alzheimer's pathology. The decrease in CREB5 correlates with reduced CREB-mediated transcription, which affects neuronal survival and function. This suggests that CREB5 downregulation

contributes to the neurodegenerative processes seen in Alzheimer's disease [167]. CREB5 cooperates with TGF-β signaling to regulate the expression of FGF18, which is crucial for the development of pharyngeal muscles. This interaction is essential for proper muscle formation in the developing embryo, highlighting CREB5's role in orchestrating complex developmental processes [168]. These examples highlight the importance of CREB5 in both cancer progression and neurodegenerative diseases, indicating that its regulation plays a critical role in maintaining cellular homeostasis and function. CREB5 is a transcription factor specifically expressed in the superficial zone of articular cartilage. It plays a crucial role in regulating Prg4 (lubricin) expression through TGF-β and EGFR signaling, which is essential for maintaining joint lubrication and cartilage integrity. Disruption of CREB5 expression can lead to reduced Prg4 levels, potentially contributing to cartilage degradation and osteoarthritis [169].

The SANT and BTB domain regulator of the CSR (SANBR) gene is primarily known for its role in cellular processes involving transcription regulation and chromatin remodeling. There is evidence that SANBR is expressed during early embryonic development, particularly in various embryonic tissues such as the ectoderm, mesoderm, and endoderm. This suggests that SANBR may play a role in the development and differentiation of these tissues during embryogenesis [170]. Information on the downregulation of the SANBR gene is sparse. General understanding of gene regulation suggests that downregulation mechanisms can involve epigenetic modifications, transcriptional repression, or post-transcriptional modifications, impacting the gene's expression levels. Understanding the specifics of SANBR gene regulation would require further experimental studies or database searches that focus on transcriptional profiling under various biological conditions.

The UQCRC2 (Ubiquinol-cytochrome c reductase core protein 2) gene, which encodes a subunit of the mitochondrial complex III, is involved in the electron transport chain and oxidative phosphorylation pathway, crucial for cellular energy production and UQCRC2 deficiency is a rare cause of mitochondrial disorders in humans, manifesting, among others, hypoglycemia, lactic acidosis and liver failure, which, however, show rapid improvement after glucose administration [173]. Downregulation of UQCRC2 has been associated with several types of cancer, including gastric cancer, breast cancer, and glioma. In gastric cancer, reduced expression of UQCRC2 correlates with poor prognosis and mitochondrial dysfunction, contributing to tumorigenesis by impairing oxidative phosphorylation and promoting a metabolic switch to glycolysis, known as the Warburg effect. Additionally, in breast cancer

cells, significantly lower levels of UQCRC2 have been observed compared to normal cells, suggesting a broader role in cancer pathogenesis. This downregulation and resultant mitochondrial dysfunction highlight the gene's potential as a therapeutic target and a biomarker for cancer prognosis [165, 172]. The UQCRC2 gene encodes a core protein of the mitochondrial respiratory chain complex III, crucial for cellular energy production. Its role in embryonic development is significant due to its involvement in mitochondrial function and cellular energy metabolism, which are vital for the rapidly dividing and differentiating cells in an embryo [173]. Disturbances in the level of UQCRC2 or its activity may lead to impaired sperm motility, decreased ATP production, reduced capacitation capacity, and adversely affect fertilization and embryo development [174]. Disrupted UQCRC2 function may result in reduced mitochondrial efficiency, decreased energy production, and impaired embryo development, which may ultimately cause embryonic lethality at an early stage of embryogenesis [175]. In embryos from younger cows, UQCRC2 gene expression could have been reduced due to immaturity of regulatory and metabolic systems in germ cells and in the early stage of embryo development. UQCRC2 is a key element of the respiratory chain in mitochondria, and the early period of embryogenesis requires efficient energy production for intensively dividing cells. In younger cows, restrictions in the access of transcription factors, cooperating mitochondrial proteins, or epigenetic regulation mechanisms could have resulted in impaired normal UQCRC2 levels. Such dysfunction causes reduced mitochondrial efficiency and limited ATP production, which can translate into weaker embryo development and, in extreme cases, even lead to early embryonic death.

The Feminization 1 homolog b (FEM1B) gene contributes to the regulation of cell differentiation and growth, both of which are essential during the development of embryos. By participating in signaling pathways that dictate cell fate, FEM1B ensures that cells differentiate appropriately into various tissue types needed for a developing embryo [176]. In humans, FEM1B expression has been demonstrated in the cerebellum, where a particularly high number of transcripts were observed, as well as in the testes [177]. Studies show that FEM1 family proteins (including FEM1B) in C. elegans regulate SLBP protein levels in oocytes – when FEM1 levels decrease, the expression of the SLBP ortholog (CDL-1) in oocytes increases. This indicates an important role of FEM1B in the control of SLBP stability and, indirectly, in processes related to oogenesis [178]. In studies on embryos from younger cows, the reduced expression level of the FEM1B gene may be due to the immaturity of regulatory systems in the germ cells of young females. FEM1B plays an important role in the processes of cell

differentiation and growth during early embryonic development [179], so changes in its expression may be the result of, among others, a different (compared to older cows) pool of cytoplasmic or epigenetic factors transferred to the oocyte. Additionally, because FEM1B regulates the stability of the SLBP protein [178], disturbances in these relationships could also affect the reduced level of FEM1B in younger cows and ultimately result in a less organized control of germ cell growth and differentiation.

JMY (Junction-Mediating And -Regulatory Protein) is a protein that was originally identified as a p300 cofactor regulating the TP53/p53 response to DNA damage, and under physiological conditions, it is mainly responsible for the nucleation of actin filaments in the cytoplasm via the WCA domain and activation of the ARP2/3 complex [180]. JMY is crucial in Sertoli cells because it is responsible for maintaining the integrity of the blood–testicular barrier and the proper organization of the actin cytoskeleton and vesicular transport, which translates into maintaining proper spermatogenesis and male fertility in mice [180]. Furthermore, JMY is crucial for proper meiotic maturation of the oocyte, being responsible for spindle migration, cell polarization, and asymmetric division, which has a direct impact on fertility in mice. [181]. Downregulation of the JMY gene, which encodes a multifunctional protein involved in both actin nucleation and apoptosis, can significantly affect cellular processes [182].

V-Akt Murine Thymoma Viral Oncogene Homolog 2 (AKT2) is a central element of the pathway regulating cellular homeostasis, especially in the context of protein degradation and recycling [183]. Downregulation of the AKT2 gene, which encodes a key protein in the PI3K/AKT signaling pathway, has significant implications for cancer progression and therapy [184]. AKT2 is involved in cell survival, proliferation, and metabolism, and its dysregulation is linked to various cancers. For example, in breast cancer, AKT2 downregulation has been associated with decreased tumor cell survival and reduced metastatic potential. Metformin-induced upregulation of miR-200c can downregulate AKT2, highlighting a potential therapeutic approach. Additionally, in colon cancer, downregulation of AKT2 can sensitize cells to chemotherapeutic agents by promoting apoptosis [185].

A study involving zebrafish embryos demonstrated that disruption of the K-ras/PI3K-Akt signaling pathway, which includes AKT2, led to defects in hematopoiesis and angiogenesis. This underscores the essential role of AKT2 in the development of blood cells and blood vessels during embryogenesis [186]. It has been shown that AKT2 is stably present in mause embryos from an early stage and translocates to the nucleus, and its deficiency disrupts

blastomere division and slows embryo maturation, and the nuclear localization of AKT2 depends on the Tcl1 protein, the deficiency of which causes the accumulation of this kinase in the cell cortex [187]. A possible explanation is that embryos from younger cows may develop in conditions that are less "demanding" in terms of metabolism and adaptation, and therefore do not need to activate the PI3K/AKT pathway to such an extent or maintain high AKT2 expression. In other words, the younger parent organism may have more favorable proportions of hormones, growth factors, or other regulators (e.g., microRNAs) that reduce the embryo's need for intensive AKT2 signaling. As a result, embryo development is not impaired despite the reduced level of this gene, because processes such as cell proliferation or metabolism are supported by other, sufficiently effective regulatory mechanisms under these conditions [188].

The genes described above have defined roles in embryogenesis. Among them, special attention should be given to NPSR1, SYT9, ARL13A, PROM1, RBMS3, ATP7A, UQCRC2, JMY, and AKT2, which are directly linked to critical processes such as placental function, implantation, cell differentiation, mitochondrial energy production, cytoskeletal organization, and key signaling pathways. In particular, SYT9, ATP7A, UQCRC2, ARL13A, JMY, AKT2, and NPSR1 stand out as especially important for bovine embryo development, since their dysregulation or deletion can lead to severe developmental defects or embryonic lethality.

The SERPINB4 gene, also known as Serpin Family B Member 4, is primarily recognized for its role in inhibiting serine proteases and is associated with inflammatory responses and various cancers. However, its specific role in embryonic development is less well-documented compared to some other genes. One study of interest, although not directly about SERPINB4, discusses the role of related serpins in developmental pathways. The research highlights how these proteins modulate protease activity to ensure proper cellular function and development [87]. Most serpins play a key role in the homeostasis of the epidermal barrier, and their abnormal expression and changes in their activity are associated with chronic skin diseases [189]. They also inhibit serine proteases. SERPINB4 is involved in various processes in cells, such as their development, differentiation, and transcription regulation (Shiiba et al., 2010). Studies have shown the presence of this gene in non-healing wounds (Eming et al., 2010). Moreover, it has been shown that downregulation of this gene may attenuate early inflammation [189].

CAPSL (Calcyphosine-like) expression was minimal or undetectable in histological samples of subcutaneous adipose tissue from 10 patients with sporadic MSL. This indicates a significant

regulation of CAPSL in these cases. CAPSL was discovered in a family with four generations affected by MSL. Unlike MSL patients, CAPSL is expressed in adipose tissue from control subjects. In 3T3-L1 pre-adipocytes, CAPSL plays a role in regulating lipid accumulation. Cells lacking CAPSL show increased resistance to oxidative stress, though they do not exhibit increased resistance to ER stress [190]. CAPSL was among the genes with increased expression associated with the frequency of epileptic seizures [191]. Calcyphosine-like (CAPSL) is a calcium-binding protein implicated in various physiological processes. Recent studies have highlighted its roles in adipogenesis and retinal angiogenesis [192]. Research indicates that CAPSL is downregulated in adipose tissues of MSL patients, suggesting its involvement in adipocyte biology. Functional studies using cell models have shown that alterations in CAPSL expression can affect autophagy, adipogenesis, lipogenesis, and Sirtuin-1 (SIRT1) expression, pointing to a potential role in the pathogenesis of MSL [193]. Research suggests that CAPSL plays a role in cellular signaling and regulation. The gene is expressed in various tissues, and its calcium-binding function implies a potential involvement in calcium-dependent processes. While there is some evidence of its expression in certain developmental stages, detailed information regarding its specific role in early embryogenesis and its influence on processes like cell differentiation and proliferation is limited. According to the Mouse Genome Informatics (MGI) database, CAPSL is expressed in multiple tissues, though its precise involvement in early embryonic development requires further investigation [194].

The LYPD6B gene, also known as LY6/PLAUR Domain Containing 6B, plays a role in the modulation of nicotinic acetylcholine receptor (nAChR) activity, particularly within the nervous system, and is expressed in various tissues, including the testis, lungs, stomach, and prostate [195]. Downregulation of LYPD6B has been associated with certain pathological conditions, such as cancer. Specifically, hypermethylation of the LYPD6B gene has been linked to decreased expression and increased invasive capacity of melanoma cells [187]. RNA sequencing studies in non-small cell lung cancer (NSCLC) have shown that LYPD6B is downregulated in tumor tissue compared to non-malignant lung tissue. This suggests that LYPD6B may have a tumor-suppressive role, and its reduced expression could contribute to the progression of NSCLC.

The LYZ (Lysozyme) gene, which encodes the enzyme lysozyme, plays a crucial role in the immune system by breaking down bacterial cell walls. Its downregulation has been observed in various contexts, including in response to environmental factors and disease conditions

[196]. LYZ is expressed in many cell types and tissues, and the protein is present in almost all body fluids, with the highest concentrations in tears, gastric juice, and milk [197]. In a study involving Pacific white shrimp, the LYZ gene was significantly downregulated after prolonged exposure to microplastic-contaminated feed. This led to weakened immune responses and increased susceptibility to infections, highlighting the environmental impact on gene expression and immune function [198]. Another study indicated that acute hyperglycemia can globally downregulate gene expression, including that of LYZ, in human tissues. This downregulation may contribute to the increased infection risk observed in diabetic patients, highlighting the broader impact of metabolic disturbances on immune function [199]. These findings illustrate the variable expression of the LYZ gene in response to different environmental and pathological conditions, underscoring its importance in immune regulation. There are no data available on LYZ and embryos; we can speculate that in embryos from younger cows, reduced LYZ gene expression may result from underdeveloped or susceptible to disruption immune and metabolic regulatory pathways.

The genes described above do not yet have clearly defined roles in embryogenesis. SERPINB4 is mainly linked to inflammation and cancer but lacks direct evidence for functions in early development. CAPSL is involved in adipogenesis, calcium signaling, and retinal angiogenesis, suggesting possible roles in cell regulation, though its contribution to embryogenesis remains poorly understood. LYPD6B modulates nicotinic acetylcholine receptors and may act as a tumor suppressor, but data on its role in embryos are missing. LYZ is a key immune-related gene with strong antimicrobial activity, and although not studied in embryos, its regulation may influence early immune and metabolic pathways. Among these genes, CAPSL deserves particular attention, as its involvement in calcium-dependent signaling, lipid metabolism, and angiogenesis points to potential importance in processes fundamental for early embryonic development. The following age-dependent down-regulated genes in bovine embryos lack documented roles in embryogenesis or reproduction. The genes encode proteins mainly associated with innate immunity (SERPINB4, LYZ), neuromodulation (LYPD6B), and metabolic or angiogenic processes (CAPSL). Although their direct contribution to early bovine development is unverified, age-related repression of these genes might still influence the embryonic micro-environment, for example, by altering inflammatory tone or nutrient signalling - thereby indirectly affecting embryo quality. Functional studies will be needed to determine whether their downregulation is merely correlative or plays a contributory role in age-linked developmental differences.

5.2. Transcriptome analysis of bovine embryos based on the bulk scRNA-seq experiment (season comparison between summer vs spring)

5.2.1. The up-regulated genes associated with embryos collected from cows in different seasons

This section of discussion describes the up-regulated genes associated with embryos collected from cows in different seasons. First, genes with clearly defined and previously established roles in embryogenesis are discussed, followed by genes whose function in bovine embryos has not yet been characterized but may still play an important role in determining embryo quality. In this dissertation, the season-dependent up-regulated genes (warm vs. cold season) in bovine embryos with established roles in embryogenesis and reproduction. Study identified the following DE genes that showed significantly higher transcript abundance in embryos collected during the warm-season versus the cold-season (or vice-versa, depending on directionality in the dataset) and have well-documented functions directly supporting embryogenesis or reproductive success. Several transcripts enhance cellular stress tolerance and proper protein folding under thermal challenge (HSPA6) or guide chemotactic cell movements critical for organ patterning and germ-cell survival (CXCR4). Up-regulation of endocrine regulators - including FSHR and the steroidogenic enzyme CYP11A1 - suggests seasonal modulation of folliculogenesis, oocyte competence, and early hormonal signalling. Metabolic support genes (BCAT2) and vascular/implantation mediators (BMPER, FGB, KLK) may bolster nutrient delivery and embryo–maternal interactions when environmental conditions fluctuate. Cardiac (MYL7) and immune-maturation factors (CD8B) further indicate that seasonally altered expression profiles could influence organogenesis and immunological priming. Together, these expression changes provide molecular evidence that ambient temperature or photoperiod affects key developmental pathways, potentially contributing to seasonal variation in embryo quality and implantation success observed in vivo.

The HSPA6 gene, also known as Heat Shock 70kDa Protein 6 (HSP70B'), is part of the HSP70 family, which plays a crucial role in the cellular stress response. The HSPA6 gene encodes a heat shock protein that is involved in protein folding, protection from stress-induced damage, and aiding in the recovery of stressed cells [200]. Unlike other HSP70 family members, HSPA6 is not constitutively expressed but is highly inducible under stress conditions such as heat shock, oxidative stress, and exposure to heavy metals. Upregulation of HSPA6 is typically

triggered by heat shock, which activates heat shock transcription factors (HSFs) [201]. These factors then bind to the heat shock elements (HSEs) in the promoter region of HSPA6, initiating its transcription. The primary mechanism of upregulation involves the activation of HSF1, a transcription factor that responds to elevated temperatures and other stressors by binding to HSEs in the HSPA6 promoter [202]. Reactive oxygen species (ROS) can also trigger the upregulation of HSPA6 through similar pathways involving HSF1 activation. Upregulation of HSPA6 helps in protecting cells from proteotoxic stress by preventing protein aggregation and assisting in the refolding of denatured proteins [202]. Its involvement in embryo development is less well-documented compared to other HSPs like HSPA1A and HSPA1B. However, heat shock proteins in general, including HSPA6, are crucial during embryogenesis for proper protein folding, protection against stress, and ensuring normal cellular functions during the rapid growth and differentiation phases [203].

The C-X-C Motif Chemokine Receptor 4 (CXCR4) gene, encoding the C-X-C chemokine receptor type 4, plays a pivotal role in embryonic development. This receptor, along with its ligand CXCL12 (SDF-1), is involved in several crucial processes, including stem cell proliferation, differentiation, migration, and organogenesis [204]. The CXCR4/SDF-1 axis is essential for the migration and homing of various stem cell types during embryogenesis. This pathway guides primordial germ cells (PGCs) to the genital ridge, which is critical for proper gonadal development. In CXCR4-deficient embryos, there is a marked decrease in PGCs in the genital ridge, indicating its role in PGC survival and proliferation during migration [205]. In zebrafish, CXCR4 and SDF-1 are required for the proper formation of skeletal muscles. The expression patterns of CXCR4 and its ligand SDF-1 during somitogenesis indicate their involvement in early and late myogenesis, crucial for the development of fast muscles [206]. The CXCR4/SDF-1 axis also influences the development of the pituitary gland. Studies in both humans and mice have shown the expression of CXCR4 in stromal cells within the developing pituitary [207]. In chick embryos, CXCR4 expression is noted at various stages, particularly in the primitive streak and somites, indicating its role in early developmental processes [208]. The CXCR4 gene plays a significant role in various biological processes, including immune cell trafficking and tumor metastasis. Its upregulation is often associated with cancer progression and metastasis [209]. The observed upregulation of the CXCR4 gene in embryos collected from cows during the cold season may reflect an adaptive developmental response to environmental stress. CXCR4 plays a pivotal role in cell migration, survival, and organogenesis, particularly in the migration of primordial germ cells (PGCs) and the development of muscles and the

pituitary gland. Cold conditions may stimulate the activation of protective molecular pathways to ensure proper embryonic development despite environmental challenges. Seasonal differences in the maternal hormonal profile or uterine environment may also influence CXCR4 expression, enhancing mechanisms that support stem cell function and tissue formation during early embryogenesis.

The FSHR gene encodes the follicle-stimulating hormone receptor (FSHR), a critical protein in reproductive biology [210]. FSHR, a receptor exclusively expressed in granulosa cells, mediates the essential actions of follicle-stimulating hormone in follicular development and ovarian function, and its genetic mutations have been linked to various reproductive disorders and fertility traits in both humans and livestock [211, 212]. Multiple mutations in the 5′-upstream region of the FSHR gene have been identified across various species, including humans, goats, sheep, and cattle, and are significantly associated with reproductive disorders and fertility traits such as amenorrhea, infertility, and litter size [210]. FSHR expression was evaluated in cumulus and granulosa cells to explore its relationship with oocyte developmental capacity in cattle. While its involvement in follicular activity is well-established, this study did not find a clear link between FSHR levels and successful embryo development [213]. The observed upregulation of FSHR in embryos from cows maintained under normal thermal conditions may reflect a more favorable follicular environment before fertilization, where optimal FSH signaling supported oocyte maturation and follicular function. In contrast, exposure to elevated environmental temperatures may impair FSHR-mediated pathways, potentially compromising oocyte competence and early embryonic development.

CYP11A1 (cytochrome P450 family 11 subfamily A member 1) encodes a key enzyme involved in steroidogenesis, catalyzing the first step in the conversion of cholesterol to pregnenolone, a precursor for all steroid hormones. CYP11A1 encodes a mitochondrial enzyme essential for the initiation of steroidogenesis, and its regulated degradation—particularly via LONP1—is crucial for controlling androgen production, with implications for disorders like PCOS [214]. In the context of polycystic ovary syndrome (PCOS), CYP11A1 plays a crucial role in ovarian androgen overproduction. Recent studies have shown that artemisinins, a class of compounds with known anti-malarial properties, can reduce androgen levels in PCOS by promoting the proteasomal degradation of CYP11A1, mediated through enhanced interaction with LONP1, a mitochondrial protease. This degradation limits excessive androgen synthesis, offering a potential therapeutic strategy for managing hyperandrogenism in PCOS [215].

CYP11A1 is the only known enzyme that initiates steroidogenesis by producing pregnenolone, but its role in the central nervous system remains unclear due to inconsistent evidence of its protein expression, especially in humans [216]. Environmental stress, modeled by cadmium exposure, downregulates CYP11A1 expression in the placenta, leading to impaired progesterone synthesis and fetal growth restriction, a process mitigated by melatonin through inhibition of BNIP3-dependent mitophagy [217]. In zebrafish, CYP11A1 is expressed early in development and in steroidogenic tissues like the gonads and interrenal gland, indicating its essential role in initiating steroidogenesis and suggesting a potential function for steroids during early embryogenesis [218]. During ovarian development, CYP11A1 expression is significantly lower in GREL cells compared to granulosa cells, highlighting its association with the differentiation and steroidogenic function of mature ovarian cell types [219]. In our study, the upregulation of CYP11A1 in embryos derived from cows kept under thermoneutral conditions may be attributed to its essential role in initiating steroidogenesis, particularly during early embryonic development. Previous research has shown that environmental stress, such as heat exposure, can downregulate CYP11A1 expression, leading to impaired progesterone synthesis and fetal growth restriction. Therefore, the higher expression of CYP11A1 in embryos from the control group likely reflects a more favorable environment for activating the steroidogenic pathway and supporting proper embryonic development.

BCAT2 (Branched-Chain Amino Acid Transaminase 2) was identified as one of the metabolism-related genes associated with both prenatal exposure to metabolism-disrupting chemicals and birth weight, suggesting its potential involvement in environmentally influenced fetal growth regulation [220]. In the fetal liver, chronic hyperinsulinemia led to downregulation of BCAT2, indicating reduced amino acid utilization as part of a broader shift in hepatic metabolism favoring altered amino acid and one-carbon metabolic pathways over glucose and lipid processing [221]. BCAT2 was identified as a differentially expressed gene in mtDNA-deficient oocytes, and its expression was restored by mitochondrial supplementation, highlighting its potential role in amino acid metabolism and early embryonic development [222]. In our study, increased expression of the BCAT2 gene was observed in embryos derived from cows kept under normal temperature conditions, compared to those exposed to elevated temperatures. BCAT2, which is involved in branched-chain amino acid metabolism, has previously been linked to environmentally influenced fetal growth regulation and birth weight in response to metabolism-disrupting exposures [219]. The upregulation of BCAT2 may reflect a more favorable metabolic environment in embryos developing under optimal temperature

conditions, supporting more efficient amino acid utilization. This interpretation is consistent with findings that chronic hyperinsulinemia leads to BCAT2 downregulation in the fetal liver, suggesting impaired amino acid metabolism under disrupted metabolic states [221]. Additionally, BCAT2 has been identified as important for early embryonic development and amino acid metabolism, particularly in the context of mitochondrial quality [222], indicating that its elevated expression could be a marker of improved metabolic and developmental potential in embryos.

BMPER (BMP-Binding Endothelial Regulatoris) a key regulator of BMP signaling in pericardial adipose stem cells, and its dysregulation under obese conditions may impair stem cell function and influence cardiac cell behavior [223]. BMPER is essential for proper coronary artery development, as it regulates endothelial cell migration and tubulogenesis through BMP signaling, with its absence leading to abnormal coronary artery connections in the embryonic heart [224]. BMPER is a key extracellular matrix protein produced by endothelial cells that fine-tunes BMP signaling in a dose-dependent manner, promoting endothelial cell sprouting and migration by enabling BMP-4 - driven activation of Smad 1/5 and Erk1/2 pathways, thus playing a crucial role in angiogenesis [225]. In our study, the upregulation of the BMPER gene in embryos from cows kept under normal temperature conditions may reflect a more favorable environment for early vascular development. As a critical regulator of BMP signaling, BMPER supports endothelial cell migration, sprouting, and tubulogenesis, all essential processes during angiogenesis and organogenesis. Since exposure to elevated environmental temperatures can disrupt vascular function and embryonic development, the higher expression of BMPER in embryos from cows in thermoneutral conditions likely indicates enhanced vascular integrity and developmental potential under optimal environmental conditions.

The FGB (Fibrinogen Beta Chain) gene, present in endometrial extracellular vesicles from fertile women, is linked to endometrial receptivity and may contribute to creating a supportive environment for embryo implantation and successful pregnancy [226]. The FGB gene, specifically the rs1800790 variant, has been associated with an increased risk of early pregnancy loss, suggesting that genetic alterations in fibrinogen production may influence maternal-fetal interactions and contribute to complications in early gestation [227]. DNA methylation within the FGB gene at birth was significantly associated with an increased risk of early-onset myopia in children, suggesting that epigenetic regulation of this gene may play a role in ocular development and early visual outcomes [228]. In our study, the upregulation of

the FGB gene in embryos from cows kept under normal temperature conditions may reflect a more favorable and receptive developmental environment. Given FGB's known role in enhancing endometrial receptivity and supporting early embryo implantation, its increased expression likely indicates improved maternal-embryonic communication and developmental potential. In contrast, exposure to elevated environmental temperatures may disrupt this regulatory balance, leading to lower FGB expression and potentially reduced embryo viability.

Quantitative analysis of kallikrein (KLK - Kallikrein-Related Peptidase Family) proteins across human tissues and fluids reveals distinct expression patterns, offering insights into their physiological roles and potential involvement in proteolytic cascades [229]. Kallikrein genes, including Klk1, Klk3, Klk9, and Klk21, show specific temporal and tissue expression during early embryonic development and may be involved in implantation and further embryogenesis [230]. The kallikrein gene family appears to participate in early developmental processes by regulating protein activation, extracellular matrix remodeling, and cellular proliferation during embryo implantation [230]. In the porcine species, various kallikrein genes (KLK1, KLK4, KLK11, and KLK14) show dynamic expression patterns in the endometrium and conceptus during the estrous cycle and early pregnancy, suggesting their role in growth factor activation and tissue remodeling during implantation [231]. In our study, the upregulation of the KLK gene in embryos derived from cows exposed to cooler environmental conditions, compared to those exposed to elevated environmental temperatures, may be explained by the role of kallikreins in early development. Kallikrein genes are known to regulate protein activation, extracellular matrix remodeling, and cellular proliferation during implantation and embryogenesis. Given their dynamic and tissue-specific expression during early development, as observed in both human and porcine models, it is likely that cooler conditions provided a more favorable environment for proper activation of these developmental processes, leading to increased KLK expression.

In mice, the reduction of MYL7 (Myosin Light Chain 7) levels due to VASN deficiency leads to structural abnormalities in the myocardium and may cause pathological cardiac hypertrophy [232]. In zebrafish embryos, selenium overload led to an enlargement of the atrial region, as observed through MYL7 reporter expression [233]. MYL7 expression was found to be upregulated in blastocysts derived from cows with subclinical endometritis, suggesting an impact of uterine inflammation on embryonic gene expression related to development [234]. In our study, the upregulation of MYL7 in embryos from cows kept under cooler conditions,

compared to those exposed to elevated environmental temperatures, may indicate better support for early cardiac development, as cooler environments favor normal physiological processes. However, previous studies have also shown that MYL7 expression can increase under stress or inflammatory conditions, such as in embryos from cows with subclinical endometritis. Therefore, it is possible that in addition to promoting development, cooler conditions may have triggered a mild adaptive stress response in the embryos.

The CD8B (Cluster of Differentiation 8 Beta) gene, which encodes the T-cell surface glycoprotein beta chain, is highly expressed in various sheep tissues, and its genetic variants are associated with increased body weight and size traits, making it a potential marker for breeding selection [235]. In chickens, CD8B expression was upregulated following vaccination against infectious laryngotracheitis, indicating its role in enhancing T cell activation and immune response [236]. In cows, the population of CD8B+ lymphocytes was influenced during early pregnancy, suggesting that changes in T cell subsets are part of the immune modulation associated with the establishment of pregnancy [237]. In calves with poor prognosis, reduced CD8B expression was associated with severe thymic histological abnormalities, suggesting impaired T cell development linked to acute thymic involution [238]. In our study, the upregulation of CD8B observed in embryos from cows exposed to cooler conditions compared to those exposed to elevated environmental temperatures may reflect a more balanced or enhanced immune preparedness. Previous studies indicate that CD8B expression is associated with immune system activation and proper T cell development, as seen after vaccination in chickens and during early pregnancy in cows. Moreover, reduced CD8B levels have been linked to thymic dysfunction and poor prognosis in calves. Therefore, the increased expression of CD8B in embryos from cooler environments may suggest a more favorable immunological status, supporting better developmental outcomes compared to embryos affected by elevated environmental temperatures.

The NR1I3 gene, known as the Nuclear Receptor Subfamily 1 Group I Member 3 or Constitutive Androstane Receptor (CAR), is a nuclear receptor that regulates the expression of genes involved in xenobiotic and endobiotic metabolism. Certain endogenous and exogenous ligands, including steroids, bilirubin, and various xenobiotics, can bind to and activate CAR, leading to its upregulation. Specific transcription factors and coactivators, such as hepatocyte nuclear factor 4 alpha (HNF4α) and peroxisome proliferator-activated receptor gamma coactivator 1-alpha (PGC-1α), can enhance NR1I3 transcription [239]. NR1I3 was initially

described as a key factor regulating the metabolism of xenobiotics, i.e., substances foreign to the body. More recent biochemical and structural findings indicate that this protein can be activated in response to metabolic and nutritional stresses in a ligand-independent manner. To gain deeper insight into its role, the NR1I3 gene was sequenced in 155 purebred Nellore bulls, leading to the identification of 24 distinct SNP polymorphisms. The results suggest that the expression and regulation of NR1I3 play a significant role in the feed efficiency of this breed, potentially providing a basis for developing new breeding strategies aimed at improving feed utilization [240]. NR1I3 was among the genes that showed the largest decrease in expression within granulosa cells from cows previously affected by metritis, pointing to a lasting alteration in the ovarian follicle's gene expression profile even after the disease had subsided [241]. In placental mammals, the detoxification gene NR1I3 can be repeatedly lost in strictly carnivorous lineages with low toxin exposure, highlighting its critical role in dietary toxin metabolism and the impact of relaxed selection on genomic evolution [242]. In our studies conducted on cows not exposed to high temperatures, there may have been an intensification of certain transcription factors (including HNF4α and PGC-1α) as well as an increased presence or activity of endogenous ligands (e.g., steroids or dietary metabolites) that stimulate NR1I3 expression. Because this gene is responsible for regulating detoxification mechanisms and endogenous metabolism, its higher level could result from optimal environmental conditions that allow for greater cellular sensitivity to metabolic signals. Furthermore, in line with reports of ligand-independent CAR activation, various nutrition- or homeostasis-related stimuli may have contributed to increased NR1I3 transcription, ultimately enhancing metabolic efficiency and the organism's adaptation to prevailing conditions.

CYP4V2 (Cytochrome P450 Family 4 Subfamily V Member 2) is a unique member of the CYP4 family that plays a key role in regulating lipid metabolism, particularly in cholesterol synthesis and lipid droplet formation, potentially influencing metabolic syndrome and nonalcoholic fatty liver disease progression. This gene encodes a member of the cytochrome P450 superfamily of enzymes, which are involved in drug metabolism and the synthesis of cholesterol, steroids, and other lipids [243]. CYP4V2 expression has been studied in the context of liver diseases, including hepatocellular carcinoma (HCC). Increased expression of this gene has been observed in certain cancerous tissues, suggesting a potential role in tumor biology. Gene Set Enrichment Analysis (GSEA) has indicated that high CYP4V2 expression is associated with specific biological pathways in HCC, impacting patient survival rates [244, 245]. The expression and regulation of CYP4V2 have also been studied in various contexts. In

zebrafish, for example, the expression of CYP4V2 and related genes is crucial for normal embryonic development, particularly in processes involving cell migration and organ formation [246].

The (Immunoglobulin Heavy Constant Mu) IGHM gene encodes the constant region of the immunoglobulin heavy chain mu, which defines the IgM isotype. IgM is one of the first antibodies produced during an immune response and is primarily found in the blood and lymphatic fluid. Upregulation of the IGHM gene can occur in various contexts, particularly in response to infections or immune challenges [247]. It has been demonstrated that IGHM—the earliest immunoglobulin isotype to emerge during evolution—is expressed in $CD34^{+}$ hematopoietic stem and progenitor cells (HSCs/HPCs) from umbilical cord blood, suggesting a potential role for immunoglobulin expression in early hematopoietic cell function [248]. In bovine species, IGHM exhibits notable genetic variability and has been mapped alongside the FES oncogene on chromosome 21, indicating that the genomic arrangement of immunoglobulin heavy chain genes in cattle differs from that observed in other mammals [249]. A sequential gene-editing approach enabled the successful knockout of both alleles of the transcriptionally inactive IGHM gene in bovine fibroblasts, leading to the creation of both heterozygous and homozygous knockout calves, and offering a promising alternative to germline-based genetic engineering in livestock [250]. The upregulation of the IGHM gene in embryos derived from cows maintained under normal temperature conditions may reflect proper activation of early immune mechanisms characteristic of physiologically developing hematopoietic cells. Since IGHM encodes the earliest immunoglobulin isotype produced during the immune response, its increased transcription could indicate enhanced immunological readiness in embryos developing under thermoneutral conditions, without exposure to elevated environmental temperatures.

The Hypoxanthine Phosphoribosyltransferase 1 (HPRT1) gene encodes the enzyme hypoxanthine-guanine phosphoribosyltransferase, which is involved in the purine salvage pathway, a critical process for recycling purines to synthesize nucleotides. This pathway is essential for cellular metabolism, DNA synthesis, and repair. The HPRT1 gene is crucial during embryonic development because it ensures that cells have a sufficient supply of nucleotides for rapid cell division and growth [251, 252]. In human cells, exposure to elevated glucose and fructose concentrations consistently suppressed HPRT1 expression, indicating a potential link between metabolic stress, disrupted purine metabolism, and increased cardiometabolic risk

[253]. HPRT1 was identified as one of the most stable reference genes for quantitative gene expression analysis in porcine placenta across gestation, ensuring reliable normalization of qPCR data during dynamic developmental changes [254]. HPRT1 expression proved highly variable in porcine immature Sertoli cells subjected to acute high-temperature exposure, highlighting its inadequacy as a reference gene for reliable normalization in transcriptomic analyses under these conditions [255]. The upregulation of HPRT1 observed in embryos from cows maintained under normal temperature conditions may reflect the absence of metabolic stress, allowing efficient activation of the purine salvage pathway. This pathway is essential for nucleotide synthesis during rapid cell proliferation and DNA replication in early embryonic development. In contrast, exposure to elevated ambient temperature may disturb this metabolic balance, potentially resulting in reduced HPRT1 expression and altered nucleotide availability, which could influence normal embryonic progression.

The MAGE Family Member B2 (MAGEB2) gene is part of the melanoma antigen (MAGE) gene family, which is primarily known for its expression in tumors and its role in immunotherapy [256]. However, MAGE genes, including MAGEB2, are also expressed in normal tissues, including during embryonic development. These genes are involved in various cellular processes, including apoptosis, cell cycle regulation, and differentiation, which are crucial for proper embryonic development [112, 257]. MAGE genes, particularly those involved in embryonic development in cattle, exhibit distinct promoter activity and are regulated primarily by zinc-finger transcription factors, with in silico analysis revealing strong promoter predictions and CpG island presence—highlighting their potential role in germ cell differentiation and early development [257]. The FosB Proto-Oncogene, AP-1 Transcription Factor Subunit (FOSB) gene encodes a protein that belongs to the Fos family of transcription factors, which are involved in regulating cell proliferation, differentiation, and survival [258]. FOSB was among twelve newly assigned gene loci mapped to the telomeric region of bovine chromosome BTA18q2.4–q2.6, confirming its conserved synteny with human chromosome 19q [259]. FOSB is a transcription factor that gradually accumulates in the nucleus accumbens in response to repeated stimuli, where it plays a pivotal role in mediating addiction, stress resilience, and the effects of antidepressant treatments [260]. FosB is broadly expressed during mouse development, particularly in forming bone, and although its absence does not cause overt developmental defects, it contributes functionally to gene regulation through AP-1-dependent pathways [261]. In rat 3Y1 embryonic cells, estrogen-induced nuclear translocation

of DeltaFosB alters cell morphology, reduces F-actin levels, halts proliferation, and modulates the expression of specific proteins, including a novel processed form of galectin-1 [262].

During the differentiation of bovine satellite cells into myotubes, Fos and FosB-members of the AP-1 transcription factor family were shown to positively regulate this process, as demonstrated by siRNA knockdown experiments targeting active enhancers marked by H3K27ac [263]. In bovine granulosa cells, FosB contributes to the gonadotropin-induced activation of the TNFAIP6 promoter during the ovulatory process, functioning through AP-1 and CRE elements in cooperation with other transcription factors [264].

In my study, increased expression of the FOSB gene was observed in embryos derived from cows kept under thermoneutral conditions. This upregulation may be related to FOSB's role in cell differentiation, environmental stimulus response, and AP-1 - dependent transcriptional regulation. As a transcription factor, FOSB is involved in controlling gene expression during development and differentiation, including in muscle and embryonic cells. Its higher expression under optimal conditions may reflect a more favorable environment for activating developmental programs, whereas exposure to elevated temperature in the other group may have disrupted these processes and suppressed FOSB induction.

The ZBBX gene (Zinc Finger B-Box and Coiled-Coil Domain Containing) encodes a protein that is part of the zinc finger protein family, which is known for its role in DNA binding and transcriptional regulation [100]. ZBBX is a cilia-associated gene found to be upregulated in the endometrial tissue of women with ectopic pregnancy, serving as one of the five key markers in a highly accurate molecular classifier for determining pregnancy location in nonviable pregnancies of unknown location [100]. ZBBX was identified as a high-degree hub gene within a co-expression network of early-stage cervical cancer, suggesting its potential as a diagnostic biomarker and therapeutic target in the disease [265]. ZBBX was identified among the genes with exonic variants potentially affecting protein function in Labrador retrievers with lumbosacral stenosis, suggesting it as a novel candidate gene for further investigation into the genetic basis of this condition [266]. In my study, increased expression of the ZBBX gene was observed in embryos from cows maintained under thermoneutral conditions, which may be linked to its role in transcriptional regulation and its association with cilia function—both of which are important during early embryonic development. Elevated temperatures can negatively affect cilia-related processes, so the upregulation of ZBBX under optimal conditions likely reflects proper molecular activity essential for normal embryogenesis.

It has been shown that the Forkhead Box A1 (FOXA1) gene is upregulated in lung, prostate, esophageal, and pancreatic cancer [267]. FOXA1 acts as a pioneer transcription factor during liver organogenesis, initiating chromatin opening to enable access for other transcriptional regulators and establishing epigenetic bookmarking essential for future hepatic gene activation [268].

FOXA1 serves as a specific marker of urogenital sinus epithelium and its pelvic derivatives, providing key evidence that the human vaginal epithelium originates exclusively from the urogenital sinus rather than Müllerian duct tissue [269]. Disruption of FOXA1 in mouse embryos creates a permissive environment for human cell integration, highlighting its essential role in nasopharyngeal epithelium development and its potential in generating humanized tissues through blastocyst complementation [270]. In mammals, FOXA1 and FOXA2 play essential roles in urethral development and cloacal division, functioning in a regulatory feedback loop with Sonic hedgehog (SHH) to coordinate genital tubercle formation and prevent malformations such as hypospadias and urethral fistula [271]. In cattle, FOXA1 acts as a key transcriptional activator of the ANGPTL4 gene, directly regulating its promoter activity and thereby influencing lipid metabolism and fat deposition [272]. In our study, the upregulation of FOXA1 in embryos derived from cows maintained under thermoneutral conditions may be attributed to its role as a pioneer transcription factor that initiates chromatin opening and activates key developmental pathways. Under elevated ambient temperature, these regulatory functions may be impaired, limiting access to essential regulatory sequences. Therefore, the higher FOXA1 expression observed in the control group likely reflects proper activation of developmental programs unaffected by environmental stress.

Lysosomal protein transmembrane 5 (LAPTM5) is a lysosome-associated transmembrane protein predominantly expressed in hematopoietic cells, suggesting a specialized role in immune cell function and development, particularly during embryogenesis and in adult lymphoid and myeloid tissues [273, 274]. LAPTM5 is upregulated during the differentiation of yolk sac-derived hematopoietic cells, suggesting a functional role in the maturation of adult hematopoietic lineages, particularly within lysosome-rich immune cell types [274]. In our study, the upregulation of LAPTM5 in embryos from cows maintained under thermoneutral conditions may be linked to its role in hematopoietic cell differentiation and the maturation of immune lineages. Exposure to elevated ambient temperature may disrupt normal immune

system development, so the higher expression of LAPTM5 in the control group likely reflects proper progression of hematopoiesis and lysosome-rich immune cell function.

MAGED2 inhibits stress-induced autophagy under hypoxic conditions by modulating the cAMP/PKA pathway, and its deficiency may lead to enhanced autophagic activity, contributing to impaired renal salt reabsorption as seen in transient Bartter's syndrome [275].

Melanoma Antigen Family D2 (MAGED2) is predominantly expressed in mesoderm-derived tissues during mouse embryogenesis, indicating its likely involvement in the development of non-neuronal structures [276]. MAGED2 is upregulated in renal tubular cells during both experimental and human acute kidney injury, indicating its potential involvement in the cellular stress response and pathophysiology of kidney damage [277]. In our study, the upregulation of MAGED2 in embryos from cows maintained under thermoneutral conditions may be linked to its role in cellular protection against stress, particularly through the inhibition of hypoxia-induced autophagy. Since MAGED2 is expressed in mesoderm-derived tissues during embryogenesis and is involved in the stress response, its higher expression under non-stressful conditions likely reflects normal developmental progression without the activation of compensatory stress pathways.

EVA1C (Eva-1 Homolog C) is significantly upregulated in neuronal cells under hypoxic-ischemic conditions, and its silencing enhances neuron survival and growth, suggesting a potential role in neurodevelopmental damage and a novel target for therapeutic intervention in neonatal hypoxic-ischemic encephalopathy [278]. EVA1C is overexpressed in WHO grade II/III gliomas and is strongly associated with increased immune cell infiltration and poor patient prognosis, highlighting its potential as a prognostic biomarker and indicator of immune activity in glioma [278]. EVA1C is expressed in axonal pathways of the developing mouse nervous system and may contribute to both Robo-dependent and Robo-independent Slit signaling, implicating it in the formation of neural circuits during development [279]. In our study, the upregulation of EVA1C in embryos from cows maintained under thermoneutral conditions may be associated with its role in axon guidance and neural circuit formation during early development. As EVA1C expression increases under hypoxic conditions and is linked to neurodevelopmental vulnerability, its elevated expression in the absence of elevated ambient temperature likely reflects proper activation of neurodevelopmental pathways essential for healthy nervous system formation.

SH3BGR (SH3 Domain-Binding Glutamic Acid-Rich Protein) acts as a negative regulator of endothelial cell migration and angiogenesis by inhibiting STAT 3 activity, and its suppression by KSHV-encoded miR-K6-3p facilitates tumor dissemination and vascular growth [280]. SH3BGR is maternally expressed during early zebrafish development and shows specific localization to the sarcomere, suggesting a potential role in muscle formation and early organogenesis, particularly in neural and digestive system development [281].

SH3BGR is essential for proper sarcomere assembly and heart development, as its loss disrupts muscle structure and segmentation in Xenopus, likely through regulation of Enah protein localization [282]. In our study, the upregulation of SH3BGR in embryos from cows maintained under thermoneutral conditions may reflect its critical role in early organogenesis, particularly in heart and muscle development. Given its involvement in sarcomere assembly and tissue segmentation, the absence of elevated ambient temperature likely allows for proper activation of developmental pathways requiring SH3BGR, whereas exposure to elevated ambient temperature in the comparison group may impair these processes and suppress gene expression.

The CA2 (Carbonic Anhydrase 2) gene, previously discussed in the context of its upregulation in embryos from younger cows, was also found to be upregulated in embryos derived from cows exposed to colder months. This recurring pattern suggests that CA2 expression may be sensitive to physiological environments characterized by increased metabolic or environmental stress, such as seasonal temperature changes. In colder months, mild hypoxia or shifts in metabolic and hormonal activity-such as changes in glucocorticoid levels-may stimulate CA2 expression as part of a broader adaptive response to maintain acid-base balance and cellular homeostasis during early development [283; 124]

The SH3-Domain GRB2-Like 2 (SH3GL2) gene, located within a QTL region linked to reproductive traits, contains intronic variants (T32742468C and G32742603A) that show a strong association with egg production at 300 days of age in chickens, suggesting its potential as a genetic marker for improving reproductive performance through selective breeding [284]. The SH3GL2 gene is involved in vesicular transport in the liver and may contribute to the regulation of yolk formation in ducks with high yolk ratios, highlighting its potential role in molecular trafficking related to yolk deposition [285]. The SH3GL2 gene has been identified as a maternal genetic locus associated with levels of the environmental pollutant BDE-28, suggesting its involvement in xenobiotic and lipid metabolism and highlighting its potential

role in modulating prenatal exposure to neurodevelopmental risk factors such as organohalogens [286]. In our study, upregulation of the SH3GL2 gene in embryos from cows maintained under normal temperature conditions may reflect a more stable and favorable environment for metabolic and reproductive processes. SH3GL2 is known to play roles in vesicular transport and lipid metabolism, both of which are essential for nutrient delivery and cellular communication during early embryonic development. Its involvement in reproductive traits and environmental response mechanisms, as shown in other species, suggests that normal thermal conditions may enhance SH3GL2 expression to support efficient molecular trafficking and metabolic homeostasis, potentially contributing to improved embryonic quality and developmental potential.

In our study, the FAM13C (Family With Sequence Similarity 13, Member C) gene was upregulated in embryos derived from cows during the cold season compared to those from the warm season. Although the role of this gene in embryogenesis remains unknown, its previously observed upregulation in embryos from younger cows may suggest that FAM13C responds to conditions associated with higher embryo quality or more favorable developmental environments. The cold season, typically associated with lower ambient temperatures, may provide such conditions, potentially explaining the increased expression of this gene in embryos developed during that period. The Metazoan SRP (Metazoan signal recognition particle RNA) gene was among the most highly upregulated transcripts in pancreatic cancer patients who experienced early death, suggesting its potential as a molecular marker associated with poor prognosis [287]. There is currently no significant information regarding the upregulation of the Metazoa_SRP gene in the context of embryos or embryogenesis.

The genes listed here were detected as differentially expressed transcripts in the analyzed embryos but lack well-established functions directly supporting mammalian embryogenesis. Some, such as ADRB2 and DOCK8, may indirectly influence early development through modulation of stress signaling or immune pathways, potentially affecting reproductive tissues and maternal–embryo interactions. Other transcripts (FBXO48, ABCC3) are primarily involved in cellular metabolism or detoxification processes, suggesting ancillary roles in maintaining tissue homeostasis during gestation. CDSN, while critical for epithelial proliferation and placental remodeling, does not have a clearly defined role in preimplantation embryos. Finally, ZNF845 has been characterized in invertebrate developmental systems without known functions in bovine or mammalian embryogenesis. Overall, while these genes

may contribute to broader physiological processes surrounding reproduction, their specific relevance to early bovine embryonic development requires further investigation.

5.2.2. The downregulated genes associated with embryos collected from cows in different seasons

This section describes down-regulated genes associated with embryos collected from cows in different seasons, beginning with those whose roles in embryogenesis are already defined, followed by genes whose functions in bovine embryonic development remain unclear. In the dissertation, the Season-dependent down-regulated genes (warm vs. cold season) in bovine embryos with established roles in embryogenesis and reproduction were identified (Table4 results section). The following genes were identified as differentially expressed transcripts in bovine embryos and were implicated in essential developmental pathways. Several encode key regulators of metabolism and energy balance (UQCRC2, AQP7, HAMP), ensuring adequate ATP production, nutrient transport, and iron homeostasis critical for rapid cellular proliferation. Transcripts involved in cytoskeletal organization and morphogenesis (DNAH12) or vesicle-mediated communication (SYT9) highlight the orchestration of intracellular trafficking and structural integrity during cleavage and implantation. Factors such as RBMS3 and FSD1L participate in stabilizing mRNA networks and epigenetic programming, underscoring their importance for lineage specification and adaptive responses to environmental cues. Transcriptional modulators (ETV5, BEND4) further govern early differentiation events and germ cell maturation. Additionally, components of proteasomal degradation and cell cycle regulation (PSMC6, FEM1B) reflect dynamic turnover and precise control of embryonic protein homeostasis. Together, these expression profiles provide insight into the molecular mechanisms driving preimplantation development and reveal potential pathways sensitive to maternal or environmental influences on embryonic competence.

RBMS3 (RNA Binding Motif Single Stranded Interacting Protein 3) is an RNA-binding protein important for embryonic development and cancer progression, influencing microRNA regulation and epithelial-mesenchymal transition, and may serve as a prognostic marker, although its molecular mechanisms remain incompletely understood [147]. RBMS3 supports cranial neural crest development by stabilizing transcripts in the TGF-β signaling pathway, crucial for promoting chondrogenesis [288]. RBMS3 supports early pancreas development by binding to the 3'UTR of Ptf1a mRNA, enhancing its translation and indirectly regulating downstream gene expression [149]. In Indian cattle breeds such as Gir and Tharparkar, which

are known for their adaptability and resilience, RBMS3 was identified as a gene under positive selection, particularly associated with reproductive functions. Its detection highlights the genetic mechanisms that support fertility and survival in challenging arid environments [289]. In our study, the downregulation of RBMS3 in embryos derived from cows exposed to colder conditions, compared to those exposed to elevated ambient temperature, may reflect reduced activation of pathways crucial for early developmental processes such as TGF-β signaling, chondrogenesis, and pancreas formation. Since RBMS3 stabilizes key transcripts involved in embryonic tissue development and supports the regulation of microRNA networks, its lower expression could indicate a slower or less dynamic progression of molecular events essential for rapid growth and differentiation. Additionally, considering that RBMS3 has been positively selected in cattle adapted to harsher, arid environments, it is possible that under colder and less metabolically demanding conditions, the selective pressure for high RBMS3 activity is reduced, leading to its decreased transcriptional activity during early embryogenesis.

The UQCRC2 (Ubiquinol-cytochrome c reductase core protein 2) gene has already been described above as downregulated in embryos derived from younger cows. Its downregulation in embryos originating from cows kept under cooler conditions may similarly reflect impaired mitochondrial function and energy production, potentially due to altered metabolic demands or mitochondrial adaptation mechanisms in response to the environmental temperature.

PSMC6 (Proteasome 26S Subunit, ATPase 6), a subunit of the proteasome, has been linked to the aggressiveness of ovarian carcinoma, with higher expression levels associated with advanced tumor stages and reduced progression-free survival. Knockdown of PSMC6 impaired cell growth, especially in cisplatin-resistant ovarian cancer cells, suggesting its potential as a diagnostic marker and therapeutic target [290]. PSMC6 was found to be significantly upregulated in embryonic stem cell-cloned mouse blastocysts, suggesting its involvement in developmental arrest and abnormalities in cloned embryos [291]. PSMC6 was identified as a target of bta-miR-26b, which downregulates immune-related genes in bovine endometrial epithelial cells to support conceptus implantation [292]. In our study, the downregulation of PSMC6 in embryos from cows kept under cold conditions, compared to those from cows exposed to elevated ambient temperature, may be related to the regulation of immune responses and protective mechanisms within the endometrial environment. As a component of the 26S proteasome, PSMC6 is involved in cell growth and stress response processes; its reduced expression could reflect lower immune activation and a limitation of stress-related pathways

in the endometrium, creating a more favorable environment for implantation. Additionally, since PSMC6 is a target of bta-miR-26b, which supports conceptus implantation by downregulating immune-related genes, the observed downregulation in cold conditions may indicate enhanced activation of these implantation-supportive pathways, contributing to better early embryonic development.

DNAH12 (Dynein Axonemal Heavy Chain 12) is a dynein protein lacking a microtubule-binding domain, essential for sperm flagellar structure but not for cilia function. Mutations in DNAH12 were identified as a recessive cause of male infertility (asthenoteratozoospermia), leading to defects in inner dynein arms and loss of the central pair in sperm flagella. In both human patients and mouse models, disruption of DNAH12 impaired the recruitment of dynein components DNALI1 and DNAH1, compromising sperm development, while intracytoplasmic sperm injection (ICSI) could bypass the infertility. These discoveries highlight DNAH12 as a critical factor in axoneme assembly and a potential diagnostic marker for male infertility [293]. In this study, DNAH12 was found to be significantly downregulated in sperm with IQUB deficiency, suggesting that DNAH12 is located near the RS1 structure and plays a role in maintaining proper inner dynein arm function, which is critical for normal sperm motility [294]. In a PTSD rat model, DNAH12 expression was found to be upregulated in the hippocampus, suggesting its involvement in axon extension processes linked to synaptic dysfunction [295]. In our study, the downregulation of DNAH12 in embryos from cows exposed to cold conditions, compared to those exposed to elevated ambient temperature, may reflect a reduced requirement for axonemal extension and remodeling. Given that DNAH12 is critical for inner dynein arm function and axoneme organization, its lower expression under colder conditions suggests greater stabilization of cellular structures, with less dynamic cytoskeletal remodeling required. This is consistent with a cellular environment less influenced by elevated temperature–associated adaptive demands, in contrast to embryos from cows exposed to elevated ambient temperature, where higher DNAH12 levels may reflect compensatory mechanisms aimed at maintaining axonemal integrity and structural organization.

ETV5 (ETS Variant Transcription Factor 5) is an ETS family transcription factor involved in the control of hepatic lipid metabolism. Its expression rises in steatotic livers caused by diet or genetic factors, and it operates in a nutrient-sensitive manner through the mTORC1 pathway. Loss of ETV5 function, either genetically or via viral depletion, results in greater lipid

accumulation in the liver. Transcriptomic analyses showed that ETV5 deficiency downregulates PPAR signaling and fatty acid metabolism pathways. Mechanistically, ETV5 enhances the activity of PPAR-responsive genes, supporting efficient β-oxidation. These findings position ETV5 as an important regulator of liver lipid balance and a promising target for therapies against hepatic steatosis [296]. ETV5, together with ETV4, acts as a key downstream effector of FGF signaling in early mouse embryos, essential for primitive endoderm formation, timely exit from naïve pluripotency, and proper epiblast maturation; its deficiency disrupts early lineage specification and embryonic patterning [297]. ETV5 is essential for female fertility in mice, playing a key role in maintaining ovarian structure, regulating mating behavior, and ensuring the developmental competence of embryos; its absence leads to impaired ovulation, reduced mating interest, and compromised early embryonic development [298]. In our study, the downregulation of ETV5 in embryos from cows exposed to cold conditions, compared to those exposed to elevated ambient temperature, may reflect a reduced requirement for metabolic adaptation during early development. Since ETV5 is involved in nutrient-sensitive pathways, including lipid metabolism via mTORC1 and PPAR signaling, its lower expression under colder conditions suggests that embryos experienced fewer temperature-associated metabolic challenges and maintained more stable developmental processes. Additionally, given ETV5's role in early lineage specification and epiblast maturation, reduced expression may indicate a slower or more tightly regulated progression of developmental stages in embryos derived from colder environments, potentially favoring improved embryo quality relative to those exposed to elevated ambient temperature.

SYT9 (Synaptotagmin 9) has already been described as a downregulated gene related to aging, highlighting its sensitivity to developmental and physiological changes over time. SYT9 belongs to the synaptotagmin family, proteins that act as calcium and phospholipid sensors during exocytosis, especially in neurotransmission. Although closely related to SYT1, SYT9 has distinct binding properties and biological functions. Studies in mouse models revealed that mutations or loss of SYT9 lead to severe developmental defects, including approximately 50% embryonic lethality, emphasizing its crucial role in cellular signaling during early embryogenesis. These findings point to SYT9 as an essential factor for proper development and cellular communication.

FSD1L (Fibronectin Type III and SPRY Domain Containing 1-Like) was identified as a gene where DNA methylation levels are significantly reduced in children exposed in utero to higher

maternal blood glucose levels, suggesting that fetal epigenetic programming of FSD1L may be influenced by maternal hyperglycemia and potentially impact long-term health outcomes [154]. FSD1L was highlighted as a positional candidate gene near a major genomic region associated with early fertility traits in Brahman cattle, such as first mating pregnancy and rebreeding success. Its location in a region also linked to puberty timing in humans suggests a possible role for FSD1L in regulating reproductive maturation and function [151]. Higher maternal blood glucose levels during pregnancy were associated with reduced DNA methylation at a CpG site within the FSD1L gene in offspring from birth to five years of age, suggesting that FSD1L may be epigenetically regulated by prenatal exposure to hyperglycemia and could be linked to long-term health risks [154]. In our study, the downregulation of FSD1L in embryos from cows exposed to cold conditions, compared to those exposed to elevated ambient temperature, may be related to environmental influences on early epigenetic programming. Since reduced DNA methylation and altered FSD1L expression have been associated with prenatal conditions such as maternal hyperglycemia, it is possible that exposure to colder environmental conditions similarly affects epigenetic regulation of this gene. Given the proposed role of FSD1L in reproductive development and metabolic adaptation, its lower expression under colder conditions may reflect a shift in developmental pathways favoring energy conservation and modified growth trajectories.

FEM1B has already been described in the context of downregulation related to age. Based on the available information, the reduced expression of FEM1B in embryos from cows exposed to colder conditions may be linked to seasonal influences on early developmental regulation. Since FEM1B is critical for proper cell differentiation and growth during embryogenesis, its downregulation under cold conditions could reflect an adaptive response, where lower metabolic activity and slower cell differentiation are favored to conserve energy and maintain embryo viability in a less favorable environment.

HAMP (Hepcidin Antimicrobial Peptide) is essential for regulating iron balance during early development, as shown in zebrafish where its deletion caused maternal iron overload, reduced hemoglobin levels, and disrupted blood progenitor cell development through increased ferroptosis. These findings highlight HAMP's critical role in maintaining proper hematopoiesis and iron homeostasis during embryogenesis [299]. In human embryonic liver cells, exposure to fluoride increased HAMP (hepcidin) expression, leading to disrupted iron metabolism and oxidative stress. Treatment with grape seed proanthocyanidin extract (GSPE) reversed these

effects by lowering HAMP levels, reducing iron accumulation, and improving antioxidant defenses, suggesting that HAMP plays a key role in mediating fluoride-induced cellular damage through iron regulation [300]. In a β-thalassemia mouse model, fetal iron overload triggered the activation of HAMP (hepcidin) in the fetal liver. Increased fetal hepcidin then suppressed placental ferroportin expression, reducing iron transfer across the placenta and partially protecting the fetus from excessive iron accumulation. This highlights HAMP's key role in regulating iron balance during thalassemic pregnancy [301]. In our study, the downregulation of HAMP in embryos from cows exposed to cold conditions, compared to those exposed to elevated ambient temperature, may reflect adjustments in iron metabolism under lower environmental temperature. Since HAMP is a key regulator of iron homeostasis and its overexpression has been associated with oxidative imbalance and altered hematopoietic processes, lower HAMP expression in embryos from colder conditions may help maintain a more balanced iron status and limit potential oxidative damage. In contrast, embryos exposed to elevated ambient temperature may exhibit higher HAMP expression as part of adaptive regulatory mechanisms aimed at maintaining iron homeostasis under temperature-associated physiological demands.

BEND4 (BEN Domain Containing 4) is a member of the BEN-domain protein family, identified as a novel regulator involved in early germ cell development. Working together with BEND5, BEND4 helps establish chromatin boundaries and promotes the differentiation of epiblast-like cells, suggesting its role as a transcriptional modulator crucial for primordial germ cell specification [302]. A pathogenic variant of BEND4 (p.Gly433Ser) was linked to infection-induced acute necrotizing encephalopathy in a family study, where affected individuals experienced severe neurological deterioration [303]. In our study, the downregulation of BEND4 in embryos from cows exposed to cold conditions, compared to those exposed to elevated ambient temperature, may reflect seasonal modulation of early developmental regulation. Since BEND4 is involved in chromatin organization and differentiation of early germ cell lineages, its reduced expression under colder conditions may indicate a more gradual or energy-conserving developmental progression, potentially prioritizing embryo survival over rapid differentiation. Additionally, as alterations in BEND4 function have been associated with increased cellular vulnerability, lower expression in embryos derived from colder environments may contribute to maintaining cellular stability during early development.

AQP7 (Aquaporin 7) is expressed throughout early stages of human and mouse embryo development, from the oocyte to the blastocyst. Functional studies showed that knocking down AQP7 in 2-cell mouse embryos significantly impaired preimplantation development, suggesting that AQP7 plays a crucial role in maintaining water homeostasis necessary for early embryonic growth [304]. AQP7 is a key glycerol channel in adipocytes, and its expression is downregulated by elevated FSH levels in post-menopausal women. This downregulation reduces glycerol efflux, promoting lipid accumulation. Mechanistically, FSH inhibits AQP7 transcription by activating CREB, which competes with c-Jun for binding at AP-1 sites in the AQP7 promoter, contributing to post-menopausal fat accumulation [305]. In our study, the downregulation of AQP7 in embryos from cows exposed to cold conditions, compared to those exposed to elevated ambient temperature, may reflect adjustments in metabolic and osmotic regulation. Since AQP7 plays a crucial role in water and glycerol transport during early embryonic development, its lower expression under colder environmental conditions may contribute to energy conservation and adaptation to reduced cellular metabolic activity. Similar to the association of AQP7 downregulation with altered lipid metabolism in other contexts, embryos developing under lower environmental temperature may modulate AQP7 expression to maintain balanced water and energy homeostasis.

ABCC3 (ATP Binding Cassette Subfamily C Member 3), also known as MRP3 is an ATP-dependent membrane transporter from the ABC protein family that exports xenobiotics and anionic molecules. It has a conserved structure across species, including sharks and humans, with especially high similarity in the nucleotide-binding domains. In shark mesenchymal stem cells, ABCC3 expression can be strongly induced by peptide growth factors, serum, and lipid components, highlighting its role in cellular responses to environmental and nutritional signals [306]. ABCC3 is one of the key transplacental transporters associated with the movement of environmental pollutants, such as flame retardants and perfluoroalkyl substances, from maternal to fetal circulation. Its expression levels correlate with the efficiency of pollutant transfer across the placenta, highlighting its potential role in fetal exposure to harmful compounds [307]. ABCC3 expression in the human placenta increases significantly from the first to the third trimester of pregnancy. This gestational age-dependent regulation suggests that ABCC3 may play an important role in supporting placental barrier function, nutrient transport, and fetal protection as pregnancy progresses [308]. In our study, the downregulation of ABCC3 in embryos from cows exposed to cold conditions, compared to those exposed to elevated ambient temperature, may reflect adjustments to lower environmental and metabolic demands.

Since ABCC3 is involved in xenobiotic export and regulation of substance transfer across the placenta, its reduced expression under colder conditions may indicate a diminished requirement for active transport and detoxification processes during early development. In a colder and more thermoneutral environment, embryos may encounter fewer metabolic or environmental challenges, which could contribute to lower ABCC3 expression relative to embryos developing under elevated ambient temperature.

Fbxo48 (F-Box Protein 48) is an orphan E3 ubiquitin ligase subunit that promotes the degradation of phosphorylated AMPKα (pAMPKα), a key regulator of metabolism. A novel inhibitor, BC1618, prevents this degradation, thereby sustaining AMPK activity without directly activating it. By stabilizing pAMPKα, BC1618 enhances mitochondrial fission, supports autophagy, and improves insulin sensitivity in obese mice, highlighting a new therapeutic strategy to regulate metabolic health [309]. FBXO48 is located in a genomic region linked to Parkinson's disease type 3 (PARK3) and is a paralog of FBXO7, a gene associated with Parkinson's disease type 15. However, genetic screening of Parkinson's patients revealed no mutations in the coding region of FBXO48, suggesting it likely does not contribute significantly to Parkinson's disease development [310]. In our study, the downregulation of FBXO48 in embryos from cows exposed to cold conditions, compared to those exposed to elevated ambient temperature, may reflect a metabolic adjustment aimed at maintaining energy balance. Since FBXO48 promotes the degradation of phosphorylated AMPKα, a central regulator of cellular energy homeostasis, its reduced expression under colder environmental conditions may contribute to sustained AMPK activity. This would support better mitochondrial function, autophagy, and overall energy efficiency, which are crucial for embryo survival and development in a low-temperature environment. Thus, the downregulation of FBDOCK8 (Dedicator of Cytokinesis 8) is crucial for proper immune function, as mutations in this gene cause a form of combined immunodeficiency known as DOCK8 deficiency, characterized by recurrent infections and increased cancer risk. DOCK8 supports lymphocyte survival, migration, and immune synapse formation, and also regulates signaling pathways that influence cytokine production and immune cell polarization, making it essential for both innate and adaptive immune responses [311]. Microduplications involving the DOCK8 gene at 9p24.3 have been identified in prenatal diagnoses, but they generally appear to be benign, as most cases showed no major abnormalities after birth. Although one fetus exhibited increased nuchal translucency, follow-up data indicated normal development in the majority of cases. These findings suggest that duplications involving DOCK8 may have limited clinical impact, but

ongoing monitoring and larger studies are needed to fully understand their significance [99]. DOCK8 was identified as a Z-linked gene that can be used for molecular sexing in paleognath bird species. By measuring gene copy number variation through qPCR, researchers demonstrated that DOCK8 helps distinguish males (ZZ) from females (ZW), contributing to a broader and more accurate method for sex identification across different bird lineages [312]. In our study, the downregulation of DOCK8 in embryos from cows exposed to cold conditions, compared to those exposed to elevated ambient temperature, may reflect modulation of immune-related pathways during early development. Since DOCK8 plays an important role in lymphocyte function, cytokine signaling, and immune synapse formation, its reduced expression under colder environmental conditions may indicate a relative shift toward prioritizing core developmental processes over immune-related activity. In a colder and more thermoneutral environment, embryos may experience fewer physiological challenges, potentially resulting in lower activation of immune-associated pathways compared to embryos developing under elevated ambient temperature.

ADRB2 (Adrenoceptor Beta 2) plays a crucial role in mediating the depletion of ovarian primordial follicles under sleep deprivation conditions by enhancing stress hormone signaling. It promotes the activation of the KITL-KIT/PI3K-mTOR pathway through norepinephrine and epinephrine stimulation, leading to increased follicle activation. Blocking ADRB2 could offer a therapeutic strategy to prevent premature follicle loss associated with sleep deprivation [313]. ADRB2 is essential for regulating epithelial tissue flexibility during development by promoting actomyosin relaxation, which allows apical cell expansion and body elongation. Loss of ADRB2 leads to excessive cell contraction and impaired tissue growth, highlighting its crucial role in coordinating epithelial morphogenesis through ligand-dependent signaling [312]. ADRB2 expression increases during decidualization, and elevated maternal epinephrine levels impair this process by suppressing stromal cell proliferation and key decidualization regulators, leading to delayed embryonic development and early pregnancy failure [313]. In our study, the downregulation of ADRB2 in embryos from cows exposed to cold conditions, compared to those exposed to elevated ambient temperature, may reflect reduced activation of adrenergic signaling pathways during early development. Since ADRB2 mediates cellular responses to catecholamines such as norepinephrine and epinephrine and has been implicated in processes including follicular dynamics, epithelial remodeling, and decidualization, its lower expression under colder environmental conditions may indicate a more stable developmental environment. Reduced ADRB2 expression may be associated with diminished adrenergic pathway

activation, potentially supporting balanced tissue regulation and early developmental progression relative to embryos developing under elevated ambient temperature.

ZNF845 (Zinc Finger Protein 845) is a C2H2-type zinc finger transcription factor that directs the development of cnidocytes in sea anemones by promoting the acquisition of new cell-specific traits while suppressing ancestral neural features. This gene, which originated through domain shuffling in early cnidarians, plays a key role in transforming neurons into the novel stinging cells essential for prey capture. Currently, there is limited information about the function of ZNF845, particularly regarding its role in embryonic development.

CDSN (corneodesmosin) was found to be upregulated in a mouse model of cleft palate induced by all-trans retinoic acid. Its expression is regulated through a ceRNA network involving LncRNA-NONMMUT100923.1 and miR-200a-3p. Increased CDSN levels promote the proliferation of palatal shelf epithelial cells and may interfere with proper adhesion during palatogenesis by maintaining desmosome junctions, contributing to cleft palate formation [316]. However, in a study on sow placental tissues, CDSN was identified as one of the genes upregulated in sows giving birth to low birth weight litters. Gene enrichment analysis linked CDSN to biological processes such as cornification and cell proliferation regulation, suggesting that its transcriptional activation may influence placental development and impact fetal growth [317]. In our study, the downregulation of CDSN in embryos from cows exposed to cold conditions, compared to those exposed to elevated ambient temperature, may reflect modulation of pathways involved in tissue organization during early development. Since CDSN has been associated with epithelial cell proliferation and the maintenance of cell–cell adhesion structures such as desmosomes, altered expression levels may influence tissue remodeling dynamics. Under colder environmental conditions, reduced CDSN expression may be consistent with a more regulated pattern of epithelial proliferation and structural organization, potentially supporting stable developmental progression relative to embryos developing under elevated ambient temperature.

In this dissertation, the season-dependent down-regulated genes (warm vs. cold season) in bovine embryos with uncharacterized or indirect roles in embryogenesis were also identified. The following genes that were detected as differentially expressed transcripts in the analyzed embryos but lack well-established functions directly supporting mammalian embryogenesis were: ADRB2 and DOCK8, which may indirectly influence early development through modulation of stress signaling or immune pathways, potentially affecting reproductive tissues

and maternal–embryo interactions. Other transcripts (FBXO48, ABCC3) are primarily involved in cellular metabolism or detoxification processes, suggesting ancillary roles in maintaining tissue homeostasis during gestation. CDSN, while critical for epithelial proliferation and placental remodeling, does not have a clearly defined role in preimplantation embryos. Finally, ZNF845 has been characterized in invertebrate developmental systems without known functions in bovine or mammalian embryogenesis. Overall, while these genes may contribute to broader physiological processes surrounding reproduction, their specific relevance to early bovine embryonic development requires further investigation.

5.3 Deconvolution

In this study, a deconvolution-inspired approach was applied as an analytical framework to comparatively assess similarities and differences in transcriptional profiles across stages of bovine preimplantation development. Bulk RNA-seq data derived from individual, in vivo–collected embryos were analyzed, meaning that each sample represented the transcriptome of an entire embryo rather than a mixture of cells originating from different tissues. In this context, deconvolution was not used to estimate true cellular proportions, but rather as an analytical framework enabling the identification of shared gene expression signatures and the evaluation of transcriptional similarity between successive developmental stages.

Results from hierarchical clustering and UMAP visualization demonstrated clear separation of transcriptional profiles corresponding to individual stages of preimplantation development. Embryos representing early stages (oocyte, zygote, 2-cell, and 4-cell stages) exhibited high transcriptional similarity among themselves, whereas the 8-cell stage, morula, and late blastocyst formed distinct clusters. These observations are consistent with previous reports indicating pronounced transcriptomic transitions during preimplantation development, particularly during embryonic genome activation and subsequent functional differentiation of cells [68].

Analysis of marker genes using Venn diagrams revealed that the majority of genes were specific to individual developmental stages, with only a small fraction shared between clusters. The highest number of unique markers was observed for the 8-cell stage and for the group encompassing the earliest developmental stages (oocyte/zygote/2-cell/4-cell), indicating the presence of clearly defined, stage-specific gene expression programs. The limited overlap of

marker genes between stages further confirms that transcriptomic changes during preimplantation development are dynamic and strongly dependent on developmental stage.

Application of the MuSiC algorithm enabled a comparative assessment of transcriptional similarity between the analyzed embryos and reference developmental stages. Heatmap-based visualization indicated that transcriptional profiles characteristic of the late blastocyst stage predominated across all analyzed samples, while signatures corresponding to the 8-cell stage and morula were absent and those associated with the earliest developmental stages were detected only at low levels. These findings suggest that the whole-embryo transcriptome is largely shaped by later-stage gene expression programs, which may reflect biological synchronization of embryo development as well as higher transcriptional activity characteristic of later developmental stages, resulting in their dominance in bulk RNA-seq data [319].

Comparison of results obtained using MuSiC and DeTREM revealed overall agreement regarding the predominance of late blastocyst–associated transcriptional signatures, while also highlighting differences in the detection of low-level signals from earlier developmental stages. DeTREM identified slightly stronger indications of early-stage and 8-cell–associated signatures in a subset of samples, which may result from differences in algorithmic design and increased sensitivity to subtle transcriptional variation. These differences underscore that the choice of analytical method influences the interpretation of transcriptomic similarity across developmental stages and should be carefully considered during data analysis [320].

In summary, the application of a deconvolution-inspired framework to bulk RNA-seq data from individual embryos enabled a detailed assessment of transcriptional similarity across stages of bovine preimplantation development. The results confirm the existence of distinct, stage-specific gene expression programs and indicate that whole-embryo transcriptomes are largely dominated by signatures of later developmental stages. This analysis provides coherent and biologically meaningful insights into transcriptomic dynamics during preimplantation development and establishes a solid foundation for future studies integrating bulk and single-cell RNA-seq data.

6. Conclusions

This study investigated the effects of maternal age and seasonal environmental conditions on the transcriptomic profile of in vivo-derived preimplantation bovine embryos obtained from Polish Holstein-Friesian cows. The RNA-seq-based approach enabled the identification of differences in gene expression and biological processes potentially associated with embryo

developmental competence, metabolism, and the capacity to adapt to the maternal environment.

Comparison of embryos derived from older cows relative to younger donors revealed increased expression of genes involved in immune signaling, cellular differentiation, metabolic regulation, and endocrine activity, including *STAT4, EGR2, PDK4, HPRT1*, and *CYP11A1*, as well as transcripts related to cell migration and embryo–endometrium interactions (e.g., CCL24, ZBBX). Concurrently, embryos from older cows exhibited reduced expression of numerous genes with well-established roles in early development, encompassing mitochondrial and energy-producing pathways (UQCRC2, IMPDH1), cytoskeletal organization and cell division (AKT2, JMY), cell polarity and cilia-dependent signaling (ARL13A, PROM1), and genomic stability maintenance (FANCA). Collectively, these changes indicate that advanced maternal age is associated with attenuation of molecular programs essential for efficient metabolism, structural integrity, and normal progression of early embryogenesis.

Seasonal analysis, conducted by comparing embryos collected during the warm season relative to the cold season, revealed pronounced activation of genes associated with cellular stress response and adaptation, as well as endocrine regulation and implantation-related processes. Warm-season embryos displayed increased expression of *HSPA6, FSHR, CXCR4, and CYP11A1,* alongside genes supporting angiogenesis and maternal–embryo interactions (BMPER, FGB, KLK) and markers related to cardiac development and immune function (MYL7, CD8B). In parallel, embryos obtained during the warm season showed reduced expression of genes involved in mitochondrial respiration and metabolic homeostasis (UQCRC2, AQP7, HAMP), cytoskeletal organization and morphogenesis (DNAH12), vesicle trafficking (SYT9), as well as transcriptional and epigenetic regulators (ETV5, RBMS3, BEND4, FSD1L) and a proteasomal component (PSMC6). This transcriptional pattern suggests that warm seasonal conditions promote activation of stress-adaptive and hormonal pathways, while simultaneously altering energy-related and regulatory mechanisms that may influence the tempo and stability of embryonic development.

In addition, a deconvolution-inspired analytical framework employing both MuSiC and DeTREM algorithms was applied to enable comparative assessment of transcriptional similarity between individual embryos and reference developmental stages. These analyses demonstrated that whole-embryo bulk transcriptomes were largely dominated by late blastocyst-associated transcriptional signatures, whereas contributions from earlier

developmental stages were limited. This observation indicates that bulk embryo transcriptomes primarily reflect later developmental gene expression programs and highlights the utility of deconvolution-based approaches as an interpretative framework for analyzing preimplantation developmental transcriptomes.

Taken together, the results demonstrate that maternal age and seasonal environmental conditions exert significant and partially overlapping effects on embryonic transcriptional programs, modulating genes and pathways critical for metabolism, cellular organization, genomic stability, implantation readiness, and stress response. The identified transcriptomic signatures provide a foundation for further investigation of molecular markers of embryo developmental competence and may support optimization of reproductive management strategies, including consideration of donor age and environmental conditions, in assisted reproduction programs in cattle.

7. References

1. Baruselli PS, Ferreira RM, Vieira LM, Souza AH, Bó GA, Rodrigues CA. Use of embryo transfer to alleviate infertility caused by heat stress. Theriogenology. 2020 Oct 1;155:1-11. doi: 10.1016/j.theriogenology.2020.04.028. Epub 2020 Jun 2. PMID: 32562738.
2. Kenny DA, Heslin J, Byrne CJ. Early onset of puberty in cattle: implications for gamete quality and embryo survival. Reprod Fertil Dev. 2017 Jan;30(1):101-117. doi: 10.1071/RD17376. PMID: 29539307.
3. Duittoz, A. H., Tillet, Y., Le Bourhis, D., & Schibler, L. (2016). The timing of puberty (oocyte quality and management). Animal Reproduction, 13(3), 313–333. https://doi.org/10.21451/1984-3143-AR874
4. Perry GA. Factors affecting puberty in replacement beef heifers. Theriogenology. 2016 Jul 1;86(1):373-8. doi: 10.1016/j.theriogenology.2016.04.051. Epub 2016 Apr 21. PMID: 27160450.
5. Abah KO, Fontbonne A, Partyka A, Nizanski W. Effect of male age on semen quality in domestic animals: potential for advanced functional and translational research? Vet Res Commun. 2023 Sep;47(3):1125-1137. doi: 10.1007/s11259-023-10159-1. Epub 2023 Jul 11. PMID: 37433886; PMCID: PMC10485126.
6. Roth Z. Effect of Heat Stress on Reproduction in Dairy Cows: Insights into the Cellular and Molecular Responses of the Oocyte. Annu Rev Anim Biosci. 2017 Feb 8;5:151-170. doi: 10.1146/annurev-animal-022516-022849. Epub 2016 Oct 12. PMID: 27732786.
7. Diskin MG, Kenny DA. Optimising reproductive performance of beef cows and replacement heifers. Animal. 2014 May;8 Suppl 1:27-39. doi: 10.1017/S175173111400086X. Epub 2014 Apr 7. PMID: 24703426.
8. Lonergan P, Fair T, Corcoran D, Evans AC. Effect of culture environment on gene expression and developmental characteristics in IVF-derived embryos. Theriogenology. 2006 Jan 7;65(1):137-52. doi: 10.1016/j.theriogenology.2005.09.028. Epub 2005 Nov 9. PMID: 16289260.
9. Westwood CT, Lean IJ, Garvin JK. Factors influencing fertility of Holstein dairy cows: a multivariate description. J Dairy Sci. 2002 Dec;85(12):3225-37. doi: 10.3168/jds.S0022-0302(02)74411-1. PMID: 12512596.

10. Wang Y, Wu ZW, Fang T, Zhang YQ, Chen L, Du ZQ, Yang CX. Identification of internal reference genes for porcine immature Sertoli cells under heat stress. Reprod Domest Anim. 2022 Nov;57(11):1344-1352. doi: 10.1111/rda.14211. Epub 2022 Jul 29. PMID: 35869802.
11. Wrenzycki C. Gene expression analysis and in vitro production procedures for bovine preimplantation embryos: Past highlights, present concepts and future prospects. Reprod Domest Anim. 2018 Sep;53 Suppl 2:14-19. doi: 10.1111/rda.13260. PMID: 30238652.
12. Lockhart KN, Drum JN, Balboula AZ, Spinka CM, Spencer TE, Ortega MS. Sire modulates developmental kinetics and transcriptome of the bovine embryo. Reproduction. 2023 Oct 4;166(5):337-348. doi: 10.1530/REP-23-0030. PMID: 37672361.
13. Ribeiro ES, Greco LF, Bisinotto RS, Lima FS, Thatcher WW, Santos JE. Biology of Preimplantation Conceptus at the Onset of Elongation in Dairy Cows. Biol Reprod. 2016 Apr;94(4):97. doi: 10.1095/biolreprod.115.134908. Epub 2016 Mar 2. PMID: 26935601.
14. Smith SL, Everts RE, Sung LY, Du F, Page RL, Henderson B, Rodriguez-Zas SL, Nedambale TL, Renard JP, Lewin HA, Yang X, Tian XC. Gene expression profiling of single bovine embryos uncovers significant effects of in vitro maturation, fertilization and culture. Mol Reprod Dev. 2009 Jan;76(1):38-47. doi: 10.1002/mrd.20927. Erratum in: Mol Reprod Dev. 2009 May;76(5):523. PMID: 18449896.
15. Shirasuna K, Iwata H. Effect of aging on the female reproductive function. Contracept Reprod Med. 2017 Oct 3;2:23. doi: 10.1186/s40834-017-0050-9. PMID: 29201428; PMCID: PMC5683335.
16. Zhang D-X, Park W-J, Sun S-C, Xu Y-N, Li Y-H, Cui X-S, Kim N-H. Regulation of Maternal Gene Expression by MEK/MAPK and MPF Signaling in Porcine Oocytes during In Vitro Meiotic Maturation. J Reprod Dev. 2011;57(1):49–56. doi: 10.1262/jrd.10-087H.
17. Xu F, Sun J, Gu X, Zhou Q. An innovative prognostic auxiliary for colon adenocarcinoma based on zinc finger protein genes. Transl Cancer Res. 2024 Apr 30;13(4):1623-1641. doi: 10.21037/tcr-23-2158. Epub 2024 Apr 25. PMID: 38737696; PMCID: PMC11082816.

18. de Barros FRO, Paula-Lopes FF. Cellular and epigenetic changes induced by heat stress in bovine preimplantation embryos. Mol Reprod Dev. 2018 Nov;85(11):810-820. doi: 10.1002/mrd.23040. Epub 2018 Nov 8. PMID: 29956856.
19. Nabenishi H, Ohta H, Nishimoto T, Morita T, Ashizawa K, Tsuzuki Y. The effects of cysteine addition during in vitro maturation on the developmental competence, ROS, GSH and apoptosis level of bovine oocytes exposed to heat stress. Zygote. 2012 Aug;20(3):249-59. doi: 10.1017/S0967199411000220. Epub 2011 May 18. PMID: 21729376.
20. Roth Z. Heat stress, the follicle, and its enclosed oocyte: mechanisms and potential strategies to improve fertility in dairy cows. Reprod Domest Anim. 2008 Jul;43 Suppl 2:238-44. doi: 10.1111/j.1439-0531.2008.01168.x. PMID: 18638130.
21. De Rensis F, Scaramuzzi RJ. Heat stress and seasonal effects on reproduction in the dairy cow--a review. Theriogenology. 2003 Oct 1;60(6):1139-51. doi: 10.1016/s0093-691x(03)00126-2. PMID: 12935853.
22. Payton RR, Romar R, Coy P, Saxton AM, Lawrence JL, Edwards JL. Susceptibility of bovine germinal vesicle-stage oocytes from antral follicles to direct effects of heat stress in vitro. Biol Reprod. 2004 Oct;71(4):1303-8. doi: 10.1095/biolreprod.104.029892. Epub 2004 Jun 16. PMID: 15201201.
23. Edwards JL, Hansen PJ. Elevated temperature increases heat shock protein 70 synthesis in bovine two-cell embryos and compromises function of maturing oocytes. Biol Reprod. 1996 Aug;55(2):341-6. doi: 10.1095/biolreprod55.2.341. PMID: 8828838.
24. Hooper LM, Payton RR, Rispoli LA, Saxton AM, Edwards JL. Impact of heat stress on germinal vesicle breakdown and lipolytic changes during in vitro maturation of bovine oocytes. J Reprod Dev. 2015;61(5):459-64. doi: 10.1262/jrd.2014-168. Epub 2015 Jun 29. PMID: 26120041; PMCID: PMC4623152.
25. Ozawa M, Hirabayashi M, Kanai Y. Developmental competence and oxidative state of mouse zygotes heat-stressed maternally or in vitro. Reproduction. 2002 Nov;124(5):683-9. doi: 10.1530/rep.0.1240683. PMID: 12417007.
26. Naranjo-Gómez JS, Uribe-García HF, Herrera-Sánchez MP, Lozano-Villegas KJ, Rodríguez-Hernández R, Rondón-Barragán IS. Heat stress on cattle embryo: gene regulation and adaptation. Heliyon. 2021 Mar 26;7(3):e06570. doi: 10.1016/j.heliyon.2021.e06570. PMID: 33869831; PMCID: PMC8035499.

27. Ealy AD, Drost M, Hansen PJ. Developmental changes in embryonic resistance to adverse effects of maternal heat stress in cows. J Dairy Sci. 1993 Oct;76(10):2899-905. doi: 10.3168/jds.S0022-0302(93)77629-8. PMID: 8227617.
28. Hansen PJ, Drost M, Rivera RM, Paula-Lopes FF, al-Katanani YM, Krininger CE 3rd, Chase CC Jr. Adverse impact of heat stress on embryo production: causes and strategies for mitigation. Theriogenology. 2001 Jan 1;55(1):91-103. doi: 10.1016/s0093-691x(00)00448-9. PMID: 11198091.
29. Sakatani M, Kobayashi S, Takahashi M. Effects of heat shock on in vitro development and intracellular oxidative state of bovine preimplantation embryos. Mol Reprod Dev. 2004 Jan;67(1):77-82. doi: 10.1002/mrd.20014. PMID: 14648877.
30. Rivera RM, Hansen PJ. Development of cultured bovine embryos after exposure to high temperatures in the physiological range. Reproduction. 2001 Jan;121(1):107-15. PMID: 11226033.
31. Bonilla L, Block J, Denicol AC, Hansen PJ. Consequences of transfer of an in vitro-produced embryo for the dam and resultant calf. J Dairy Sci. 2014;97(1):229-39. doi: 10.3168/jds.2013-6943. Epub 2013 Nov 7. PMID: 24210495.
32. Fear JM, Hansen PJ. Developmental changes in expression of genes involved in regulation of apoptosis in the bovine preimplantation embryo. Biol Reprod. 2011 Jan;84(1):43-51. doi: 10.1095/biolreprod.110.086249. Epub 2010 Sep 1. PMID: 20811013.
33. Miętkiewska K, Kordowitzki P, Pareek CS. Effects of Heat Stress on Bovine Oocytes and Early Embryonic Development-An Update. Cells. 2022 Dec 16;11(24):4073. doi: 10.3390/cells11244073. PMID: 36552837; PMCID: PMC9776454.
34. Chandolia RK, Peltier MR, Tian W, Hansen PJ. Transcriptional control of development, protein synthesis, and heat-induced heat shock protein 70 synthesis in 2-cell bovine embryos. Biol Reprod. 1999 Dec;61(6):1644-8. doi: 10.1095/biolreprod61.6.1644. PMID: 10570014.
35. Hassan FU, Nawaz A, Rehman MS, Ali MA, Dilshad SMR, Yang C. Prospects of HSP70 as a genetic marker for thermo-tolerance and immuno-modulation in animals under climate change scenario. Anim Nutr. 2019 Dec;5(4):340-350. doi: 10.1016/j.aninu.2019.06.005. Epub 2019 Jun 28. PMID: 31890910; PMCID: PMC6920399.
36. Camargo LSA, Aguirre-Lavin T, Adenot P, Araujo TD, Mendes VRA, Louro ID, Beaujean N, Souza ED. Heat shock during in vitro maturation induces chromatin

modifications in the bovine embryo. Reproduction. 2019 Oct;158(4):313-322. doi: 10.1530/REP-19-0245. PMID: 31426029.

37. Pavani KC, Baron E, Correia P, Lourenço J, Bettencourt BF, Sousa M, da Silva FM. Gene expression, oocyte nuclear maturation and developmental competence of bovine oocytes and embryos produced after in vivo and in vitro heat shock. Zygote. 2016 Oct;24(5):748-59. doi: 10.1017/S0967199416000071. Epub 2016 Mar 28. PMID: 27019120.
38. Khan I, Lee KL, Xu L, Mesalam A, Chowdhury MM, Joo MD, Ihsan-Ul-Haq, Mirza B, Kong IK. Improvement of in vitro-produced bovine embryo treated with coagulansin-A under heat-stressed condition. Reproduction. 2017 Apr;153(4):421-431. doi: 10.1530/REP-16-0530. Epub 2017 Jan 9. PMID: 28069903.
39. Corcoran D, Rizos D, Fair T, Evans AC, Lonergan P. Temporal expression of transcripts related to embryo quality in bovine embryos cultured from the two-cell to blastocyst stage in vitro or in vivo. Mol Reprod Dev. 2007 Aug;74(8):972-7. doi: 10.1002/mrd.20677. PMID: 17219429.
40. Bustin SA, Nolan T. Pitfalls of quantitative real-time reverse-transcription polymerase chain reaction. J Biomol Tech. 2004 Sep;15(3):155-66. PMID: 15331581; PMCID: PMC2291693.
41. Pareek CS, Smoczynski R, Tretyn A. Sequencing technologies and genome sequencing. J Appl Genet. 2011 Nov;52(4):413-35. doi: 10.1007/s13353-011-0057-x. Epub 2011 Jun 23. PMID: 21698376; PMCID: PMC3189340.
42. Chitwood DH, Kumar R, Headland LR, Ranjan A, Covington MF, Ichihashi Y, Fulop D, Jiménez-Gómez JM, Peng J, Maloof JN, Sinha NR. A quantitative genetic basis for leaf morphology in a set of precisely defined tomato introgression lines. Plant Cell. 2013 Jul;25(7):2465-81. doi: 10.1105/tpc.113.112391. Epub 2013 Jul 19. PMID: 23872539; PMCID: PMC3753377.
43. Xu F, Sun J, Gu X, Zhou Q. An innovative prognostic auxiliary for colon adenocarcinoma based on zinc finger protein genes. Transl Cancer Res. 2024 Apr 30;13(4):1623-1641. doi: 10.21037/tcr-23-2158. Epub 2024 Apr 25. PMID: 38737696; PMCID: PMC11082816.
44. Noguchi T, Aizawa T, Munakata Y, Iwata H. Comparison of gene expression and mitochondria number between bovine blastocysts obtained in vitro and in vivo. J Reprod Dev. 2020 Feb 14;66(1):35-39. doi: 10.1262/jrd.2019-100. Epub 2019 Nov 20. PMID: 31748448; PMCID: PMC7040209.

45. Wang LN, Jia JS, Yang XL, Wen YT, Liu JX, Li DK, Chen XR, Wang JH, Li JK, Huang ZX, Yao KT. Foxa1 disruption enhances human cell integration in human-mouse interspecies chimeras. Cell Tissue Res. 2025 Feb;399(2):231-245. doi: 10.1007/s00441-024-03941-3. Epub 2024 Dec 21. PMID: 39708115
46. Adjaye J, Herwig R, Brink TC, Herrmann D, Greber B, Sudheer S, Groth D, Carnwath JW, Lehrach H, Niemann H. Conserved molecular portraits of bovine and human blastocysts as a consequence of the transition from maternal to embryonic control of gene expression. Physiol Genomics. 2007 Oct 22;31(2):315-27. doi: 10.1152/physiolgenomics.00041.2007. Epub 2007 Jun 26. PMID: 17595343.
47. Bermejo-Alvarez P, Lonergan P, Rizos D, Gutiérrez-Adan A. Low oxygen tension during IVM improves bovine oocyte competence and enhances anaerobic glycolysis. Reprod Biomed Online. 2010 Mar;20(3):341-9. doi: 10.1016/j.rbmo.2009.12.006. Epub 2009 Dec 16. PMID: 20093090.
48. Fan, Jiaxin, Yafei Lyu, Qihuang Zhang, Xuran Wang, Mingyao Li, and Rui Xiao. 2022. "MuSiC2: cell-type deconvolution for multi-condition bulk RNA-seq data." Briefings in Bioinformatics 23 (6): bbac430. https://doi.org/10.1093/bib/bbac430.
49. Bó GA, Baruselli PS, Chesta PM, Martins CM. The timing of ovulation and insemination schedules in superstimulated cattle. Theriogenology. 2006;65(1):89–101. doi: 10.1016/j.theriogenology.2005.10.008.
50. Stringfellow DA, Givens MD. Manual of the International Embryo Transfer Society: a procedural guide and general information for the use of embryo transfer technology emphasizing sanitary procedures. 4th ed. Savoy: IETS Publish; 2009.
51. Bo, Gabriel and Mapletoft, Reuben. (2013). Evaluation and classification of bovine embryos. Animal reproduction. 10. 344-348.
52. Cock P.J.A. et al (2010). The Sanger FASTQ file format for sequences with quality scores, and the Solexa/Illumina FASTQ variants. Nucleic acids research 38, 1767-1771.
53. Hansen K.D. et al (2010). Biases in Illumina transcriptome sequencing caused by random hexamer priming. Nucleic acids research 38, e131-e131.
54. Erlich Y.et al (2008). Alta-Cyclic: a self-optimizing base caller for next-generation sequencing.Nature Methods,5,679-682.
55. Jiang L.C. et al (2011). Synthetic spike-in standards for RNA-seq experiments. Genome research 21, 1543-1551.

56. Andrews, S. FastQC: A quality control tool for high-throughput sequence data. Available online at: http://www.bioinformatics.babraham.ac.uk/projects/fastqc/ (2010).
57. Chen, S., Zhou, Y., Chen, Y. & Gu, J. fastp: An ultra-fast all-in-one FASTQ preprocessor. Bioinformatics 34, i884–i890 (2018).
58. Yan L.Y. et al (2013). Single-cell RNA-Seq profiling of human preimplantation embryos and embryonic stem cells. Nat Struct Mol Biol.
59. Li, B. & Dewey, C. N. RSEM: Accurate transcript quantification from RNA-Seq data with or without a reference genome. BMC Bioinform. 12, 323 (2011).
60. Dobin, A. et al. STAR: Ultrafast universal RNA-seq aligner. Bioinformatics 29, 15–21 (2013).
61. Lassmann, T., Hayashizaki, Y. & Daub, C. O. SAMStat: Monitoring biases in next generation sequencing data. Bioinformatics 27, 130–131 (2011).
62. Graubert, A., Aguet, F., Ravi, A., Ardlie, K. G. & Getz, G. RNA-SeQC 2: Efficient RNA-seq quality control and quantification for large cohorts. Bioinformatics 37, 3048–3050 (2021).
63. Ewels, P., Magnusson, M., Lundin, S. & Käller, M. MultiQC: Summarize analysis results for multiple tools and samples in a single report. Bioinformatics 32, 3047–3048 (2016).
64. Love, M. I., Huber, W. & Anders, S. Moderated estimation of fold change and dispersion for RNA-seq data with DESeq2. Genome Biol. 15, 550 (2014).
65. Leek, J. T. et al. The sva package for removing batch effects and other unwanted variation in high-throughput experiments. Bioinformatics 28, 882–883 (2012)
66. Bindea G, Mlecnik B, Hackl H, Charoentong P, Tosolini M, Kirilovsky A, Fridman WH, Pagès F, Trajanoski Z, Galon J. ClueGO: a Cytoscape plug-in to decipher functionally grouped gene ontology and pathway annotation networks. Bioinformatics. 2009 Apr 15;25(8):1091-3. doi: 10.1093/bioinformatics/btp101.
67. Tang D, Chen M, Huang X, Zhang G, Zeng L, Zhang G, et al. (2023) SRplot: A free online platform for data visualization and graphing. PLoS ONE 18(11): e0294236. https://doi.org/10.1371/journal.pone.0294236
68. Yan L, Yang M, Guo H, Yang L, Wu J, Li R, Liu P, et al. Single-Cell RNA-Seq Profiling of Human Preimplantation Embryos and Embryonic Stem Cells. Nat Struct Mol Biol. 2013 Aug;20:1131–1139. doi: 10.1038/nsmb.2660. PMID: 23851493.

69. Edgar, Ron, Michael Domrachev, and Alex Lash. 2002. “Gene Expression Omnibus: NCBI Gene Expression and Hybridization Array Data Repository.” Nucleic Acids Research 30 (February): 207–10. https://doi.org/10.1093/nar/30.1.207.
70. Martin F, Amode M, Aneja A, Austine-Orimoloye O, Azov A, Barnes I, Becker A, et al. Ensembl 2023. Nucleic Acids Res. 2022 Nov;51. https://doi.org/10.1093/nar/gkac958.
71. O’Neill N, Stein T, Hu J, Rehman H, Campbell J, Yajima M, Zhang X, Farrer L. Bulk Brain Tissue Cell-Type Deconvolution with Bias Correction for Single-Nuclei RNA Sequencing Data Using DeTREM. BMC Bioinformatics. 2023 Sep;24. https://doi.org/10.1186/s12859-023-05476-w.
72. Khatib H, Huang W, Mikheil D, Schutzkus V, Monson RL. Effects of STAT1 and STAT3 genotypic combinations on fertilization and embryonic survival rates in Holstein cattle. J Dairy Sci. 2009 Dec;92(12):6186-91. doi: 10.3168/jds.2009-2439. PMID: 19923622.
73. Darnell, J. E. 1997. STATs and gene regulation. Science 277:1630–1635.
74. Takeda K, Noguchi K, Shi W, Tanaka T, Matsumoto M, Yoshida N, Kishimoto T, Akira S. Targeted disruption of the mouse Stat3 gene leads to early embryonic lethality. Proc Natl Acad Sci U S A. 1997;94:3801–3804.
75. Maj T, Chelmonska-Soyta A. Pleiotropy and redundancy of STAT proteins in early pregnancy. Reprod. Domest. Anim. 2007;42:343–353
76. Upadhyay R, Dua B, Sharma B, Natrajan M, Jain AK, Kithiganahalli Narayanaswamy B, Joshi B. Transcription factors STAT-4, STAT-6 and CREB regulate Th1/Th2 response in leprosy patients: effect of M. leprae antigens. BMC Infect Dis. 2019 Jan 14;19(1):52. doi: 10.1186/s12879-018-3601-z. PMID: 30642265; PMCID: PMC6332553.
77. Zhong Z, Wen Z, Darnell JE Jr. Stat3 and Stat4: members of the family of signal transducers and activators of transcription. Proc Natl Acad Sci U S A. 1994;91(11):4806–4810. doi: 10.1073/pnas.91.11.4806.
78. Price PA, Caputo JM, Williamson MK. Bone origin of the serum complex of calcium, phosphate, fetuin, and matrix Gla protein: biochemical evidence for the cancellous bone-remodeling compartment. J Bone Miner Res. 2002;17:1171-1179.
79. Cancela M L, laizé v, conceição n (2014). Matrix Gla protein and osteocalcin: from gene duplication to neofunctionalization. Arch Biochem Biophys 1; 561: 56-63.

80. Correia E, Conceição N, Cancela ML, Belo JA. Matrix Gla Protein expression pattern in the early avian embryo. Int J Dev Biol. 2016;60(1-3):71-6. doi: 10.1387/ijdb.150365jb. PMID: 26934291.
81. Hu MC, Hsu HJ, Guo IC, Chung BC. Function of Cyp11a1 in animal models. Mol Cell Endocrinol. 2004 Feb 27;215(1-2):95-100. doi: 10.1016/j.mce.2003.11.024. PMID: 15026180.
82. Manna PR, Stetson CL, Slominski AT, Pruitt K. Role of the steroidogenic acute regulatory protein in health and disease. Endocrine. 2016 Jan;51(1):7-21. doi: 10.1007/s12020-015-0715-6. Epub 2015 Aug 14. PMID: 26271515; PMCID: PMC4707056.
83. Watanabe MX, Jones SP, Iwata H, Kim EY, Kennedy SW. Effects of co-exposure to 2,3,7,8-tetrachlorodibenzo-p-dioxin and perfluorooctane sulfonate or perfluorooctanoic acid on expression of cytochrome P450 isoforms in chicken (Gallus gallus) embryo hepatocyte cultures. Comp Biochem Physiol C Toxicol Pharmacol. 2009 May;149(4):605-12. doi: 10.1016/j.cbpc.2009.01.001. Epub 2009 Jan 10. PMID: 19167519.
84. Shen N, Li C, Yang S, Ma Y, Wang HL. Liver proteomics analysis reveals the differentiation of lipid mechanism and antioxidant enzyme activity during chicken embryonic development. Int J Biol Macromol. 2023 Dec 31;253(Pt 7):127417. doi: 10.1016/j.ijbiomac.2023.127417. Epub 2023 Oct 16. PMID: 37848110.
85. Singh R, Kumar K, Ranjan R, Kumar M, Yasotha T, Singh RK, Das BC, Sarkar M, Bag S. Comparative expression analysis of embryonic development-related genes at different stages of parthenogenetic and in vitro fertilized embryos in caprine. Zygote. 2015 Apr;23(2):198-204. doi: 10.1017/S096719941300049X. Epub 2013 Nov 11. PMID: 24229648.
86. Garcia-Zepeda EA, Rothenberg ME, Ownbey RT, Celestin J, Leder P, Luster AD. Human eotaxin is a specific chemoattractant for eosinophil cells and provides a new mechanism to explain tissue eosinophilia. Nat Med. 1996 Apr;2(4):449-56. doi: 10.1038/nm0496-449. PMID: 8597956.
87. Li H, Huang YH, Li MQ, Meng YH, Chen X, Shao J, Tang CL, Du MR, Jin LP, Li DJ. Trophoblasts-derived chemokine CCL24 promotes the proliferation, growth and apoptosis of decidual stromal cells in human early pregnancy. Int J Clin Exp Pathol. 2013 May 15;6(6):1028-37. PMID: 23696919; PMCID: PMC3657354.

88. Li H, Meng YH, Shang WQ, Liu LB, Chen X, Yuan MM, Jin LP, Li MQ, Li DJ. Chemokine CCL24 promotes the growth and invasiveness of trophoblasts through ERK1/2 and PI3K signaling pathways in human early pregnancy. Reproduction. 2015 Nov;150(5):417-27. doi: 10.1530/REP-15-0119. Epub 2015 Aug 27. PMID: 26316550.
89. Negrón-Pérez VM, Vargas-Franco D, Hansen PJ. Role of chemokine (C-C motif) ligand 24 in spatial arrangement of the inner cell mass of the bovine embryo. Biol Reprod. 2017 May 1;96(5):948-959. doi: 10.1093/biolre/iox037. PMID: 28449095.
90. Goupil S, Maréchal L, El Hajj H, Tremblay MÈ, Richard FJ, Leclerc P. Identification and Localization of the Cyclic Nucleotide Phosphodiesterase 10A in Bovine Testis and Mature Spermatozoa. PLoS One. 2016 Aug 22;11(8):e0161035. doi: 10.1371/journal.pone.0161035. PMID: 27548062; PMCID: PMC4993467.
91. Fujishige K, Kotera J, Michibata H, Yuasa K, Takebayashi S, Okumura K, Omori K. Cloning and characterization of a novel human phosphodiesterase that hydrolyzes both cAMP and cGMP (PDE10A). J Biol Chem. 1999 Jun 25;274(26):18438-45. doi: 10.1074/jbc.274.26.18438. PMID: 10373451.
92. Sasseville' M, Gagnon MC, Guillemette C, Sullivan R, Gilchrist RB, Richard FJ. Regulation of gap junctions in porcine cumulus-oocyte complexes: contributions of granulosa cell contact, gonadotropins, and lipid rafts. Mol Endocrinol. 2009 May;23(5):700-10. doi: 10.1210/me.2008-0320. Epub 2009 Feb 19. PMID: 19228792; PMCID: PMC5419259.
93. Lv Y, Lu G, Cai Y, Su R, Liang L, Wang X, Mu W, He X, Huang T, Ma J, Zhao Y, Chen ZJ, Xue Y, Liu H, Chan WY. RBM46 is essential for gametogenesis and functions in post-transcriptional roles affecting meiotic cohesion
94. Dai X, Cheng X, Huang J, Gao Y, Wang D, Feng Z, Zhai G, Lou Q, He J, Wang Z, Yin Z. Rbm46, a novel germ cell-specific factor, modulates meiotic progression and spermatogenesis. Biol Reprod. 2021 May 7;104(5):1139-1153. doi: 10.1093/biolre/ioab016. PMID: 33524105.
95. Song X, Liu J, Kuang F, Chen X, Zeh HJ 3rd, Kang R, Kroemer G, Xie Y, Tang D. PDK4 dictates metabolic resistance to ferroptosis by suppressing pyruvate oxidation and fatty acid synthesis. Cell Rep. 2021 Feb 23;34(8):108767. doi: 10.1016/j.celrep.2021.108767. PMID: 33626342.

96. Hong L, Xiao S, Diao L, Lian R, Chen C, Zeng Y, Liu S. Decreased AMPK/SIRT1/PDK4 induced by androgen excess inhibits human endometrial stromal cell decidualization in PCOS. Cell Mol Life Sci. 2024 Jul 30;81(1):324. doi: 10.1007/s00018-024-05362-5. PMID: 39080028; PMCID: PMC11335245.
97. Wathes DC, Clempson AM, Pollott GE. Associations between lipid metabolism and fertility in the dairy cow. Reprod Fertil Dev. 2012;25(1):48-61. doi: 10.1071/RD12272. PMID: 23244828.
98. Zhu HL, Shi XT, Xu XF, Zhou GX, Xiong YW, Yi SJ, Liu WB, Dai LM, Cao XL, Xu DX, Wang H. Melatonin protects against environmental stress-induced fetal growth restriction via suppressing ROS-mediated GCN2/ATF4/BNIP3-dependent mitophagy in placental trophoblasts. Redox Biol. 2021 Apr;40:101854. doi: 10.1016/j.redox.2021.101854. PMID: 33454563; PMCID: PMC7811044.
99. Yue L, Yu HF, Yang ZQ, Tian XC, Zheng LW, Guo B. Egr2 mediates the differentiation of mouse uterine stromal cells responsiveness to HB-EGF during decidualization. J Exp Zool B Mol Dev Evol. 2018 Jun;330(4):215-224. doi: 10.1002/jez.b.22807. Epub 2018 May 20. PMID: 29781132.
100. Du N, Kwon H, Li P, West EE, Oh J, Liao W, Yu Z, Ren M, Leonard WJ. EGR2 is critical for peripheral naïve T-cell differentiation and the T-cell response to influenza. Proc Natl Acad Sci U S A. 2014 Nov 18;111(46):16484-9. doi: 10.1073/pnas.1417215111. Epub 2014 Nov 3. PMID: 25368162; PMCID: PMC4246296.
101. Lentscher JA, Colburn ZT, Ortogero N, Gillette L, Leonard GT, Burney RO, Chow GE. An intrauterine genomic classifier reliably delineates the location of nonviable pregnancies. Fertil Steril. 2021 Jul;116(1):138-146. doi: 10.1016/j.fertnstert.2021.02.005. Epub 2021 Mar 24. PMID: 33771330.
102. Biase FH, Moorey SE, Schnuelle JG, Rodning S, Ortega MS, Spencer TE. Extensive rewiring of the gene regulatory interactions between in vitro-produced conceptuses and endometrium during attachment. PNAS Nexus. 2023 Sep 2;2(9):pgad284. doi: 10.1093/pnasnexus/pgad284. PMID: 37711857; PMCID: PMC10498941.
103. Rivière T, Bader A, Pogoda K, Walzog B, Maier-Begandt D. Structure and Emerging Functions of LRCH Proteins in Leukocyte Biology. Front Cell Dev Biol. 2020 Sep 22;8:584134. doi: 10.3389/fcell.2020.584134. PMID: 33072765; PMCID: PMC7536344.

104. Protasova MS, Gusev FE, Andreeva TV, Klyushnikov SA, Illarioshkin SN, Rogaev EI. Novel genes bearing mutations in rare cases of early-onset ataxia with cerebellar hypoplasia. Eur J Hum Genet. 2022 Jun;30(6):703-711. doi: 10.1038/s41431-022-01088-9. Epub 2022 Mar 29. PMID: 35351988; PMCID: PMC9178031.

105. Amatore F, Gorvel L, Olive D. Role of Inducible Co-Stimulator (ICOS) in cancer immunotherapy. Expert Opin Biol Ther. 2020 Feb;20(2):141-150. doi: 10.1080/14712598.2020.1693540. Epub 2019 Nov 28. PMID: 31738626.

106. Zhao X, Wang Y, Jiang X, Mo B, Wang C, Tang M, Rong Y, Zhang G, Hu M, Cai H. Comprehensive analysis of the role of ICOS (CD278) in pan-cancer prognosis and immunotherapy. BMC Cancer. 2023 Feb 28;23(1):194. doi: 10.1186/s12885-023-10564-4. PMID: 36855091; PMCID: PMC9971684.

107. Thul, P. J., & Lindskog, C. (2018). The Human Protein Atlas – A tool for pathology. Journal of Pathology, 246(5), 1–3. Retrieved from https://www.proteinatlas.org/

108. Burdelski C, Borcherding L, Kluth M, Hube-Magg C, Melling N, Simon R, Möller-Koop C, Weigand P, Minner S, Haese A, Michl HU, Tsourlakis MC, Jacobsen F, Hinsch A, Wittmer C, Lebok P, Steurer S, Izbicki JR, Sauter G, Krech T, Büscheck F, Clauditz T, Schlomm T, Wilczak W. Family with sequence similarity 13C (FAM13C) overexpression is an independent prognostic marker in prostate cancer. Oncotarget. 2017 May 9;8(19):31494-31508. doi: 10.18632/oncotarget.16357. PMID: 28415558; PMCID: PMC5458224.

109. Chi H, Gao X, Xia Z, Yu W, Yin X, Pan Y, Peng G, Mao X, Teichmann AT, Zhang J, Tran LJ, Jiang T, Liu Y, Yang G, Wang Q. FAM family gene prediction model reveals heterogeneity, stemness and immune microenvironment of UCEC. Front Mol Biosci. 2023 May 19;10:1200335. doi: 10.3389/fmolb.2023.1200335. PMID: 37275958; PMCID: PMC10235772.

110. Candels LS, Becker S, Trautwein C. PLA2G7: a new player in shaping energy metabolism and lifespan. Signal Transduct Target Ther. 2022 Jun 17;7(1):195. doi: 10.1038/s41392-022-01052-5. PMID: 35715398; PMCID: PMC9206017.

111. Shiao MS, Liu ST, Siriwatcharapibool G, Thongpradit S, Khunpanich P, Tong SK, Huang CH, Jinawath N, Chou MY. Conserved expression of the zebrafish syt4 gene in GABAergic neurons in the cerebellum of adult fishes revealed by mammalian

SYT4 immunoreactive-like signals. Heliyon. 2024 May 3;10(9):e30575. doi: 10.1016/j.heliyon.2024.e30575. PMID: 38765140; PMCID: PMC11098836.

112. Mendez JA, Bourque MJ, Fasano C, Kortleven C, Trudeau LE. Somatodendritic Dopamine Release Requires Synaptotagmin 4 and 7 and the Participation of Voltage-Gated Calcium Channels. PLoS One. 2011;6:e25657. doi: 10.1371/journal.pone.0025657.

113. Ladelfa MF, Peche LY, Amato GE, Escalada MC, Zampieri S, Pascucci FA, Benevento AF, Do Porto DF, Dardis A, Schneider C, Monte M. Expression of the tumor-expressed protein MageB2 enhances rRNA transcription. Biochim Biophys Acta Mol Cell Res. 2021 Jun;1868(7):119015. doi: 10.1016/j.bbamcr.2021.119015. Epub 2021 Mar 17. PMID: 33741433.

114. Chomez P, De Backer O, Bertrand M, De Plaen E, Boon T, Lucas S. An overview of the MAGE gene family with the identification of all human members of the family. Cancer Res. 2001 Jul 15;61(14):5544-51. PMID: 11454705.

115. Sun D, Liu L, Yan Y. Development and Evaluation of a Nomogram for INCS Insensitivity in Chinese Adults with Allergic Rhinitis. Int J Clin Pract. 2023 Apr 18;2023:3027092. doi: 10.1155/2023/3027092. PMID: 37113405; PMCID: PMC10129423.

116. Maiuthed A, Prakhongcheep O, Chanvorachote P. Microarray-based Analysis of Genes, Transcription Factors, and Epigenetic Modifications in Lung Cancer Exposed to Nitric Oxide. Cancer Genomics Proteomics. 2020 Jul-Aug;17(4):401-415. doi: 10.21873/cgp.20199. PMID: 32576585; PMCID: PMC7367602.

117. Rontani P, Perche O, Greetham L, Jullien N, Gepner B, Féron F, Nivet E, Erard-Garcia M. Impaired expression of the COSMOC/MOCOS gene unit in ASD patient stem cells. Mol Psychiatry. 2021 May;26(5):1606-1618. doi: 10.1038/s41380-020-0728-2. Epub 2020 Apr 23. PMID: 32327736; PMCID: PMC8159765.

118. Sedda D, Mackowiak C, Pailloux J, Culerier E, Dudas A, Rontani P, Erard N, Lefevre A, Mavel S, Emond P, Foucher F, Le Bert M, Quesniaux VFJ, Mihatsch MJ, Ryffel B, Erard-Garcia M. Deletion of Mocos Induces Xanthinuria with Obstructive Nephropathy and Major Metabolic Disorders in Mice. Kidney360. 2021 Sep 17;2(11):1793-1806. doi: 10.34067/KID.0001732021. PMID: 35372998; PMCID: PMC8785848.

119. Brakeman PR, Lanahan AA, O'Brien R, Roche K, Barnes CA, Huganir RL, Worley PF. Homer: a protein that selectively binds metabotropic glutamate receptors. Nature. 1997 Mar 20;386(6622):284-8. doi: 10.1038/386284a0. PMID: 9069287.

120. Sato M, Suzuki K, Nakanishi S. NMDA receptor stimulation and brain-derived neurotrophic factor upregulate homer 1a mRNA via the MAPK cascade in cultured cerebellar granule cells. J Neurosci. 2001 Jun 1;21(11):3797-805. doi: 10.1523/JNEUROSCI.21-11-03797.2001. PMID: 11356868; PMCID: PMC6762687.

121. Rietschel M, Mattheisen M, Frank J, Treutlein J, Degenhardt F, Breuer R, Steffens M, Mier D, Esslinger C, Walter H, Kirsch P, Erk S, Schnell K, Herms S, Wichmann HE, Schreiber S, Jöckel KH, Strohmaier J, Roeske D, Haenisch B, Gross M, Hoefels S, Lucae S, Binder EB, Wienker TF, Schulze TG, Schmäl C, Zimmer A, Juraeva D, Brors B, Bettecken T, Meyer-Lindenberg A, Müller-Myhsok B, Maier W, Nöthen MM, Cichon S. Genome-wide association-, replication-, and neuroimaging study implicates HOMER1 in the etiology of major depression. Biol Psychiatry. 2010 Sep 15;68(6):578-85. doi: 10.1016/j.biopsych.2010.05.038. Epub 2010 Jul 31. PMID: 20673876.

122. Jiang J, Kong K, Fang X, Wang D, Zhang Y, Wang P, Yang Z, Zhang Y, Liu X, Aung T, Li F, Yu-Wai-Man P, Zhang X. CRISPR-Cas9-mediated deletion of carbonic anhydrase 2 in the ciliary body to treat glaucoma. Cell Rep Med. 2024 May 21;5(5):101524. doi: 10.1016/j.xcrm.2024.101524. Epub 2024 Apr 25. PMID: 38670096; PMCID: PMC11148640.

123. Yan M, Cai L, Duan X, Tycksen ED, Rai MF. Carbonic anhydrase 2 is important for articular chondrocyte function and metabolic homeostasis. Bone. 2025 Jan;190:117313. doi: 10.1016/j.bone.2024.117313. Epub 2024 Oct 31. PMID: 39488239.

124. Pastorekova S, Parkkila S, Pastorek J, et al. Carbonic anhydrases: current state of the art, therapeutic applications, and future prospects. J Enzyme Inhib Med Chem. 2004 Apr;19(3):199-229.

125. Deshpande GP, Patterton HG, Faadiel Essop M. The human transketolase-like proteins TKTL1 and TKTL2 are bona fide transketolases. BMC Struct Biol. 2019 Jan 15;19(1):2. doi: 10.1186/s12900-018-0099-y. PMID: 30646877; PMCID: PMC6334435.

126. Xu X, Zur Hausen A, Coy JF, et al. Transketolase-like protein 1 (TKTL1) is associated with cell proliferation and cancer prognosis. Cancer Lett. 2009 May 8;273(2):251-9.

127. Zhang S, Yang JH, Guo CK, et al. Increased expression of transketolase-like gene 1 promotes cell proliferation and migration in human colon cancer. Tumour Biol. 2015 Jul;36(7):8953-64.

128. Valsalan J, Chakravarty AK, Patil CS, Dash SK, Mahajan AC, Kumar V, Vohra V. Enhancing milk and fertility performances using selection index developed for Indian Murrah buffaloes. Trop Anim Health Prod. 2014 Aug;46(6):967-74. doi: 10.1007/s11250-014-0596-3. Epub 2014 Apr 30. PMID: 24781153.

129. Peter HL, Giglberger M, Frank J, Streit F, Zänkert S, Kreuzpointner L, Rietschel M, Kudielka BM, Wüst S. The association between genetic variability in the NPS/NPSR1 system and chronic stress responses: A gene-environment-(quasi-) experiment. Psychoneuroendocrinology. 2022 Oct;144:105883. doi: 10.1016/j.psyneuen.2022.105883. Epub 2022 Jul 27. PMID: 35914393.

130. Robledo G, González-Gay MA, Fernández-Gutiérrez B, Lamas JR, Balsa A, Pascual-Salcedo D, Castañeda S, Blanco R, González-Alvaro I, García A, Raya E, Gómez-Vaquero C, Delgado M, Martín J. NPSR1 gene is associated with reduced risk of rheumatoid arthritis. J Rheumatol. 2012 Jun;39(6):1166-70. doi: 10.3899/jrheum.111205. Epub 2012 May 1. PMID: 22548958.

131. Peng Y, Chen L, Chen X, Lin J, Wei J, Cheng J, Zhou F, Ge L, Zhou R, Ding F, Wang X. NPSR1 promotes chronic colitis through regulating CD4+ T cell effector function in inflammatory bowel disease. Int Immunopharmacol. 2024 Dec 5;142(Pt B):113252. doi: 10.1016/j.intimp.2024.113252. Epub 2024 Sep 26. PMID: 39332092.

132. Flisikowski K, Venhoranta H, Bauersachs S, Hänninen R, Fürst RW, Saalfrank A, Ulbrich SE, Taponen J, Lohi H, Wolf E, Kind A, Andersson M, Schnieke A. Truncation of MIMT1 gene in the PEG3 domain leads to major changes in placental gene expression and stillbirth in cattle. Biol Reprod. 2012 Dec 21;87(6):140. doi: 10.1095/biolreprod.112.104240. PMID: 23100617.

133. Zhu D, Zhou W, Liang T, Yang F, Zhang RY, Wu ZX, Xu T. Synaptotagmin I and IX function redundantly in controlling fusion pore of large dense core vesicles. Biochem Biophys Res Commun. 2007 Oct 5;361(4):922-7. doi: 10.1016/j.bbrc.2007.07.083. Epub 2007 Jul 25. PMID: 17686463.

134. Zhang M, Zhou J, Ji Y, Shu S, Zhang M, Liang Y. LncRNA-NONMMUT100923.1 regulates mouse embryonic palatal shelf adhesion by sponging miR-200a-3p to modulate medial epithelial cell desmosome junction during palatogenesis. Heliyon. 2023 May 19;9(5):e16329. doi: 10.1016/j.heliyon.2023.e16329. PMID: 37251885; PMCID: PMC10208945.

135. Shin, O.-H., Rizo, J., Sudhof, T. C. Synaptotagmin function in dense core vesicle exocytosis studied in cracked PC12 cells. Nature Neurosci. 5: 649-656, 2002.

136. Song P, Perkins BD. Developmental expression of the zebrafish Arf-like small GTPase paralogs arl13a and arl13b. Gene Expr Patterns. 2018 Sep;29:82-87. doi: 10.1016/j.gep.2018.07.002. Epub 2018 Jul 17. PMID: 30009987; PMCID: PMC6136450.

137. Singla V, Reiter JF. The primary cilium as the cell's antenna: signaling at a sensory organelle. Science. 2006 Aug 4;313(5787):629-33. doi: 10.1126/science.1124534. PMID: 16888132.

138. Gigante ED, Taylor MR, Ivanova AA, Kahn RA, Caspary T. ARL13B regulates Sonic hedgehog signaling from outside primary cilia. Elife. 2020 Mar 4;9:e50434. doi: 10.7554/eLife.50434. PMID: 32129762; PMCID: PMC7075693.

139. Schoen K, Hirschberg RM, Plendl J, Kaessmeyer S. Identification of CD133-, CD34- and KDR-positive cells in the bovine ovary: a new site of vascular wall resident endothelial progenitor cells. Clin Hemorheol Microcirc. 2012;52(2-4):67-84. doi: 10.3233/CH-2012-1585. PMID: 22954638.

140. Russo MT, Racioppi C, Zanetti L, Ristoratore F. Expression of a single prominin homolog in the embryo of the model chordate Ciona intestinalis. Gene Expr Patterns. 2014 May;15(1):38-45. doi: 10.1016/j.gep.2014.04.001. Epub 2014 Apr 19. PMID: 24755348.

141. Kim H, Ju JH, Son S, Shin I. Silencing of CD133 inhibits GLUT1-mediated glucose transport through downregulation of the HER3/Akt/mTOR pathway in colon cancer. FEBS Lett. 2020 Mar;594(6):1021-1035. doi: 10.1002/1873-3468.13686. Epub 2019 Nov 29. PMID: 31736063.

142. Liou GY. CD133 as a regulator of cancer metastasis through the cancer stem cells. Int J Biochem Cell Biol. 2019 Jan;106:1-7. doi: 10.1016/j.biocel.2018.10.013. Epub 2018 Nov 3. PMID: 30399449; PMCID: PMC6309463.

143. Karbanová J, Missol-Kolka E, Fonseca AV, Lorra C, Janich P, Hollerová H, Jászai J, Ehrmann J, Kolár Z, Liebers C, Arl S, Subrtová D, Freund D, Mokry J, Huttner

WB, Corbeil D. The stem cell marker CD133 (Prominin-1) is expressed in various human glandular epithelia. J Histochem Cytochem. 2008 Nov;56(11):977-93. doi: 10.1369/jhc.2008.951897. Epub 2008 Jul 21. PMID: 18645205; PMCID: PMC2569896.

144. Wang Y, Chen M, Wu Z, Tong C, Dai H, Guo Y, Liu Y, Huang J, Lv H, Luo C, Feng KC, Yang QM, Li XL, Han W. CD133-directed CAR T cells for advanced metastasis malignancies: A phase I trial. Oncoimmunology. 2018 May 7;7(7):e1440169. doi: 10.1080/2162402X.2018.1440169. PMID: 29900044; PMCID: PMC5993480.

145. Dowland SN, Madawala RJ, Poon CE, Lindsay LA, Murphy CR. Prominin-1 glycosylation changes throughout early pregnancy in uterine epithelial cells under the influence of maternal ovarian hormones. Reprod Fertil Dev. 2017 Jun;29(6):1194-1208. doi: 10.1071/RD15432. PMID: 27166505.

146. Niki T, Galli I, Ariga H, Iguchi-Ariga SM. MSSP, a protein binding to an origin of replication in the c-myc gene, interacts with a catalytic subunit of DNA polymerase alpha and stimulates its polymerase activity. FEBS Lett. 2000 Jun 23;475(3):209-12. doi: 10.1016/s0014-5793(00)01679-3. PMID: 10869558.

147. Górnicki T, Lambrinow J, Mrozowska M, Podhorska-Okołów M, Dzięgiel P, Grzegrzółka J. Role of RBMS3 Novel Potential Regulator of the EMT Phenomenon in Physiological and Pathological Processes. Int J Mol Sci. 2022 Sep 17;23(18):10875. doi: 10.3390/ijms231810875. PMID: 36142783; PMCID: PMC9503485.

148. Yang Y, Quan L, Ling Y. RBMS3 Inhibits the Proliferation and Metastasis of Breast Cancer Cells. Oncol Res. 2018 Jan 19;26(1):9-15. doi: 10.3727/096504017X14871200709504. Epub 2017 Apr 12. PMID: 28409548; PMCID: PMC7844557.

149. Lu CK, Lai YC, Chen HR, Chiang MK. Rbms3, an RNA-binding protein, mediates the expression of Ptf1a by binding to its 3'UTR during mouse pancreas development. DNA Cell Biol. 2012 Jul;31(7):1245-51. doi: 10.1089/dna.2012.1619. Epub 2012 Feb 28. PMID: 22372950.

150. Gao Y, Liu J, Zhao D, Diao G. A novel prognostic model for identifying the risk of hepatocellular carcinoma based on angiogenesis factors. Front Genet. 2022;13:857215.

151. Tahir MS, Porto-Neto LR, Gondro C, Shittu OB, Wockner K, Tan AWL, Smith HR, Gouveia GC, Kour J, Fortes MRS. Meta-Analysis of Heifer Traits Identified Reproductive Pathways in Bos indicus

152. Perry JR, Stolk L, Franceschini N, Lunetta KL, Zhai G, McArdle PF, Smith AV, Aspelund T, Bandinelli S, Boerwinkle E, Cherkas L, Eiriksdottir G, Estrada K, Ferrucci L, Folsom AR, Garcia M, Gudnason V, Hofman A, Karasik D, Kiel DP, Launer LJ, van Meurs J, Nalls MA, Rivadeneira F, Shuldiner AR, Singleton A, Soranzo N, Tanaka T, Visser JA, Weedon MN, Wilson SG, Zhuang V, Streeten EA, Harris TB, Murray A, Spector TD, Demerath EW, Uitterlinden AG, Murabito JM. Meta-analysis of genome-wide association data identifies two loci influencing age at menarche. Nat Genet. 2009 Jun;41(6):648-50. doi: 10.1038/ng.386. Epub 2009 May 17. PMID: 19448620; PMCID: PMC2942986.

153. Banerjee A, Biswas D, Barpanda A, Halder A, Sibal S, Kattimani R, Shah A, Mahadevan A, Goel A, Srivastava S. The First Pituitary Proteome Landscape From Matched Anterior and Posterior Lobes for a Better Understanding of the Pituitary Gland. Mol Cell Proteomics. 2023 Jan;22(1):100478. doi: 10.1016/j.mcpro.2022.100478. Epub 2022 Dec 5. PMID:

154. Taschereau A, Thibeault K, Allard C, Juvinao-Quintero D, Perron P, Lutz SM, Bouchard L, Hivert MF. Maternal glycemia in pregnancy is longitudinally associated with blood DNAm variation at the FSD1L gene from birth to 5 years of age. Clin Epigenetics. 2023 Jun 29;15(1):107. doi: 10.1186/s13148-023-01524-7. PMID: 37386647; PMCID: PMC10308691.

155. Mendelsohn BA, Yin C, Johnson SL, Wilm TP, Solnica-Krezel L, Gitlin JD. Atp7a determines a hierarchy of copper metabolism essential for notochord development. Cell Metab. 2006 Aug;4(2):155-62. doi: 10.1016/j.cmet.2006.05.001. PMID: 16890543.

156. Wang Y, Zhu S, Weisman GA, Gitlin JD, Petris MJ. Conditional Knockout of the Menkes Disease Copper Transporter Demonstrates Its Critical Role in Embryogenesis. PLoS One. 2012;7(8):e43039. doi: 10.1371/journal.pone.0043039.

157. Kaler SG. ATP7A-related copper transport diseases-emerging concepts and future trends. Nat Rev Neurol. 2011 Jan;7(1):15-29. doi: 10.1038/nrneurol.2010.180. PMID: 21221114; PMCID: PMC4214867.

158. Sakti DH, Cornish EE, Nash BM, Jamieson RV, Grigg JR. IMPDH1-associated autosomal dominant retinitis pigmentosa: natural history of novel variant Lys314Gln

and a comprehensive literature search. Ophthalmic Genet. 2023 Oct;44(5):437-455. doi: 10.1080/13816810.2023.2215310. Epub 2023 May 31. PMID: 37259572.

159. Burrell AL, Nie C, Said M, Simonet JC, Fernández-Justel D, Johnson MC, Quispe J, Buey RM, Peterson JR, Kollman JM. IMPDH1 retinal variants control filament architecture to tune allosteric regulation. Nat Struct Mol Biol. 2022 Jan;29(1):47-58. doi: 10.1038/s41594-021-00706-2. Epub 2022 Jan 10. PMID: 35013599; PMCID: PMC9044917.

160. Giroto AB, Fontes PK, Franchi FF, Dos Santos PH, Razza EM, Nogueira MFG, Maioli MA, Nogueira GP, Nunes GB, Mingoti GZ, Mareco EA, Castilho ACS. Use of pregnancy-associated plasma protein-A during oocyte in vitro maturation increases IGF-1 and affects the transcriptional profile of cumulus cells and embryos from Nelore cows. Mol Reprod Dev. 2019 Nov;86(11):1694-1704. doi: 10.1002/mrd.23259. Epub 2019 Aug 29. PMID: 31468638.

161. Abu-Issa, R., Eichele, G., & Youssoufian, H. (1999). Expression of the Fanconi anemia group A gene (Fanca) during mouse embryogenesis. Blood, 94(2), 818-820. https://doi.org/10.1182/blood.V94.2.818

162. Tulpule A, Lensch MW, Miller JD, Austin K, D'Andrea A, Schlaeger TM, Shimamura A, Daley GQ. Knockdown of Fanconi anemia genes in human embryonic stem cells reveals early developmental defects in the hematopoietic lineage. Blood. 2010 Apr 29;115(17):3453-62. doi: 10.1182/blood-2009-10-246694. Epub 2010 Jan 20. PMID: 20089964; PMCID: PMC2867260.

163. Chang L, Zhang L, Zhao B, Cheng X, Wan Y, Zhang R, Yuan W, Gao X, Zhu X. Mutation spectrum, expression profiling, and prognosis evaluation of Fanconi anemia signaling pathway genes for 4259 patients with myelodysplastic syndromes or acute myeloid leukemia. BMC Med Genomics. 2023 Nov 16;16(1):290. doi: 10.1186/s12920-023-01730-5. PMID: 37974167; PMCID: PMC10652513.

164. Castella M, Pujol R, Callén E, Trujillo JP, Casado JA, Gille H, Lach FP, Auerbach AD, Schindler D, Benítez J, Porto B, Ferro T, Muñoz A, Sevilla J, Madero L, Cela E, Beléndez C, de Heredia CD, Olivé T, de Toledo JS, Badell I, Torrent M, Estella J, Dasí A, Rodríguez-Villa A, Gómez P, Barbot J, Tapia M, Molinés A, Figuera A, Bueren JA, Surrallés J. Origin, functional role, and clinical impact of Fanconi anemia FANCA mutations. Blood. 2011 Apr 7;117(14):3759-69. doi: 10.1182/blood-2010-08-299917. Epub 2011 Jan 27. PMID: 21273304; PMCID: PMC3083295.

165. Lensch MW, Tischkowitz M, Christianson TA, Reifsteck CA, Speckhart SA, Jakobs PM, O'Dwyer ME, Olson SB, Le Beau MM, Hodgson SV, Mathew CG, Larson RA, Bagby GC Jr. Acquired FANCA dysfunction and cytogenetic instability in adult acute myelogenous leukemia. Blood. 2003 Jul 1;102(1):7-16. doi: 10.1182/blood-2002-09-2781. Epub 2003 Mar 13. PMID: 12637330.

166. Wang S, Qiu J, Liu L, Su C, Qi L, Huang C, Chen X, Zhang Y, Ye Y, Ding Y, Liang L, Liao W. CREB5 promotes invasiveness and metastasis in colorectal cancer by directly activating MET. J Exp Clin Cancer Res. 2020 Aug 25;39(1):168. doi: 10.1186/s13046-020-01673-0. PMID: 32843066; PMCID: PMC7446182.

167. Pugazhenthi S, Wang M, Pham S, Sze CI, Eckman CB. Downregulation of CREB expression in Alzheimer's brain and in Aβ-treated rat hippocampal neurons. Mol Neurodegener. 2011 Aug 19;6:60. doi: 10.1186/1750-1326-6-60. PMID: 21854604; PMCID: PMC3174124.

168. Feng J, Han X, Yuan Y, Cho CK, Janečková E, Guo T, Pareek S, Rahman MS, Zheng B, Bi J, Jing J, Zhang M, Xu J, Ho TV, Chai Y. TGF-β signaling and Creb5 cooperatively regulate Fgf18 to control pharyngeal muscle development. Elife. 2022 Dec 21;11:e80405. doi: 10.7554/eLife.80405. PMID: 36542062; PMCID: PMC9771365.

169. Zhang CH, Gao Y, Jadhav U, Hung HH, Holton KM, Grodzinsky AJ, Shivdasani RA, Lassar AB. Creb5 establishes the competence for Prg4 expression in articular cartilage. Commun Biol. 2021 Mar 12;4(1):332. doi: 10.1038/s42003-021-01857-0. PMID: 33712729; PMCID: PMC7955038.

170. Zheng S, Matthews AJ, Rahman N, Herrick-Reynolds K, Sible E, Choi JE, Wishnie A, Ng YK, Rhodes D, Elledge SJ, Vuong BQ. The uncharacterized SANT and BTB domain-containing protein SANBR inhibits class switch recombination. J Biol Chem. 2021 Jan-Jun;296:100625. doi: 10.1016/j.jbc.2021.100625. Epub 2021 Apr 6. PMID: 33831416; PMCID: PMC8141524.

171. Bansept C, Gaignard P, Lebigot E, Eyer D, Delplancq G, Hoebeke C, Mazodier K, Ledoyen A, Rouzier C, Fragaki K, Ait-El-Mkadem Saadi S, Philippe C, Bruel AL, Faivre L, Feillet F, Abi Warde MT. UQCRC2-related mitochondrial complex III deficiency, about 7 patients. Mitochondrion. 2023 Jan;68:138-144. doi: 10.1016/j.mito.2022.12.001. Epub 2022 Dec 9. PMID: 36509339.

172. Shang Y, Zhang F, Li D, Li C, Li H, Jiang Y, Zhang D. Overexpression of UQCRC2 is correlated with tumor progression and poor prognosis in colorectal cancer.

Pathol Res Pract. 2018 Oct;214(10):1613-1620. doi: 10.1016/j.prp.2018.08.012. Epub 2018 Aug 11. PMID: 30115536.

173. Burska D, Stiburek L, Krizova J, Vanisova M, Martinek V, Sladkova J, Zamecnik J, Honzik T, Zeman J, Hansikova H, Tesarova M. Homozygous missense mutation in UQCRC2 associated with severe encephalomyopathy, mitochondrial complex III assembly defect and activation of mitochondrial protein quality control. Biochim Biophys Acta Mol Basis Dis. 2021 Aug 1;1867(8):166147. doi: 10.1016/j.bbadis.2021.166147. Epub 2021 Apr 15. PMID: 33865955.

174. Shukla KK, Kwon WS, Rahman MS, Park YJ, You YA, Pang MG. Nutlin-3a decreases male fertility via UQCRC2. PLoS One. 2013 Oct 9;8(10):e76959. doi: 10.1371/journal.pone.0076959. PMID: 24130818; PMCID: PMC3793967.

175. Shan W, Li J, Xu W, Li H, Zuo Z. Critical role of UQCRC1 in embryo survival, brain ischemic tolerance and normal cognition in mice. Cell Mol Life Sci. 2019 Apr;76(7):1381-1396. doi: 10.1007/s00018-019-03007-6. Epub 2019 Jan 21. PMID: 30666338; PMCID: PMC6421091.

176. Wang J, Liu W, Zhang T, Cui M, Gao K, Lu P, Yao S, Cao Z, Zheng Y, Tian W, Li Y, Yin R, Hu J, Han G, Liang J, Zhou F, Chai J, Zhang H. An epitranscriptomic program maintains skeletal stem cell quiescence via a METTL3-FEM1B-GLI1 axis. EMBO J. 2025 Apr;44(8):2263-2278. doi: 10.1038/s44318-025-00399-z. Epub 2025 Feb 27. PMID: 40016417; PMCID: PMC12000498.

177. Ventura-Holman, T., et al. 1998. The murine fem1 gene family: homologs of the Caenorhabditis elegans sex-determination protein FEM-1. Genomics 54: 221-230

178. Dankert JF, Pagan JK, Starostina NG, Kipreos ET, Pagano M. FEM1 proteins are ancient regulators of SLBP degradation. Cell Cycle. 2017 Mar 19;16(6):556-564. doi: 10.1080/15384101.2017.1284715. Epub 2017 Jan 24. PMID: 28118078; PMCID: PMC5384579.

179. Lei J, Li Q, Gao Y, Zhao L, Liu Y. Increased PKCα activity by Rack1 overexpression is responsible for chemotherapy resistance in T-cell acute lymphoblastic leukemia-derived cell line. Sci Rep. 2016 Sep 20;6:33717. doi: 10.1038/srep33717. PMID: 27644318; PMCID: PMC5028770.

180. Zuchero JB, Coutts AS, Quinlan ME, Thangue NB, Mullins RD. p53-cofactor JMY is a multifunctional actin nucleation factor. Nat Cell Biol. 2009 Apr;11(4):451-9. doi: 10.1038/ncb1852. Epub 2009 Mar 15. PMID: 19287377; PMCID: PMC2763628.

181. Sun SC, Sun QY, Kim NH. JMY is required for asymmetric division and cytokinesis in mouse oocytes. Mol Hum Reprod. 2011 May;17(5):296-304. doi: 10.1093/molehr/gar006. Epub 2011 Jan 25. PMID: 21266449.

182. Adighibe O, Pezzella F. The Role of JMY in p53 Regulation. Cancers (Basel). 2018 May 31;10(6):173. doi: 10.3390/cancers10060173. PMID: 29857553; PMCID: PMC6025294.

183. Ghosh S, Hose S, Sinha D. AKT2-mediated lysosomal dysfunction promotes secretory autophagy in retinal pigment epithelium (RPE) cells. Autophagy. 2024 Dec;20(12):2841-2842. doi: 10.1080/15548627.2024.2413305. Epub 2024 Oct 16. PMID: 39412071; PMCID: PMC11587834.

184. Honardoost M, Rad SMAH. Triangle of AKT2, miRNA, and Tumorigenesis in Different Cancers. Appl Biochem Biotechnol. 2018 Jun;185(2):524-540. doi: 10.1007/s12010-017-2657-3. Epub 2017 Dec 4. PMID: 29199386.

185. Zhang J, Li G, Chen Y, Fang L, Guan C, Bai F, Ma M, Lyu J, Meng QH. Metformin Inhibits Tumorigenesis and Tumor Growth of Breast Cancer Cells by Upregulating miR-200c but Downregulating AKT2 Expression. J Cancer. 2017 Jul 2;8(10):1849-1864. doi: 10.7150/jca.19858. PMID: 28819383; PMCID: PMC5556649.

186. Liu L, Zhu S, Gong Z, Low BC. K-ras/PI3K-Akt signaling is essential for zebrafish hematopoiesis and angiogenesis. PLoS One. 2008 Aug 6;3(8):e2850. doi: 10.1371/journal.pone.0002850. PMID: 18682746; PMCID: PMC2483249.

187. Fiorenza MT, Russo G, Narducci MG, Bresin A, Mangia F, Bevilacqua A. Protein kinase Akt2/PKBβ is involved in blastomere proliferation of preimplantation mouse embryos. J Cell Physiol. 2020 Apr;235(4):3393-3401. doi: 10.1002/jcp.29229. Epub 2019 Sep 25. PMID: 31552693.

188. Miwa JM, Anderson KR, Hoffman KM. Lynx Prototoxins: Roles of Endogenous Mammalian Neurotoxin-Like Proteins in Modulating Nicotinic Acetylcholine Receptor Function to Influence Complex Biological Processes. Front Pharmacol. 2019 Apr 30;10:343. doi: 10.3389/fphar.2019.00343. PMID: 31114495; PMCID: PMC6502960.

189. Sivaprasad U, Kinker KG, Ericksen MB, Lindsey M, Gibson AM, Bass SA, Hershey NS, Deng J, Medvedovic M, Khurana Hershey GK. SERPINB3/B4 contributes to early inflammation and barrier dysfunction in an experimental murine model of atopic dermatitis. J Invest Dermatol. 2015 Jan;135(1):160-169. doi: 10.1038/jid.2014.353. Epub 2014 Aug 11. PMID: 25111616; PMCID: PMC4268075.

190. Lindner A., Marbach F., Tschernitz S. et al. Calcyphosine-like (CAPSL) is regulated in Multiple Symmetric Lipomatosis and is involved in Adipogenesis. Sci Rep. 2019;9:8444. doi: 10.1038/s41598-019-44382-1.

191. Zhang R, Chen Y, He J, Gou HY, Zhu YL, Zhu YM. WGCNA combined with GSVA to explore biomarkers of refractory neocortical epilepsy. IBRO Neurosci Rep. 2022 Oct 3;13:314-321. doi: 10.1016/j.ibneur.2022.09.010. PMID: 36247523; PMCID: PMC9561751.

192. Liu W, Li S, Yang M, Ma J, Liu L, Fei P, Xiang Q, Huang L, Zhao P, Yang Z, Zhu X. Dysfunction of Calcyphosine-Like gene impairs retinal angiogenesis through the MYC axis and is associated with familial exudative vitreoretinopathy. Elife. 2024 Sep 12;13:RP96907. doi: 10.7554/eLife.96907. PMID: 39264149; PMCID: PMC11392532.

193. Lindner A, Marbach F, Tschernitz S, Ortner C, Berneburg M, Felthaus O, Prantl L, Kye MJ, Rappl G, Altmüller J, Thiele H, Schreml S, Schreml J. Calcyphosine-like (CAPSL) is regulated in Multiple Symmetric Lipomatosis and is involved in Adipogenesis. Sci Rep. 2019 Jun 11;9(1):8444. doi: 10.1038/s41598-019-44382-1. PMID: 31186450; PMCID: PMC6559987.

194. https://www.informatics.jax.org/marker/MGI:1922818

195. Ochoa V, George AA, Nishi R, Whiteaker P. The prototoxin LYPD6B modulates heteromeric α3β4-containing nicotinic acetylcholine receptors, but not α7 homomers. FASEB J. 2016 Mar;30(3):1109-19. doi: 10.1096/fj.15-274548. Epub 2015 Nov 19. PMID: 26586467; PMCID: PMC4750422.

196. Gu Z, Wang L, Dong Q, Xu K, Ye J, Shao X, Yang S, Lu C, Chang C, Hou Y, Zhai Y, Wang X, He F, Sun A. Aberrant LYZ expression in tumor cells serves as the potential biomarker and target for HCC and promotes tumor progression via csGRP78. Proc Natl Acad Sci U S A. 2023 Jul 18;120(29):e2215744120. doi: 10.1073/pnas.2215744120. Epub 2023 Jul 10. PMID: 37428911; PMCID: PMC10629575.

197. Cieslak J, Wodas L, Borowska A, Sadoch J, Pawlak P, Puppel K, Kuczynska B, Mackowski M. Variability of lysozyme and lactoferrin bioactive protein concentrations in equine milk in relation to LYZ and LTF gene polymorphisms and expression. J Sci Food Agric. 2017 May;97(7):2174-2181. doi: 10.1002/jsfa.8026. Epub 2016 Oct 4. PMID: 27611486.

198. Niemcharoen S, Haetrakul T, Palić D, Chansue N. Microplastic-Contaminated Feed Interferes with Antioxidant Enzyme and Lysozyme Gene Expression of Pacific White Shrimp (Litopenaeus vannamei) Leading to Hepatopancreas Damage and Increased Mortality. Animals (Basel). 2022 Nov 26;12(23):3308. doi: 10.3390/ani12233308. PMID: 36496829; PMCID: PMC9740652.

199. Meugnier E, Faraj M, Rome S, Beauregard G, Michaut A, Pelloux V, Chiasson JL, Laville M, Clement K, Vidal H, Rabasa-Lhoret R. Acute hyperglycemia induces a global downregulation of gene expression in adipose tissue and skeletal muscle of healthy subjects. Diabetes. 2007 Apr;56(4):992-9. doi: 10.2337/db06-1242. Epub 2007 Feb 15. PMID: 17303805.

200. Becirovic L, Brown IR. Targeting of Heat Shock Protein HSPA6 (HSP70B') to the Periphery of Nuclear Speckles is Disrupted by a Transcription Inhibitor Following Thermal Stress in Human Neuronal Cells. Neurochem Res. 2017 Feb;42(2):406-414. doi: 10.1007/s11064-016-2084-9. Epub 2016 Oct 14. PMID: 27743288.

201. Kuballa P, Baumann AL, Mayer K, Bär U, Burtscher H, Brinkmann U. Induction of heat shock protein HSPA6 (HSP70B') upon HSP90 inhibition in cancer cell lines. FEBS Lett. 2015 Jun 4;589(13):1450-8. doi: 10.1016/j.febslet.2015.04.053. Epub 2015 May 7. PMID: 25957766.

202. Khalouei S, Chow AM, Brown IR. Localization of heat shock protein HSPA6 (HSP70B') to sites of transcription in cultured differentiated human neuronal cells following thermal stress. J Neurochem. 2014 Dec;131(6):743-54. doi: 10.1111/jnc.12970. Epub 2014 Dec 2. PMID: 25319762.

203. Alharbi BM, Bugshan A, Almozel A, Alenzi R, Bouchama A, Khatlani T, Mohammad S, Malik SS. Heat-Induced Proteotoxic Stress Response in Placenta-Derived Stem Cells (PDSCs) Is Mediated through HSPA1A and HSPA1B with a Potential Higher Role for HSPA1B. Curr Issues Mol Biol. 2022 Oct 10;44(10):4748-4768. doi: 10.3390/cimb44100324. PMID: 36286039; PMCID: PMC9600182.

204. Lyu F, Burzynski C, Fang YY, Tal A, Chen AY, Kisa J, Agrawal K, Kluger Y, Taylor HS, Tal R. Maternal CXCR4 deletion results in placental defects and pregnancy loss mediated by immune dysregulation. JCI Insight. 2023 Nov 8;8(21):e172216. doi: 10.1172/jci.insight.172216. PMID: 37815869; PMCID: PMC10721256.

205. Molyneaux KA, Zinszner H, Kunwar PS, Schaible K, Stebler J, Sunshine MJ, O'Brien W, Raz E, Littman D, Wylie C, Lehmann R. The chemokine SDF1/CXCL12

and its receptor CXCR4 regulate mouse germ cell migration and survival. Development. 2003 Sep;130(18):4279-86. doi: 10.1242/dev.00640. PMID: 12900445.

206. Chong SZ, Evrard M, Devi S, Chen J, Lim JY, See P, Zhang Y, Adrover JM, Lee B, Tan L, Li JL, Liong KH, Phua C, Balachander A, Boey A, Liebl D, Tan SM, Chan JK, Balabanian K, Harris JE, Bianchini M, Weber C, Duchene J, Lum J, Poidinger M, Chen Q, Rénia L, Wang CI, Larbi A, Randolph GJ, Weninger W, Looney MR, Krummel MF, Biswas SK, Ginhoux F, Hidalgo A, Bachelerie F, Ng LG. CXCR4 identifies transitional bone marrow premonocytes that replenish the mature monocyte pool for peripheral responses. J Exp Med. 2016 Oct 17;213(11):2293-2314. doi: 10.1084/jem.20160800. Epub 2016 Oct 10. PMID: 27811056; PMCID: PMC5068243.

207. Gonzalez-Meljem JM, Ivins S, Andoniadou CL, Le Tissier P, Scambler P, Martinez-Barbera JP. An expression and function analysis of the CXCR4/SDF-1 signalling axis during pituitary gland development. PLoS One. 2023 Feb 17;18(2):e0280001. doi: 10.1371/journal.pone.0280001. PMID: 36800350; PMCID: PMC9937476.

208. Yusuf F, Rehimi R, Moroşan-Puopolo G, Dai F, Zhang X, Brand-Saberi B. Inhibitors of CXCR4 affect the migration and fate of CXCR4+ progenitors in the developing limb of chick embryos. Dev Dyn. 2006 Nov;235(11):3007-15. doi: 10.1002/dvdy.20951. PMID: 16958136.

209. Urosevic J, Blasco MT, Llorente A, Bellmunt A, Berenguer-Llergo A, Guiu M, Cañellas A, Fernandez E, Burkov I, Clapés M, Cartanà M, Figueras-Puig C, Batlle E, Nebreda AR, Gomis RR. ERK1/2 Signaling Induces Upregulation of ANGPT2 and CXCR4 to Mediate Liver Metastasis in Colon Cancer. Cancer Res. 2020 Nov 1;80(21):4668-4680. doi: 10.1158/0008-5472.CAN-19-4028. Epub 2020 Aug 19. PMID: 32816905.

210. Yang WC, Li SJ, Chen L, Yang LG. FSHR genotype affects estrogen levels but not pregnancy rates in Luxi cattle subjected to embryo transfer. Genet Mol Res. 2014 Mar 12;13(1):1563-9. doi: 10.4238/2014.March.12.8. PMID: 24668630.

211. Achrekar SK, Modi DN, Meherji PK, Patel ZM, et al. (2010). Follicle stimulating hormone receptor gene variants in women with primary and secondary amenorrhea. J. Assist. Reprod. Genet. 27: 317-326.

212. Livshyts G, Podlesnaja S, Kravchenko S, Sudoma I, et al. A distribution of two SNPs in exon 10 of the FSHR gene among the women with a diminished ovarian reserve in Ukraine. J. Assist. Reprod. Genet. 2009;26:29-34.

213. Kussano NR, Franco MM, Dode MAN. Biochemical profiling of the follicular environment to predict oocyte competence in cattle. PLoS One. 2024 Mar 11;19(3):e0298316. doi: 10.1371/journal.pone.0298316. PMID: 38466703; PMCID: PMC10927144.

214. Chien Y, Rosal K, Chung BC. Function of CYP11A1 in the mitochondria. Mol Cell Endocrinol. 2017 Feb 5;441:55-61. doi: 10.1016/j.mce.2016.10.030. Epub 2016 Nov 2. PMID: 27815210.

215. Liu Y, Jiang JJ, Du SY, Mu LS, Fan JJ, Hu JC, Ye Y, Ding M, Zhou WY, Yu QH, Xia YF, Xu HY, Shi YJ, Qian SW, Tang Y, Li W, Dang YJ, Dong X, Li XY, Xu CJ, Tang QQ. Artemisinins ameliorate polycystic ovarian syndrome by mediating LONP1-CYP11A1 interaction. Science. 2024 Jun 14;384(6701):eadk5382. doi: 10.1126/science.adk5382. Epub 2024 Jun 14. PMID: 38870290.

216. Lin YC, Papadopoulos V. Neurosteroidogenic enzymes: CYP11A1 in the central nervous system. Front Neuroendocrinol. 2021 Jul;62:100925. doi: 10.1016/j.yfrne.2021.100925. Epub 2021 May 18. PMID: 34015388.

217. Zhu M, Wang M, Shao Y, Nan Y, Blair HT, Morris ST, Zhao Z, Zhang H. Characterization of muscle development and gene expression in early embryos of chicken, quail, and their hybrids. Gene. 2021 Feb 5;768:145319. doi: 10.1016/j.gene.2020.145319. PMID: 33246031.

218. Hsu HJ, Lin JC, Chung BC. Zebrafish cyp11a1 and hsd3b genes: structure, expression and steroidogenic development during embryogenesis. Mol Cell Endocrinol. 2009 Nov 27;312(1-2):31-4. doi: 10.1016/j.mce.2009.07.030. Epub 2009 Aug 12. PMID: 19682541.

219. Liu M, Hummitzsch K, Bastian NA, Hartanti MD, Wan Q, Irving-Rodgers HF, Anderson RA, Rodgers RJ. Isolation, culture, and characterisation of bovine ovarian fetal fibroblasts and gonadal ridge epithelial-like cells and comparison to their adult counterparts. PLoS One. 2022 Jul 8;17(7):e0268467. doi: 10.1371/journal.pone.0268467. PMID: 35802560; PMCID: PMC9269465.

220. Cai A, Portengen L, Ertaylan G, Legler J, Vermeulen R, Lenters V, Remy S. Prenatal Exposure to Metabolism-Disrupting Chemicals, Cord Blood Transcriptome Perturbations, and Birth Weight in a Belgian Birth Cohort. Int J Mol Sci. 2023 Apr 20;24(8):7607. doi: 10.3390/ijms24087607. PMID: 37108768; PMCID: PMC10141364.

221. Rozance PJ, Jones AK, Bourque SL, D'Alessandro A, Hay WW Jr, Brown LD, Wesolowski SR. Effects of chronic hyperinsulinemia on metabolic pathways and insulin signaling in the fetal liver. Am J Physiol Endocrinol Metab. 2020 Oct 1;319(4):E721-E733. doi: 10.1152/ajpendo.00323.2020. Epub 2020 Aug 24. PMID: 32830555; PMCID: PMC7864241.

222. Tsai TS, Tyagi S, St John JC. The molecular characterisation of mitochondrial DNA deficient oocytes using a pig model. Hum Reprod. 2018 May 1;33(5):942-953. doi: 10.1093/humrep/dey052. PMID: 29546367.

223. Pérez LM, de Lucas B, Gálvez BG. BMPER is upregulated in obesity and seems to have a role in pericardial adipose stem cells. J Cell Physiol. 2021 Jan;236(1):132-145. doi: 10.1002/jcp.29829. Epub 2020 May 29. PMID: 32468630.

224. Dyer L, Wu Y, Moser M, Patterson C. BMPER-induced BMP signaling promotes coronary artery remodeling. Dev Biol. 2014 Feb 15;386(2):385-94. doi: 10.1016/j.ydbio.2013.12.019. Epub 2013 Dec 27. PMID: 24373957; PMCID: PMC4112092.

225. Heinke J, Wehofsits L, Zhou Q, Zoeller C, Baar KM, Helbing T, Laib A, Augustin H, Bode C, Patterson C, Moser M. BMPER is an endothelial cell regulator and controls bone morphogenetic protein-4-dependent angiogenesis

226. Rai A, Poh QH, Fatmous M, Fang H, Gurung S, Vollenhoven B, Salamonsen LA, Greening DW. Proteomic profiling of human uterine extracellular vesicles reveal dynamic regulation of key players of embryo implantation and fertility during menstrual cycle. Proteomics. 2021 Jul;21(13-14):e2000211. doi: 10.1002/pmic.202000211. Epub 2021 Mar 19. PMID: 33634576.

227. Tisato V, Silva JA, Scarpellini F, Capucci R, Marci R, Gallo I, Salvatori F, D'Aversa E, Secchiero P, Serino ML, Zauli G, Singh AV, Gemmati D. Epigenetic role of LINE-1 methylation and key genes in pregnancy maintenance. Sci Rep. 2024 Feb 8;14(1):3275. doi: 10.1038/s41598-024-53737-2. PMID: 38332006; PMCID: PMC10853191.

228. Seow WJ, Ngo CS, Pan H, Barathi VA, Tompson SW, Whisenhunt KN, Vithana E, Chong YS, Juo SH, Hysi P, Young TL, Karnani N, Saw SM. In-utero epigenetic factors are associated with early-onset myopia in young children. PLoS One. 2019 May 17;14(5):e0214791. doi: 10.1371/journal.pone.0214791. PMID: 31100065; PMCID: PMC6524791.

229. Shaw JL, Diamandis EP. Distribution of 15 human kallikreins in tissues and biological fluids. Clin Chem. 2007 Aug;53(8):1423-32. doi: 10.1373/clinchem.2007.088104. Epub 2007 Jun 15. PMID: 17573418.

230. Chan CS, Harvey MB, Clements JA. Temporal and tissue-specific expression of kallikrein (Klk) genes and identification of a novel Klk messenger ribonucleic acid transcript during early development in the mouse. Biol Reprod. 1999 Sep;61(3):621-8. doi: 10.1095/biolreprod61.3.621. PMID: 10456837.

231. Fernando SC, Buck JS, Ashworth MD, Ross JW, Geisert RD, DeSilva U. Porcine endometrial and conceptus tissue kallikrein 1, 4, 11, and 14 gene expression. Reproduction. 2006 Dec;132(6):939-47. doi: 10.1530/rep.1.01013. PMID: 17127754.

232. Sun J, Guo X, Yu P, Liang J, Mo Z, Zhang M, Yang L, Huang X, Hu B, Liu J, Ouyang Y, He M. Vasorin deficiency leads to cardiac hypertrophy by targeting MYL7 in young mice. J Cell Mol Med. 2022 Jan;26(1):88-98. doi: 10.1111/jcmm.17034. Epub 2021 Dec 2. PMID: 34854218; PMCID: PMC8742182.

233. Zhao G, Zhu Y, Hu J, Gao M, Hong Y. L-selenomethionine induces zebrafish embryo cardiovascular defects via down-regulating expression of lrp2b. Chemosphere. 2022 Mar;290:133351. doi: 10.1016/j.chemosphere.2021.133351. PMID: 34933029.

234. Hoelker M, Salilew-Wondim D, Drillich M, Christine GB, Ghanem N, Goetze L, Tesfaye D, Schellander K, Heuwieser W. Transcriptional response of the bovine endometrium and embryo to endometrial polymorphonuclear neutrophil infiltration as an indicator of subclinical inflammation of the uterine environment. Reprod Fertil Dev. 2012;24(6):778-93. doi: 10.1071/RD11171. PMID: 22781929.

235. Lin C, Li F, Zhang X, Zhang D, Li X, Zhang Y, Zhao Y, Song Q, Wang J, Zhou B, Cheng J, Xu D, Li W, Zhao L, Wang W. Expression and polymorphisms of CD8B gene and its associations with body weight and size traits in sheep. Anim Biotechnol. 2023 Nov;34(4):1214-1222. doi: 10.1080/10495398.2021.2016432. Epub 2021 Dec 20. PMID: 34928779.

236. Luo J, Carrillo JA, Menendez KR, Tablante NL, Song J. Transcriptome analysis reveals an activation of major histocompatibility complex 1 and 2 pathways in chicken trachea immunized with infectious laryngotracheitis virus vaccine. Poult Sci. 2014 Apr;93(4):848-55. doi: 10.3382/ps.2013-03624. PMID: 24706961.

237. da Silva MI, Oli N, Gambonini F, Ott T. Effects of parity and early pregnancy on peripheral blood leukocytes in dairy cattle. J Dairy Sci. 2024 Dec;107(12):11728-11743. doi: 10.3168/jds.2024-25063. Epub 2024 Aug 30. PMID: 39216517.

238. Wakitani S, Kawabata R, Yasuda M. Insufficiency of CD205-positive cortical thymic epithelial cells in immature Japanese Black cattle with severe thymic abnormalities and poor prognosis. Vet Immunol Immunopathol. 2022 Mar;245:110379. doi: 10.1016/j.vetimm.2021.110379. Epub 2022 Jan 4. PMID: 35038635.

239. Mazin ME, Yarushkin AA, Pustylnyak YA, Prokopyeva EA, Pustylnyak VO. Promotion of NR1I3-mediated liver growth is accompanied by STAT3 activation. Mol Biol Rep. 2022 May;49(5):4089-4093. doi: 10.1007/s11033-022-07340-1. Epub 2022 Mar 19. PMID: 35305226.

240. Alexandre PA, Gomes RC, Santana MH, Silva SL, Leme PR, Mudadu MA, Regitano LC, Meirelles FV, Ferraz JB, Fukumasu H. Bovine NR1I3 gene polymorphisms and its association with feed efficiency traits in Nellore cattle. Meta Gene. 2014 Feb 20;2:206-17. doi: 10.1016/j.mgene.2014.01.003. PMID: 25606404; PMCID: PMC4287810.

241. Piersanti RL, Horlock AD, Block J, Santos JEP, Sheldon IM, Bromfield JJ. Persistent effects on bovine granulosa cell transcriptome after resolution of uterine disease. Reproduction. 2019 Jul;158(1):35-46. doi: 10.1530/REP-19-0037. PMID: 30933928; PMCID: PMC6773536.

242. Wagner F, Ruf I, Lehmann T, Hofmann R, Ortmann S, Schiffmann C, Hiller M, Stefen C, Stuckas H. Reconstruction of evolutionary changes in fat and toxin consumption reveals associations with gene losses in mammals: A case study for the lipase inhibitor PNLIPRP1 and the xenobiotic receptor NR1I3. J Evol Biol. 2022 Feb;35(2):225-239. doi: 10.1111/jeb.13970. Epub 2022 Jan 11. PMID: 34882899.

243. Osborne N, Leahy C, Lee YK, Rote P, Song BJ, Hardwick JP. CYP4V2 fatty acid omega hydroxylase, a druggable target for the treatment of metabolic associated fatty liver disease (MAFLD). Biochem Pharmacol. 2022 Jan;195:114841. doi: 10.1016/j.bcp.2021.114841. Epub 2021 Nov 16. PMID: 34798124.

244. Eun HS, Cho SY, Lee BS, Seong IO, Kim KH. Profiling cytochrome P450 family 4 gene expression in human hepatocellular carcinoma. Mol Med Rep. 2018 Dec;18(6):4865-4876. doi: 10.3892/mmr.2018.9526. Epub 2018 Oct 1. PMID: 30280198; PMCID: PMC6236316

245. Safdar H, Cleuren AC, Cheung KL, Gonzalez FJ, Vos HL, Inoue Y, Reitsma PH, van Vlijmen BJ. Regulation of the F11, Klkb1, Cyp4v3 gene cluster in livers of metabolically challenged mice. PLoS One. 2013 Sep 16;8(9):e74637. doi: 10.1371/journal.pone.0074637. PMID: 24066149; PMCID: PMC3774739.

246. Goldstone JV, McArthur AG, Kubota A, Zanette J, Parente T, Jönsson ME, Nelson DR, Stegeman JJ. Identification and developmental expression of the full complement of Cytochrome P450 genes in Zebrafish. BMC Genomics. 2010 Nov 18;11:643. doi: 10.1186/1471-2164-11-643. PMID: 21087487; PMCID: PMC3012610.

247. Ferjeni Z, Raouia F, Abida O, Penha-Gonçalves C, Masmoudi H. Association of IGHM polymorphisms with susceptibility to type 1 diabetes. Immunol Res. 2022 Jun;70(3):325-330. doi: 10.1007/s12026-021-09252-x. Epub 2022 Jan 20. PMID: 35048256.

248. Liu J, Xia M, Wang P, Wang C, Geng Z, Cameron Yin C, Zhang C, Qiu X. Immunoglobulin gene expression in umbilical cord blood-derived $CD34^{+}$ hematopoietic stem/progenitor cells. Gene. 2016 Jan 1;575(1):108-17. doi: 10.1016/j.gene.2015.08.046. Epub 2015 Sep 11. PMID: 26364572.

249. Tobin-Janzen TC, Womack JE. Comparative mapping of IGHG1, IGHM, FES, and FOS in domestic cattle. Immunogenetics. 1992;36(3):157-65. doi: 10.1007/BF00661092. PMID: 1612649.

250. Kuroiwa Y, Kasinathan P, Matsushita H, Sathiyaselan J, Sullivan EJ, Kakitani M, Tomizuka K, Ishida I, Robl JM. Sequential targeting of the genes encoding immunoglobulin-mu and prion protein in cattle. Nat Genet. 2004 Jul;36(7):775-80. doi: 10.1038/ng1373. Epub 2004 Jun 6. PMID: 15184897.

251. Solano ME, Thiele K, Kowal MK, Arck PC. Identification of suitable reference genes in the mouse placenta. Placenta. 2016 Mar;39:7-15. doi: 10.1016/j.placenta.2015.12.017. Epub 2015 Dec 25. PMID: 26992668.

252. Sood TJ, Lagah SV, Sharma A, Singla SK, Mukesh M, Chauhan MS, Manik R, Palta P. Selection of Suitable Internal Control Genes for Accurate Normalization of Real-Time Quantitative PCR Data of Buffalo (Bubalus bubalis) Blastocysts Produced by SCNT and IVF. Cell Reprogram. 2017 Oct;19(5):302-310. doi: 10.1089/cell.2017.0010. Epub 2017 Sep 7. PMID: 28880574.

253. Schiano C, Grimaldi V, Franzese M, Fiorito C, De Nigris F, Donatelli F, Soricelli A, Salvatore M, Napoli C. Non-nutritional sweeteners effects on endothelial vascular function. Toxicol In Vitro. 2020 Feb;62:104694. doi: 10.1016/j.tiv.2019.104694. Epub 2019 Oct 23. PMID: 31655124.

254. Steinhauser CB, Wing TT, Gao H, Li X, Burghardt RC, Wu G, Bazer FW, Johnson GA. Identification of appropriate reference genes for qPCR analyses of

placental expression of SLC7A3 and induction of SLC5A1 in porcine endometrium. Placenta. 2017 Apr;52:1-9. doi: 10.1016/j.placenta.2017.02.003. Epub 2017 Feb 4. PMID: 28454689.

255. Wang Y, Wu ZW, Fang T, Zhang YQ, Chen L, Du ZQ, Yang CX. Identification of internal reference genes for porcine immature Sertoli cells under heat stress. Reprod Domest Anim. 2022 Nov;57(11):1344-1352. doi: 10.1111/rda.14211. Epub 2022 Jul 29. PMID: 35869802.

256. Zhao X, Huang Z, Chen Y, Zhou Q, Zhu F, Zhang H, Zhou D. MAGEB2-Mediated Degradation of EGR1 Regulates the Proliferation and Apoptosis of Human Spermatogonial Stem Cell Lines. Stem Cells Int. 2023 Jun 2;2023:3610466. doi: 10.1155/2023/3610466. PMID: 37304127; PMCID: PMC10256451.

257. Abera B, Dinka H. MAGE genes encoding for embryonic development in cattle is mainly regulated by zinc finger transcription factor family and slightly by CpG Islands. BMC Genom Data. 2022 Mar 18;23(1):19. doi: 10.1186/s12863-022-01034-0. PMID: 35303799; PMCID: PMC8932067.

258. Stephens GS, Park J, Eagle A, You J, Silva-Pérez M, Fu CH, Choi S, Romain CPS, Sugimoto C, Buffington SA, Zheng Y, Costa-Mattioli M, Liu Y, Robison AJ, Chin J. Persistent ΔFosB expression limits recurrent seizure activity and provides neuroprotection in the dentate gyrus of APP mice. Prog Neurobiol. 2024 Jun;237:102612. doi: 10.1016/j.pneurobio.2024.102612. Epub 2024 Apr 19. PMID: 38642602; PMCID: PMC11406539.

259. Brunner RM, Sanftleben H, Goldammer T, Kühn C, Weikard R, Kata SR, Womack JE, Schwerin M. The telomeric region of BTA18 containing a potential QTL region for health in cattle exhibits high similarity to the HSA19q region in humans. Genomics. 2003 Mar;81(3):270-8. doi: 10.1016/s0888-7543(03)00019-3. PMID: 12659811.

260. Nestler EJ. ΔFosB: a transcriptional regulator of stress and antidepressant responses. Eur J Pharmacol. 2015 Apr 15;753:66-72. doi: 10.1016/j.ejphar.2014.10.034. Epub 2014 Nov 7. PMID: 25446562; PMCID: PMC4380559.

261. Gruda MC, van Amsterdam J, Rizzo CA, Durham SK, Lira S, Bravo R. Expression of FosB during mouse development: normal development of FosB knockout mice. Oncogene. 1996 May 16;12(10):2177-85. PMID: 8668344.

262. Nishioka T, Sakumi K, Miura T, Tahara K, Horie H, Kadoya T, Nakabeppu Y. FosB gene products trigger cell proliferation and morphological alteration with an increased expression of a novel processed form of galectin-1 in the rat 3Y1 embryo cell line. J Biochem. 2002 May;131(5):653-61. doi: 10.1093/oxfordjournals.jbchem.a003148. PMID: 11983071.

263. Lyu P, Settlage RE, Jiang H. Genome-wide identification of enhancers and transcription factors regulating the myogenic differentiation of bovine satellite cells. BMC Genomics. 2021 Dec 16;22(1):901. doi: 10.1186/s12864-021-08224-7. PMID: 34915843; PMCID: PMC8675486.

264. Sayasith K, Bouchard N, Doré M, Sirois J. Regulation of bovine TNFAIP6 in ovarian follicles during the ovulatory process and promoter activation in granulosa cells. Endocrinology. 2008 Dec;149(12):6213-25. doi: 10.1210/en.2008-0459. Epub 2008 Aug 7. PMID: 18687781.

265. Yari AH, Aghbash PS, Bayat M, Lahouti S, Jalilzadeh N, Zadeh LN, Yari AM, Tabrizi-Nezhadi P, Nahand JS, MotieGhader H, Baghi HB. Novel bioinformatic approaches show the role of driver genes in the progression of cervical cancer: An in-silico study. Heliyon. 2024 Nov 14;10(22):e40179. doi: 10.1016/j.heliyon.2024.e40179. PMID: 39634417; PMCID: PMC11616557.

266. Mukherjee M, Jones JC, Yao J. Lumbosacral stenosis in Labrador retriever military working dogs - an exomic exploratory study. Canine Genet Epidemiol. 2017 Oct 23;4:12. doi: 10.1186/s40575-017-0052-6. PMID: 29085643; PMCID: PMC5651560.

267. Dong HY, Ding L, Zhou TR, Yan T, Li J, Liang C. FOXA1 in prostate cancer. Asian J Androl. 2023 May-Jun;25(3):287-295. doi: 10.4103/aja202259. PMID: 36018068; PMCID: PMC10226509.

268. Tachmatzidi EC, Galanopoulou O, Talianidis I. Transcription Control of Liver Development. Cells. 2021 Aug 8;10(8):2026. doi: 10.3390/cells10082026. PMID: 34440795; PMCID: PMC8391549.

269. Cunha GR, Robboy SJ, Kurita T, Isaacson D, Shen J, Cao M, Baskin LS. Development of the human female reproductive tract. Differentiation. 2018 Sep-Oct;103:46-65. doi: 10.1016/j.diff.2018.09.001. Epub 2018 Sep 6. PMID: 30236463; PMCID: PMC6234064.

270. Wang LN, Jia JS, Yang XL, Wen YT, Liu JX, Li DK, Chen XR, Wang JH, Li JK, Huang ZX, Yao KT. Foxa1 disruption enhances human cell integration in human-

mouse interspecies chimeras. Cell Tissue Res. 2025 Feb;399(2):231-245. doi: 10.1007/s00441-024-03941-3. Epub 2024 Dec 21. PMID: 39708115.

271. Gredler ML, Patterson SE, Seifert AW, Cohn MJ. Foxa1 and Foxa2 orchestrate development of the urethral tube and division of the embryonic cloaca through an autoregulatory loop with Shh. Dev Biol. 2020 Sep 1;465(1):23-30. doi: 10.1016/j.ydbio.2020.06.009. Epub 2020 Jul 6. PMID: 32645357; PMCID: PMC7484041.

272. Mi X, Ning Y, Wang X, Junjvlieke Z, Wang L, Wang S, Zhang W, Su X, Zan L. GR and Foxa1 promote the transcription of ANGPTL4 in bovine adipocytes. Mol Cell Probes. 2019 Dec;48:101443. doi: 10.1016/j.mcp.2019.101443. Epub 2019 Sep 2. PMID: 31487539.

273. Cortese R, Hartmann O, Berlin K, Eckhardt F. Correlative gene expression and DNA methylation profiling in lung development nominate new biomarkers in lung cancer. Int J Biochem Cell Biol. 2008;40(8):1494-508. doi: 10.1016/j.biocel.2007.11.018. Epub 2007 Dec 7. PMID: 18203646.

274. Adra CN, Zhu S, Ko JL, Guillemot JC, Cuervo AM, Kobayashi H, Horiuchi T, Lelias JM, Rowley JD, Lim B. LAPTM5: a novel lysosomal-associated multispanning membrane protein preferentially expressed in hematopoietic cells. Genomics. 1996 Jul 15;35(2):328-37. doi: 10.1006/geno.1996.0364. PMID: 8661146.

275. Nasrah S, Radi A, Daberkow JK, Hummler H, Weber S, Seaayfan E, Kömhoff M. MAGED2 Depletion Promotes Stress-Induced Autophagy by Impairing the cAMP/PKA Pathway. Int J Mol Sci. 2023 Aug 30;24(17):13433. doi: 10.3390/ijms241713433. PMID: 37686237; PMCID: PMC10488052.

276. Bertrand M, Huijbers I, Chomez P, De Backer O. Comparative expression analysis of the MAGED genes during embryogenesis and brain development. Dev Dyn. 2004 Jun;230(2):325-34. doi: 10.1002/dvdy.20026. PMID: 15162511.

277. Reusch B, Bartram MP, Dafinger C, Palacio-Escat N, Wenzel A, Fenton RA, Saez-Rodriguez J, Schermer B, Benzing T, Altmüller J, Beck BB, Rinschen MM. MAGED2 controls vasopressin-induced aquaporin-2 expression in collecting duct cells. J Proteomics. 2022 Feb;252:104424. doi: 10.1016/j.jprot.2021.104424. Epub 2021 Nov 12. PMID: 34775100.

278. Hu Z, Qu S. EVA1C Is a Potential Prognostic Biomarker and Correlated With Immune Infiltration Levels in WHO Grade II/III Glioma. Front Immunol. 2021 Jun

29;12:683572. doi: 10.3389/fimmu.2021.683572. PMID: 34267752; PMCID: PMC8277382.

279. James G, Foster SR, Key B, Beverdam A. The expression pattern of EVA1C, a novel Slit receptor, is consistent with an axon guidance role in the mouse nervous system. PLoS One. 2013 Sep 9;8(9):e74115. doi: 10.1371/journal.pone.0074115. PMID: 24040182; PMCID: PMC3767613.

280. Li H, Meng YH, Shang WQ, Liu LB, Chen X, Yuan MM, Jin LP, Li MQ, Li DJ. Chemokine CCL24 promotes the growth and invasiveness of trophoblasts through ERK1/2 and PI3K signaling pathways in human early pregnancy. Reproduction. 2015 Nov;150(5):417-27. doi: 10.1530/REP-15-0119. Epub 2015 Aug 27. PMID: 26316550.

281. Tong F, Zhang M, Guo X, Shi H, Li L, Guan W, Wang H, Yang S. Expression patterns of SH3BGR family members in zebrafish development. Dev Genes Evol. 2016 Jul;226(4):287-95. doi: 10.1007/s00427-016-0552-5. Epub 2016 May 28. PMID: 27233781.

282. Jang DG, Sim HJ, Song EK, Medina-Ruiz S, Seo JK, Park TJ. A thioredoxin fold protein Sh3bgr regulates Enah and is necessary for proper sarcomere formation. Dev Biol. 2015 Sep 1;405(1):1-9. doi: 10.1016/j.ydbio.2015.06.005. Epub 2015 Jun 24. PMID: 26116879; PMCID: PMC4561413.

283. Yan M, Cai L, Duan X, Tycksen ED, Rai MF. Carbonic anhydrase 2 is important for articular chondrocyte function and metabolic homeostasis. Bone. 2025 Jan;190:117313. doi: 10.1016/j.bone.2024.117313. Epub 2024 Oct 31. PMID: 39488239.

284. Xu H, Zeng H, Zhang DX, Jia XL, Luo CL, Fang MX, Nie QH, Zhang XQ. Polymorphisms associated with egg number at 300 days of age in chickens. Genet Mol Res. 2011 Oct 3;10(4):2279-89. doi: 10.4238/2011.October.3.5. PMID: 22002122.

285. Du X, Ren JD, Xu XQ, Chen GH, Huang Y, Du JP, Tao ZR, Cai ZX, Lu LZ, Yang H. Comparative transcriptome analysis reveals genes related to the yolk ratio of duck eggs. Anim Genet. 2019 Oct;50(5):484-492. doi: 10.1111/age.12820. Epub 2019 Jul 1. PMID: 31260130.

286. Traglia M, Croen LA, Lyall K, Windham GC, Kharrazi M, DeLorenze GN, Torres AR, Weiss LA. Independent Maternal and Fetal Genetic Effects on Midgestational Circulating Levels of Environmental Pollutants. G3 (Bethesda). 2017 Apr 3;7(4):1287-1299. doi: 10.1534/g3.117.039784. PMID: 28235828; PMCID: PMC5386877.

287. Salgado I, Prado Montes de Oca E, Chairez I, Figueroa-Yáñez L, Pereira-Santana A, Rivera Chávez A, Velázquez-Fernandez JB, Alvarado Parra T, Vallejo A. Deep Learning Techniques to Characterize the RPS28P7 Pseudogene and the Metazoa-SRP Gene as Drug Potential Targets in Pancreatic Cancer Patients. Biomedicines. 2024 Feb 8;12(2):0. doi: 10.3390/biomedicines12020395. PMID: 38397997; PMCID: PMC11154313.

288. Jayasena CS, Bronner ME. Rbms3 functions in craniofacial development by posttranscriptionally modulating TGF-β signaling. J Cell Biol. 2012 Oct 29;199(3):453-66. doi: 10.1083/jcb.201204138. Epub 2012 Oct 22. PMID: 23091072; PMCID: PMC3483135.

289. Sukhija N, Malik AA, Devadasan JM, Dash A, Bidyalaxmi K, Ravi Kumar D, Kousalaya Devi M, Choudhary A, Kanaka KK, Sharma R, Tripathi SB, Niranjan SK, Sivalingam J, Verma A. Genome-wide selection signatures address trait specific candidate genes in cattle indigenous to arid regions of India. Anim Biotechnol. 2024 Nov;35(1):2290521. doi: 10.1080/10495398.2023.2290521. Epub 2023 Dec 13. PMID: 38088885.

290. Costantino M, Mirra L, D'arcy P, Corno C, Carenini N, Corna E, Gubat J, Ciniselli CM, Pratesi P, Verderio P, Linder S, Beretta GL, Perego P. PSMC6 regulation of ovarian cancer cisplatin resistance unravels a new mode for proteasome targeting. Int J Biol Sci. 2025 Feb 26;21(5):2258-2274. doi: 10.7150/ijbs.104612. PMID: 40083690; PMCID: PMC11900818.

291. Jincho Y, Sotomaru Y, Kawahara M, Ono Y, Ogawa H, Obata Y, Kono T. Identification of genes aberrantly expressed in mouse embryonic stem cell-cloned blastocysts. Biol Reprod. 2008 Apr;78(4):568-76. doi: 10.1095/biolreprod.107.064634. Epub 2007 Oct 31. PMID: 17978277.

292. Nakamura K, Kusama K, Hori M, Imakawa K. The effect of bta-miR-26b in intrauterine extracellular vesicles on maternal immune system during the implantation period. Biochem Biophys Res Commun. 2021 Oct 8;573:100-106. doi: 10.1016/j.bbrc.2021.08.019. Epub 2021 Aug 9. PMID: 34403805.

293. Yang M, Hussain HMJ, Khan M, Muhammad Z, Zhou J, Ma A, Huang X, Ye J, Chen M, Zhi A, Liu T, Khan R, Asim A, Shah W, Zeb A, Ahmad N, Zhang H, Xu B, Ma H, Shi Q, Shi B. Deficiency in DNAH12 causes male infertility by impairing DNAH1 and DNALI1 recruitment in humans and mice. Elife. 2025 Mar

27;13:RP100350. doi: 10.7554/eLife.100350. PMID: 40146200; PMCID: PMC11949491.

294. Hu Y, Rong R, Wang Y, Yan SS, Liu S, Wang L. Downregulating EVA1C exerts the potential to promote neuron growth after neonatal hypoxic-ischemic encephalopathy injury associated with alternative splicing. Ibrain. 2022 Jul 21;8(4):481-491. doi: 10.1002/ibra.12053. PMID: 37786591; PMCID: PMC10529346.

295. Guan Y, Chen X, Zhao B, Shi Y, Han F. What Happened in the Hippocampal Axon in a Rat Model of Posttraumatic Stress Disorder. Cell Mol Neurobiol. 2022 Apr;42(3):723-737. doi: 10.1007/s10571-020-00960-w. Epub 2020 Sep 15. PMID: 32930942; PMCID: PMC11441271.

296. Mao Z, Feng M, Li Z, Zhou M, Xu L, Pan K, Wang S, Su W, Zhang W. ETV5 Regulates Hepatic Fatty Acid Metabolism Through PPAR Signaling Pathway. Diabetes. 2021 Jan;70(1):214-226. doi: 10.2337/db20-0619. Epub 2020 Oct 22. PMID: 33093014.

297. Simon CS, Hur W, Garg V, Kuo YY, Niakan KK, Hadjantonakis AK. ETV4 and ETV5 orchestrate FGF-mediated lineage specification and epiblast maturation during early mouse development. Development. 2025 Mar 15;152(6):dev204278. doi: 10.1242/dev.204278. Epub 2025 Mar 24. PMID: 40007475.

298. Eo J, Shin H, Kwon S, Song H, Murphy KM, Lim JH. Complex ovarian defects lead to infertility in Etv5-/- female mice. Mol Hum Reprod. 2011 Sep;17(9):568-76. doi: 10.1093/molehr/gar021. Epub 2011 Apr 8. PMID: 21478265.

299. Yang M, Hussain HMJ, Khan M, Muhammad Z, Zhou J, Ma A, Huang X, Ye J, Chen M, Zhi A, Liu T, Khan R, Asim A, Shah W, Zeb A, Ahmad N, Zhang H, Xu B, Ma H, Shi Q, Shi B. Deficiency in DNAH12 causes male infertility by impairing DNAH1 and DNALI1 recruitment in humans and mice. Elife. 2025 Mar 27;13:RP100350. doi: 10.7554/eLife.100350. PMID: 40146200; PMCID: PMC11949491.

300. Niu Q, Mu L, Li S, Xu S, Ma R, Guo S. Proanthocyanidin Protects Human Embryo Hepatocytes from Fluoride-Induced Oxidative Stress by Regulating Iron Metabolism. Biol Trace Elem Res. 2016 Feb;169(2):174-9. doi: 10.1007/s12011-015-0409-1. Epub 2015 Jun 25. PMID: 26105545.

301. Yu Y, Woloshun RR, Lee JK, Ebea PO, Zhu S, Nemeth E, Garrick LM, Garrick MD, Collins JF. Fetal factors disrupt placental and maternal iron homeostasis in murine

β-thalassemia. Blood. 2023 Jul 13;142(2):185-196. doi: 10.1182/blood.2022018839. PMID: 37146247; PMCID: PMC10352602.

302. Shi G, Bai Y, Zhang X, Su J, Pang J, He Q, Zeng P, Ding J, Xiong Y, Zhang J, Wang J, Liu D, Ma W, Huang J, Songyang Z. Bend family proteins mark chromatin boundaries and synergistically promote early germ cell differentiation. Protein Cell. 2022 Oct;13(10):721-741. doi: 10.1007/s13238-021-00884-1. Epub 2021 Nov 3. PMID: 34731408; PMCID: PMC9233729.

303. Kara B, Uyguner O, Maraş Genç H, İşlek EE, Kasap M, Toksoy G, Akpınar G, Uyur Yalçın E, Anık Y, Üstek D. BEND4 as a Candidate Gene for an Infection-Induced Acute Encephalopathy Characterized by a Cyst and Calcification of the Pons and Cerebellar Atrophy. Mol Syndromol. 2022 Feb;13(1):12-22. doi: 10.1159/000517541. Epub 2021 Sep 28. PMID: 35221871; PMCID: PMC8832206.

304. Xiong Y, Tan YJ, Xiong YM, Huang YT, Hu XL, Lu YC, Ye YH, Wang TT, Zhang D, Jin F, Huang HF, Sheng JZ. Expression of aquaporins in human embryos and potential role of AQP3 and AQP7 in preimplantation mouse embryo development. Cell Physiol Biochem. 2013;31(4-5):649-58. doi: 10.1159/000350084. Epub 2013 May 6. PMID: 23652731.

305. Chen L, Chen H, Liu X, Li J, Gao Q, Shi S, Wang T, Ye X, Lu Y, Zhang D, Sheng J, Jin L, Huang H. AQP7 mediates post-menopausal lipogenesis in adipocytes through FSH-induced transcriptional crosstalk with AP-1 sites. Reprod Biomed Online. 2020 Dec;41(6):1122-1132. doi: 10.1016/j.rbmo.2020.08.008. Epub 2020 Aug 18. PMID: 33132060.

306. Kobayashi H, Parton A, Czechanski A, Durkin C, Kong CC, Barnes D. Multidrug resistance-associated protein 3 (Mrp3/Abcc3/Moat-D) is expressed in the SAE Squalus acanthias shark embryo-derived cell line. Zebrafish. 2007 Winter;4(4):261-75. doi: 10.1089/zeb.2007.0520. PMID: 18284333; PMCID: PMC2597096.

307. Yuan KY, Gu YH, Pei YH, Yu SY, Li TZ, Feng T, Liu Y, Tian J, Miao X, Xiong J, Hu M, Yuan BF. Comprehensive analysis of transplacental transfer of environmental pollutants detected in paired maternal and cord serums. J Hazard Mater. 2025 Mar 15;486:136970. doi: 10.1016/j.jhazmat.2024.136970. Epub 2024 Dec 24. PMID: 39740555.

308. Imperio GE, Javam M, Lye P, Constantinof A, Dunk CE, Reis FM, Lye SJ, Gibb W, Matthews SG, Ortiga-Carvalho TM, Bloise E. Gestational age-dependent gene

expression profiling of ATP-binding cassette transporters in the healthy human placenta. J Cell Mol Med. 2019 Jan;23(1):610-618. doi: 10.1111/jcmm.13966. Epub 2018 Nov 8. PMID: 30407748; PMCID: PMC6307765.

309. Liu Y, Jurczak MJ, Lear TB, Lin B, Larsen MB, Kennerdell JR, Chen Y, Huckestein BR, Nguyen MK, Tuncer F, Jiang Y, Monga SP, O'Donnell CP, Finkel T, Chen BB, Mallampalli RK. A Fbxo48 inhibitor prevents pAMPKα degradation and ameliorates insulin resistance. Nat Chem Biol. 2021 Mar;17(3):298-306. doi: 10.1038/s41589-020-00723-0. Epub 2021 Jan 25. PMID: 33495648; PMCID: PMC8529588.

310. Xiu X, Song Z, Gao K, Deng X, Qi Y, Zhu A, Gong L, Deng H. Genetic analysis of the FBXO48 gene in Chinese Han patients with Parkinson disease. Neurosci Lett. 2013 Apr 29;541:224-6. doi: 10.1016/j.neulet.2013.02.031. Epub 2013 Feb 26. PMID: 23485738.

311. Kearney CJ, Randall KL, Oliaro J. DOCK8 regulates signal transduction events to control immunity. Cell Mol Immunol. 2017 May;14(5):406-411. doi: 10.1038/cmi.2017.9. Epub 2017 Apr 3. PMID: 28366940; PMCID: PMC5423093.

312. Mazzoleni S, Němec P, Albrecht T, Lymberakis P, Kratochvíl L, Rovatsos M. Long-term stability of sex chromosome gene content allows accurate qPCR-based molecular sexing across birds. Mol Ecol Resour. 2021 Aug;21(6):2013-2021. doi: 10.1111/1755-0998.13381. Epub 2021 Apr 2. PMID: 33720488.

313. Weng L, Hong H, Zhang Q, Xiao C, Zhang Q, Wang Q, Huang J, Lai D. Sleep Deprivation Triggers the Excessive Activation of Ovarian Primordial Follicles via β2 Adrenergic Receptor Signaling. Adv Sci (Weinh). 2024 Nov;11(41):e2402393. doi: 10.1002/advs.202402393. Epub 2024 Sep 4. PMID: 39229959; PMCID: PMC11538700.

314. Mizoguchi Y, Nakashima K, Sato A, Shindo A. β-adrenergic receptor regulates embryonic epithelial extensibility through actomyosin inhibition. iScience. 2023 Nov 15;26(12):108469. doi: 10.1016/j.isci.2023.108469. PMID: 38213788; PMCID: PMC10783608.

315. Wu J, Kong S, Guo C, Wang J, Lu J, Jiang R, Wang H. An exaggerated epinephrine-adrenergic receptor signaling impairs uterine decidualization in mice. Reprod Toxicol. 2019 Dec;90:109-117. doi: 10.1016/j.reprotox.2019.09.003. Epub 2019 Sep 11. PMID: 31520687.

316. Zhang M, Zhou J, Ji Y, Shu S, Zhang M, Liang Y. LncRNA-NONMMUT100923.1 regulates mouse embryonic palatal shelf adhesion by sponging miR-200a-3p to modulate medial epithelial cell desmosome junction during palatogenesis. Heliyon. 2023 May 19;9(5):e16329. doi: 10.1016/j.heliyon.2023.e16329. PMID: 37251885; PMCID: PMC10208945.

317. Linck Moroni J, Tsoi S, Wenger II, Plastow GS, Dyck MK. Placental Transcriptome Analysis in Connection with Low Litter Birth Weight Phenotype (LBWP) Sows. Genes (Basel). 2024 May 28;15(6):703. doi: 10.3390/genes15060703. PMID: 38927639; PMCID: PMC11203121.

318. Yan L, Yang M, Guo H, Yang L, Wu J, Li R, Liu P, Lian Y, Zheng X, Yan J, Huang J, Li M, Wu X, Wen L, Lao K, Li R, Qiao J, Tang F. Single-cell RNA-Seq profiling of human preimplantation embryos and embryonic stem cells. Nat Struct Mol Biol. 2013 Sep;20(9):1131-9. doi: 10.1038/nsmb.2660. Epub 2013 Aug 11. PMID: 23934149.

319. Xue Z, Huang K, Cai C, Cai L, Jiang CY, Feng Y, Liu Z, Zeng Q, Cheng L, Sun YE, Liu JY, Horvath S, Fan G. Genetic programs in human and mouse early embryos revealed by single-cell RNA sequencing. Nature. 2013 Aug 29;500(7464):593-7. doi: 10.1038/nature12364. Epub 2013 Jul 28. PMID: 23892778; PMCID: PMC4950944.

320. Wang X, Park J, Susztak K, Zhang NR, Li M. Bulk tissue cell type deconvolution with multi-subject single-cell expression reference. Nat Commun. 2019 Jan 22;10(1):380. doi: 10.1038/s41467-018-08023-x. PMID: 30670690; PMCID: PMC6342984.

8. Supplementary materials

Table Captions and Figure Legends

Table Captions:

Table 1. Individual embryo recovery outcomes in relation to donor age.

Table 2. Embryo yield under two experimental designs: age-based and season-based grouping.

Table 3. Morphological classification and quality assessment of *in vivo*–derived bovine embryos according to IETS criteria.

Morphological characteristics, developmental stage, and quality grading of individual bovine embryos recovered *in vivo* from Holstein–Friesian cows. Embryos were evaluated under a stereomicroscope and classified according to the International Embryo Transfer Society (IETS) guidelines. Developmental stages include compact morula (stage code 4), early blastocyst (stage code 5), and blastocyst (stage code 6). Embryo quality was graded on a scale from 1 (excellent/good) to 3 (poor), based on morphological features such as blastocoel formation, degree of compaction, differentiation of the inner cell mass and trophoblast, integrity of the zona pellucida, cellular symmetry, fragmentation, and overall viability of the embryonic mass.

Table 4. Quality control and statistics of RNA-seq data of in vivo-derived embryo of Polish HF cattle

Table 5. TOP 30 Age-dependent up-regulated genes from in vivo-derived embryo of Polish HF cattle

Table 6. TOP 30 Age-dependent down-regulated genes from in vivo-derived embryo of Polish HF cattle

Table 7. Age-dependent up-regulated genes in bovine embryos with established roles in embryogenesis and reproductive pathways. This table lists genes that were significantly up-regulated in embryos obtained from cows of different ages and whose documented functions are directly linked to embryogenesis or reproductive processes. The annotations highlight key pathways—including steroidogenesis (e.g., CYP11A1), immune and cellular differentiation signalling (STAT4, LRCH2), metabolic support for rapid cell proliferation (HPRT1, PDK4), and cell migration crucial for implantation (CCL24). Collectively, the elevated expression of these transcripts may underpin age-related variations in embryo competence, developmental trajectory, and implantation potential observed in the study.

Table 8. Age-dependent up-regulated genes in bovine embryos with no currently validated roles in embryogenesis or reproduction

This table compiles genes that were significantly up-regulated in embryos derived from cows of different ages, but for which the literature does not yet provide clear evidence of direct involvement in embryogenesis or reproductive processes. Although many encode proteins with well-characterised functions—such as immune-cell activation (ICOS), lipid and pH homeostasis (PLA2G7, CA2), neuronal signalling (SYT4, HOMER1), and nucleotide metabolism (MOCOS, TKTL2)—their contribution to early bovine development remains speculative. Several genes (e.g., CT47B1, MAGEB2) are chiefly known as cancer/testis antigens, while others (C5H12orf75) are largely uncharacterized. Their differential expression may reflect age-related systemic influences on the embryo rather than direct developmental roles, underscoring the need for functional validation to determine whether any of these transcripts modulate embryo quality, stress resilience, or later physiological traits.

Table 9. Age-dependent down-regulated genes in bovine embryos with established roles in embryogenesis and reproduction

This table lists genes whose transcript levels decreased significantly in embryos collected from cows of different ages and whose documented functions are tightly linked to core developmental or reproductive pathways. The down-regulation affects diverse processes, including cilia-mediated signalling (ARL13A), copper and purine metabolism essential for energy production (ATP7A, IMPDH1, UQCRC2), cytoskeletal dynamics during oocyte maturation and cleavage (JMY, AKT2), and placental or uterine interactions critical for implantation (PROM1, NPSR1). Reduced expression of key genome-maintenance and DNA-repair factors (FANCA) further suggests compromised genomic stability. Collectively, these changes may help explain age-related declines in embryo viability, altered metabolic competence, and reduced implantation success observed in the study.

Table 10. Age-dependent down-regulated genes in bovine embryos lacking documented roles in embryogenesis or reproduction

This table summarises transcripts whose abundance fell significantly in embryos derived from cows of different ages, yet whose known functions do not presently include embryogenesis or reproductive regulation. The genes encode proteins mainly associated with innate immunity (SERPINB4, LYZ), neuromodulation (LYPD6B), and metabolic or angiogenic processes (CAPSL). Although their direct contribution to early bovine development is unverified, age-related repression of these genes might still influence the embryonic micro-environment—for example, by altering inflammatory tone or nutrient signalling—thereby indirectly affecting embryo quality. Functional studies will be needed to determine whether their down-regulation is merely correlative or plays a contributory role in age-linked developmental differences.

Table 11. TOP 30 season-dependent up-regulated genes from in vivo-derived embryo of Polish HF cattle

Table 12. TOP 30 season-dependent down-regulated genes from in vivo-derived embryo of Polish HF cattle

Table 13. Season-dependent up-regulated genes in bovine embryos with established roles in embryogenesis and reproductive pathways

Table 14. Season-dependent up-regulated genes in bovine embryos with no currently validated roles in embryogenesis or reproduction

Table 15. Season-dependent down-regulated genes in bovine embryos with established roles in embryogenesis and reproduction

Table 16. Season-dependent down-regulated genes in bovine embryos lacking documented roles in embryogenesis or reproduction

Figure Legends:

Figure 1: Representative images of bovine embryos derived *in vivo* from seven Holstein–Friesian cows, examined under a stereomicroscope (working magnification 40–60×).

Figure 2. Overview of the experimental workflow and a bioinformatics pipeline. This schematic illustrates the experimental workflow conducted in two complementary experiments. In the first experiment, embryos were collected from cows at different lactation stages (first lactation and beyond the sixth lactation). In the second experiment, embryos were obtained from cows exposed to distinct environmental conditions: thermoneutral and elevated temperature. In both experiments, cows were synchronized for oestrus and inseminated. Recovered embryos were flushed by using PBS supplemented with PVA and subsequently cryopreserved at –80°C until further processing. For molecular analysis, total RNA was extracted and subjected to library preparation, which included embryo lysis, cDNA synthesis, LD-PCR amplification, validation of cDNA libraries, and dilution of prepared libraries. Next-generation sequencing (RNA-seq) was then performed, followed by quality control, read mapping, group assignment, and identification of differentially expressed genes (DEGs). Finally, bioinformatics and pathway analyses were carried out to investigate gene expression dynamics and functional networks associated with embryonic development under the studied conditions.

Figure 2. Experimental design and RNA-seq workflow for *in vivo*–derived bovine embryos.
Schematic overview of the experimental design and analytical workflow. Bovine embryos were obtained *in vivo* from Holstein–Friesian cows differing in lactation status and exposed to thermoneutral or elevated environmental temperature conditions. Following oestrus synchronization and insemination, embryos were recovered by uterine flushing, transferred to PBS supplemented with PVA, and immediately deep-frozen at −80 °C. RNA was extracted from individual embryos and processed for next-generation sequencing (NGS)-based RNA-seq, including cDNA synthesis, LD-PCR amplification, library preparation, and validation. Sequencing data were subjected to bioinformatic analyses, including quality control, read

filtering, mapping, experimental group design, and differential gene expression analysis, followed by functional pathway analysis.

Figure 3. Age-dependent: Density plot displaying the distribution of raw gene expression counts across individual bovine embryo RNA-seq samples. The X-axis indicates mean gene expression counts, while the Y-axis represents density. Each coloured curve corresponds to a unique embryo sample (legend). The high degree of overlap among curves reflects consistent expression distributions across samples, supporting uniform sequencing depth and sample quality prior to normalization.

Figure 4. Age-dependent: Principal component analysis (PCA) plot showing sample classification of embryo samples based on their gene expression profiles. Each point represents an individual sample plotted according to their scores on principal components PC1 (x-axis) and PC2 (y-axis), reflecting the highest variability within the dataset. Samples are classified by developmental stage (blastocyst, cleavage, or embryo) indicated by different shapes (circle, triangle, and square, respectively), and grouped into two distinct clusters (Group 1 in red and Group 2 in blue). Clear separation between these two groups on PC1 suggests pronounced differences in gene expression profiles related to distinct biological conditions or developmental characteristics.

Figure 5. Age-dependent: Bar plot showing the proportion of variance explained by each principal component (PC) in the PCA analysis. PC1 explains the largest proportion (29.7%) of total variance, followed by PC2 (13.7%) and PC3 (8.9%), indicating that these first few components capture most of the variability present in the gene expression data. This plot emphasizes the significance of the first principal components in differentiating embryo samples based on their gene expression profiles.

Figure 6. Age-dependent: Histogram showing the distribution of nominal p-values obtained from differential gene expression analysis using DESeq2. The X-axis represents nominal p-value ranges, and the Y-axis indicates the number of genes falling within each range. The noticeable peak near zero indicates a substantial proportion of genes with statistically significant differential expression between the analysed conditions. This p-value distribution highlights the robustness and sensitivity of the differential expression analysis performed in this study.

Figure 7. Age-dependent: Normal Q-Q plot representing the distribution of the gene expression data residuals against a theoretical normal distribution. The X-axis shows theoretical quantiles, while the Y-axis shows observed sample quantiles. Points deviating significantly from the diagonal line indicate departures from normality, suggesting potential presence of outliers or non-normal distribution in the data. Notable deviations observed at both tails of the plot indicate that some genes significantly differ from a normal distribution, a common scenario in high-throughput gene expression datasets.

Figure 8. Age-dependent: Volcano plots illustrating the differential gene expression between the compared embryo conditions. The x-axis represents the magnitude of change in gene expression (log2 Fold Change), while the y-axis shows the statistical significance (-log10 False Discovery Rate, FDR). Each dot represents a gene: Red dots indicate significantly upregulated genes, blue dots indicate significantly downregulated genes, and grey dots indicate genes without significant expression changes. Genes located in the upper corners of each plot

represent those with the highest fold change and greatest statistical significance, highlighting key differentially expressed genes that may have biological importance.

Figure 9. Age-dependent: MA plot showing differential gene expression between embryos derived from younger (≤3 years) and older (6–7 years) Holstein–Friesian cows. Each dot represents a gene, plotted by its $\log_2$ mean expression (x-axis) and $\log_2$ fold change (y-axis). Red and blue dots indicate significantly up- and downregulated transcripts, respectively (FDR-adjusted $p < 0.05$), while grey dots represent non-significant genes. The top 20 differentially expressed genes are annotated by Ensembl IDs based on effect size. Dashed lines denote the fold change thresholds used to determine biological significance.

Figure 10. Age-dependent: ClueGO Gene Ontology (GO) and KEGG pathway enrichment analysis of RNA-seq upregulated target genes associated with cow's age. Bar chart displaying significantly enriched GO biological process terms and KEGG pathways among RNA-seq target genes upregulated in association with age in cattle. The y-axis lists enriched terms, while the x-axis represents the percentage of genes annotated to each term within the input set. Numbers at the end of each bar indicate the number of associated genes. Functional terms are color-coded based on biological groupings. The analysis reveals age-associated upregulation of key processes including development (e.g., **lung and forebrain development**, **urogenital system development**), immune signaling, lipid metabolism, synaptic transmission, and peptide transport, highlighting molecular pathways potentially linked to physiological aging in cattle.

Figure 11. Age-dependent: ClueGO pie chart showing GO biological process and KEGG pathway enrichment of RNA-seq upregulated target genes associated with cow's age. Pie chart illustrating the distribution of significantly enriched GO biological processes and KEGG pathways identified by ClueGO among RNA-seq target genes upregulated with advancing age in cattle. Each slice represents a functional term or pathway group, with its proportion expressed as a percentage of the total enriched terms. Major enriched categories include *dipeptide transmembrane transport* (18.18%), *negative regulation of short-term neuronal synaptic plasticity* (18.18%), *fatty acid omega-oxidation* (16.67%), *rhomboid morphogenesis* (14.39%), and *lipid oxidation* (11.36%). Additional pathways include *purine nucleoside biosynthetic process* (7.58%), *skeletal muscle contraction* (5.3%), and others. Asterisks (**) indicate statistically significant enrichment after multiple testing corrections. Functional groups are color-coded to reflect biological similarity. This analysis highlights age-associated changes in metabolism, neuroregulation, morphogenesis, and transport processes in cattle.

Figure 12. Age-dependent: ClueGO Gene Ontology (GO) and KEGG pathway enrichment analysis of RNA-seq downregulated target genes associated with cow's age. Bar chart displaying significantly enriched GO biological process terms and KEGG pathways among RNA-seq target genes downregulated with increasing age in cattle, as identified using ClueGO. The y-axis lists the enriched GO terms, while the x-axis represents the percentage of genes in the input set annotated to each term. Numbers at the end of each bar indicate the gene count per term. Terms are color-coded based on functional groupings. Notable enriched terms include 'de novo' actin filament nucleation, defense response to tumor cell, epithelial cell differentiation, prostate gland morphogenesis, positive regulation of kidney development, glucose and glycogen metabolic processes, regulation of fatty acid beta-oxidation, fatty acid transport, anion transmembrane transport, regulation of membrane potential, and cellular response to light intensity. These results reflect age-associated downregulation of genes involved in cellular signaling, transport, metabolism, and developmental processes in cattle.

Figure13. Age-dependent: ClueGO pie chart showing GO biological process and KEGG pathway enrichment of RNA-seq downregulated target genes associated with cow's age. Pie chart illustrating the proportional distribution of significantly enriched GO biological process terms and KEGG pathways among RNA-seq target genes downregulated with advancing age in cattle, identified using ClueGO. Each slice represents a functional group, with its proportion expressed as a percentage of the total number of enriched terms. Dominant categories include *cellular response to light intensity* (55.7%), *positive regulation of kidney development* (15.19%), and *prostate gland morphogenesis* (8.86%), with additional terms such as *GTP metabolic process* (8.86%), *regulation of CD40 signaling pathway* (5.06%), *cellular copper ion homeostasis* (2.53%), *defense response to tumor cell* (2.53%), and *'de novo' actin filament nucleation* (1.27%). Terms marked with asterisks (**) are statistically significant after multiple testing corrections. Color coding represents functionally grouped biological processes. This analysis highlights age-related downregulation of pathways linked to cellular signaling, immune function, development, and environmental response in cattle.

Figure 14. Season dependent: Density plot displaying the distribution of raw gene expression counts across individual bovine embryo RNA-seq samples. The X-axis indicates mean gene expression counts, while the Y-axis represents density. Each coloured curve corresponds to a unique embryo sample (legend). The high degree of overlap among curves reflects consistent expression distributions across samples, supporting uniform sequencing depth and sample quality prior to normalization.

Figure 15. Season dependent: Principal component analysis (PCA) plot showing sample classification of embryo samples based on their gene expression profiles. Each point represents an individual sample plotted according to their scores on principal components PC1 (x-axis) and PC2 (y-axis), reflecting the highest variability within the dataset. Samples are classified by developmental stage (blastocyst, cleavage, or embryo) indicated by different shapes (circle, triangle, and square, respectively), and grouped into two distinct clusters (Group 1 in red and Group 2 in blue). Clear separation between these two groups on PC1 suggests pronounced differences in gene expression profiles related to distinct biological conditions or developmental characteristics.

Figure 16. Season dependent: Bar plot showing the proportion of variance explained by each principal component (PC) in the PCA analysis. PC1 explains the largest proportion (29.7%) of total variance, followed by PC2 (13.7%) and PC3 (8.9%), indicating that these first few components capture most of the variability present in the gene expression data. This plot emphasizes the significance of the first principal components in differentiating embryo samples based on their gene expression profiles.

Figure 17. Season dependent: Histogram showing the distribution of nominal p-values obtained from differential gene expression analysis using DESeq2. The X-axis represents nominal p-value ranges, and the Y-axis indicates the number of genes falling within each range. The noticeable peak near zero indicates a substantial proportion of genes with statistically significant differential expression between the analysed conditions. This p-value distribution highlights the robustness and sensitivity of the differential expression analysis performed in this study.

Figure 18. Season dependent: Normal Q-Q plot representing the distribution of the gene expression data residuals against a theoretical normal distribution. The X-axis shows theoretical quantiles, while the Y-axis shows observed sample quantiles. Points deviating

significantly from the diagonal line indicate departures from normality, suggesting potential presence of outliers or non-normal distribution in the data. Notable deviations observed at both tails of the plot indicate that some genes significantly differ from a normal distribution, a common scenario in high-throughput gene expression datasets.

Figure 19. Season dependent: Volcano plots illustrating the differential gene expression between the compared embryo conditions. The x-axis represents the magnitude of change in gene expression (log2 Fold Change), while the y-axis shows the statistical significance (-log10 False Discovery Rate, FDR). Each dot represents a gene: Red dots indicate significantly upregulated genes, blue dots indicate significantly downregulated genes, and grey dots indicate genes without significant expression changes. Genes located in the upper corners of each plot represent those with the highest fold change and greatest statistical significance, highlighting key differentially expressed genes that may have biological importance.

Figure 20. Season dependent: MA plot showing differential gene expression between embryos derived from sumer and spring season of Polish Holstein–Friesian cows. Each dot represents a gene, plotted by its $\log_2$ mean expression (x-axis) and $\log_2$ fold change (y-axis). Red and blue dots indicate significantly up- and downregulated transcripts, respectively (FDR-adjusted $p < 0.05$), while grey dots represent non-significant genes. The top 20 differentially expressed genes are annotated by Ensembl IDs based on effect size. Dashed lines denote the fold change thresholds used to determine biological significance.

Figure 21. Season dependent: Gene Ontology (GO) Biological Process and KEGG pathway enrichment analysis of genes significantly upregulated in bovine embryos derived from cows collected during two distinct seasons (warm and cold), performed using ClueGO. The bar plot illustrates enriched GO terms and KEGG pathways, with bar length proportional to the number of genes associated with each term. The x-axis represents the percentage of genes annotated to a given term within the input gene set, while numbers at the end of each bar indicate the absolute number of associated genes. Functionally related terms are grouped and color-coded according to shared biological categories. The analysis reveals age-associated upregulation of key biological processes, including developmental pathways (e.g., lung and forebrain development, urogenital system development), immune signaling, lipid metabolism, synaptic transmission, and peptide transport, highlighting molecular pathways potentially linked to physiological aging in cattle.

Figure 22: Season dependent: ClueGO pie chart of GO biological process and KEGG pathway enrichment for season-associated upregulated genes in bovine embryos.

Figure 22. Pie chart illustrating the distribution of significantly enriched Gene Ontology (GO) Biological Process terms and KEGG pathways identified by ClueGO among RNA-seq target genes upregulated with advancing maternal age in cattle. Each slice represents a functional term or pathway group, with its proportion expressed as a percentage of the total enriched terms. The major enriched categories include dipeptide transmembrane transport (18.18%), negative regulation of short-term neuronal synaptic plasticity (18.18%), fatty acid omega-oxidation (16.67%), rhomboid morphogenesis (14.39%), and lipid oxidation (11.36%). Additional enriched pathways include purine nucleoside biosynthetic process (7.58%), skeletal muscle contraction (5.30%), and others. Asterisks (**) indicate statistically significant enrichment after correction for multiple testing. Functional groups are color-coded to reflect biological similarity. Overall, the analysis highlights age-associated alterations in metabolic, neuroregulatory, morphogenetic, and transport-related processes in bovine embryos.

Figure 23. Season dependent: ClueGO Gene Ontology (GO) enrichment analysis of season-associated downregulated genes in bovine embryos.

ClueGO-based Gene Ontology (GO) Biological Process enrichment analysis of RNA-seq target genes significantly downregulated in bovine embryos in association with seasonal variation. The bar chart displays enriched GO terms related to key biological processes, including vesicle trafficking, cytoskeletal organization, regulation of apoptosis, and sensory perception, identified from RNA-seq analysis of embryos collected under different seasonal conditions. Bar length corresponds to the number of genes annotated to each GO term.

Figure24: Season dependent: ClueGO pie chart showing GO biological process and KEGG pathway enrichment of RNA-seq downregulated target genes associated with seasonal variation.

Figure 25. Expression profiles of five developmentally relevant genes during bovine preimplantation stages.

This violin plot illustrates the expression profiles of CYP11A1, AKT2, UQCRC2, CXCR4, and BMPER during bovine preimplantation development, from oocyte to late blastocyst. Distinct expression patterns highlight the potential roles of these genes at specific developmental stages: CYP11A1: Expression is minimal at early cleavage stages but increases markedly in morula and late blastocyst, suggesting a role in steroidogenesis and metabolic regulation necessary for later embryonic differentiation. AKT2: Shows moderate expression starting from the 2-cell stage, with a steady increase towards the late blastocyst, consistent with its function in cell survival, proliferation, and metabolism during rapid cell divisions. UQCRC2: Highly expressed in morula and late blastocyst stages, reflecting its role in mitochondrial function and energy production, which are essential as the embryo undergoes compaction and differentiation. CXCR4: Expression emerges strongly in morula and late blastocyst, indicating its importance in cell signaling, migration, and lineage allocation within the embryo. BMPER: Displays low expression in early cleavage stages but becomes more prominent at the zygote and late blastocyst levels, pointing to a potential regulatory role in BMP signaling pathways during embryonic patterning.

Figure 26. MuSiC dendrograms visualizing hierarchical clustering of bovine preimplantation embryos based on the design matrix (left) and the mean relative abundance (right) following group revision.

Dendrograms showing hierarchical clustering of developmental stage structure (left) and MuSiC-derived mean relative abundance across bovine preimplantation embryos (right). The left panel presents clustering based on the design matrix of gene expression, while the right panel depicts the clustering based on the mean relative abundance (RA). Both approaches consistently demonstrate the separation of early developmental stages (oocyte, zygote, 2-cell, 4-cell), from later stages (8-cell, morula, late blastocyst), reflecting transcriptional similarities within these groups. The clustering results served as the basis for grouping developmental stages into broader categories for deconvolution analysis.

Figure 27. UMAP visualization of RNA-seq samples across developmental stages

Uniform Manifold Approximation and Projection (UMAP) plot displaying the transcriptional similarity between RNA-seq samples corresponding to distinct developmental stages: late blastocyst (red), morula (purple), 8-cell (blue), and the combined early-stage group comprising oocyte, zygote, 2-cell, and 4-cell (green). The clear separation between clusters indicates consistent stage-specific expression profiles across the samples, validating the categorization strategy applied for further analyses.

Figure 28. Venn diagram of marker genes assigned to developmental stage clusters

Venn diagram showing the overlap of marker genes identified for four embryo developmental stages: 8-cell (yellow), morula (grey), late blastocyst (red), and the early-stage group comprising 2-cell/4-cell embryos (blue). Most marker genes exhibit stage specificity, with the majority being unique to the 8-cell stage (2832; 45.6%) and the early-stage group (1444; 23.3%), followed by morula (895; 14.4%) and late blastocyst (640; 10.3%). Only limited overlap was detected between clusters, indicating that each developmental stage is characterized by a distinct gene expression profile.

Figure 29. Heatmap of MuSiC-estimated developmental stage contributions across embryo RNA-seq samples.

The heatmap displays the estimated proportions of transcriptional signatures characteristic of four developmental stages - oocyte/zygote/2-cell/4-cell, 8-cell, morula, and late blastocyst - across individual embryo RNA-seq samples. Each row represents one sample, and the color gradient (0–1) reflects the relative abundance of each signature. Late-blastocyst transcriptional profiles dominate all samples, while 8-cell and morula signatures are absent. A faint signal corresponding to the oocyte/zygote/2-cell/4-cell group is detectable in several samples.

Figure 30. Heatmap of estimated developmental stage proportions in embryo RNA-seq samples using DeTREM

Figure 30. Heatmap of estimated developmental stage proportions in embryo RNA-seq samples using DeTREM

The heatmap displays the estimated proportions of transcriptional signatures characteristic of four developmental stages - oocyte/zygote/2-cell/4-cell, 8-cell, morula, and late blastocyst - across individual embryo RNA-seq samples. Each row represents one sample, and the color gradient (0–1) reflects the relative abundance of each signature. Late-blastocyst transcriptional profiles dominate most samples. Low-level contributions from the oocyte/zygote/2-cell/4-cell group and the 8-cell stage are detectable in several samples, whereas morula signatures are nearly absent.

Supplementary Tables (S1-S8):

Supplementary Table S1: Quality control check of qualified scRNA-seq libraries from in vivo-derived embryo of Polish HF cattle

Supplementary Table S2: The normalization and quantification of age-dependent gene transcripts of in vivo-derived embryo of Polish HF cattle with the Fragments Per Kilobase of transcript per Million (FPKM) / Transcript per Million (TPM) values

Sheet-1: The normalization and quantification of 27607 gene transcripts without filtering of in vivo-derived embryos of Polish HF cattle.

Sheet-2: The normalization and quantification of 11571 gene transcripts after filtering of the in vivo-derived embryo of Polish HF cattle.

Supplementary Table S3: Identification of 11571 age-dependent gene transcripts of in vivo-derived embryo of Polish HF cattle.

Sheet-1: Identification of 11571 gene transcripts of the in vivo-derived embryo of Polish HF cattle. (cutoff p<1.0)

Sheet-2: Identification of 159 gene transcripts of the in vivo-derived embryo of Polish HF cattle (cutoff <0.001)

Sheet-3: Identification of 236 gene transcripts of the in vivo-derived embryo of Polish HF cattle (cutoff <0.002)

Sheet-4: Identification of 488 gene transcripts of the in vivo-derived embryo of Polish HF cattle (cutoff <0.005)

Sheet-5: Identification of 647 gene transcripts of the in vivo-derived embryo of Polish HF cattle (cutoff <0.01)

Supplementary Table S4: Identification of age-dependent upregulated gene transcripts of in vivo-derived embryo of Polish HF cattle

Supplementary Table S5: Identification of age-dependent downregulated gene transcripts of in vivo-derived embryo of Polish HF cattle

Supplementary Table S6: Identification of 12571 season-dependent gene transcripts of in vivo-derived embryo of Polish HF cattle.

Sheet-1: Identification of 12571 gene transcripts of the in vivo-derived embryo of Polish HF cattle. (cutoff p<1.0)

Sheet-2: Identification of 159 gene transcripts of the in vivo-derived embryo of Polish HF cattle (cutoff <0.001)

Sheet-3: Identification of 236 gene transcripts of the in vivo-derived embryo of Polish HF cattle (cutoff <0.002)

Sheet-4: Identification of 488 gene transcripts of the in vivo-derived embryo of Polish HF cattle (cutoff <0.005)

Sheet-5: Identification of 647 gene transcripts of the in vivo-derived embryo of Polish HF cattle (cutoff <0.01)

Supplementary Table S7: Identification of season-dependent upregulated gene transcripts of in vivo-derived embryo of Polish HF cattle

Supplementary Table S8: Identification of season-dependent downregulated gene transcripts of in vivo-derived embryo of Polish HF cattle

Supplementary Figures (S1-S5):

Supplementary Figure S1: The determination of the qualitative and quantitative assessments (QC check) of libraries by the Agilent 2100 Bioanalyzer.

Supplementary Figure (S2): ClueGO network showing enriched Gene Ontology (GO) terms for genes upregulated with increasing cow age based on RNA-seq data. The Figures show the functionally grouped network with terms as nodes (hubs) linked based on their kappa score level (≥0.3) and p-value after Bonferroni correction < 0.05, where only the label of the most significant term per group is shown. The node size represents the term enrichment significance. Node color represents the functional groups.

Supplementary Figure (S3): ClueGO network showing enriched Gene Ontology (GO) terms for genes downregulated with increasing cow age based on RNA-seq data.

The Figure shows the functionally grouped network with terms as nodes (hubs) linked based on their kappa score level (≥0.3) and p-value after Bonferroni correction < 0.05, where only the label of the most significant term per group is shown. The node size represents the term enrichment significance. Node color represents the functional groups.

Supplementary Figure (S4): ClueGO network showing enriched Gene Ontology (GO) terms for genes upregulated with the season based on RNA-seq data. The Figure shows the functionally grouped network with terms as nodes (hubs) linked based on their kappa score level (≥0.3) and p-value after Bonferroni correction < 0.05, where only the label of the most significant term per group is shown. The node size represents the term enrichment significance. Node color represents the functional groups.

Supplementary Figure (S5): ClueGO network showing enriched Gene Ontology (GO) terms for genes downregulated with the season based on RNA-seq data. The Figure shows the functionally grouped network with terms as nodes (hubs) linked based on their kappa score level (≥0.3) and p-value after Bonferroni correction < 0.05, where only the label of the most significant term per group is shown. The node size represents the term enrichment significance. Node color represents the functional groups.